An indirectly controlled high-speed servo valve using piezo actuators

Master's Thesis

for the qualification towards

Master of Engineering (MEng): Mechatronics

Faculty of Engineering, the Built Environment and Information Technology

Department of Mechatronics

Nelson Mandela Metropolitan University

by

Leander Behre

promoters: Prof. Dr.-Ing. U. Becker

Prof. Dr.-Ing. T. van Niekerk

March 3, 2015

Leander Behre
45 Rubin Crescent
Summerstrand
Port Elizabeth 6001
-South Africa-

I hereby declare that the work done in this dissertation is my own and that all sources used or referred to have been documented and recognized.

Port Elizabeth
March 3, 2015

Leander Behre

Copyright statement

The copy of this thesis has been supplied on condition that anyone who consults it is understood to recognize that its copyright rests with the author and that no quotation from this thesis and no information derived from it may be published without the author's prior consent.

Abstract

Since the exhaust emissions legislation for motor vehicles with combustion engines is complicating the manufacturing of environmental yet powerful engines more than ever, automobile manufacturers have approached this challenge by means of downsizing, hybridization of combustion and electric engines and variable valve opening times. In these cases conventional, mechanical valve trains are still used.

The subject of this master thesis is the development of a mechatronic control unit as replacement for the camshaft driven valve train of common combustion engines. The system's aim is a contribution to the progression of the development of modern combustion engines satisfying current demands in terms of economy and efficiency. The developed system is based on the "Full Variable Valve Train" project, founded at the "Institute of Vehicle Construction Wolfsburg" at the "Ostfalia University of Applied Sciences".

An indirectly controlled high speed servo valve that is actuated by a piezo-electric actuator and pressurized hydraulic fluid is being developed. The overall aim is to obtain advantages from a control engineering perspective, being able to reduce the size of the used piezo actuator and hence solve the packaging and regulation issues of the overall system. After manufacturing and improvement activities, a system could be developed that allows a variable control of the engine valve movement. The best results are achieved using a rectangular function for the engine valve actuator. The system allows engine valve operation independent from the crankshaft position and shows the potential to generate higher engine torque and power output while decreasing fuel consumption and emissions at the same time.

Acknowledgements

I express my appreciation to Prof. Dr.-Ing. Udo Becker from the "Ostfalia University of Applied Sciences" who gave me the opportunity to participate in the "Full Variable Valve Train" project while engaged in my bachelor studies in Wolfsburg, Germany, since the beginning of the year 2012. I express my gratitude to Prof. Becker for introducing me to the "Nelson Mandela Metropolitan University" during my visit in the year 2012; also for the trust put in my abilities as a researcher and young engineer and for promoting this master's project.

My utmost appreciation also belongs to Prof. Dr.-Ing. Theo van Niekerk from the "Nelson Mandela Metropolitan University" in Port Elizabeth, South Africa, who started to encourage my master's project during my bachelor studies. I am deeply grateful for his support throughout all formalities I faced as an international student and the support from the beginning of my proposal until the completion of this work.

I thank the Research Capacity Development (RCD) of the "Nelson Mandela Metropolitan University" for awarding me an "NMMU Postgraduate Scholarship".

I wholeheartedly thank my fellow student and friend Dr Oluwole Ayodeji Olufayo for his selfless and unfailing support and imaginative input during troubleshooting and testing.

I also want to mention Dr Thomas Wilm and especially Mr Ian Oberholzer from the "Volkswagen South Africa (Pty) Ltd" (VWSA) and emphasize their outstanding assistance within the early stage of the project.

Contents

Copyright statement III

Abstract IV

Acknowledgements V

List of tables X

List of figures XII

Nomenclature XIII

1 Introduction 1

1.1 Overall aim 4

1.2 Statement of sub-objectives 4

1.3 Delimitation of the research 5

1.4 Methodologies and thesis layout 6

1.5 Conclusion 7

2 Principles of engine valve control 8

2.1 Research engine and valve operation 8

2.1.1 BMW K71 engine 8

2.1.2 Four-stroke cycle of the petrol engine 10

2.2 Potential of the valve train regarding engine performance and efficiency 12

2.2.1 Emissions of the spark ignition engine 13

2.2.2 Effect of valve control timing on emissions and engine performance 16
2.3 Existing fully variable valve trains 21
2.3.1 Fiat "TwinAir" and "MultiAir" 21
2.3.2 "Electrohydraulic camless valvetrain" 24
2.4 Conclusion 27

3 "Full Variable Valve Train" at the Ostfalia University 28
3.1 Valve train composition 28
3.2 Piezo technology and actuator 30
3.3 Switching positions of the servo valve 34
3.4 Conclusion 37

4 Indirectly controlled "Full Variable Valve Train" system 38
4.1 Design background 38
4.2 Requirements 40
4.3 Solution 43
4.3.1 Control unit 45
4.3.2 Servo valve 47
4.3.3 Switching positions of the redesigned system 50
4.4 Conclusion 53

5 Mathematical fundamentals 55
5.1 Lever transmission ratio and travel range 55
5.2 Layout of the compression springs 58
5.2.1 Single compression spring of the control unit 58
5.2.2 Identical compression springs of the servo valve 66
5.3 Servo cylinder discharge section layout 71
5.4 Conclusion 81

6 Manufacturing and FVVT system components 83
6.1 Rapid prototyping 83
6.1.1 Utilized 3D printers 84

6.1.2 Rapid prototyping results 84
6.2 Material choice 86
6.2.1 Properties of the material AlZnMgCu 86
6.2.2 Properties of the material 42CrMo4 87
6.2.3 Material attribution 88
6.3 Peripheral electric and electronic devices 90
6.3.1 Block diagram of the redesigned FVVT sytem 90
6.3.2 Displacement sensors 92
6.3.3 Pressure transducer 98
6.3.4 Piezo amplifier 99
6.3.5 Development control system 100
6.3.6 Function generator 101
6.3.7 Power supply 101
6.4 Peripheral mechanical devices 102
6.4.1 Rod seals for moved pistons 102
6.4.2 Properties of the chosen o-rings 103
6.4.3 Compression springs 103
6.5 Conclusion 104

7 Experimental setup and test results 105
7.1 System setup on mobile test bench 105
7.1.1 System component composition 105
7.1.2 Cylinder head and piezo actuator fixture 107
7.1.3 Substituted compression springs 108
7.1.4 Sensor mounts 108
7.1.5 Hydraulic equipment 109
7.1.6 Sensor connection to MicroAutoBox 110
7.2 Model of the electrohydraulic actuator 111
7.2.1 Simulink model of the redesigned FVVT system 111
7.2.2 Matlab m-File of the redesigned FVVT system 114

7.2.3 Modified dSPACE ControlDesk layout 115
7.3 Modifications and optimizations 117
7.3.1 Improvements of the servo valve 118
7.3.2 Improvements of the control unit 119
7.4 Test results 121
7.4.1 Control piston movement 121
7.4.2 Servo piston motion 126
7.4.3 Engine valve lift curve 130
7.4.4 Engine valve brake 140
7.5 Conclusion 143

8 Research summary and future development 144

9 Appendices 146
9.1 Technical specifications BMW K71 engine [44] 146
9.2 Technical drawings: control unit 147
9.3 Technical drawings: redesigned servo valve 161
9.4 Technical specifications of the "Fortus 250mc" printer [24] 171
9.5 Technical specifications of the "Dimension Elite" printer [25] 172
9.6 Datasheet Al 7075: material properties [26] 173
9.7 Datasheet 4137 steel: material properties [27] 177
9.8 Datasheet of the Sensitec GLM7xxASB-Ax family sensors [45] 179
9.9 Datasheet of the Gefran PY2 series sensors [35] 182
9.10 Datasheet of the Parker Hannifin PTD ASIC pressure transducers [36] 186
9.11 Datasheet of the Physik Instrumente HVPZT E-482 amplifier [37] 191
9.12 Technical specifications: dSPACE MicroAutoBox type 1401/1501 [46] 194
9.13 Digimess FG 200 function generator datasheet [47] 197
9.14 Technical data: profitec switchable power supply type SPS 12103 [42] 199
9.15 Technical drawing of the Guilliard & Dörr rod seals 200
9.16 List of dimensions and quantity of used o-rings 202
9.17 Properties of the compression spring used in the control unit 204
9.18 Properties of the compression springs used in the servo valve 206

List of Tables

6.1 Material attribution 89

6.2 Displacement transducer selection 97

List of Figures

2.1 Crankshaft and valve train assembly of the BMW K71 engine [5] 9
2.2 Otto-cycle of a four-stroke petrol engine [6] 11
2.3 Emission components of a four-stroke petrol engine [8] 13
2.4 pV graph of Atkinson-cycle (left) and Miller-cycle (right) 17
2.5 Fiat "Multiair" valve train components [13] 22
2.6 Electrohydraulic camless vavletrain by Schechter at al. [18] 25

3.1 Previous FVVT system of the Ostfalia University [20] 29
3.2 Internal structure of a piezo stack actuator [21] 31
3.3 Relation between force and travel distance of the P-235.90 actuator [20] 32
3.4 Basic control positions of the FVVT system 34

4.1 Concept presented in the feasibility study [23] 39
4.2 Standard K71 valve lift curve at 8000 $^1/_{min}$ [23] 42
4.3 Redesigned indirectly controlled FVVT system 44
4.4 Exploded view of the control unit 45
4.5 Internal structure of the control unit 46
4.6 Exploded view of the redesigned servo valve 48
4.7 Internal structure of the redesigned servo valve 49
4.8 Altered basic control positions of the redesigned FVVT system 50

5.1 Servo cylinder of the control unit 57
5.2 Partial bodies of the translation piston 60
5.3 Partial bodies of the control piston 62

5.4 Partial bodies of the servo piston 67
5.5 Oil volume displaced during reciprocating servo piston motion 72

6.1 RP components of the control unit (left); assembled parts (right) 85
6.2 RP components of the servo valve (left); assembled parts (right) 85
6.3 Block diagram of the indirectly controlled FVVT system 91
6.4 Sensitec GLM7xxASB-Ax sensor composition [29] 93
6.5 Sensitec GLM700 FVVT valve travel sensor application 94
6.6 Principle of magnetostrictive displacement measurement [33] 95
6.7 Gefran PY2C25 displacement transducer [35] 96

7.1 Test setup of the indirectly controlled FVVT system 106
7.2 Adjustable sensor mount 108
7.3 Sensor signal input of the MicroAutoBox 110
7.4 Modified Simulink model 113
7.5 Modified Matlab m-File 115
7.6 ControlDesk layout 116
7.7 Oil catch reservoir with pump 118
7.8 Oil cut-off cock for lever transmission 120
7.9 Installed spacer for lever transmission 121
7.10 Control piston displacement in dependency of chosen return spring preload 122
7.11 Control piston displacement: increased piezo amplitude 125
7.12 Control piston displacement: increased frequency 126
7.13 Servo piston movement in dependency of control piston position; sine function 127
7.14 Servo piston movement in dependency of control piston position; rectangular function 130
7.15 Full experimental setup; sine function 131
7.16 Full experimental setup; rectangular function 134
7.17 Full experimental setup; optimized rectangular function 137
7.18 Dynamic lever transmission pressure; optimized rectangular function 138
7.19 FVVT engine valve brake concept 141

Nomenclature

Symbol	Unit	Meaning
a	$[\frac{m}{s^2}]$	acceleration
a_{sp}	$[\frac{m}{s^2}]$	maximum acceleration of the servo piston
A_{cp}	$[m^2]$	front surface of the control piston
A_{dis}	$[m^2]$	required oil displacement section
$\hat{A}_{dis}$	$[m^2]$	actual oil displacement section
A_{hyd}	$[m^2]$	servo piston area the particular compressive force acts upon
A_{sp}	$[m^2]$	front surface of the servo piston
A_{tp}	$[m^2]$	front surface of the translation piston
$\hat{A}_{tp}$	$[m^2]$	front surface of the modified translation piston
$c_{1/2}$	$[\frac{N}{m}]$	spring stiffness
C	$[F]; [\frac{A^2 s^4}{kg \cdot m^2}]$	electrical capacitance
d_{1-15}	$[m]$	diameter of the partial bodies
d_{piezo}	$[m]$	diameter of the piezo stack
d_{cp}	$[m]$	diameter of the control piston
d_{sp}	$[m]$	diameter of the servo piston
d_{tp}	$[m]$	diameter of the translation piston
$\hat{d}_{tp}$	$[m]$	diameter of the modified translation piston
d_w	$[m]$	wire diameter
D_e	$[m]$	external wire diameter
f_0	$[Hz]$	resonance frequency

Symbol	Unit	Meaning
$\hat{f}_0$	$[Hz]$	actual resonance frequency
$f_{0,piezo}$	$[Hz]$	resonance frequency of the piezo actuator
F_c	$[N]$	compressive force resistance
F_f	$[N]$	frictional force to be overcome to enable servo piston motion
F_{hyd}	$[N]$	compressive force acting at full hydraulic pressure
F_m	$[N]$	mass force to be overcome to enable servo piston motion
F_{red}	$[N]$	compressive force acting at reduced hydraulic pressure
F_s	$[N]$	spring force to be overcome to enable servo piston motion
$F_{s,max}$	$[N]$	maximum spring force
$F_{s,min}$	$[N]$	minimum spring force
F_t	$[N]$	tensile strength
F_{tot}	$[N]$	total force to be overcome to allow servo piston motion
h_{1-15}	$[m]$	height of the partial bodies
h_{dis}	$[m]$	height of the oil displacement volume
h_{oil}	$[m]$	height of the oil volume in the lever transmission
i	$[-]$	lever transmission ratio
$\hat{i}$	$[-]$	modified lever transmission ratio
k_T	$[\frac{N}{m}]$	rigidity
l_{piezo}	$[m]$	length of the piezo stack
l_{window}	$[m]$	length of one oil displacement window
Δl_0	$[m]$	maximum travel range of the piezo actuator
Δl_{eff}	$[m]$	effectively used travel range of the piezo actuator
L_0	$[m]$	free length of the spring
L_1	$[m]$	length of the compressed spring
L_{st}	$[-]$	stoichiometric air requirement
m_{cp}	$[kg]$	mass of the control piston
m_K	$[kg]$	fuel mass
m_L	$[kg]$	actual air mass in the cylinder
$m_{L,St}$	$[kg]$	air mass under stoichiometric conditions
m_{oil}	$[kg]$	mass of the hydraulic oil in the lever transmission

Symbol	Unit	Meaning
m_s	$[kg]$	mass of the spring
m_{sp}	$[kg]$	mass of the servo piston
m_{tp}	$[kg]$	mass of the translation piston
m_{trans}	$[kg]$	mass of the components in motion
m_w	$[kg]$	wire mass
n	$[\frac{1}{min}]$	engine speed
n_c	$[-]$	number of coils
n_{cs}	$[\frac{1}{min}]$	rotational speed of the camshaft(s)
p_{hyd}	$[Pa]; [\frac{kg}{m \cdot s^2}]$	hydraulic system pressure
p_{red}	$[Pa]; [\frac{kg}{m \cdot s^2}]$	reduced hydraulic pressure
Δp	$[Pa]; [\frac{kg}{m \cdot s^2}]$	required hydraulic pressure difference
$Q_{2-3,v}$	$[\frac{J}{kg}]$	isochoric heat supply
$Q_{3-4,p}$	$[\frac{J}{kg}]$	isobaric heat supply
$Q_{5-6,v}$	$[\frac{J}{kg}]$	isochoric heat removal
Q_{dis}	$[\frac{m^3}{s}]$	flow rate of the oil displacement volume
r_2	$[m]$	radius of volume V_2
s	$[m]$	displacement
s_0	$[m]$	initial displacement
s_{cp}	$[m]$	travel range of the control piston
$s_{s,max}$	$[m]$	maximum spring compression displacement
$s_{s,pre}$	$[m]$	preload displacement of the springs in the servo valve
s_{sp}	$[m]$	travel range of the servo piston
s_{tp}	$[m]$	travel range of the translation piston
t	$[s]$	time
t_2	$[m]$	width of cylinder segment V_2
t_{act}	$[s]$	time available for one valve actuation
t_{dis}	$[s]$	time available for displacing the oil volume V_{dis}
t_{open}	$[s]$	actual time available for one valve operation
v_0	$[\frac{m}{s}]$	initial velocity
V_{1-15}	$[m^3]$	volume of the partial bodies

Symbol	Unit	Meaning
V_c	$[m^3]$	cubic capacity
V_{cp}	$[m^3]$	volume of the control piston
V_{dis}	$[m^3]$	oil displacement volume
V_{oil}	$[m^3]$	oil volume in the lever transmission
V_{sp}	$[m^3]$	volume of the servo piston
V_{tp}	$[m^3]$	volume of the translation piston
w_{dis}	$[\frac{m}{s}]$	displacement oil flow velocity
w_{window}	$[m]$	width of one oil displacement window

Symbol	Unit	Meaning
α	$[^\circ]$	angle
α_{cs}	$[^\circ]$	camshaft rotation angle
α_{open}	$[^\circ]$	valve actuation angle of the camshaft
ϵ	$[-]$	compression ratio
$\epsilon_{Atkinson}$	$[-]$	compression ratio of the Atkinson-cycle
ϵ_{max}	$[-]$	theoretical maximum compression ratio
ϵ_{Miller}	$[-]$	compression ratio of the Miller-cycle
λ	$[-]$	excess-air factor
ω_0	$[\frac{1}{s}]$	eigen angular frequency
$\hat{\omega}_0$	$[\frac{1}{s}]$	actual eigen angular frequency
$\rho_{42CrMo4}$	$[\frac{kg}{m^3}]$	density of the employed chromium steel
$\rho_{AlZnMgCu}$	$[\frac{kg}{m^3}]$	density of the employed aluminium alloy
ρ_{oil}	$[\frac{kg}{m^3}]$	density of the hydraulic oil in the lever transmission

Abbreviation	**Meaning**
.csv	comma-separated values
3D	three-dimensional
ABS	Acrylonitrile-Butadiene-Styrene
AD	analogue/digital
AFR	air-fuel ratio
AISI	American Iron and Steel Institute
Al	aluminium
AMP	piezo amplifier
ASIC	Application Specific Integrated Circuit
BMW AG	Bayerische Motoren Werke Aktiengesellschaft
BNC	Bayonet Neill-Concelman Connector
BDC	bottom dead center
CAD	computer aided design
CO	carbon monoxide
CO_2	carbon dioxide
CP	control piston displacement
Cr	chromium
Cu	copper
CU	control unit
DC	direct current
DIN	German Institute for Standardization
DOHC	double overhead camshaft
ECU	engine control unit
EIVC	early intake valve closing
EN	Europäische Norm = European Standard
EV	engine valve body
FDM	Fused Deposition Modelling
FG	function generator
FPGA	Field Programmable Gate Array
FVVT	Full Variable Valve Train

Abbreviation	**Meaning**
GMR	Giant MagnetoResistive
HC	hydrocarbon
I/O	Input/Output
ISO	International Organization for Standardization
iv(s)	intake valve(s)
IVs	engine valve displacement
KJ-ZEM	engine code of a Mazda engine utilizing the Atkinson-cycle
LIVC	late intake valve closing
LIVO	late intake valve opening
LT	lever transmission
Mg	magnesium
Mn	manganese
Mo	molybdenum
MOE	Ministry of the Environment
NMMU	Nelson Mandela Metropolitan University
NO_x	nitrogen oxides
PI	Physik Instrumente GmbH & Co. KG
PM	particulate matter
PI	piezo actuator displacement
p_{oil}	pressure transducer
PWM	pulse width modulation
PZT	lead zirconate titanate
pV graph	pressure volume graph
RP	rapid prototyping
SOHC	single overhead camshaft
SP	servo piston displacement
STL	Standard Tessellation Language
SV	servo valve
TDC	top dead center
USA	United States of America

Abbreviation	**Meaning**
UTS	ultimate tensile strength
VTEC	Variable Valve Timing and Lift Electronic Control
VWSA	Volkswagen South Africa (Pty) Ltd
Zn	zinc

1 Introduction

The worldwide steadily increasing number of new motor vehicle registrations proves that the demand for automobiles is significantly growing globally. In China alone the number of registrations increased by 32.4 % from the year 2009 to 2010. At the same time worldwide registrations have risen by an overall 14.2 % while roughly 81 % of the total registrations have been passenger cars according to the demographic trends and as a consequence thereof the rise in population density especially in Asia [1].

The customers' expectations in terms of vehicle safety and comfort aspects are further increasing. At the same time a modern motor vehicle is expected to have a powertrain strong enough to meet the demands of effortless driving comfort even though motor vehicle kerb weights as a general rule advance gradually as a consequence of the afore-mentioned customers' expectations. On the other hand the customer's choice for a certain vehicle is determined by a low fuel consumption, being the key buying criterion in general.

The emissions legislation continues to become more and more sharp worldwide. In Europe the "Euro 6" standard limits the emissions of carbon monoxide (CO), nitrogen oxides (NO_x), hydrocarbon (HC), and particulate matter (PM). With the "Tier 2" limits in the United States of Aermica (USA) and the emission regulations defined by the "Ministry of the Environment" (MOE) in Japan, mentioning only the most important, similar regulations apply throughout the world. Additionally the carbon dioxide (CO_2) emissions are strictly limited. These are directly proportional to the fuel consumption of a vehicle. Accordingly, the automotive industry faces

the challenge that with increasing vehicle weights very efficient engines need to be developed which deliver a high power and torque output while at the same time offering low fuel consumption and emissions.

The operation of the intake and exhaust valves of a four stroke combustion engine offers the largest potential concerning a positive influence on emissions and torque and power output, hence on the efficiency of an engine. Since the 1990s several systems have been developed in order to vary the actuation of the engine valves with the engine speed range. Examples for current systems are Honda's "Variable Valve Timing and Lift Electronic Control" (VTEC) system or "VarioCam" by Porsche. Looking at a valve lift curve the parameters that are influenced by the camshaft profile are the:

- Phasing
- Valve lift
- Valve opening time
- Valve lift function.

Most of the variable valve systems on the market are able to influence only valve lift and timing depending on engine speed. The systems are still a compromise between increased engine performance and low emissions. The beneficial effects are limited to a specific engine speed range of a few hundred revolutions, usually above $4000\,rpm$.

These variable valve systems are technically mature to the highest extent. Another attempt to develop very efficient combustion engines is the so-called downsizing. The displacement is being reduced while keeping the engine performance in reference to power and torque output. These engines are usually being turbocharged. Downsized engines can be combined with variable valve systems but still the cam profiles will be conventional and the complete potential of the valve train cannot be used.

Electromobility as an alternative solution to the utilization of the combustion engine still features problems regarding high vehicle prices, a limited obtainable range of around 200 km only and high overall vehicle weights. A study of the Graz University of Technology reveals that as an example the batteries used within the electric vehicle "Tesla Roadster" amongst other materials contain 24 kilogramme of copper (Cu). The extraction of this amount of copper, according to Mr Schmidt-Bleek, former vice president of the "Wuppertal Institute for Climate, Environment and Energy", involves an environmental impact that destroys more than eight tons of nature. Hence, the environmental balance might not yet be as promising as suggested by the manufacturers of electric vehicles. Futher disadvantages are the fact that low ambient temperatures reduce the performance of the batteries and that a quick charging procedure of the batteries increases the amount of required energy by around ten per cent [2]. All these factors lead to an uncertain market penetration of electromobility at this state of development.

This research project will deal with a different approach to reveal the whole potential of the valve train. Based on the "Full Variable Valve Train" (FVVT) project founded at the Ostfalia University, an indirectly controlled fully adjustable mechatronic valve train control unit for a combustion engine as replacement for the mechanically driven valve trains used until the present time is developed. The FVVT is working electrohydraulically and without camshafts. It is not bound to a fixed cam timing and even inclination of the valve lift curve, the phasing and the valve lift function can be fully adjusted. The system also aims at dethrottling of the combustion engine, where the use of a throttle and hence pumping losses can be eliminated, while the task of the throttle is transferred to the engine intake valve motion, directly determining how much air enters the combustion chamber.

Finally, the development of an innovative intake/exhaust cycle change system for piston stroke engines can reveal the complete yet unused potential of the valve train. It is a serious alternative to electromobility without drastically increasing the kerb weight of a motor vehicle. The system gives consideration to the demand for combustion engines with maximized performance and ecological efficiency.

1.1 Overall aim

Based on a feasibility study from the year 2010 [3] and a bachelor thesis from the year 2013 [4] the electrohydraulic FVVT system has to be redesigned so that the core component, the high speed servo valve, is operated indirectly by a pressure difference on the end faces of the servo piston that is moving inside of the servo valve. To achieve this, an additional control unit, driven by the utilized piezo actuator, will be implemented. By these means advantages in terms of an enhanced system control and increased precision will be achieved.

1.2 Statement of sub-objectives

The following sub-objectives need to be accomplished in order to achieve the overall aim:

1. Literature research/study on the valve controller
    - evaluation of overall requirements of the system
    - consideration of the performance that needs to be met
2. Finalizing the design and evaluation of the components
    - dimensioning of springs and component parts
    - material choice for manufacturing
3. Assembly of the system
    - manufacturing of components
    - assembly of the overall system

4. Literature review and selection of measurement instrumentation
    - implementation of displacement sensors
    - implementation of pressure sensors

5. Programming of the system
    - arrange a program so that system can be operated
    - design program freely adjustable to any control-specific demands

6. Initial testing
    - test and evaluation of the system
    - modification of system components wherever necessary
    - production of a system ready for installation on the test engine.

1.3 Delimitation of the research

The following parts of the overall system are based on existing components and need not be designed in this project:

- piezo actuator and housing
- internal structure of the servo valve:
    1. servo valve body
    2. servo cylinder
- engine valve body, bolted to the servo valve.

1.4 Methodologies and thesis layout

In order to solve the research problem the following methods will be used:

- Literature research

A literature research will be conducted in order to obtain general information on the topic of this master project and to explain some of the principles, following in Chapter 2. A literature review will also be carried out so as to select the measurement instrumentation of the overall system.

- Feasibility study/preliminary work

The basic concept for the FVVT system developed within this work arose from the afore-mentioned feasibility study dealing with the creation of a concept of an indirectly controlled fully variable valve train based on a piezo actuator. Within the mentioned bachelor thesis [4] an FVVT system, based on the idea stated in the feasibility study, has been developed in a completely redesigned way with changed components in order to achieve a reliable control of the system. Based on this result the overall system is being re-scrutinized and improved further, see Chapters 3 and 4. To gain new ideas and utilize suggestions for improvement all persons participating in the FVVT project are being asked for their feedback.

- Mathematical proofs

In Chapter 5 calculation measures will be used to predict the system behaviour, especially on high simulated engine speeds, as accurately as possible. The layout of all hydraulic ducts and moving parts is crucial for a successful and reliable system operation subsequently. Also physical laws and fluid mechanics will be used to estimate the dynamic processes and ensure an appropriate layout of all components.

- Computer aided design

With the assistance of the computer aided design (CAD) program "Catia V5 R20" by Dassault Systèmes the developed system is transferred into a three-dimensional model. The results of all calculations and the system's layout are incorporated in this model.

- Rapid prototyping

Subsequently, in order to be able to validate the theoretical thoughts the manufacturing of the designed system as rapid prototyping (RP) components will be carried out in Chapter 6. Any weak points in design or misfits would be easily visible in the prototype and time could be saved due to a possible fault removal before the consequent manufacturing process of the eventual system begins.

- Programming

After the system has been assembled physically the software "MatLab/Simulink" will be used to program the dynamic processes taking place while the system is being operated (compare Chapter 7).

- Experiments

Concluding Chapter 7, the designed system will be evaluated in terms of reliability and usability by testing it on an engine valve test bench.

1.5 Conclusion

After solving all sub-objectives by using the stated methodologies, a final system design will be achieved, allowing the assembly of a first prototype and in the course of this research leading to a physical and usable test setup of an innovative mechatronic engine valve actuator. According to the afore-mentioned, the research thesis commences explaining the principles of engine valve control.

2 Principles of engine valve control

For a complete understanding of the FVVT system that is being developed within this thesis it is important to understand the basics of a conventional valve train as used in common four-stroke combustion engines until today. Initially the BMW K71 engine that is being used for this research project will be presented. To demonstrate the reasons for substituting the conventional valve train by a mechatronic control unit the basics of a four-stroke engine and its valve actuation are explained in detail. Furthermore, the influence of the engine valve control with regard to performance and emissions is explained. The chapter closes with research results on existing (fully) variable valve trains.

2.1 Research engine and valve operation

This section introduces the BMW K71 research engine used within the FVVT project and explains the valve train and working cycle of this engine.

2.1.1 BMW K71 engine

The research engine used for the FFVT project is the K71 two-cylinder four-stroke petrol engine which has been developed by the "Bayerische Motoren Werke Aktiengesellschaft" (BMW AG) in cooperation with the "Bombardier Recreational Products

(BRP)-Rotax GmbH & Co. KG". The Parallel Twin[1] engine originally has been used in the BMW F800 series motorcycles. It features a cubic capacity of $V_c = 798\,cm^3$ and a top engine speed of $n = 9000\,{}^1/_{min}$. Intake manifold injection is used. The crank assembly and valve train of the K71 engine is shown in Figure 2.1.

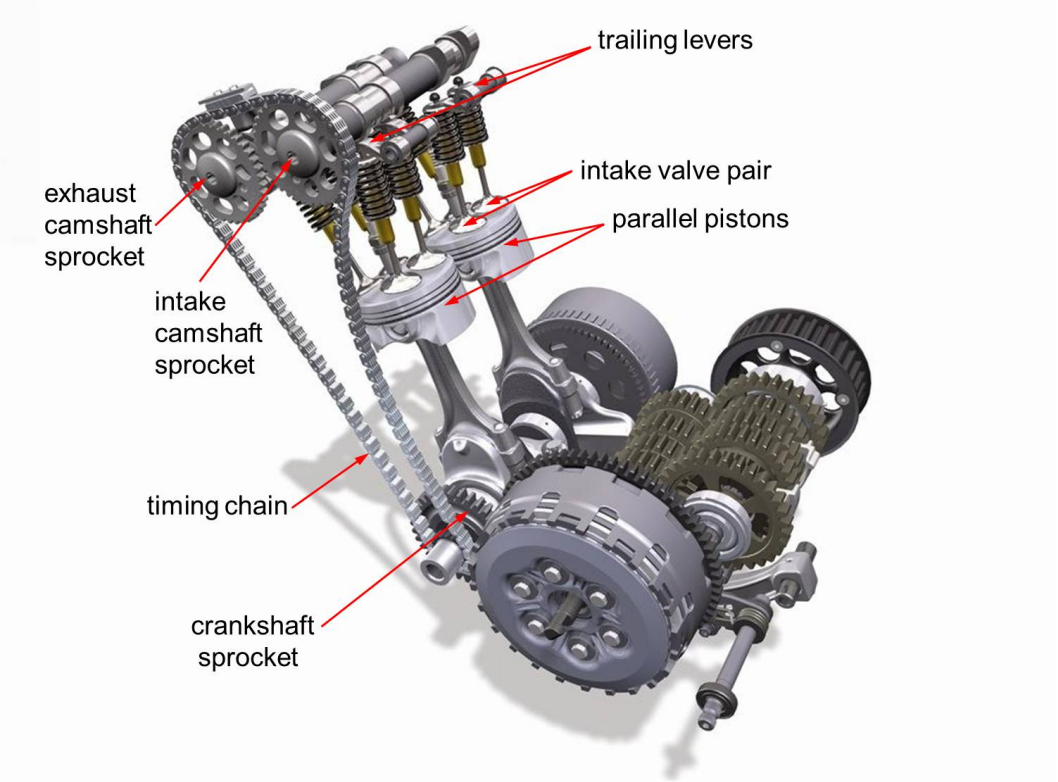

Figure 2.1: Crankshaft and valve train assembly of the BMW K71 engine [5]

A datasheet with all technical specifications of the research engine can be found in Appendix 9.1. The K71 is equipped with a double overhead camshaft (DOHC) arrangement employing eight engine valves. The intake and exhaust camshafts are driven by the crankshaft via the timing chain. Each shaft has a sprocket on which the chain is engaged. The intake and exhaust valves are opened by the cam lobe profiles running over the cam followers while the corresponding camshaft is being rotated by the crankshaft and chain assembly when the engine is running. The valve

[1] movement of both pistons accordant; crankpin offset and angular ignition spacing $\alpha = 360\,°$

closing is carried out by the force of a strong spring mounted between every cam lobe and valve. The part of the camshaft circumference within which there is no cam lift determines the angle respectively time in which the valve is being closed. While this surface rotates over the cam follower no pressure is applied onto the afore-mentioned springs and the valves stay closed. The K71 engine uses trailing levers to operate the valves. This configuration comes into use especially in high-revving and racing engines as it keeps the masses in motion as low as possible and reduces friction significantly compared to a hydraulic valve lifter. The disadvantage here is the fact that when using trailing levers the valve-clearance compensation cannot be carried out automatically as by the use of hydraulic valve lifters which have become standard in most engines with usual engine speed range today. Valve-clearance compensation will not be necessary at all for the developed mechatronic FVVT system as the mechanical components camshafts, cam followers and valve springs are being replaced.

While the valves are being operated in the way described above the pistons move up and downwards in the cylinders. The crankpins on the crankshaft guide the connecting rods that are directly connected to the pistons on the other end. The crankpins are mounted eccentrically on the crankshaft. By this the transformation of the piston movement into a rotation of the crankshaft is realized.

2.1.2 Four-stroke cycle of the petrol engine

Figure 2.2 (next page) illustrates all strokes of the so-called Otto-cycle[2] which is the basic principle of a common four-stroke petrol engine.

[2]named after Nicolaus August Otto, 1832-1891, German inventor of the first internal-combustion engine "Ottomotor"

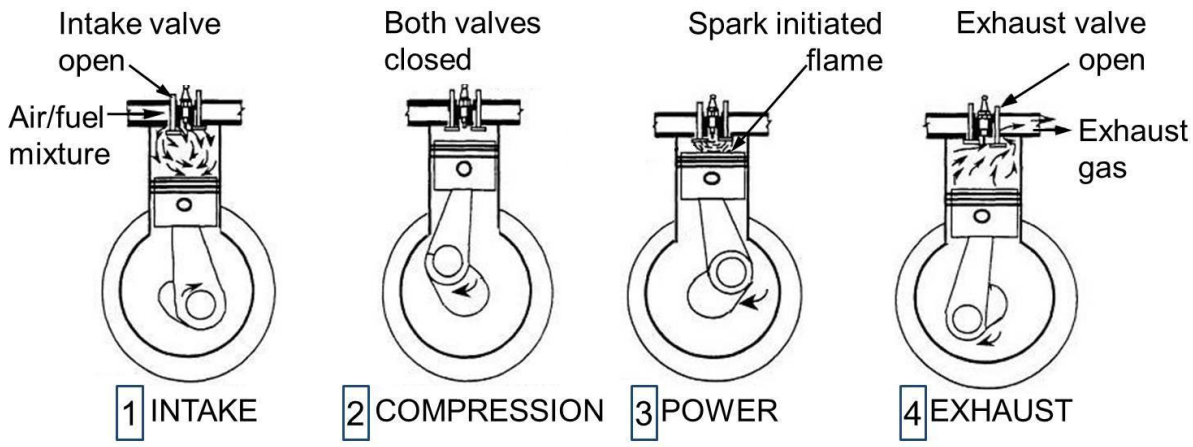

Figure 2.2: Otto-cycle of a four-stroke petrol engine [6]

Each stroke will be explained below for a non-turbocharged DOHC engine with four valves per cylinder.

1. Intake

   The piston moves downwards, starting from the top dead center (TDC)[3]. The intake camshaft pushes the intake valves open. The volume in the cylinder is increased until the piston reaches the bottom dead center (BDC)[4]. While this is in process the intake valves are open and the charge consisting of an air and fuel mixture is brought into the combustion chamber due to the negative pressure in the cylinder and the attached intake manifold.

2. Compression

   The intake valves are closed by the valve springs as the cam lift of the rotating intake camshaft becomes zero on the according part of the camshaft circumference. The combustion chamber is equivalent to a closed volume in this stroke. While the piston changes its direction of movement and moves back to TDC, the working chamber is reduced and the charge is compressed against the cylinder head.

[3]piston in closest position to cylinder head; no piston movement in axial direction

[4]piston in furthest position from cylinder head; no piston movement in axial direction

3. Power

   Usually a few degrees before reaching the TDC the compressed charge is ignited externally by the spark plug. Subsequently, an expansion of the working gas takes place forcing the piston back downwards to BDC. Work is applied to the piston which drives the crankshaft via the connecting rod and the eccentrical crankpin. Intake and exhaust valves are still closed in this stroke.

4. Exhaust

   The exhaust valves are pushed open by the exhaust camshaft while the piston moves upwards to TDC. The combustion gases are pushed out by the piston through the open exhaust valves that lead into the exhaust. When TDC is reached the exhaust valves are closed by the valve springs. The four-stroke cycle starts from the beginning.

Because four strokes are necessary for the Otto-cycle and each stroke has to complete the distance between BDC and TDC the crankshaft needs to turn by 180 ° in order to perform one stroke. Therefore the crankshaft needs to rotate 720 ° in total so as to carry out one complete Otto-cycle. As both the intake and exhaust camshaft only need to operate the valves once in a complete cycle and then again only in the following cycle the speed ratio between crankshaft and camshafts is $2 : 1$. While the crankshaft does two full rotations within one complete cycle each camshaft only rotates once around its own axis.

2.2 Potential of the valve train regarding engine performance and efficiency

This section explains in which way the valve operation timing affects the emissions and overall efficiency of an internal combustion engine. In this case, however, all mentioned considerations apply to a four-stroke petrol engine as this is the engine type used for the FVVT project.

2.2.1 Emissions of the spark ignition engine

Figure 2.3 shows a composition of the emissions of a four-stroke spark ignition engine. There are significant differences in the emissions produced by two-stroke engines or diesel engines as contrasted with the four-stroke petrol engine. Two-stroke engines feature scavenging losses[5] emitting un-burnt hydrocarbons as a consequence [7] and expelling oil needed for lubrication into the exhaust. On the other hand diesel engines produce particulate matter and nitrogen oxides in large amounts due to the high pressure, increased burning temperatures and a lean air fuel ratio.

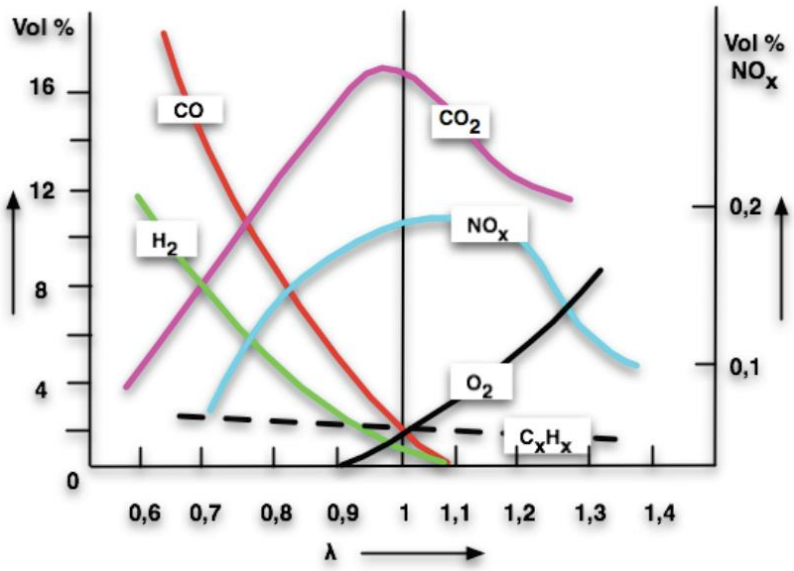

Figure 2.3: Emission components of a four-stroke petrol engine [8]

Figure 2.3 shows the percentage by volume of emissions for carbon monoxide, carbon dioxide, hydrogen (H_2), oxygen (O_2) and hydrocarbon on the left ordinate and the percentage by volume of emitted nitrogen oxides on the right ordinate versus the excess-air factor λ on the abscissa.

[5]the part of the fresh charge that flows unused from the intake into the exhaust due to overlapping

The stoichiometric air requirement L_{st} describes the relation between air mass and fuel mass that enter a combustion engine as inflammable charge under stoichiometric[6] conditions:

$$L_{st} = \frac{m_{L,St}}{m_K} \tag{2.1}$$

where

$m_{L,St}$ = air mass under stoichiometric conditions
m_K = fuel mass

In a petrol engine the value for the stoichiometric air requirement is $L_{st} = 14.7 : 1$, meaning that $14.7\,kg$ of air is used to burn $1\,kg$ of petrol. "The stoichiometric air requirement can be calculated from the percentage by weight of the chemical elements contained in the fuel" [9].

The air-fuel equivalence ratio or excess-air factor λ describes the correlation between the air mass that is actually brought into the cylinder and the stoichiometric air mass:

$$\lambda = \frac{m_L}{m_{L,St}} = \frac{m_L}{m_K \cdot L_{St}} \tag{2.2}$$

where

m_L = actual air mass in the cylinder

Subsequently, the excess-air factor can be described as specific air-fuel ratio (AFR), being the quotient of actual air mass and fuel mass in relation to the stoichiometric air requirement. The excess-air factor can be located within the following range:

[6] all fuel molecules react entirely with the atmospheric oxygen, such that neither oxygen is missing for the combustion nor un-burnt oxygen remains afterwards

- $\lambda = 1$: stoichiometric air/fuel mixture
- $\lambda < 1$: air deficiency, "rich mixture"
- $\lambda > 1$: excess air, "lean mixture".

As emerging from Figure 2.3 there is a strong dependency between the emissions and the λ value. Modern engines that feature intake manifold injection as the K71 are operated almost exclusively with stoichiometric mixture $\lambda = 1$ today [9]. It is impossible to operate an engine with maximum power output and low emissions at the same time. Peak engine performance is reached at a λ value of approximately 0.85 or at rich mixture respectively. Here also the highest flame propagation rate of the mixture occurs and the maximum cylinder mean pressure is reached. The performance is being increased by this as the effective mean pressure is directly proportional to the effective power of a combustion engine [10].

Even though CO_2 and NO_x emissions are decreased in this λ-range compared to the stoichiometric value, the value of the hazardous CO emission component and HC rise significantly. Especially CO shows a very sharp increase from around $2\,vol\%$ up to almost $7\,vol\%$ which is equal to an increase by $250\,\%$. As CO is very dangerous to health petrol engines in passenger cars are not being operated with a rich mixture in general. The utilization of a rich mixture is reserved for peripheral areas like motorsports where it is used to maximize the engine power output while exhaust emissions are of minor importance.

Operating a petrol engine with a lean mixture ($\lambda > 1$) on the other hand to reduce CO, CO_2 and HC emissions results in extremely high combustion temperatures as the evaporation enthalpy[7] with the use of less fuel is reduced and hence the combustion chamber is not cooled sufficiently. This quickly results in a deterioration of the engine.

[7] energy that is needed to transform a given quantity of a substance from the liquid into the gaseous state

Concluding Figure 2.3 illustrates that for the stoichiometric mixture ($\lambda = 1$) as used in modern passenger vehicles the two main emission components are CO_2 and NO_x. The following subsection explains in which way these emissions can be reduced by a sophisticated valve actuation and shows the opportunities in this matter that arise from using a fully variable valve train.

2.2.2 Effect of valve control timing on emissions and engine performance

The valve actuation timing exhibits large potential when it comes to an influence on the emissions of an internal combustion engine. CO_2, as one of the two critical exhaust emission components mentioned above, arises from a complete combustion of hydrocarbon in the fuel molecules [9]. This is why the concentration of CO_2 is very close to its maximum of around $17\,vol\%$ for the stoichiometric mixture ($\lambda = 1$) in Figure 2.3. The formation of NO_x on the other hand is highly pressure and temperature dependent and reaches its maximum amount at a temperature between 2200 and $2400\,K$.

As the intake valve closing time has got the most significant influence on the above-mentioned emissions, this will be more closely analysed in this subsection. Two pioneering strategies are the so-called Miller-cycle[8] and Atkinson-cycle[9]. Both cycles are displayed in Figure 2.4 (next page).

[8] named after its inventor and American engineer Ralph Miller who patented this principle 1957

[9] named after the British engineer James Atkinson, 1846-1914, who invented the Atkinson cycle engine in 1882

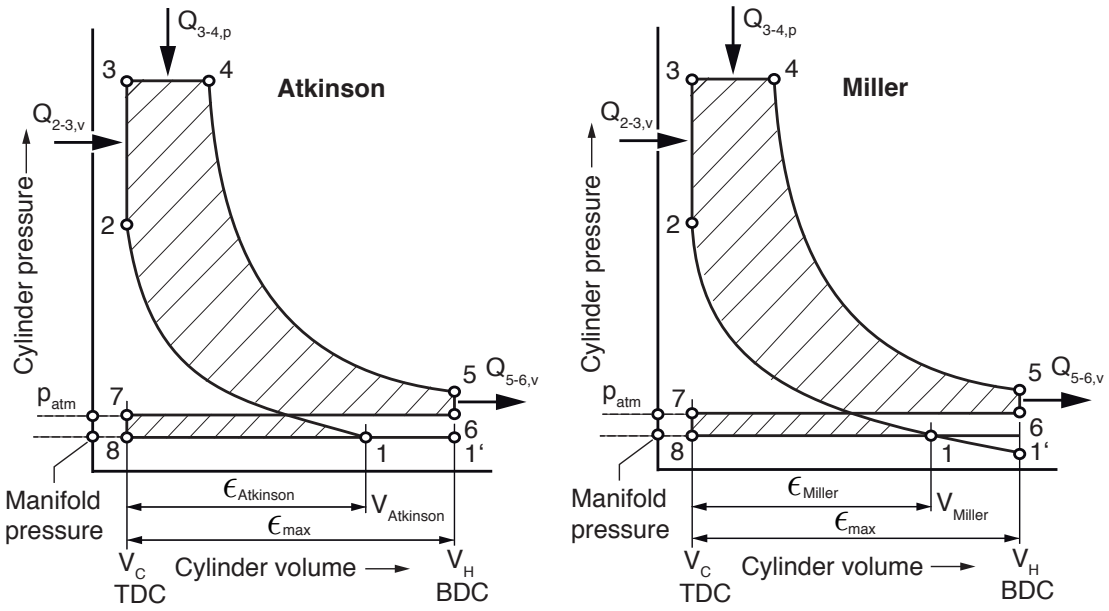

Figure 2.4: pV graph of Atkinson-cycle (left) and Miller-cycle (right)

The graphs show the cylinder pressure versus cylinder volume, typically referred to as pV graph. Both cycles are displayed as Seiliger-cycle. This cycle combines the constant volume (isochoric) cycle according to Otto and the constant pressure (isobaric) cycle as seen in the Diesel-cycle[10] and reflects the cycle of the ideal engine. The state changes in both cycles are as follows:

Atkinson	**Miller**
1-2: isentropic compression	1-2: isentropic compression
2-3: isochoric heat supply	2-3: isochoric heat supply
3-4: isobaric heat supply	3-4: isobaric heat supply
4-5: isentropic expansion	4-5: isentropic expansion
5-6: isochoric heat removal	5-6: isochoric heat removal
charge cycle loop:	
6-7: exhaust stroke	6-7: exhaust stroke
8-1′: intake stroke, iv(s) open	8-1′: intake stroke, iv(s) partly closed
1′-1: piston movement: open iv(s)	1′-1: piston movement: closed iv(s)

[10]named after Rudolf Diesel, 1858-1913, German engineer and inventor of the diesel engine

The abbreviation "iv(s)" used above stands for "intake valve(s)". Cycle direction is clockwise in both cases and underneath the actual cycle the charge cycle loop is included (6-7-8-1′). State changes 1-2 represent the compression stroke and 3-5 the power stroke respectively. BDC and TDC positions have been added to the cycles for better understanding. Isochoric and isobaric heat supply $Q_{2-3,v}$ and $Q_{3-4,p}$, as well as removed heat $Q_{5-6,v}$, are also entered into the cycles. The manifold pressure course can also be taken from the diagram. Both Atkinson- and Miller-cycles are closely related and have the common aim of decreasing the heat produced in the combustion chamber by reducing the effective compression ratio compared to a usual cycle [12].

The compression ratio ϵ is defined as the sum of cubic capacity and compression volume[11] divided by the latter. This heat reduction leads to reduced NO_x emissions due to their temperature dependent behaviour. Both cycles do not utilize the available cubic capacity entirely and in Figure 2.4 on the abscissa the reduced compression ratios $\epsilon_{Atkinson}$ and ϵ_{Miller} are compared to the theoretical maximum ϵ_{max}.

The maximum air charge can be brought into the cylinder by closing the intake valve(s) in BDC. The compression ratio then reaches its maximum. If the intake valve closing time is altered, regardless of before or after BDC, less air enters the engine in general and hence the compression ratio is reduced. The decisive factor in this case is the cubic capacity used at the moment when the intake valve(s) close(s).

In the case of the Atkinson-cycle, also referred to as late intake valve closing (LIVC), a part of the air charge gets pushed out of the cylinder again while the piston moves from BDC to TDC with intake valve(s) still open at the beginning of the compression stroke. As seen in Figure 2.4 the piston fulfils a full intake stroke (8-1′) at constant manifold pressure with open intake valve(s). While the cycle continues (1′-1) the manifold pressure does not change as intake valve closing and thus the beginning of compression take place delayed (1).

[11] remaining volume between the piston top and cylinder head when piston is in TDC at the end of the compression stroke

The Miller-cycle on the other hand makes use of an early intake valve closing (EIVC). While the piston moves from TDC to BDC within the intake stroke (8-1′), the closing of the intake valve(s) occurs before BDC is reached (1). As a difference to Atkinson the cylinder pressure drops below manifold pressure as the volume is increased with closed intake valve(s) due to the piston downward movement. This generates negative pressure. As a consequence 1′ is at a lower vertical position in the Miller-cycle compared to that of Atkinson. The subsequent piston movement (1′-1) takes place with closed intake valve(s) before the actual compression stroke begins (1). Consequently, both Atkinson- and Miller-cycles exhibit the same reduced cubic capacity and compression ratio.

Research by He, Durrett, and Sun (2008) on this topic shows that a reduction of NO_x emissions by 30-50 % can be reached with LIVC, depending on the operation conditions and injection method. The experiments that have been carried out with a single cylinder engine clearly show the potential of a valve train that can implement the LIVC strategy [11]. Disadvantages concerning engine performance output occur though as with LIVC the cubic capacity and maximum amount of fresh charge partly remain unused. Thus the engine torque output is decreased. This disadvantage is often compensated by turbocharging of the combustion engine. Through this measure the reduced compression ratio is transferred into a raise in boost of the turbocharger. Hence for turbocharged engines the Atkinson cycle can be seen as partial outsourcing of the compression from the combustion chamber into the compressor of the turbocharger [12].

As mentioned in Chapter 1, the CO_2 emissions are directly proportional to the fuel consumption. For this reason it is necessary to control the valves as variably as possible to keep the fuel consumption and consequently CO_2 emissions as low as possible within the entire engine speed range. By making use of the Atkinson- or Miller-cycle CO_2 emissions can be reduced significantly as because of the reduced air mass brought into the cylinder less fuel is necessary to reach the stoichiometric mixture or complete combustion respectively. The fuel consumption is reduced by

this measure. The Mazda 2 1.3, brought to the market in 2007 is an example of a motor vehicle that is equipped with a petrol engine making use of the Atkinson-cycle.

In the higher engine speed range above $n = 3000\,{}^{1}/_{min}$, however, LIVC can be beneficial regarding the engine performance. It increases the cylinder fill factor[12] significantly as more fresh charge enters the combustion chamber. Only on higher engine speeds the dynamic of the intake charge is of sufficient velocity to enter the combustion chamber while the piston moves into the direction of TDC at the beginning compression stroke with intake valve(s) still open. This of course increases power output and torque.

Then again this leads to the opposite of what the Atkinson-cycle originally aims at. Both CO_2 emissions and fuel consumption on the one hand and cylinder pressure, process temperature and hence NO_x emissions on the other hand will rise. For the best results concerning low emissions and a low fuel consumption the Atkinson-cycle needs to be used in the lower engine speed range exclusively before the effects explained above set in. In order to guarantee this Mazda uses variable valve timing on their "KJ-ZEM" engine which also works according to the Atkinson-cycle.

However, no existing valve train on the market is able to combine an Atkinson-cycle in the low engine speed range with the possibility of either using LIVC on high engine speed ranges to increase performance at the cost of risen emissions or—at low torque request in the high engine speed range—close the intake valve(s) at BDC or even switch to Miller-cycling to reduce the emissions topmost.

To enable an engine speed dependent operation of the intake valve(s) in the above-mentioned way a common camshaft driven valve train will quickly reach its limit even when used in combination with a variable valve timing. The FVVT system due to the absence of camshafts and full adjustability offers significant potential

[12] ratio between the mixture actually brought into the cylinder and the filling theoretically possible at a given cubic capacity

regarding the simultaneous implementation of several valve actuation strategies within the same valve train.

2.3 Existing fully variable valve trains

The following section outlines the current developments in terms of fully variable valve trains. The first system in use in an automotive application will be introduced and the advantages and disadvantages will be pointed out. Furthermore research results on a fully variable valve train with strong analogy to the developed FVVT system will be explained.

2.3.1 Fiat "TwinAir" and "MultiAir"

The "TwinAir" (two-cylinder version)/"MultiAir" (four-cylinder version) technology appears in two different engines developed by Fiat with cubic capacities of 875 and $1368\,cm^3$ respectively. Released in 2009 it is the first system on the market and often referred to as the first fully variable valve train even though it only features variability for the intake valve actuation. A sectional view through the cylinder head that includes all system components for one cylinder can be seen in Figure 2.5 (next page).

Both the "TwinAir" and the "MultiAir" engine feature a single overhead camshaft layout (SOHC). The exhaust camshaft operates both the exhaust valves directly and the intake valves indirectly. As in conventional modern combustion engines the engine viewed here features two intake valves and two exhaust valves per cylinder. The exhaust valves are actuated by cam lobes and valve lifters similar to those in usual modern combustion engines.

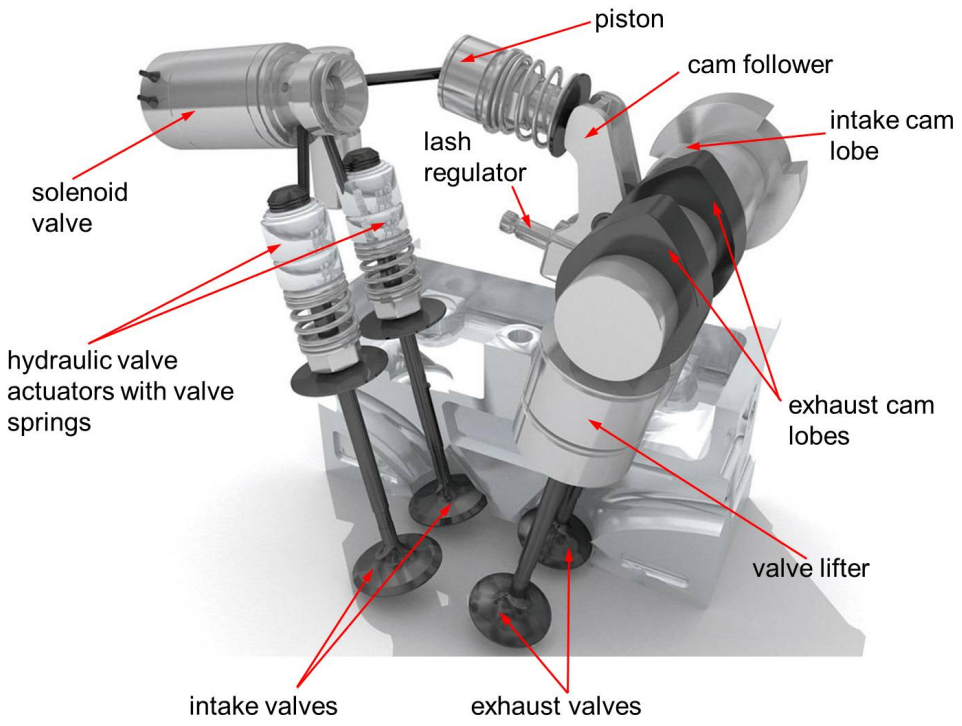

Figure 2.5: Fiat "Multiair" valve train components [13]

The intake valves are operated with the aid of hydraulic valve actuators as seen in Figure 2.5 in the following way. First the intake cam lobe actuates a piston via a cam follower. The solenoid valve regulates the hydraulic flow from the piston into the valve actuators on the intake side of the engine. When the solenoid is being closed, the almost incompressible fluid directly transfers the cam lobe lift into a movement of the intake valves resulting in a fixed valve timing as used in a conventional valve train. By opening the solenoid the hydraulic pressure within the system is reduced as the oil bypasses the paths leading to the valve actuators. This allows variable intake valve actuation. By means of switching the solenoid between its open and closed positions at certain times the timing and lift of the intake valves can be varied. The closing of the intake valves takes place by valve springs as used in a traditional valve train [14]. In summary, "[t]he final part of the valve closing is controlled by a dedicated hydraulic brake to ensure soft and regular landing phase in any engine operating conditions" [15]. This is fairly important as the valves require a certain reduction in force before impinging on the valve seat and the touchdown velocity must not exceed the allowed values in order not to damage the valve seat and cylinder head in a long-term view.

Fiat claims that the system can reduce exhaust emissions significantly at increased fuel-economy and higher power output. Advantageous also is the fact that the throttle plate remains fully open while the engine is used under conditions in which "TwinAir"/"MultiAir" can be utilized. In a traditional petrol engine the throttle plate is used to regulate the required amount of air mass flowing into the cylinder. This leads to throttling losses which can be avoided to a certain extent with the "TwinAir"/"MultiAir" technology.

The system features the following five operation modes for variable valve timing and lift [16] [17]:

1. Full Lift: fixed valve lift according to cam lobe
2. EIVC: early intake valve closing; Miller-cycling
3. LIVO: late intake valve opening
4. Multi Lift: multiple valve lifts within one stroke
5. Partial Load: similar to EIVC with larger maximum lift.

The benefits arising from the above listed operation modes have partly already been explained in Subsection 2.2.2. All mentioned measures aim at a reduction of emissions and fuel consumption while the "Multi Lift" mode is used at very low engine speeds to improve both turbulence within the cylinder and the velocity of the subsequent combustion. All modes enable the operation of the combustion engine at a raised degree of efficiency.

One of the major disadvantages is the fact that this variety of operation modes can be fully made use of only in the low- to mid-revolution range of the engine. This also explains why the throttle plate is still necessary even though it remains fully open while the mentioned operation modes are being used. On high revolutions the throttle plate is necessary to control the amount of air entering the engine as

the intake valves alone cannot be used as only throttle machanism under these conditions. For instance, the "Multi Lift" mode cannot be used at higher engine speeds. Hence, the system is not fully variable. Additionally, only the intake valves are being operated in a variable way while the exhaust valves maintain a fixed valve timing.

The FVVT system developed within this research project will be independent from engine speed and usable for both intake and exhaust valves of an internal combustion engine.

2.3.2 "Electrohydraulic camless valvetrain"

As not any functioning fully variable valve train has been introduced to the market yet a hydraulic approach that has been researched on will be looked at more closely. The "Electrohydraulic camless valvetrain" system, assigned by the "Ford Motor Company" and patented by Schechter and Levin (1996), shows certain analogies to the system that is being developed within this research project and is shown in Figure 2.6 (next page).

The main components of this system are an engine valve assembly (10), a hydraulic system (8) and a rotary valve (34). As opposed to Fiat's "TwinAir"/"MultiAir" technology this electrohydraulic solution is usable for both intake and exhaust valves. As seen in Figure 2.6 the system still employs poppet valves (12) as used in common combustion engines. The hydraulic system basically consists of an oil sump (46), a low pressure pump (54) and a high pressure pump (50). Thus it features a low (70) and a high pressure branch (68). A piston (16) is attached to the engine valve stem. While the volume underneath the piston (42) is continuously supplied by the high pressure branch using the high pressure lines (26), the rotary valve is used to distribute hydraulic pressure from either the low pressure branch or the high pressure branch to the volume above the piston (20) in order to open and close the corresponding engine valve. The rotary valve is driven by a motor (60) and controlled by the engine control system (48). Low and high pressure windows are imbedded into the cylindrical body of the rotary valve.

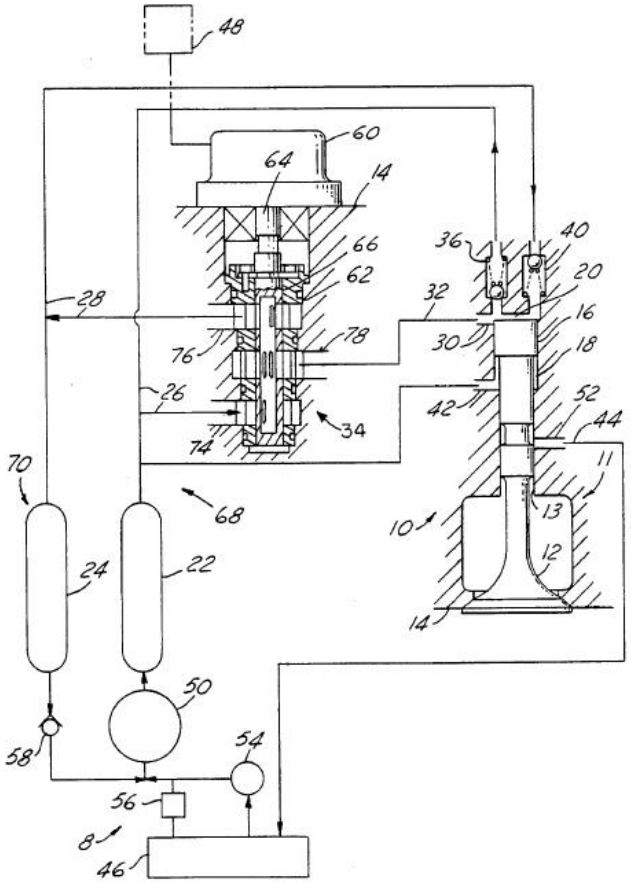

Figure 2.6: Electrohydraulic camless vavletrain by Schechter at al. [18]

Depending on the position of the rotary valve, the piston on the valve stem can fulfil a reciprocating motion within the limits of the piston chamber according to the hydraulic pressure applied above the piston. The pressure surface area above the valve stem piston in volume (20) is significantly larger than the effective surface underneath it in volume (42). Therefore, the opening of the engine valve becomes possible. Even though at this stage both volumes underneath and above the valve stem piston are connected to identical pressure from the high pressure branch, the difference in surface area results in a larger force acting on top of the piston and hence pushes the engine valve open. In this case oil is led from the high pressure reservoir (22) to volume (20) via the hydraulic lines (26) and (32).

Engine valve closing is carried out by changing the position of the rotary valve as to allow the hydraulic fluid to run from volume (20) to the low pressure fluid reservoir (24) via lines (32) and (28). By altering the position of the rotary valve body with the embedded windows the engine valve acceleration and deceleration can be influenced. The high pressure check valve (36) opens as the engine valve is closing and the displacement above the valve stem piston decreases. Hydraulic fluid gets pushed out into the high pressure lines (26) so the valve is being decelerated just before it seats. In this way a hydraulic valve brake is realized. With the aid of this the consequences resulting from a hard valve seating as explained in Subsection 2.3.1 are avoided.

The low pressure check valve (40) opens while the valve stem piston moves downwards as the engine valve is opening. As the valve possesses kinetic energy while reciprocating with high velocity, the engine valve still moves downwards while the corresponding window in the rotary valve body supplying volume (20) with high pressure has already been closed. With the volume above the valve stem piston further increasing void formation in volume (20) can be avoided by opening the low pressure check valve and allowing hydraulic oil to enter. This is highly important and needs to be considered during developing the FVVT system as air is highly compressible and void formation will affect a precise control of the engine valve movement.

The system shows large variability concerning the valve operation. For instance, by altering the timing of window crossings within the rotary valve body the timing of engine valve opening and closing can be influenced. By varying the alignment of certain windows the valve lift can be modified. Depending on the applied pressure engine valve velocity and acceleration can be adjusted [18].

2.4 Conclusion

In conclusion, the BMW K71 engine, originally designated for the use in the "Formula Student" racing competition with a reduced cubic capacity of $610\,cm^3$, is utilized as the research engine for the FVVT project. The K71 complies with contemporary engine technology and being compact it faciliates an easy implementation of the FVVT system as only two cylinders and eight valves need to be operated.

Same as in the FVVT system the presented valve train systems aim at full adjustability of the valve operation and increasing the potential of the reciprocating piston engine. Most of these valve train systems offer large potential regarding the achievable performance and pollution improvements that have been explained before.

However, the "TwinAir" and "MultiAir" approach by Fiat still shows strong limitations in its functionality. A hydraulic valve actuator that is in development at "Sturman Industries" in Colorado, USA has not been presented due to the very limited published information on the system. The developers claim the ability to amongst others incorporate Atkinson and Miller cycle into the valve motion, but the system still features a valve return spring, which will cause limitations regarding full adjustability of the engine valve movement, especially at high engine speeds [19].

The FVVT system features the main advantage that the mechanically moving parts like cam followers and engine valve springs will be removed from the valve train. This will enable fully variable engine valve control, independent from limitations occurring due to spring properties or large oscillating components. Identical to the presented systems the transmitting medium of the engine valve actuator will be hydraulic oil, enabling a sufficient reaction time of the system, allowing to adjust the engine valve position for best efficiency with lowest possible emissions at any time. The "Electrohydraulic camless valvetrain" (Schechter and Levin, 1996) shows significant similarity to the FFVT system at the "Ostfalia University of Applied Sciences", which will be introduced in the following chapter.

3 "Full Variable Valve Train" at the Ostfalia University

This chapter presents the electrohydraulic FVVT system that has been developed at the "Ostfalia University of Applied Sciences" in the way it is currently being used. Continuous research and development work on the system is still being carried out within one doctorate and different research projects, both at the "Ostfalia University of Applied Sciences" and the "Nelson Mandela Metropolitan University" (NMMU), in order to enhance system packaging and control engineering.

3.1 Valve train composition

To guarantee a thorough understanding of the fundamentals of the previous FVVT system that is the basis for the system developed within this project, the former is illustrated in Figure 3.1 (next page). The FVVT system involves the main components valve assembly (1), high speed servo valve (2), piezo actuator with lever transmission (3), control system (4) and hydraulic unit (5). By using an oil pickup (A) and hydraulic line (B) an adjustable hydraulic axial piston pump delivers hydraulic oil from the oil reservoir (6) to the lever transmission that is directly connected to the piezo actuator. Line (C) is used to eject oil from the lever transmission into the oil reservoir when a pressure adjustment is needed or to bleed the oil-filled volume of the transmission. The system pressure is $150\,bar$ or $15\,MPa$ respectively. A hydraulic line (D) supplies the servo valve with hydraulic oil.

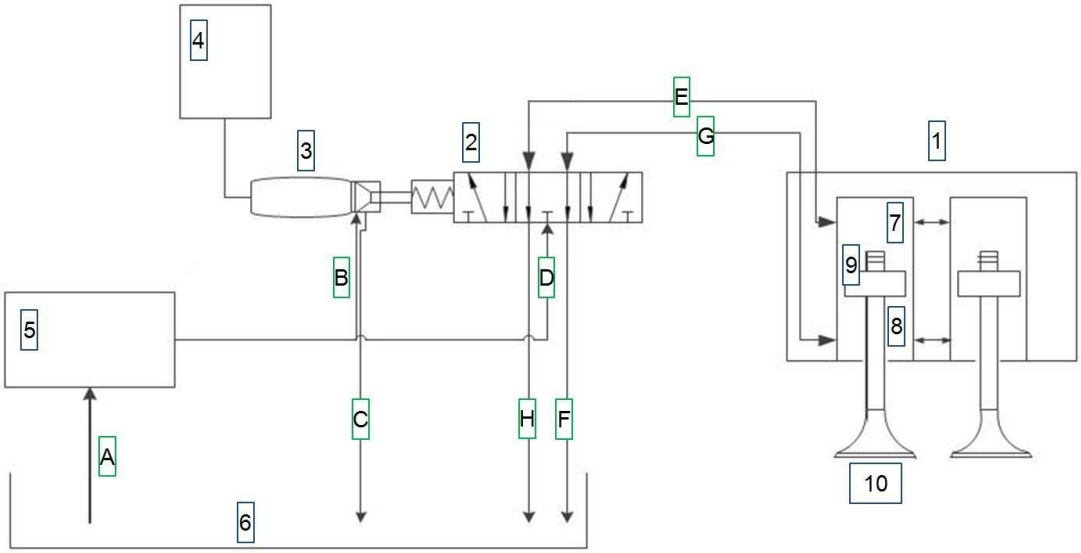

1: Valve assembly | 2: Servo valve | 3: Piezo actuator

4: Control system | 5: Hydraulic unit | 6: Oil reservoir

7: Volume above piston | 8: Volume under piston | 9: Valve stem piston

10: Engine valves | A-H: Hydraulic lines

Figure 3.1: Previous FVVT system of the Ostfalia University [20]

The voltage applied to the piezo actuator is delivered by an amplifier (see Subsection 6.3.4) that is part of the control system. In dependency on voltage value and cycle time the piezo actuator fulfils a reciprocating movement as the crystals extend when voltage is applied and contract when the supply is interrupted. This movement is transferred onto a translation piston featuring a diameter of $40\,mm$ that is positioned within the lever transmission. The latter is oil-filled under any condition and as a consequence of the piston movement pressure is applied to the hydraulic transmitting medium. As the oil is almost incompressible and the lever transmission is closed towards the atmosphere, the force of the piezo actuator is transferred onto the effective surface area of the servo piston with a substantially smaller diameter of $4\,mm$ that is positioned at the other end of the lever transmission and extends into the servo valve. Within this the servo piston features three piston elements extending the diameter of $4\,mm$ that open or close the hydraulic ducts within the servo valve. These ducts are connected to the hydraulic lines (D), (E), (F), (G) and (H).

The valve assembly contains two poppet valves (10) that each have a piston (9) on the valve stem. A volume above the piston (7) is connected to hydraulic line (E) and a volume underneath the piston (8) to line (G). Lines (E) and (G) are included into the engine valve body and can be used in both directions indicated by the arrows in Figure 3.1. Depending on the position of the servo piston in the servo valve either the volume above or underneath the piston is supplied with hydraulic oil or both volumes are disconnected from the pressure supply. In any piston position it is impossible to connect both volumes to the hydraulic pressure supply at the same time. Both valves can be moved within the displacement of the valve stem piston chamber formed by volume (7) and (8). Contingent on the operating mode of the system lines (F) and (H) are used to eject excess oil into the oil reservoir when the displacement of the oil-filled volume (8) or (7) is being reduced due to the valve movement. Both valves are operated in the same way due to the fact that both volumes above the valve stem pistons are connected and attached to the same line (E). The same is valid for the volumes underneath the pistons in respect of line (G).

3.2 Piezo technology and actuator

For the following explanations it is necessary to understand how the piezo actuator is working and in which way it can be used in the FVVT system. The term “piezo” derives from the Greek and means “push”/“compress”. The effect can be seen on crystals that produce an electric potential on their surface due to an application of external force. This is known as direct piezo effect. On the contrary, a piezo actuator transforms electrical energy into mechanical energy. If voltage is applied to the piezo crystals this results in an extension of the crystals. This is called inverted piezo effect.

The materials used for piezo actuators basically are polycrystalline, ferromagnetic ceramics as barium titanate or lead zirconate titanate (PZT) due to the fact that the piezo effect is very low in natural crystals like quartz or tourmaline [21] [22].

The piezo effect comes into use in different automotive applications. For example, in engine knock[13] sensors utilizing the direct piezo effect and in certain fuel injectors utilizing the inverted effect. Figure 3.2 shows a stack of an piezo actuator as used within this project.

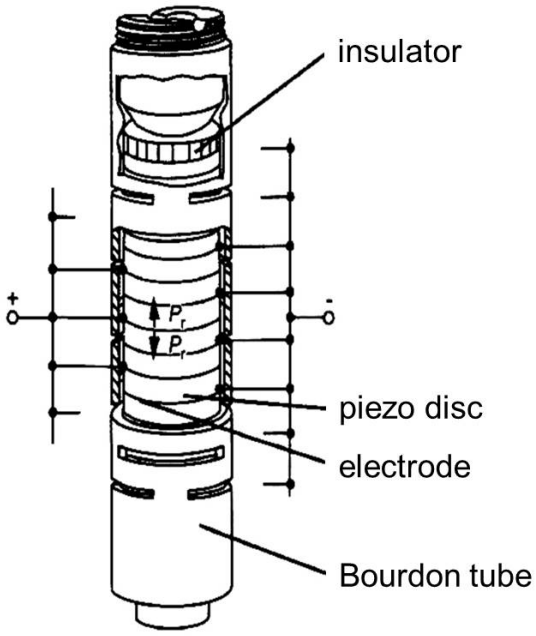

Figure 3.2: Internal structure of a piezo stack actuator [21]

The piezo stack actuator uses the inverted piezo effect. Mechanically the discs are connected in series while electrically they feature a parallel connection. A large number of discs is used with a maximum thickness of $1\,mm$ each. As the thickness of the ceramic is inversely proportional to the electric field strength it is aimed at a low ceramic thickness. This at a specified voltage ensures a sufficient field strength and expansion of the ceramic. In order to work as an actuator many discs need to be coupled. The overall expansion range of the actuator is equivalent to the sum of the thickness changes of the individual discs. A Bourdon tube makes the actuator resistant against tensile forces [21] [22].

[13] uncontrolled self-ignition of the air/fuel mixture in internal combustion engines

The piezo actuator deployed within the FVVT project is the actuator type P-235.90 from the company "Physik Instrumente (PI) GmbH & Co. KG". It features the following properties:

Maximum travel range:	$\Delta l_0 = 180\,\mu m$
Diameter:	$d_{piezo} = 49.8\,mm$
Length:	$l_{piezo} = 199\,mm$
Compressive force resistance:	$F_c = 30000\,N$
Tensile strength:	$F_t = 3500\,N$
Rigidity:	$k_T = 150\,\frac{N}{\mu m}$
Electrical capacitance:	$C = 7800\,nF$
Resonance frequency:	$f_{0,piezo} = 2800\,Hz$

Figure 3.3 explains why instead of the full travel range Δl_0, a range of only $\Delta l_{eff} = 120\,\mu m$ is used within this setup.

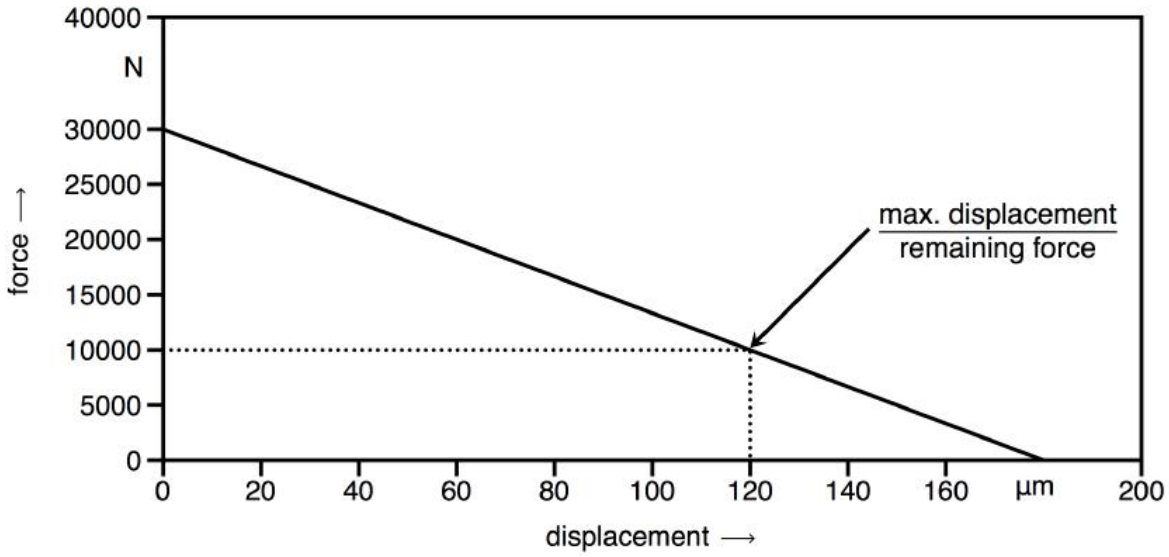

Figure 3.3: Relation between force and travel distance of the P-235.90 actuator [20]

When using the maximum travel range Δl_0, no excess force of the piezo actuator is left at all. As a certain amount of force is required to overcome friction and dynamic

forces of the overall system in motion it has been decided to use an effective travel range of $120\,\mu m$ leaving $10\,kN$ of excess force for a reliable system operation under any circumstances.

With the effective travel range and the ratio of the lever transmission the effective travel distance of the servo piston can be calculated. The ratio with the above mentioned piston diameters is as follows:

$$i = \frac{A_{tp}}{A_{sp}} = \frac{\frac{\pi}{4} \cdot d_{tp}^2}{\frac{\pi}{4} \cdot d_{sp}^2} \tag{3.1}$$

$$= \frac{\frac{\pi}{4} \cdot (40\,mm)^2}{\frac{\pi}{4} \cdot (4\,mm)^2} \tag{3.2}$$

$$= \frac{1256.64\,mm^2}{12.57\,mm^2} \tag{3.3}$$

$$\approx \underline{\underline{100}} \tag{3.4}$$

where

i = lever transmission ratio
A_{tp} = front surface of the translation piston
A_{sp} = front surface of the servo piston
d_{tp} = diameter of the translation piston
d_{sp} = diameter of the servo piston

Now that the ratio of the lever transmission is known the travel range of the servo piston is:

$$s_{sp} = s_{tp} \cdot i = 0.12\,mm \cdot 100 \tag{3.5}$$

$$= \underline{\underline{12\,mm}} \tag{3.6}$$

where

s_{sp} = travel range of the servo piston

s_{tp} = travel range of the translation piston

In practice it is enough to use a $10\,mm$ servo piston travel range to operate the system as this is the furthest distance the piston has to be moved to switch between the utmost positions within the servo valve. The $2\,mm$ excess range ensures that the piston can reach its switching positions under any change of conditions due to heat expansion of the parts or a not perfectly accurate position of the servo piston within the lever transmission.

3.3 Switching positions of the servo valve

This section presents the possible fundamental control positions of the servo piston and the resulting valve movements, as illustrated in Figure 3.4.

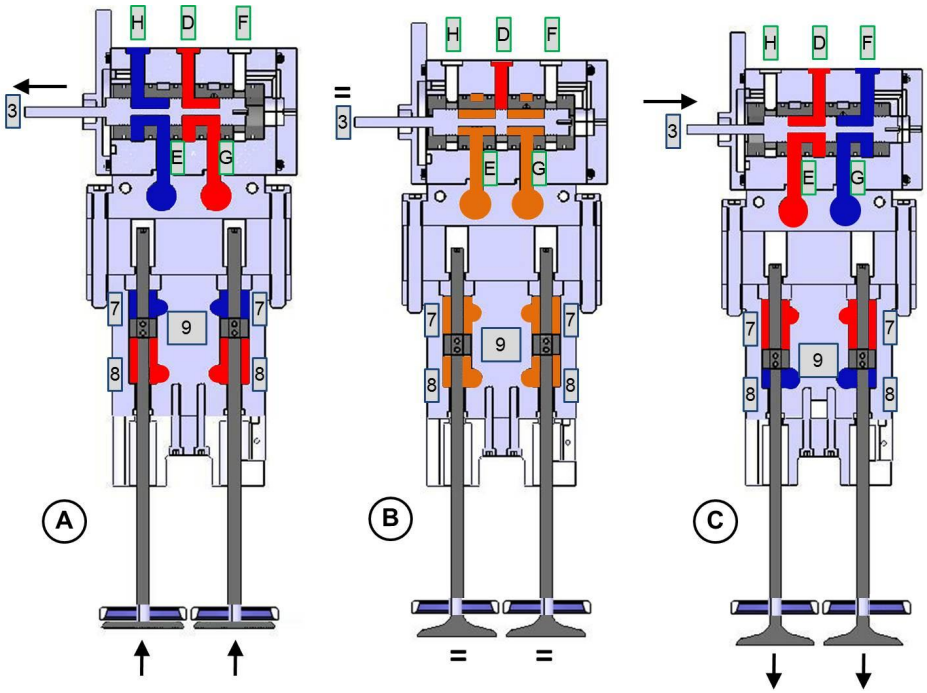

Figure 3.4: Basic control positions of the FVVT system

The piezo actuator with lever transmission (3) is positioned to the left hand side of the servo piston and not illustrated in Figure 3.4. The black arrows close to the servo valve indicate the moving direction of the piezo stack and the black arrows at the bottom show the resulting valve movement. The red lines are pressurized with full system pressure ($15\,MPa$); the blue lines are non-pressurized and the orange ducts are at lowered maintaining pressure ($<15\,MPa$).

- Case A (valve closing)

No voltage is applied to the piezo actuator. Due to the properties of piezo crystals the actuator stays in its full contracted position. The servo piston remains in its furthermost left position and is not moved out of the lever transmission. This position allows the pressurized hydraulic fluid to flow from line (D) via line (G) to volume (8). At the same time volume (7) is being drained using lines (E) and (H). As a consequence the high pressure applied underneath the valve stem pistons causes an upward movement of both valves. As volume (7) is non-pressurized in this case the resistance counteracting the piston movement is as low as possible. The servo piston closes the connection to line (F) ensuring that the hydraulic fluid cannot escape back into the oil reservoir.

- Case B (center position of the servo piston)

By applying a defined voltage to the piezo actuator with help of the lever transmission the servo piston is moved half of its maximum effective travel range of $10\,mm$. Hereby lines (H), (D) and (F) on top of the servo valve are closed. Due to this neither the hydraulic pressure supply is connected to volume (7) or (8) nor hydraulic fluid can exit the valve body. As both volumes remain constant in this configuration the current valve position is being held continuously. The center position of the servo piston at the same time is the initial point in terms of the system's control. Before the system can be operated the servo piston must be adjusted to its center position first of all.

- Case C (valve opening)

When applying a voltage to the piezo actuator that results in the servo piston's full effective travel range of $10\,mm$, lines (E) and (G) are used, as opposed to Case A. The hydraulic pressure supply (D) is connected to line (E) leading to volume (7) above the valve stem pistons. Volume (8) underneath the pistons is being drained via lines (G) and (F). The pressure distribution above and underneath the valve stem pistons is contrary to Case A. Consequently the pistons and engine valves are pushed downwards. Line (H) is closed in this configuration separating the pressure supply from the oil reservoir return and hence avoiding a drop of system pressure.

When the voltage supply to the piezo actuator is interrupted the stack contracts and the larger translation piston which the piezo actuator is acting upon is being pushed back by the hydraulic pressure within the lever transmission. As the servo piston cannot be brought back into its initial position by the hydraulic pressure in the lever transmission it is being pushed back with the aid of a return spring that is attached to the servo piston and supports itself against the body of the servo valve.

The servo piston position can be adjusted between the basic positions explained above and dependent on the voltage applied to the piezo actuator variable positions within the travel range of the servo piston can be approached. By opening or closing the ducts within the servo valve partly or fully the valve movement acceleration and deceleration can be adjusted.

A hydraulic valve brake can be included in the system's control in order to guarantee soft landing of the engine valves during the closing procedure. The valve brake will be adapted to work within the system developed in this research project and is being explained in Chapter 7.

3.4 Conclusion

The presented FVVT system is an electrohydraulic engine valve actuation technology that uses a directly controlled servo valve as one of the main components to control the engine valve lift fully adjustable.

The main advantage of this system is the combination of the piezo's precision with the force of the hydraulic actuator, which is a good basis for variable engine valve timing. On the other hand, the piezo displacement needs a large lever transmission ratio of 100, so the servo piston can reach all switching positions within the servo valve. As a consequence the piezo actuator is comparatively large. Another disadvantage is that the center position of the servo piston as initial point of experiments must gradually be adjusted.

The following chapter will introduce an altered version of this system that has been finalized within this research project. It is based on the main components piezo actuator and servo valve and builds on the main thought of combining precision and hydraulic force. Other than before, the redesigned system will be controlled indirectly. It will feature the advantage of a significantly reduced lever transmission ratio that allows to reduce the piezo's size in future projects. Additionally, the center position of the servo piston within the servo valve will be self-adjusting by the use of two identical compression springs on either side of the piston.

4 Indirectly controlled "Full Variable Valve Train" system

This chapter presents the development results of the redesigned and indirectly controlled FVVT system that is the core of this research project. Firstly, the overall task will be fully clarified by showing the results and flaws of the feasibility study this project is based on. The resulting system requirements will be discussed and the achieved solution and design of the new system components will be introduced. Finally, the three altered basic switching positions for the engine valve actuation will be explained.

4.1 Design background

The basic design idea of the indirectly controlled FVVT system arose from the feasibility study mentioned in Section 1.1. Figure 4.1 (next page) shows the design result of the feasibility study.

The illustrated system features a modified servo valve and an added control unit as basic components. The engine valve body and the core of the servo valve are being kept. The configuration shown in the figure is equivalent to Case A (valve closing) explained in Section 3.3. For enhanced comparability the hydraulic lines (D) to (H) are marked in the figure. Different to the directly controlled system in this case the piezo actuator is coupled to the control unit instead of acting directly upon the servo valve and is positioned vertically above the former, with regard to Figure 4.1.

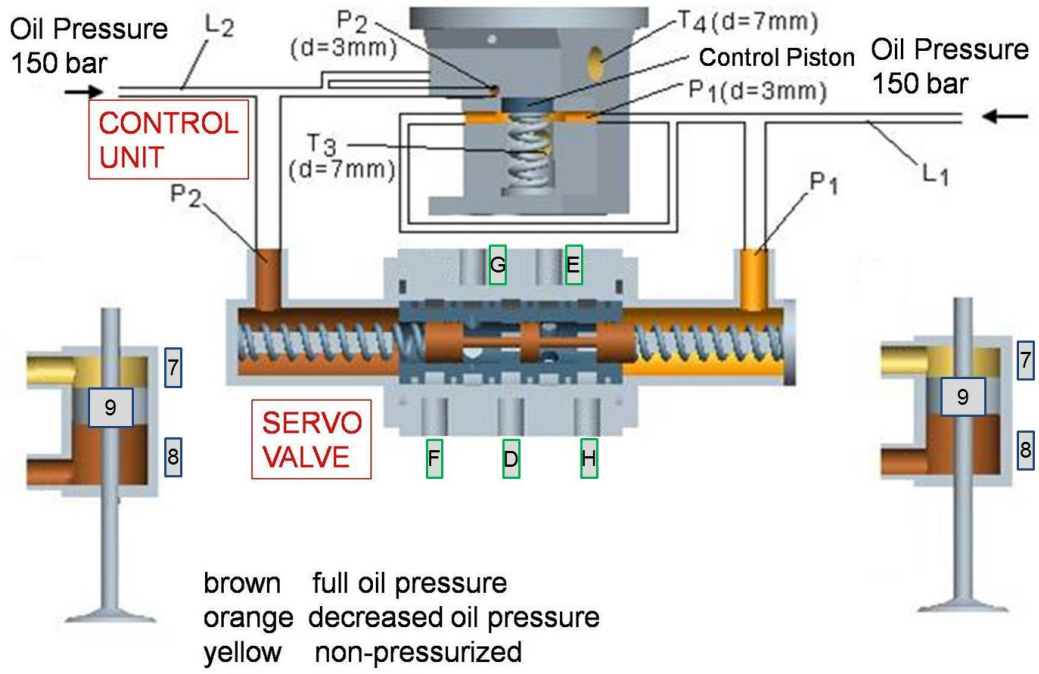

Figure 4.1: Concept presented in the feasibility study [23]

By opening or closing the ducts marked with (P1) and (P2) the pressurized hydraulic fluid can be recirculated into the oil reservoir through lines (T3) and (T4) respectively. This is realized by moving the control piston downwards or upwards. The piston can be reset to its initial position with the aid of a return spring.

In the shown case the open (P1) loop allows oil pressure on the right hand side of the servo piston (with regard to Figure 4.1) to decrease as the oil is led back into the reservoir. The control piston blocks the (P2) loop in this case as to keep full oil pressure on the left hand side of the servo piston. Due to this the servo piston is pushed into its utmost right position. As explained in Section 3.3 full system pressure is applied underneath the valve stem piston (9) in chamber (8) while the chamber above the piston (7) is being drained.

Case B (center position of the servo piston) is being reached by moving the control piston downwards, blocking off both the (P1) and (P2) loops allowing full pressure to be applied on both end surfaces of the servo piston. The servo piston is brought to and held in the center position by two identical compression springs on either side.

Case C (valve opening) is reached when the control piston is moved further downwards keeping the (P1) loop closed and opening the (P2) loop. In this case the pressure distribution between both ducts leading to the servo piston is opposite to Case A leading to a movement of the servo piston the the left (with regard to Figure 4.1) and hence opening the engine valves according to Section 3.3.

The main advantages of the system are, firstly, a more precise system control due to a decreased travel range of the control piston resulting in a decreased time required for reaching the switching positions of the piston. And, secondly, the utilization of a more compact lever transmission which uses a significantly lower ratio, advancing the setup with regard to the possible implementation of a smaller piezo actuator in future projects leading to a more compact overall system size and weight.

Research on the concept exposed a major flaw in design and potential for improvement. The largest concern arises from the fact that full oil pressure is still applied through lines (L1) and (L2) while either loop (P1) or (P2) is opened. As the applied pressure reaches up to $15\,MPa$, the pressure decrease which is necessary to control the system reliably is strongly restrained. Based on the above mentioned a redesigned FVVT system with indirect control is being developed. The system has to comply with the requirements shown subsequently.

4.2 Requirements

Due to the already mentioned facts and the overall aim of this project the following specifications need to be met:

- Design of a system that is free of a restrained pressure decrease
- Full adjustability of the valve movement under any circumstances
- Possibility of including an engine valve brake

- Closing of the engine valves when power breakdown occurs
- Enhanced control precision (compact lever transmission).

The listing of boundary conditions that are crucial for the system operation will be completed by taking a closer look at the frequency which the system will be operated with and the resulting resonance frequency of the system in motion. The FVVT system at present is being used up to a maximum theoretical engine speed of $8000\,{}^{1}/_{min}$. Due to the camshaft and crankshaft rotation ratio explained in Subsection 2.1.2 the speed of both camshafts in this case is equivalent to $4000\,{}^{1}/_{min}$. Narrowing down the view towards the FVVT system actuating two engine valves, the required actuation frequency and hence resulting system resonance frequency f_0 can be calculated as follows:

$$f_0 = \frac{n_{cs}}{60\,\frac{s}{min}} = \frac{4000\,\frac{1}{min}}{60\,\frac{s}{min}} \tag{4.1}$$

$$= \underline{\underline{66.67\,Hz}} \approx \underline{\underline{67\,Hz}} \tag{4.2}$$

where

n_{cs} = rotational speed of the camshaft(s)

This means that with regard to the conventional K71 engine the engine valves are being actuated approximately 67 times per second at the maximum engine speed referred to above. According to the reciprocal value of f_0 the time available for one valve actuation is $t_{act} = 14.9\,ms$. Due to the fact that the cam lobe profile of the camshaft viewed, only exhibits lift on circa $52\,\%$ of the camshaft circumference the actual time available for one valve operation t_{open} is as follows:

$$t_{open} = \frac{\alpha_{open} \cdot 60\,\frac{s}{min}}{\alpha_{cs} \cdot n_{cs}} = \frac{188° \cdot 60\,\frac{s}{min}}{360° \cdot 4000\,\frac{1}{min}} \tag{4.3}$$

$$= \underline{\underline{7.83\,ms}} \tag{4.4}$$

where

α_{open} = valve actuation angle of the camshaft

α_{cs} = camshaft rotation angle

The value for t_{open} seems plausible and can be proved with the aid of Figure 4.2 showing experimental results of the FVVT system as it is actually being used.

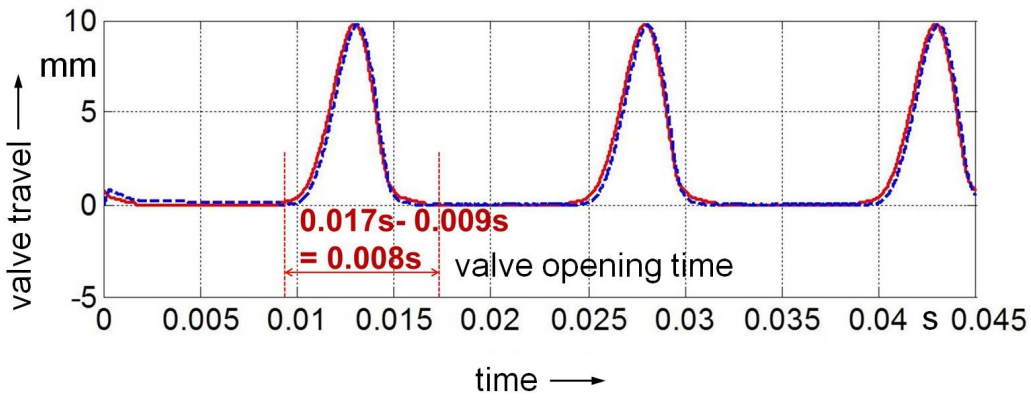

Figure 4.2: Standard K71 valve lift curve at 8000 $^1/_{min}$ [23]

The graph shows the valve lift versus the elapsed time at an engine speed of 8000 $^1/_{min}$. The blue curve shows the simulation result recorded on the valve test bench at the "Ostfalia University of Applied Sciences" in Wolfsburg while the red curve shows the original valve lift of the K71 which is of interest for considering the valve opening time of the original engine as the simulation still includes a slight deviation.

The time within which a valve is actuated once is marked and is equivalent to approximately $8\,ms$. Conventionally the engine valves are being pushed open by the cam lobe and closed again by the valve springs within t_{open}. Regarding the redesigned

FVVT system, this means that within this time the servo piston must be moved into the position illustrated in Case C in Figure 3.4 and back to the extreme left position shown in Case A. As the piezo actuator extends by the application of voltage and contracts again when voltage supply is cut it only needs to be actuated once to move the servo piston into one direction (voltage applied) and back again (voltage interrupted). The piston is moved only into one direction by an electric cause while the movement back into the other direction is caused mechanically. This can also be ensured within the redesigned system as a return spring still will be in use. This will be explained in detail in the following Section 4.3. As a consequence, the servo piston, amongst all other internal system components, moves with twice the frequency f_0 the piezo is actuated with, summing up to $2 \cdot f_0 \approx 2 \cdot 67\,Hz = 134\,Hz$.

As the resonance frequency is known the resulting eigen angular frequency ω_0 can be calculated:

$$\omega_0 = 2 \cdot \pi \cdot f_0 = 2 \cdot \pi \cdot 66.67\,Hz \tag{4.5}$$

$$= \underline{\underline{418.90\,\frac{1}{s}}} \tag{4.6}$$

All moved masses within the system core must be laid out concerning this value to ensure the system does not reach resonance. The following section shows how the requirements listed above have been implemented into the redesigned FVVT system components.

4.3 Solution

The two core components, servo valve and control unit, have been designed for the purpose of being used within an indirectly controlled system. With regard to the feasibility study the system layout needs to be altered corresponding to Figure 4.3 (next page).

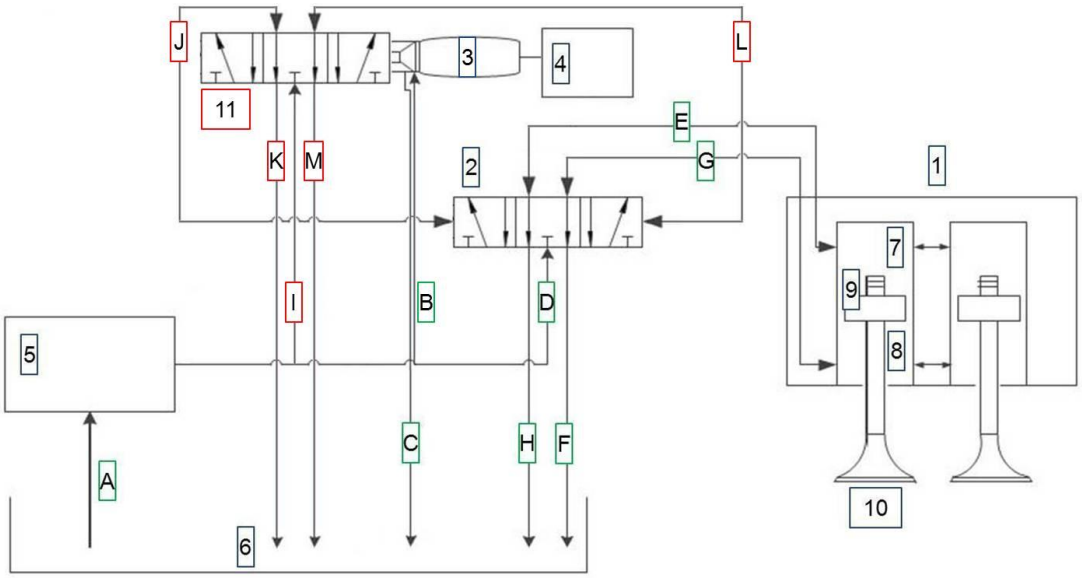

1: Valve assembly | 2: Servo valve | 3: Piezo actuator
4: Control system | 5: Hydraulic unit | 6: Oil reservoir
7: Volume above piston | 8: Volume under piston | 9: Valve stem piston
10: Engine valves | 11: Control unit | A-M: Hydraulic lines

Figure 4.3: Redesigned indirectly controlled FVVT system

In contrast to Figure 3.1 the new system has been extended by a control unit (11) and hydraulic lines (I) to (M). All added system components are marked in red. Instead of using the hydraulic loops (P1) and (P2) illustrated in Figure 4.1, the redesigned system utilizes hydraulic lines (J) and (L) that, such as lines (E) and (G) can be used in both directions, indicated by the black arrows. The following subsections will explain how this modification helps to solve the mentioned pressure distribution issues that occur in the concept of the feasibility study.

Lines (K) and (M) are oil return lines leading from the control unit into the oil reservoir similar to lines (H) and (F) used for the servo valve (2). Line (I) feeds pressurized hydraulic fluid into the control unit in order to change the servo piston position by pressurizing line (J) and/or (L). The remaining components and lines are almost exclusively used in the same way as explained in Sections 3.1 and 3.3. The following subsections will take a closer view at the redesigned servo valve and the new control unit. Both presented components have been designed with the CAD program "Catia V5 R20" by Dassault Systèmes.

4.3.1 Control unit

Many basic ideas of the feasibility study have been included into the design of the new system while especially in the case of the control unit major changes were undertaken to improve the control of the hydraulic oil flow through the body of this part. An exploded drawing of the control unit is shown in Figure 4.4.

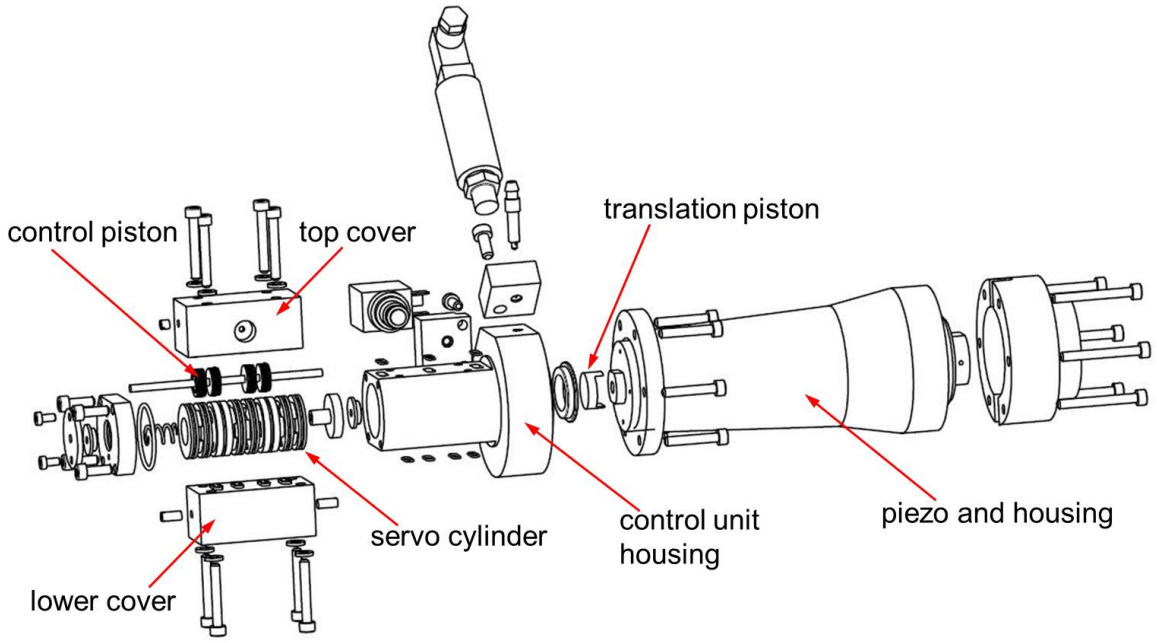

Figure 4.4: Exploded view of the control unit

A sectional view of the assembled control unit is shown in Figure 4.5 (next page).

The housing (1) of the control unit contains a servo cylinder (2) within which the control piston (3) can be moved, a compression spring (4) and seven hydraulic lines (I) to (M). The translation piston (5) is directly being operated by the piezo actuator (6). As in the previous FVVT system, a lever transmission is part of the setup. In this case it does not act directly on the servo piston in the servo valve but on the control piston instead.

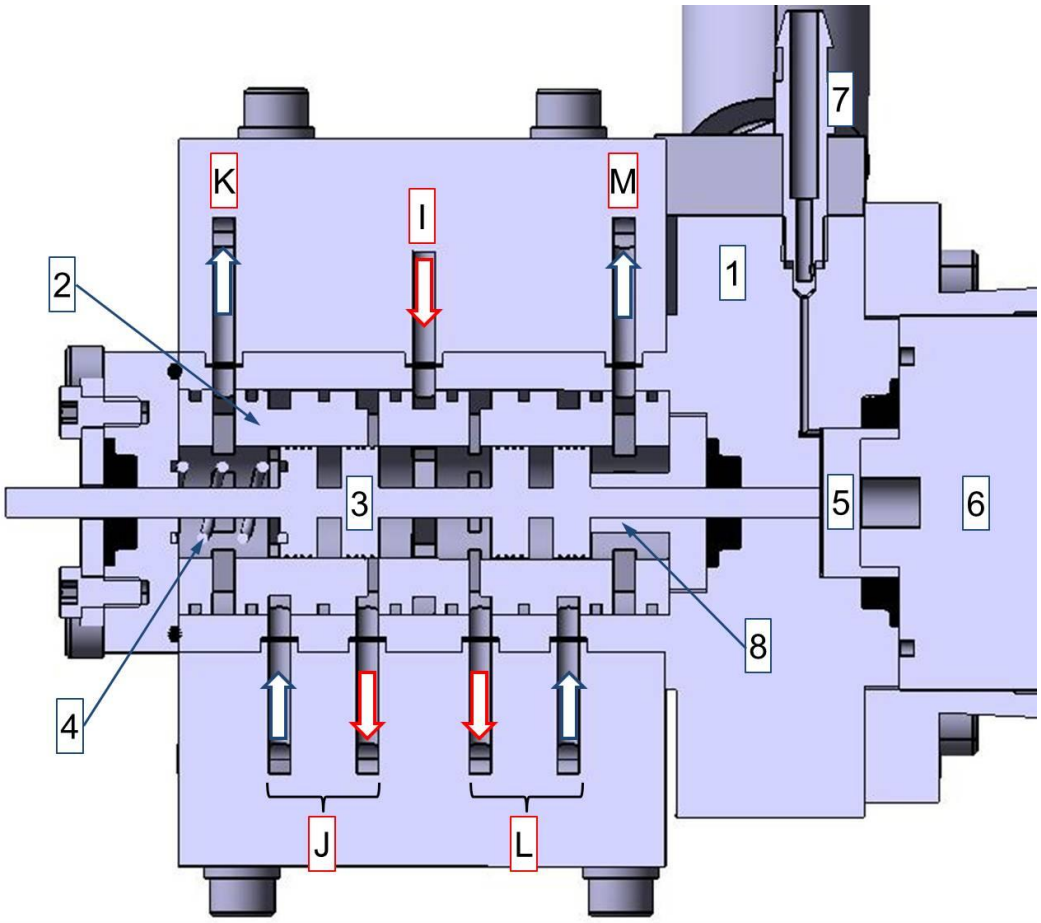

1: Housing
2: Servo cylinder
3: Control piston
4: Compression spring
5: Translation piston
6: Piezo actuator
7: Air vent
8: Mechanical stop

Figure 4.5: Internal structure of the control unit

Hydraulic fluid will be sent into a diminutive volume between translation and servo piston. The distance between the two pistons in the illustrated case is only $0.4\,mm$ in order to reduce the used oil mass. As the effectively used travel range of the piezo actuator is only $0.12\,mm$, a damage of the control unit caused by the piezo pushing the translation piston into a range of interference with the housing of the control unit can be excluded. Due to the reduced volume it is easier to maintain a constant oil level within the lever transmission as void formation can be avoided to the largest possible extent. This will be beneficial regarding the overall system control. If void formation occurs though, an air vent (7) can be used to bleed the lever transmission.

Three rod seals are used within the control unit. In Figure 4.5 these are illustrated in black. The one to the utmost left seals the control piston against the atmosphere while the remaining two rod seals are used to prevent the lever transmission from any oil leaks to either side.

As mentioned earlier, hydraulic lines (J) and (L) can each be used in two directions. This, both for (J) and (L), is realized by connecting the line indicated by the blue arrow and the line indicated by the red arrow to one common line leading to one side of the servo piston in the servo valve.

The control piston and inner ducts of the control unit have been completely changed compared to the feasibility study in order to guarantee a physical separation of the hydraulic ducts in use according to the particular switching position and to ensure an improved producibility of the core of the control unit. The control piston features four piston elements and all hydraulic ducts are arranged in a straight line. A total of four hydraulic ducts is controlled by the control piston elements. In the three basic switching positions each two of these ducts will be in use at the same time. A mechanical stop (8) to the right hand side of the control piston is used to ensure the correct position of the latter when no voltage is applied to the piezo. All technical drawings of the newly designed control unit components are included in Appendix 9.2. With reference to Section 1.3, drawings of the piezo actuator and housing are not included as these can be taken from the previous FVVT setup. The switching positions of the overall system will be introduced in Subsection 4.3.3.

4.3.2 Servo valve

In order to couple the servo valve with the control unit several modifications of the servo valve were necessary. Figure 4.6 shows the result in an exploded view drawing (next page).

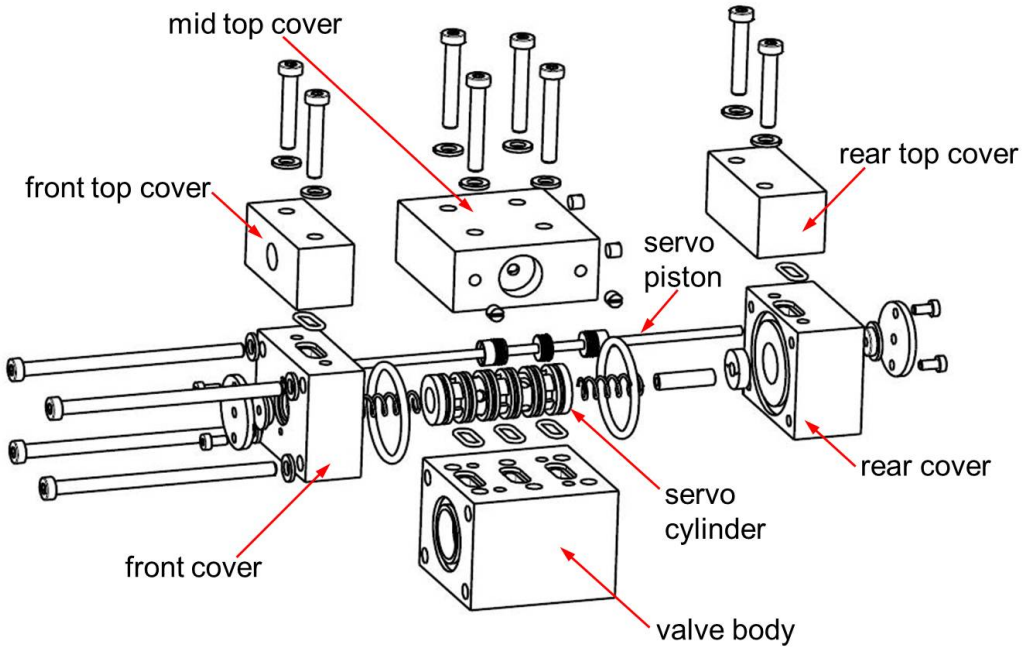

Figure 4.6: Exploded view of the redesigned servo valve

For a better understanding of the system component arrangement Figure 4.7 shows a sectional view of the servo valve (next page).

The redesign allows the retention of the servo valve body (1) and the incorporated servo cylinder (2) as used within the previous FVVT system. Hence the inner ducts connecting to lines (D) to (H) remain in the same arrangement as explained before. The servo piston (3) still consists of three piston elements but has been redesigned using a symmetrical design.

New covers to the left and the right of the servo valve have been designed that include ducts (4) for the hydraulic fluid which lines (J) and (L) connect to, coming from the control unit. The two-coloured arrows indicate that the ducts can either be pressurized or bled as mentioned in Subsection 4.3.1 with regard to lines (J) and (L).

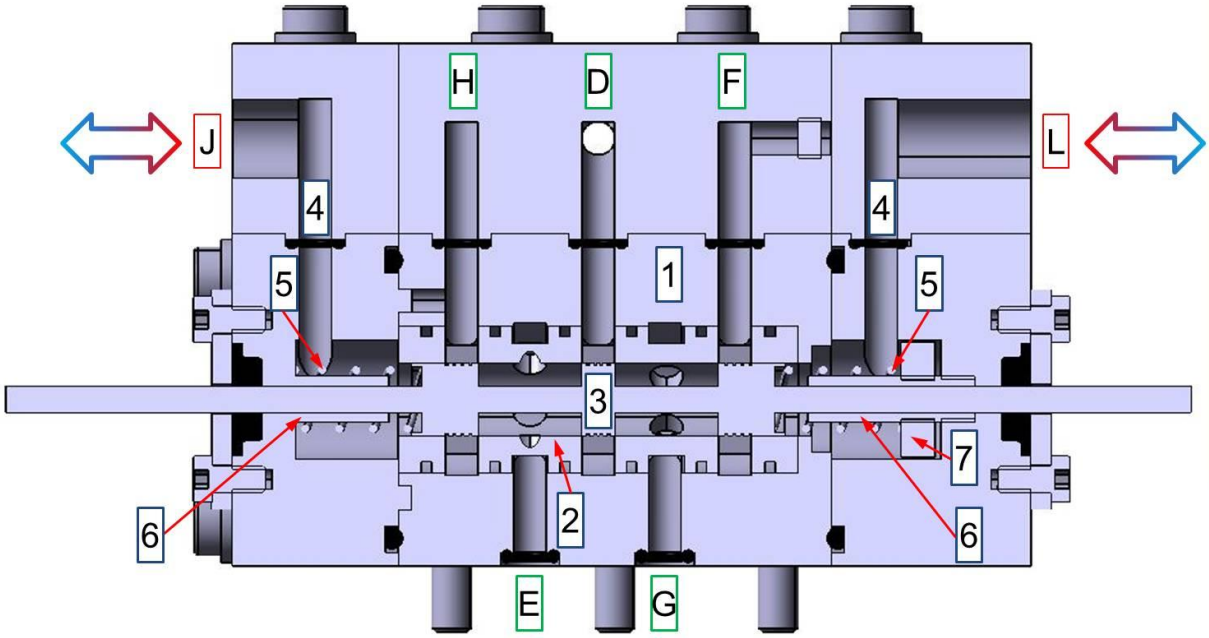

1: Valve body 2: Servo cylinder 3: Servo piston
4: Oil ducts 5: Compression springs 6: Mechanical stops
7: Spring adjuster

Figure 4.7: Internal structure of the redesigned servo valve

Two identical compression springs (5) are necessary to ensure the initial/center position of the servo piston as explained in the following Subsection 4.3.3. Mechanical stops (6) on either side of the piston are used to ensure exact end positions for valve opening and closing procedures after the translatory motion of the piston. The spring adjuster (7) is able to compensate for fabrication tolerances within the two theoretically identical compression springs. The spring on the right hand side can either be further preloaded or unloaded in order to match the other spring.

Another two rod seals, again illustrated in black in Figure 4.7 and positioned close to the outer limits of the servo valve covers, are used in order to seal the servo piston against the atmosphere. The seals prevent oil from leaking out of one of the hydraulic volumes on the left or right side of the servo piston. Appendix 9.3 contains technical drawings of all redesigned components used within the servo valve. Again, however, drawings of the existing components servo valve body, servo cylinder and engine valve body are not included, referring to Section 1.3.

4.3.3 Switching positions of the redesigned system

The three basic switching positions explained in Section 3.3 will be maintained. This subsection clarifies the combined switching positions of the control unit, directly influenced by the piezo actuator position and the servo valve that is operated indirectly by changing the pressure distribution in lines (J) and (L). Figure 4.8 illustrates the altered basic switching positions of the overall system.

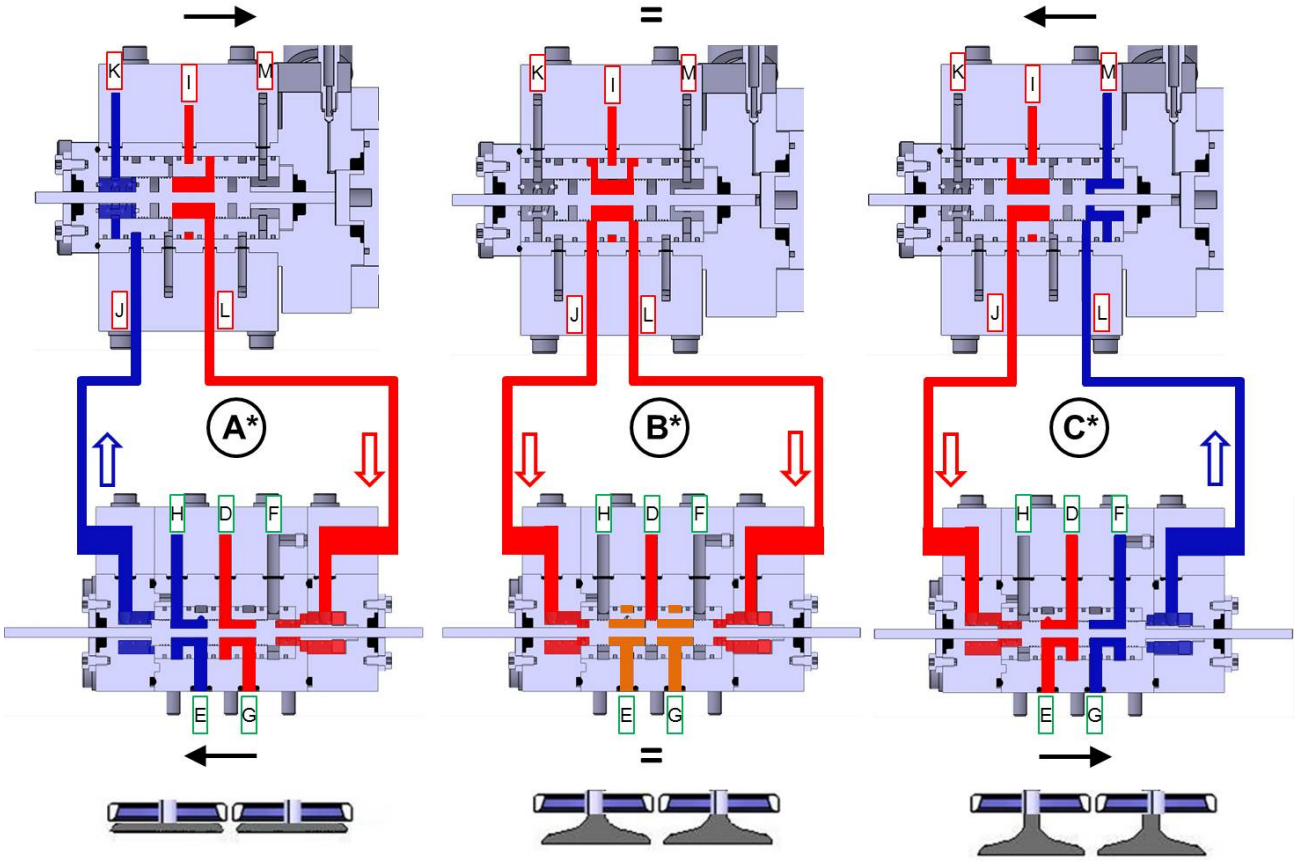

Figure 4.8: Altered basic control positions of the redesigned FVVT system

The basic layout of the illustration is equivalent to Figure 3.4 presented in Section 3.3. For all three switching positions the control unit has been added above the servo valve. The black arrows above the control unit indicate the movement of the piezo actuator and control piston, whereas the black arrows underneath the servo valve

represent the movement of the servo piston. The arrows in red and blue show the flow direction of the hydraulic lines active in the respective case.

As in Figure 3.4 the resulting valve movement can be taken out of the illustration at the bottom of Figure 4.8. The engine valve body situated underneath the servo valve as shown in Figure 3.4 has been left out for enhanced clarity in this figure as all processes within the valve body remain the same in all three Cases A* to C*. All hydraulic lines mentioned beforehand ((I) to (M) and (D) to (H)) are marked for a better understanding of the valve actuation procedures explained below:

- Case A* (valve closing)

No voltage is applied to the piezo actuator which remains fully contracted. Translation and control piston remain in their utmost right hand position (with regard to Figure 4.8). The latter is kept against its mechanical stop by the force of the compression spring used within the control unit.

Pressurized hydraulic fluid runs from line (I), which serves as a pressure supply to the control unit, via line (L) to the right hand side of the servo piston in the servo valve. At the same time the duct to the utmost left piston element of the control piston is opened, allowing the hydraulic fluid on the left hand side of the servo piston to exit the servo valve using lines (J) and (K). The duct that leads from the pressure supply (I) to line (J) is kept closed by the second control piston element from the left which ensures an unhindered pressure decrease on the left side of the servo piston.

As a consequence of the pressure difference between its left and right end surfaces the servo piston is pushed against its left mechanical stop. This results in engine valve closing according to Case A explained in Section 3.3. As no voltage is applied to the piezo actuator in this case, the valve closing as a safety measure at an electric power breakdown can be maintained in accordance with the requirements listed in Section 4.2. This way interference of the engine piston and engine valves after a

system failure can be avoided while the system is operated in a combustion engine. The control piston blocks the hydraulic line (M) so no pressurized fluid from line (L) can return into the oil reservoir.

- Case B* (center position of the servo piston)

By applying a voltage to the piezo actuator that results in half of its maximum travel range, the control piston reaches the center position within the control unit. The piston element to the furthest left closes the duct leading to line (K) and the piston element to the right of this opens a duct allowing the pressure supply to flow into line (J). Hence line (J) is used, as opposed to Case A*. The internal duct of the control unit leading from the pressure supply (I) to line (L) remains opened as in the previous case. Oil return line (M) stays blocked, so that hydraulic pressure in lines (J) and (L) cannot escape into the oil reservoir through lines (K) or (M).

This leads to a full system pressure equivalently being applied to both sides of the servo piston within the servo valve. The two identical compression springs in the servo valve ensure that the servo piston is moved into the center position as the balance of forces alone, being a consequence of the equal pressure distribution does not lead to a piston movement. In this way the initial position of the system or maintaining a certain valve position during system operation can be realized. The pressure distribution within the valve body remains as explained in Section 3.3 with regard to Case B.

- Case C* (valve opening)

When voltage supply to the piezo is increased the actuator and translation piston move further to the left (with regard to Figure 4.8). With the aid of the lever transmission the control piston is also moved and reaches its furthest left hand position within the control unit. Its second piston element from the right closes the duct leading from the pressure supply (I) to line (L). The duct leading to line (J) remains opened and line (K) is kept blocked. Full system pressure reaches the left side of the servo piston in

the servo valve. The first control piston element from the right opens another duct allowing hydraulic fluid to run from the right hand side of the servo piston into the reservoir using line (L) and return line (M).

Contrary to Case A* the servo piston is pushed against its right mechanical stop resulting in opening of the engine valves according to Case C in Section 3.3. After voltage supply has been cut, the control piston is pushed back against its mechanical stop within the control unit by the return spring, resulting in valve closing according to Case A*.

As in all mentioned cases lines (J) and (L) are strictly used either as the return line or pressurized with full system pressure, the above listed requirement of an unresisted pressure decrease is fulfilled. However, still the acceleration and deceleration of the engine valve movement can be influenced by approaching intermediate positions between the three illustrated control piston positions. This can be used to manipulate the pressure decrease in line (J) during engine valve closing and in line (L) during engine valve opening.

This again has an effect on the position of the servo piston which partly closes the hydraulic ducts within the servo valve influencing the time required to fill or drain the volumes above and underneath the valve stem pistons. Due to this fact the system keeps full variability of the valve movement control which is also of high significance for the engine valve brake that will be implemented into the new system.

4.4 Conclusion

Based upon the design results of a feasibility study from the year 2010 a new and advanced electrohydraulic "Full Variable Valve Train" system which is controlled indirectly has been designed with the aid of CAD. The existing FVVT system is expanded by a control unit that is used to manage the indirect control of the modified

servo valve. The redesigned system meets all technical and operational requirements while the inner structure of the servo valve and the engine valve body can still be kept.

In order to guarantee an optimal system operation in the following chapter the system components will be configured using the laws of mathematics and physics with regard to the mentioned maximum engine speed of $8000\,{}^{1}/_{min}$ and calculated eigen angular frequency $\omega_0 = 418.90\,{}^{1}/_{s}$.

5 Mathematical fundamentals

Initially, in this chapter the changed lever transmission ratio and the resulting travel range of the control piston will be calculated. In order to substantiate the system design presented in the previous sections this chapter contains the layout of the compression springs used within the redesigned system. Finally, the masses in motion and the maximum occurring acceleration will be calculated to determine the required oil discharge sections of the servo cylinder that is situated within the control unit. All calculations will be carried out considering the hydraulic system pressure of $15\,MPa$ and the maximum theoretical and hence critical engine speed of $8000\,{}^{1}/_{min}$.

5.1 Lever transmission ratio and travel range

Due to the fact that the oil volume within the lever transmission should be kept as small as possible the translation piston features a diameter of only $20\,mm$ instead of $40\,mm$ as in the previous FVVT setup. The $4\,mm$ diameter of the part of the control piston that extends into the lever transmission is equivalent to the diameter used in the previous setup to ensure sufficient strength of the piston. Analogous to Section 3.2 the new lever transmission ratio can be calculated:

$$\hat{i} = \frac{\hat{A}_{tp}}{A_{cp}} = \frac{\frac{\pi}{4} \cdot \hat{d}_{tp}^2}{\frac{\pi}{4} \cdot d_{cp}^2} \tag{5.1}$$

$$= \frac{\frac{\pi}{4} \cdot (20\,mm)^2}{\frac{\pi}{4} \cdot (4\,mm)^2} \tag{5.2}$$

$$= \frac{314.16\,mm^2}{12.57\,mm^2} \tag{5.3}$$

$$\approx \underline{\underline{25}} \tag{5.4}$$

where

$\hat{i}$ = modified lever transmission ratio
$\hat{A}_{tp}$ = front surface of the modified translation piston
A_{cp} = front surface of the control piston
$\hat{d}_{tp}$ = diameter of the modified translation piston
d_{cp} = diameter of the control piston

Thus the travel range of the control piston s_{cp} can be calculated as follows:

$$s_{cp} = s_{tp} \cdot \hat{i} = 0.12\,mm \cdot 25 \tag{5.5}$$

$$= \underline{\underline{3\,mm}} \tag{5.6}$$

The lever transmission ratio and maximum travel range of the control piston have been reduced by 75 % in the case of the redesigned system. As discussed before this allows a faster adjustment of the control piston position and will enhance system control as the system will be more responsive. This is important especially for high engine speeds where the time for a valve actuation is very limited. According to the modified control piston travel range a new servo cylinder for the control unit needed to be designed. Figure 5.1 shows a drawing of this cylinder (next page).

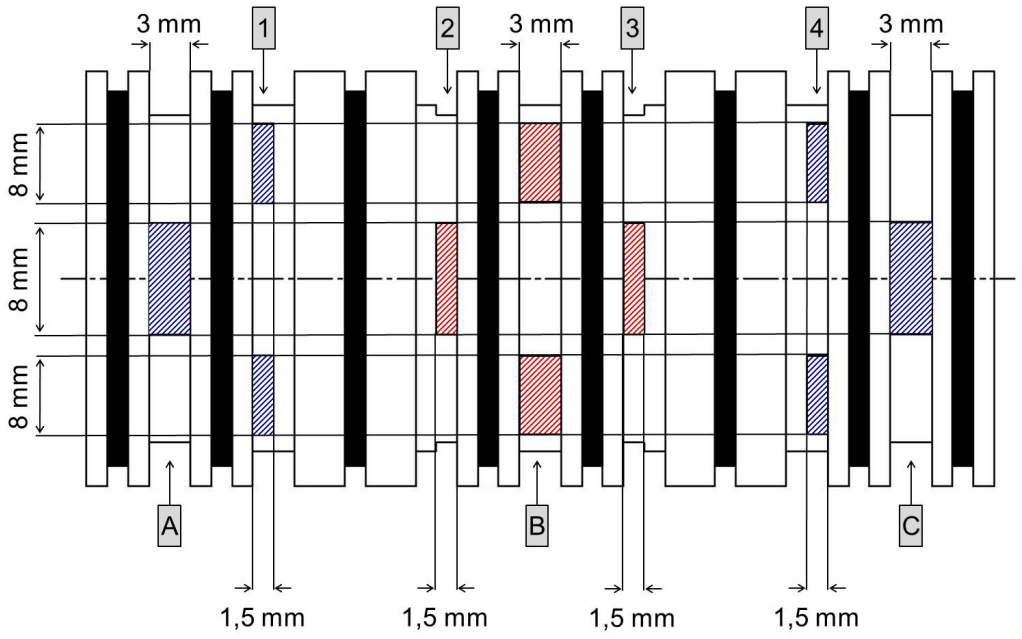

Figure 5.1: Servo cylinder of the control unit

The design of this servo cylinder is inspired by the design of the servo cylinder used within the existing servo valve. The design could be proved suitable for transferring the hydraulic transmitting medium to the correspondent hydraulic ducts within the available time in order to operate the engine valves.

The new servo cylinder features windows with sharp edges that are used to distribute the oil to the relevant hydraulic ducts within the control unit. Grooves (A), (B) and (C) each feature four large windows. In accordance with Figure 4.5 the windows in groove (B) are used for the pressure supply while the windows in grooves (A) and (C) are leading to the oil reservoir return lines.

The windows in grooves (1)-(4) are crucial for the system control. Again, four windows are embedded into each groove in order to maximize the overall section available for the oil flow. These narrower windows are so fundamental for the control as the four piston elements open or close these windows depending on the piston position, as explained in Subsection 4.3.3. The sharp edges of the rectangular windows allow a precise control of oil flow while the edges of the control piston elements are moved across them.

Due to the maximum travel range of the control piston $s_{cp} = 3\,mm$ the width of each window in grooves (1)-(4) is equivalent to $1.5\,mm$. As two movements of the control piston by $1.5\,mm$ from its initial position allow for reaching all three basic switching positions according to Subsection 4.3.3, this determines the width of the mentioned windows.

The eight grooves that are marked in black in Figure 5.1 are the areas where o-rings will be used in order to seal the oil compartments against each other. This ensures that pressurized oil is supplied only to the ducts desired.

The laws of mathematics and physics will be used in Section 5.3 to prove that the dimensions of the windows in the circumference of the servo cylinder are laid out sufficiently to ensure an unproblematic control of the system to the point of its maximum operation frequency. To conduct these calculations it is necessary to firstly lay out the compression springs used within the system due to the fact that the spring forces need to be known to calculate the sectional area required for a timely pressure decrease on one side of the servo piston. This will be thoroughly explained in Section 5.3.

5.2 Layout of the compression springs

In this section the required properties of the compression springs utilized within the control unit and servo valve will be calculated. With the aid of the critical eigen angular frequency calculated in Section 4.2, the required spring stiffness can be determined.

5.2.1 Single compression spring of the control unit

For the eigen angular frequency Equation 5.7 is valid:

$$\omega_0 = \sqrt{\frac{c_1}{m_{trans} + \frac{m_s}{3}}} \tag{5.7}$$

where

c_1 = spring stiffness
m_{trans} = mass of the components in motion
m_s = mass of the spring

Converted according to the spring stiffness this results in:

$$c_1 = \omega_0^2 \cdot (m_{trans} + \frac{m_s}{3}) \tag{5.8}$$

The mass of the components in motion and the mass of the spring are yet unknown values. For a first mathematical approach a spring mass of $m_s = 5\,g$ will be supposed. The mass of the components in motion will be calculated in the following and consists of the mass of the translation piston, the mass of the oil volume within the lever transmission and the mass of the control piston. All these components are subject to translatory inertia within the control unit while the piezo actuator extends or contracts. Hence follows:

$$m_{trans} = m_{tp} + m_{oil} + m_{cp} \tag{5.9}$$

where

m_{tp} = mass of the translation piston
m_{oil} = mass of the hydraulic oil in the lever transmission
m_{cp} = mass of the control piston

In order to calculate the overall value of m_{trans} initially the volumes of the associated components will be determined. Considering the distinct densities of the components the mass will be calculated. The translation piston consists of the partial bodies illustrated in Figure 5.2 (next page).

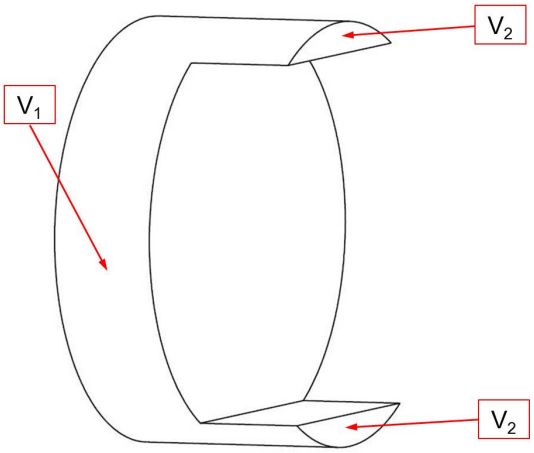

Figure 5.2: Partial bodies of the translation piston

Volume V_2 is composed of two identical cylinder segments that are used for the guidance of the translation piston on the corresponding connection piece of the piezo actuator. Thus the volume of the translation piston V_{tp} is as follows:

$$V_{tp} = V_1 + V_2 \tag{5.10}$$

$$V_1 = \frac{\pi}{4} \cdot d_1^2 \cdot h_1 = \frac{\pi}{4} \cdot (0.02\,m)^2 \cdot 0.005\,m \tag{5.11}$$

$$= \underline{\underline{1.57 \cdot 10^{-6}\,m^3}} \tag{5.12}$$

$$V_2 = 2 \cdot [h_2 \cdot (\pi \cdot \frac{r_2^2}{2} - r_2^2 \cdot arcsin(1 - \frac{t_2}{r_2}) - (r_2 - t_2) \cdot \sqrt{t_2 \cdot (2 \cdot r_2 - t_2)})] \tag{5.13}$$

$$\begin{aligned} = 2 \cdot [0.0051\,m \cdot (\pi \cdot \frac{(0.01\,m)^2}{2} - (0.01\,m)^2 \cdot arcsin(1 - \frac{0.0015\,m}{0.01\,m}) \\ -(0.01\,m - 0.0015\,m) \cdot \sqrt{0.0015\,m \cdot (2 \cdot 0.01\,m - 0.0015\,m)})] \end{aligned} \tag{5.14}$$

$$= \underline{\underline{10.92 \cdot 10^{-8}\,m^3}} \tag{5.15}$$

$$\Rightarrow V_{tp} = (1.57 \cdot 10^{-6} + 10.92 \cdot 10^{-8})\,m^3 = \underline{\underline{1.679 \cdot 10^{-6}\,m^3}} \tag{5.16}$$

where

$V_{1/2}$ = volume of the partial bodies
d_1 = diameter of volume V_1
$h_{1/2}$ = height of the partial bodies
r_2 = radius of volume V_2
t_2 = width of cylinder segment V_2

The mass of the translation piston that will be made of a suitably strong aluminium alloy is:

$$m_{tp} = \rho_{AlZnMgCu} \cdot V_{tp} = 2800 \frac{kg}{m^3} \cdot 1.679 \cdot 10^{-6}\, m^3 \tag{5.17}$$

$$= \underline{\underline{4.7 \cdot 10^{-3}\, kg}} \tag{5.18}$$

where

$\rho_{AlZnMgCu}$ = density of the employed aluminium alloy

The individual component material choice will be explained in Chapter 6.

As explained in Subsection 4.3.1 the distance between translation and control piston within the control unit is $0.4\, mm$ when no voltage is applied to the piezo actuator. Based on this distance and the diameter of the translation piston the oil volume in the lever transmission V_{oil} can be calculated:

$$V_{oil} = \frac{\pi}{4} \cdot d_1^2 \cdot h_{oil} = \frac{\pi}{4} \cdot (0.02\, m)^2 \cdot 0.0004\, m \tag{5.19}$$

$$= \underline{\underline{1.26 \cdot 10^{-7}\, m^3}} \tag{5.20}$$

where

h_{oil} = height of the oil volume in the lever transmission

For the FVVT system the hydraulic oil "HLP 46" according to DIN[14] 51524 – 2 is being used. With its density in the next step the mass of the hydraulic oil in the lever transmission can be determined:

$$m_{oil} = \rho_{oil} \cdot V_{oil} = 874 \frac{kg}{m^3} \cdot 1.26 \cdot 10^{-7}\, m^3 \tag{5.21}$$

$$= \underline{\underline{1.101 \cdot 10^{-4}\, kg}} \tag{5.22}$$

where

ρ_{oil} = density of the hydraulic oil in the lever transmission

The control piston consists of the partial bodies shown in Figure 5.3.

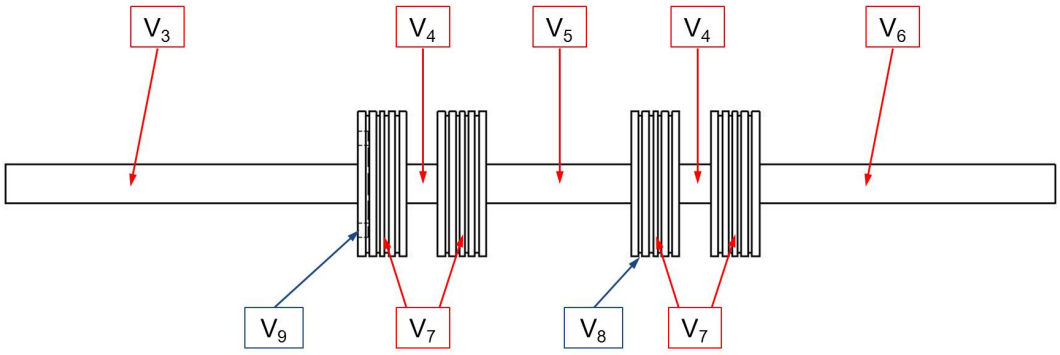

Figure 5.3: Partial bodies of the control piston

Volumes V_8 and V_9, illustrated in blue, need to be subtracted from the overall volume of the control piston. V_8 includes 16 grooves that are used to absorb excessive hydraulic oil while the piston is moving within the servo cylinder. V_9 on the other hand is a groove that carries the return spring that has been illustrated in Figures

[14]Deutsches Institut für Normung = German Institute for Standardization

4.4 and 4.5. Volume V_3 extends out of the control unit in order to connect to a displacement sensor. The use of this sensor is crucial for the system regulation.

Hence the overall volume of the control piston V_{cp} is:

$$V_{cp} = V_3 + V_4 + V_5 + V_6 + V_7 - 16 \cdot V_8 - V_9 \tag{5.23}$$

$$V_3 = \frac{\pi}{4} \cdot d_3^2 \cdot h_3 = \frac{\pi}{4} \cdot (0.004\,m)^2 \cdot 0.0365\,m \tag{5.24}$$

$$= \underline{\underline{4.59 \cdot 10^{-7}\,m^3}} \tag{5.25}$$

$$V_4 = 2 \cdot (\frac{\pi}{4} \cdot d_4^2 \cdot h_4) = 2 \cdot (\frac{\pi}{4} \cdot (0.004\,m)^2 \cdot 0.00325\,m) \tag{5.26}$$

$$= \underline{\underline{8.2 \cdot 10^{-8}\,m^3}} \tag{5.27}$$

$$V_5 = \frac{\pi}{4} \cdot d_5^2 \cdot h_5 = \frac{\pi}{4} \cdot (0.004\,m)^2 \cdot 0.015\,m \tag{5.28}$$

$$= \underline{\underline{1.88 \cdot 10^{-7}\,m^3}} \tag{5.29}$$

$$V_6 = \frac{\pi}{4} \cdot d_6^2 \cdot h_6 = \frac{\pi}{4} \cdot (0.004\,m)^2 \cdot 0.0306\,m \tag{5.30}$$

$$= \underline{\underline{3.85 \cdot 10^{-7}\,m^3}} \tag{5.31}$$

$$V_7 = 4 \cdot (\frac{\pi}{4} \cdot d_7^2 \cdot h_7) = 4 \cdot (\frac{\pi}{4} \cdot (0.015\,m)^2 \cdot 0.005\,m) \tag{5.32}$$

$$= \underline{\underline{3.53 \cdot 10^{-6}\,m^3}} \tag{5.33}$$

$$V_8 = \frac{\pi}{4} \cdot h_8 \cdot (d_7^2 - d_8^2) = \frac{\pi}{4} \cdot 0.0004\,m \cdot ((0.015\,m)^2 - (0.0142\,m)^2) \tag{5.34}$$

$$= \underline{\underline{7 \cdot 10^{-9}\,m^3}} \tag{5.35}$$

$$V_9 = \frac{\pi}{4} \cdot h_9 \cdot (d_{9,1}^2 - d_{9,2}^2) = \frac{\pi}{4} \cdot 0.001\,m \cdot ((0.011\,m)^2 - (0.0081\,m)^2) \tag{5.36}$$

$$= \underline{\underline{4.4 \cdot 10^{-8}\,m^3}} \tag{5.37}$$

$$\begin{aligned} \Rightarrow V_{cp} = (&4.59 \cdot 10^{-7} + 8.2 \cdot 10^{-8} + 1.88 \cdot 10^{-7} + 3.85 \cdot 10^{-7} \\ &+3.53 \cdot 10^{-6}\,m^3 - 16 \cdot 7 \cdot 10^{-9} - 4.4 \cdot 10^{-8})\,m^3 \end{aligned} \tag{5.38}$$

$$= \underline{\underline{4.488 \cdot 10^{-6}\,m^3}} \tag{5.39}$$

where

V_{3-9} = volume of the partial bodies
d_{3-9} = diameter of the partial bodies
h_{3-9} = height of the partial bodies

The mass of the control piston sums up to:

$$m_{cp} = \rho_{42CrMo4} \cdot V_{cp} = 7720\,\frac{kg}{m^3} \cdot 4.488 \cdot 10^{-6}\,m^3 \tag{5.40}$$

$$= \underline{\underline{3.46 \cdot 10^{-2}\,kg}} \tag{5.41}$$

where

$\rho_{42CrMo4}$ = density of the employed chromium steel

Based on these results the overall mass of the components in motion can be calculated using Equation 5.9:

$$m_{trans} = (4.7 \cdot 10^{-3} + 1.101 \cdot 10^{-4} + 3.46 \cdot 10^{-2})\,kg \tag{5.42}$$

$$= \underline{\underline{3.94 \cdot 10^{-2}\,kg}} \tag{5.43}$$

This overall mass in combination with the supposed spring mass of $5\,g$ and the eigen angular frequency leads to the determination of the required spring stiffness according to Equation 5.8:

$$c_1 = (418.90\,\frac{1}{s})^2 \cdot (3.94 \cdot 10^{-2}\,kg + \frac{0.005\,kg}{3}) \tag{5.44}$$

$$= \underline{\underline{7206.26\,\frac{N}{m}}} = \underline{\underline{7.21\,\frac{N}{mm}}} \tag{5.45}$$

In the calculated case the spring features the resonance frequency of the FVVT system of $67\,Hz$ as calculated in Section 4.2. In order to avoid the appearance of resonance in any circumstance a spring with significantly higher stiffness will be chosen. As a displacement transducer will be connected to volume V_3, the mass of the components in motion will be further increased, which leads to a higher required spring stiffness. The chosen stiffness is about 79 % higher than the minimum required value of $7.21\,{}^{N}/_{mm}$. This will allow the connection of displacement sensor parts in motion to the control piston with a total weight of $33\,g$ without reaching the resonance frequency. The spring features the following properties:

spring stiffness:	$c_1 = 12926\,\frac{N}{mm}$
wire diameter:	$d_w = 1.45\,mm$
external wire diameter:	$D_e = 11\,mm$
free length of the spring:	$L_0 = 16.5\,mm$
length of the compressed spring:	$L_1 = 10.14\,mm$
wire mass:	$m_w = 2.333\,g$
number of coils:	$n_c = 4$

The used material is spring steel according to EN $10270 - 1$ SM(B) specifications (EN stands for Europäische Norm = European Standard). As the spring properties are known the actual eigen angular frequency $\hat{\omega}_0$ can be determined:

$$\hat{\omega}_0 = \sqrt{\frac{c_1}{m_{trans} + \frac{m_s}{3}}} \tag{5.46}$$

$$= \sqrt{\frac{12926 \frac{N}{m}}{3.94 \cdot 10^{-2}\, kg + \frac{0.002333\, kg}{3}}} \tag{5.47}$$

$$= \underline{\underline{567.2 \frac{1}{s}}} \tag{5.48}$$

The calculated eigen angular frequency is situated significantly above the FVVT system frequency $\omega_0 = 418.90\, {}^1\!/_s$. With eigen angular frequency and spring mass being inversely proportional and the spring featuring a mass that is over 53 % reduced contrary to the first assumption, this leads to a further increased value of ω_0. Hence a higher safety against reaching the resonance frequency is achieved. Adapted from the above calculated the actual resonance frequency $\hat{f}_0$ is:

$$\hat{f}_0 = \frac{\hat{\omega}_0}{2 \cdot \pi} = \frac{567.2 \frac{1}{s}}{2 \cdot \pi} \tag{5.49}$$

$$= \underline{\underline{90.27\, Hz}} \approx \underline{\underline{90\, Hz}} \tag{5.50}$$

The value of $\hat{f}_0$ is more than 34 % above the system resonance frequency of $f_0 = 67\, Hz$. Hence resonance will not occur while the control unit is being operated.

5.2.2 Identical compression springs of the servo valve

Two identical compression springs are used within the servo valve. The only mass in motion within the servo valve is the servo piston that fulfils a reciprocating translation while the system is being operated. For the eigen angular frequency in the viewed case Equation 5.51 is valid:

$$\omega_0 = \sqrt{\frac{c_1 + c_2}{m_{sp} + \frac{m_s}{3}}} \tag{5.51}$$

where

$c_{1/2}$ = spring stiffness

m_{sp} = mass of the servo piston

Converted according to the spring stiffness this results in:

$$c_1 + c_2 = \omega_0^2 \cdot (m_{sp} + \frac{m_s}{3}) \tag{5.52}$$

The mass of the servo piston and the spring are yet unknown. This time an overall spring mass of $m_s = 5\,g$ will be supposed for a first mathematical approach as the same spring material will be used and the assumption taken for the spring of the control unit was around 100 % too high. The mass of the servo piston will be calculated subsequently. The partial bodies of the servo piston are shown in Figure 5.4.

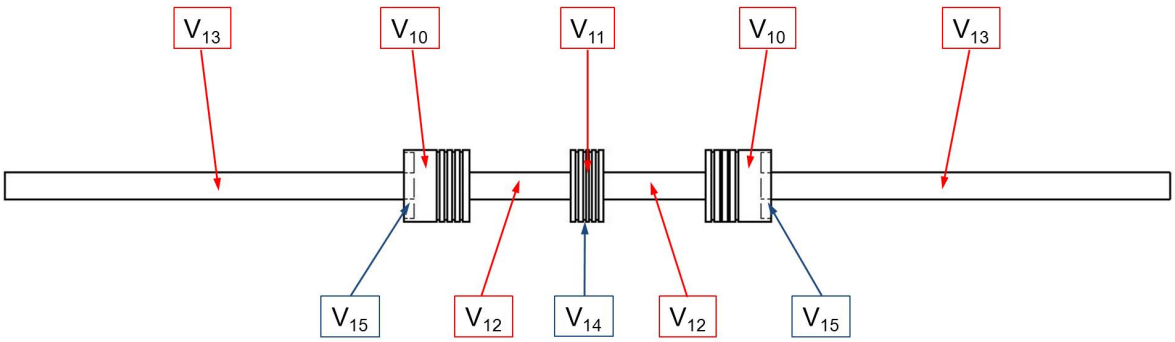

Figure 5.4: Partial bodies of the servo piston

Volumes V_{14} and V_{15}, illustrated in blue again, need to be subtracted from the overall volume of the servo piston. V_{14} includes 12 grooves that have the same purpose as in the case of the control piston. V_{15} contains the two grooves that are used to guide the two compression springs within the servo valve. Volumes V_{13} extend

out of the servo valve in order to connect to a displacement measurement device, which again is necessary for a reproducible operation of the FVVT system. It is only required to connect this transducer to one of the two volumes extending out of the servo valve body. However, the servo piston features a symmetrical design to guarantee equivalent pressure surface areas on both piston ends. These ensure that the same force is applied to both surface areas while full system pressure is maintained.

Thus the overall volume of the servo piston V_{sp} calculates as follows:

$$V_{sp} = V_{10} + V_{11} + V_{12} + V_{13} - 12 \cdot V_{14} - V_{15} \tag{5.53}$$

$$V_{10} = 2 \cdot (\frac{\pi}{4} \cdot d_{10}^2 \cdot h_{10}) = 2 \cdot (\frac{\pi}{4} \cdot (0.011\,m)^2 \cdot 0.01\,m) \tag{5.54}$$

$$= \underline{\underline{1.90 \cdot 10^{-6}\,m^3}} \tag{5.55}$$

$$V_{11} = \frac{\pi}{4} \cdot d_{11}^2 \cdot h_{11} = \frac{\pi}{4} \cdot (0.011\,m)^2 \cdot 0.005\,m \tag{5.56}$$

$$= \underline{\underline{4.75 \cdot 10^{-7}\,m^3}} \tag{5.57}$$

$$V_{12} = 2 \cdot (\frac{\pi}{4} \cdot d_{12}^2 \cdot h_{12}) = 2 \cdot (\frac{\pi}{4} \cdot (0.004\,m)^2 \cdot 0.0155\,m) \tag{5.58}$$

$$= \underline{\underline{3.9 \cdot 10^{-7}\,m^3}} \tag{5.59}$$

$$V_{13} = 2 \cdot (\frac{\pi}{4} \cdot d_{13}^2 \cdot h_{13}) = 2 \cdot (\frac{\pi}{4} \cdot (0.004\,m)^2 \cdot 0.0625\,m) \tag{5.60}$$

$$= \underline{\underline{1.57 \cdot 10^{-6}\,m^3}} \tag{5.61}$$

$$V_{14} = \frac{\pi}{4} \cdot h_{14} \cdot (d_{11}^2 - d_{14}^2) = \frac{\pi}{4} \cdot 0.0004\,m \cdot ((0.011\,m)^2 - (0.0102\,m)^2) \tag{5.62}$$

$$= \underline{\underline{5 \cdot 10^{-9}\,m^3}} \tag{5.63}$$

$$V_{15} = 2 \cdot (\frac{\pi}{4} \cdot d_{15}^2 \cdot h_{15}) = 2 \cdot (\frac{\pi}{4} \cdot (0.010\,m)^2 \cdot 0.0015\,m) \tag{5.64}$$

$$= \underline{\underline{2.36 \cdot 10^{-7}\,m^3}} \tag{5.65}$$

$$\begin{aligned} \Rightarrow V_{sp} = (1.90 \cdot 10^{-6} + 4.75 \cdot 10^{-7} + 3.9 \cdot 10^{-7} + 1.57 \cdot 10^{-6} \\ -12 \cdot 5 \cdot 10^{-9} - 2.36 \cdot 10^{-7})\,m^3 \end{aligned} \tag{5.66}$$

$$= \underline{\underline{4.04 \cdot 10^{-6}\,m^3}} \tag{5.67}$$

where

V_{10-15} = volume of the partial bodies
d_{10-15} = diameter of the partial bodies
h_{10-15} = height of the partial bodies

The mass of the servo piston sums up to:

$$m_{sp} = \rho_{42CrMo4} \cdot V_{sp} = 7720\,\frac{kg}{m^3} \cdot 4.04 \cdot 10^{-6}\,m^3 \tag{5.68}$$

$$= \underline{\underline{3.119 \cdot 10^{-2}\,kg}} \tag{5.69}$$

With the mass of the components in motion within the servo valve now known the required spring stiffness can be calculated according to Equation 5.52:

$$c_1 + c_2 = (418.90\,\frac{1}{s})^2 \cdot (3.119 \cdot 10^{-2}\,kg + \frac{0.005\,kg}{3}) \tag{5.70}$$

$$= \underline{\underline{5765.6\,\frac{N}{m}}} \tag{5.71}$$

Consequently for each of the two identical springs follows:

$$c_1 = c_2 = \frac{1}{2} \cdot 5765.6 \, \frac{N}{m} \tag{5.72}$$

$$= \underline{\underline{2882.8 \, \frac{N}{m}}} = \underline{\underline{2.88 \, \frac{N}{mm}}} \tag{5.73}$$

Considering the required stiffness and supposed spring mass of $5\,g$, both springs feature the resonance frequency of the FVVT system of $67\,Hz$ again. As in the previous case, springs with significantly higher stiffness will be chosen to avoid the appearance of resonance in any circumstance. This will allow the connection of displacement sensor parts in motion to the servo piston with a total weight of $26\,g$ without reaching the resonance frequency. Each of the identical springs features the following properties:

spring stiffness:	$c_{1/2} = 5166 \, \frac{N}{mm}$
wire diameter:	$d_w = 1.2\,mm$
external wire diameter:	$D_e = 10\,mm$
free length of the spring:	$L_0 = 26\,mm$
length of the compressed spring:	$L_1 = 11.55\,mm$
wire mass:	$m_w = 1.964\,g$
number of coils:	$n_c = 6$

As in the previous case spring steel according to EN $10270 - 1$ SM(B) specifications will be used. With the aid of the spring properties the actual eigen angular frequency $\hat{\omega}_0$ can be determined:

$$\hat{\omega}_0 = \sqrt{\frac{c_1 + c_2}{m_{sp} + \frac{m_s}{3}}} \tag{5.74}$$

$$= \sqrt{\frac{5166 \, \frac{N}{m} + 5166 \, \frac{N}{m}}{3.119 \cdot 10^{-2}\,kg + \frac{2 \cdot 0.001964\,kg}{3}}} \tag{5.75}$$

$$= \underline{\underline{563.84 \, \frac{1}{s}}} \tag{5.76}$$

The calculated eigen angular frequency is significantly higher than the FVVT system frequency $\omega_0 = 418.90\,{}^1\!/_s$. The actual resonance frequency $\hat{f}_0$ is:

$$\hat{f}_0 = \frac{\hat{\omega}_0}{2 \cdot \pi} = \frac{563.84\,\frac{1}{s}}{2 \cdot \pi} \tag{5.77}$$

$$= \underline{\underline{89.74\,Hz}} \approx \underline{\underline{90\,Hz}} \tag{5.78}$$

Again, the value of $\hat{f}_0$ is situated more than 34 % above the system resonance frequency of $f_0 = 67\,Hz$. Thus resonance will not occur while the servo valve is being operated.

5.3 Servo cylinder discharge section layout

As mentioned in Section 5.1 with the spring stiffness now known the required size of the oil displacement windows in the servo cylinder of the control unit can be determined.

To ensure that the control unit is able to reliably control the FVVT system up to the current maximum thoretical engine speed of $8000\,{}^1\!/_{min}$, the oil volume being displaced by the servo piston within the servo valve in any circumstance has to be successfully returned into the oil reservoir with the aid of control edges that are operated by the piston.

The largest possible oil volume has to be discharged when the servo piston is moved from one mechanical stop to the other. Executing this motion it travels its maximum distance of $10\,mm$. The maximum oil displacement volume is illustrated in Figure 5.5 (next page).

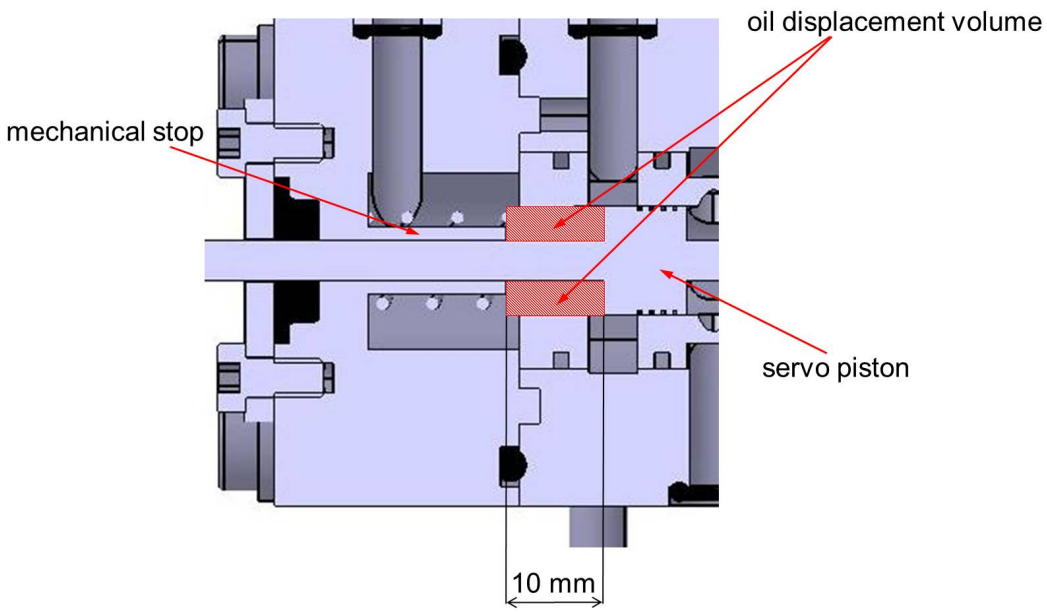

Figure 5.5: Oil volume displaced during reciprocating servo piston motion

The oil displacement volume V_{dis} calculates as follows:

$$V_{dis} = \frac{\pi}{4} \cdot h_{dis} \cdot (d_{10}^2 - d_{13}^2) = \frac{\pi}{4} \cdot 0.01\,m \cdot ((0.011\,m)^2 - (0.004\,m)^2) \tag{5.79}$$

$$= \underline{\underline{8.25 \cdot 10^{-7}\,m^3}} \tag{5.80}$$

where

h_{dis} = height of the oil displacement volume

According to Section 4.2, the time available for one valve operation is equivalent to $7.83\,ms$ at an engine speed of $8000\,{}^1/_{min}$. Within this time one valve actuation has to be completed, which includes opening the valve to the full valve lift and closing it again in accordance with the valve lift curve that has been presented in Figure 4.2. Just in the apex of the lift curve the servo piston direction has to be changed in order to proceed from the position illustrated in Case C*) to the position shown in Case A*) (see Figure 4.8) and close the engine valves. As soon as the direction of the

servo piston is inverted, the time available to close the engine valves elapses as soon as the valve lift curve again reaches a valve travel of zero. During the valve opening procedure the correspondent time available is situated between the beginning of the ascending slope of the lift curve and the apex.

As for the K71 engine the valve lift graph generally features a symmetrical progression, although the closing slope, compared to the opening slope, shows a more continuous gradient approaching the zero lift line. Due to the basic symmetry the time t_{dis} considered available for displacing the oil volume shown in Figure 5.5 is half of the valve operation time indicated in the lift curve:

$$t_{dis} = \frac{1}{2} \cdot t_{open} \tag{5.81}$$

$$= \frac{1}{2} \cdot 7.83\,ms \approx \underline{\underline{3.92\,ms}} \tag{5.82}$$

It can be assumed that within the timeframe of $3.92\,ms$, after the servo piston has reached one of the mechanical stops, also the valve opening or closing process respectively is terminated. With its beginning translation the servo piston allows oil flow through the respective hydraulic ducts (D) to (H) (compare Figure 4.8) as these are gradually opened by the edges of the piston elements moving past them. Thereby the inversion of engine valve direction begins already before the piston reaches the mechanical stop. Supportively, the system pressure of $15\,MPa$ is of such a high amount that a delayed control of the engine valve position is not expected.

Using Equation 5.83 the required discharge section of the servo cylinder that is used in the control unit can be determined. This is the section A_{dis} through which the oil volume displaced by the servo piston will be returned into the reservoir.

$$Q_{dis} = w_{dis} \cdot A_{dis} \Leftrightarrow A_{dis} = \frac{Q_{dis}}{w_{dis}} \tag{5.83}$$

where

Q_{dis} = flow rate of the oil displacement volume
w_{dis} = displacement oil flow velocity

With the equations:

$$Q_{dis} = \frac{V_{dis}}{t_{dis}} \tag{5.84}$$

and

$$\Delta p = \frac{\rho_{oil}}{2} \cdot (w_{dis})^2 \Leftrightarrow w_{dis} = \sqrt{\frac{2 \cdot \Delta p}{\rho_{oil}}} \tag{5.85}$$

inserted in Equation 5.83 this results in:

$$A_{dis} = \frac{V_{dis}}{t_{dis} \cdot \sqrt{\frac{2 \cdot \Delta p}{\rho_{oil}}}} \tag{5.86}$$

where

Δp = required hydraulic pressure difference

Within this equation Δp is the only unknown and represents the pressure difference that enables a complete translatory motion of the servo piston to one of its mechanical stops within t_{dis}. In order to determine Δp, firstly the reduced hydraulic pressure p_{red} in the according duct (J) or (L) on either side of the servo piston (compare Figure 4.7), allowing for a servo piston movement, has to be calculated. In the duct on the respective opposing side full system pressure is applied throughout the whole translation process. With the pressure being defined as force divided by area and only the front surfaces of the servo piston yet known, first the acting forces need to be identified:

$$\Delta p = p_{hyd} - p_{red} \tag{5.87}$$

$$p_{red} = \frac{F_{red}}{A_{hyd}} \tag{5.88}$$

where

p_{hyd} = hydraulic system pressure
F_{red} = compressive force acting at reduced hydraulic pressure
A_{hyd} = servo piston area the particular compressive force acts upon

whereas F_{red} is defined as follows:

$$F_{red} = F_{hyd} - F_{tot} \tag{5.89}$$

where

F_{hyd} = compressive force acting at full hydraulic pressure
F_{tot} = total force to be overcome to allow servo piston motion

The force remaining within the duct in which the pressure is being decreased must not exceed the value of the maximum compressive force F_{hyd} acting upon the opposing front surface of the servo piston minus all forces that need to be overcome from a dynamic point of view. Only in this way a translatory motion of the servo piston is possible under any conditions. F_{hyd} results in:

$$F_{hyd} = p_{hyd} \cdot A_{hyd} = p_{hyd} \cdot \frac{\pi}{4} \cdot (d_{10}^2 - d_{13}^2) \tag{5.90}$$

$$= 1.5 \cdot 10^7 \frac{N}{m^2} \cdot \frac{\pi}{4} \cdot ((0.011\,m)^2 - (0.004\,m)^2) \tag{5.91}$$

$$= \underline{\underline{1237\,N}} \tag{5.92}$$

The total force that needs to be overcome is:

$$F_{tot} = F_m + F_s + F_f \tag{5.93}$$

where

F_m = mass force to be overcome to enable servo piston motion
F_s = spring force to be overcome to enable servo piston motion
F_f = frictional force to be overcome to enable servo piston motion

Each component of F_{tot} needs to be determined subsequently. The servo piston experiences an acceleration that is directly proportional to the applied force acting upon it. Thus, the mass force F_m can be calculated according to the second axiom of Newton[15]:

$$F_m = (m_{sp} + m_s) \cdot a_{sp} \tag{5.94}$$

where

a_{sp} = maximum acceleration of the servo piston

a_{sp} is the only unknown within this equation. In the viewed case of maximal theoretical engine speed the servo piston needs to travel the full distance of $10\,mm$ between the two mechanical stops within $t_{dis} = 3.92\,ms$ in order to fulfil an engine valve opening or closing procedure. In order to determine a_{sp} a calculation based on a uniformly accelerated motion will be supposed:

[15]second of three laws of motion, formulated by and named after Isaac Newton, 1643-1727, English physicist and mathematician

$$s = \frac{1}{2} \cdot a \cdot t^2 + v_0 \cdot t + s_0 \tag{5.95}$$

where

s = displacement
a = acceleration
t = time
v_0 = initial velocity
s_0 = initial displacement

As the viewed servo piston motion begins at one of the mechanical stops just before the piston changes direction v_0 can be considered zero. As this is the initial point of the servo piston motion s_0 also is zero. This leads to the servo piston acceleration:

$$s_{sp} = \frac{1}{2} \cdot a_{sp} \cdot t_{dis}^2 \Leftrightarrow a_{sp} = 2 \cdot \frac{s_{sp}}{t_{dis}^2} \tag{5.96}$$

For the maximum servo piston acceleration follows Equation 5.97:

$$a_{sp} = 2 \cdot \frac{10 \cdot 10^{-3}\, m}{(3.92 \cdot 10^{-3}\, s)^2} \tag{5.97}$$

$$= \underline{\underline{1301.54 \, \frac{m}{s^2}}} \tag{5.98}$$

The calculated value is equivalent to approximately $133\, g$ ($1\, g = 9.81\, {}^{m}/_{s^2}$). With a_{sp} now known the maximum mass force that needs to be overcome can be determined according to Equation 5.94:

$$F_m = ((3.119 \cdot 10^{-2} + 2 \cdot 1.964 \cdot 10^{-3})\, kg) \cdot 1301.54 \, \frac{m}{s^2} \tag{5.99}$$

$$= \underline{\underline{45.71\,N}} \tag{5.100}$$

The mass force acts against the maximum compressive force F_{hyd} and hence needs to be overcome by the latter in order to allow a servo piston translation. In the next step the spring force F_s will be determined. As soon as the servo piston reaches one of the mechanical stops, the respective spring on this side of the piston is compressed to the highest extent. A preload displacement of the springs of $s_{s,pre} = 2\,mm$ has been chosen to guarantee that the spring that is placed at the adjustable side within the servo valve stays preloaded even if it is necessary to slightly unload it to match the spring on the other side (as explained in Subsection 4.3.2). This ensures a reliable guidance of the spring in any circumstance. The preload displacement will be considered in this calculation which leads to the maximum spring force $F_{s,max}$:

$$F_{s,max} = c_{1/2} \cdot (s_{s,max} + s_{s,pre}) \tag{5.101}$$

$$= 5166\,\frac{N}{m} \cdot ((10+2) \cdot 10^{-3}\,m) \tag{5.102}$$

$$= \underline{\underline{61.99\,N}} \tag{5.103}$$

where

$s_{s,max}$ = maximum spring compression displacement

The force $F_{s,max}$ has to be overcome by F_{hyd} as well. But it needs to be considered that the spring on the opposed side gradually extends from its compressed state and supports the servo piston motion due to its force having the same direction as F_{hyd}. This spring features the minimum spring force $F_{s,min}$ according to its remaining preload displacement of $2\,mm$:

$$F_{s,min} = c_{1/2} \cdot s_{s,pre} = 5166 \frac{N}{m} \cdot 2 \cdot 10^{-3}\, m \tag{5.104}$$

$$= \underline{\underline{10.33\, N}} \tag{5.105}$$

The actual spring force to be overcome can be calculated as follows:

$$F_s = F_{s,max} - F_{s,min} = (61.99 - 10.33)\, N \tag{5.106}$$

$$= \underline{\underline{51.66\, N}} \tag{5.107}$$

The frictional force which is the last unknown before the total force to be overcome can be determined originates from the oil film between the peripheral surfaces of the servo piston and servo cylinder adjacent to one another. As general tolerances according to DIN ISO 2768-1 and 2768-2 (ISO for International Organization for Standardization) in the finest classes “f” and “H” respectively are used for the manufacturing process, the clearance between servo piston and servo cylinder is minimal, increasing the friction of the hydraulic fluid-particles.

Since the basic dimensions of servo piston and cylinder remain as originally considered in the afore-mentioned feasibility sutdy, the frictional force, which already has been calculated with regard to the temperature dependent values of viscosity and density of the hydraulic oil is adopted from the study and is:

$$F_f = \underline{\underline{7.48\, N}}\ [3] \tag{5.108}$$

With all necessary values known, now the total force that needs to be overcome in order to enable a movement of the servo piston can be calculated according to Equation 5.93:

$$F_{tot} = (45.71 + 51.66 + 7.48)\, N \tag{5.109}$$

$$= \underline{\underline{104.85\,N}} \tag{5.110}$$

According to Equation 5.89 the compressive force acting at reduced hydraulic pressure that has to be reached within the available time in order to allow a servo piston movement is:

$$F_{red} = (1237 - 104.85)\,N \tag{5.111}$$

$$= \underline{\underline{1132.15\,N}} \tag{5.112}$$

Using Equations 5.87 and 5.88 the reduced hydraulic pressure and the required hydraulic pressure difference can be determined:

$$\Delta p = (1.5 - 1.37) \cdot 10^7\,\frac{N}{m^2} \tag{5.113}$$

$$= \underline{\underline{1.3 \cdot 10^6\,\frac{N}{m^2}}} \tag{5.114}$$

$$p_{red} = \frac{1132.15\,N}{\frac{\pi}{4} \cdot ((0.011\,m)^2 - (0.004\,m)^2)} \tag{5.115}$$

$$= \underline{\underline{1.37 \cdot 10^7\,\frac{N}{m^2}}} \tag{5.116}$$

The required pressure difference is equal to $13\,bar$. A translatory motion of the servo piston can be realized as soon as the pressure decreases from 150 to $137\,bar$ in the respective hydraulic duct (J) or (L). Using Equation 5.86, the required oil displacement section in the servo cylinder of the control unit results in:

$$A_{dis} = \frac{8.25 \cdot 10^{-7}\,m^3}{3.92 \cdot 10^{-3}\,s \cdot \sqrt{\frac{2 \cdot 1.3 \cdot 10^6\,\frac{N}{m^2}}{874\,\frac{kg}{m^3}}}} \tag{5.117}$$

$$= \underline{\underline{3,86 \cdot 10^{-6}\, m^2}} \tag{5.118}$$

The following considerations are based on what has been explained in Section 5.1 and refer to Figure 5.1. As the each four windows in grooves (1) and (2) feature the narrowest area through which the displaced oil enters the servo cylinder before being returned into the reservoir, the window of 8x1.5 mm will be used for the calculation of the actual oil displacement section of the servo cylinder $\hat{A}_{dis}$:

$$\hat{A}_{dis} = 4 \cdot l_{window} \cdot w_{window} = 4 \cdot 0.008\, m \cdot 0.0015\, m \tag{5.119}$$

$$= \underline{\underline{4.80 \cdot 10^{-5}\, m^2}} \tag{5.120}$$

where

l_{window} = length of one oil displacement window
w_{window} = width of one oil displacement window

The actual section is over 12 times larger than the required value. From a mathematical point of view, the oil displacement volume can be returned into the oil reservoir in any operational condition of the FVVT system while the servo piston reciprocates. As the conditions on both sides of the servo piston are the same, this is valid both for engine valve opening and closing procedures.

5.4 Conclusion

After the presentation of the redesigned indirectly controlled FVVT system in the previous chapter the laws of mathematics and physics have been used in this chapter to prove that the system design allows an operation of the FVVT system up to the maximum theoretical engine speed of 8000 $^1/_{min}$.

The acting forces, required spring stiffness and sectional areas within the hydraulic ducts have been considered, taking into account the critical resonance frequency of the system of $67\,Hz$. To enable a safe and reliable system control under any circumstance the cross-sectional areas and spring parameters have been chosen over and above the theoretical requirements. The calculations consider all parameters that have been subject to a new layout as the existing directly controlled FVVT system has been changed to an indirectly controlled system. As the remaining cross sections remain identical no additional calculations were required. In the following step a prototype will be manufactured for a final validation before the actual system will be manufactured and assembled.

6 Manufacturing and FVVT system components

The content of this chapter is the manufacturing process of the redesigned FVVT system. Firstly, the prototype of the system's components that are still required for assembly of the indirectly controlled servo valve will be presented. After this the material choice and relevant properties of the chosen materials, which already have been represented within the mathematical calculations, will be explained. Further, the transducers for an accurate displacement measurement will be chosen solving one of the mentioned sub-problems of this project. Finally, the remaining parts such as a pressure sensor for the lever transmission and the rod seals will be introduced.

6.1 Rapid prototyping

The production of the rapid prototyping (RP) parts has been carried out by Volkswagen South Africa in Uitenhage and was kindly supported by the Product Engineering department. In the following the 3D (three-dimensional) printing machines used and the produced results will be presented.

6.1.1 Utilized 3D printers

For this project the two 3D printers "Fortus 250mc" and "Dimension Elite" by the 3D printing equipment manufacturer Stratasys have been utilized. Both machines are based on the Fused Deposition Modelling (FDM) technology, which is an additive manufacturing technology printing the parts from bottom upwards with a specified number of layers of semi-liquid heated thermoplastics applying the required modelling and support material.

Both mentioned machines use the production grade thermoplastic ABS*plus* P-430 (ABS for Acrylonitrile-Butadiene-Styrene), a material that is durable enough to keep up with the properties of production parts, Stratasys claims [24] [25]. The "Fortus 250mc" offers three possible layer thicknesses between 0.178 and 0.33 mm while sharing the two lower thicknesses with the "Dimension Elite" machine. For the printing process in this project exclusively the 0.178 mm layering has been used as many of the printed components feature very small dimensions and many details requiring a very high printing accuracy [24] [25]. Datasheets with all relevant technical specifications for both "Fortus 250mc" and "Dimension Elite" printers can be found in Appendices 9.4 and 9.5.

6.1.2 Rapid prototyping results

All components that still need to be manufactured to complete the redesigned FVVT system have been exported using the CAD program Catia and transformed into files with an *.stl*[16] format. These files can be read by the 3D printers regardless of which supported CAD program they originate from. Figure 6.1 shows the printed components of the control unit (next page).

[16]STL for Standard Tessellation Language; describes exclusively the surface geometry of a CAD model

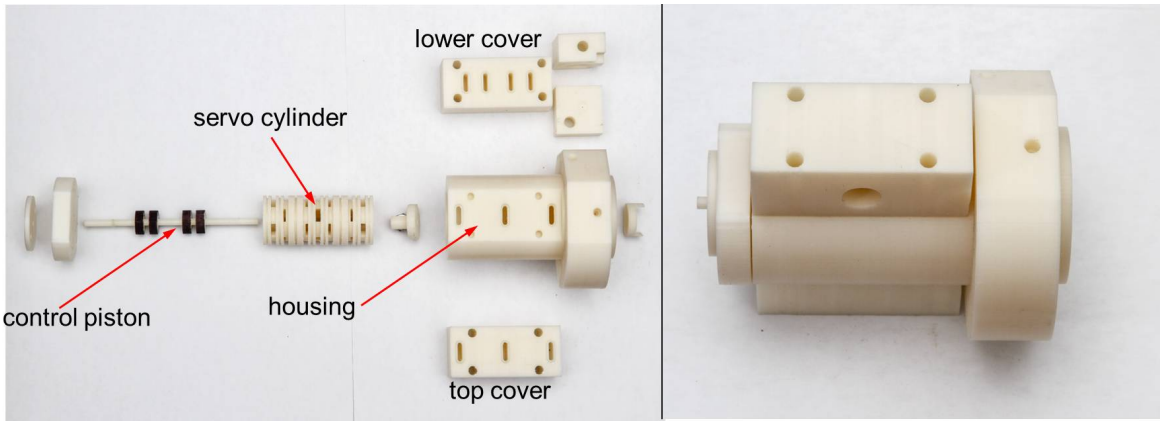

Figure 6.1: RP components of the control unit (left); assembled parts (right)

This includes all components that are shown in the technical drawings in Appendix 9.2. After a mechanical finishing using sandpaper for the peripheral surfaces adjacent to one another and drill bits for all boreholes the components are easy to assemble and feature a very good surface appearance. The remaining components that are required to assemble the servo valve are illustrated in Figure 6.2.

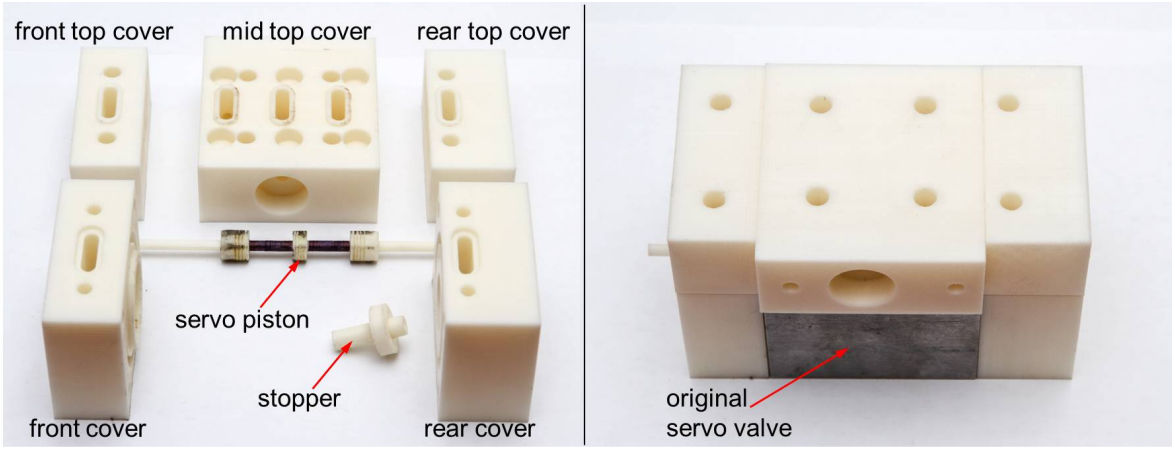

Figure 6.2: RP components of the servo valve (left); assembled parts (right)

The servo valve still used from the directly controlled FVVT system can be seen with all components attached that are required for an assembly of the new indirectly controlled system according to Appendix 9.3. To assemble the parts, again minor mechanical surface finishing was required whilst the parts show very good dimensional accuracy.

For a first attempt the servo piston has been printed horizontally from bottom to top, meaning that each layer of thermoplastic runs through the entire piston from one end to the other. This enables the piston to take a higher bending moment and prevents it from breaking but the accuracy was reduced so far by this that the grooves of the piston elements cannot be seen and the piston elements feature a tapered shape. By printing the servo piston vertically the accuracy seen on the other components could be maintained while losing some of the piston's resistance against bending.

By adjusting both the printed control piston in the assembled control unit and the servo piston within the servo valve according to the three basic switching positions in Cases A*, B* and C* (compare Figure 4.8) for engine valve closing, center position and engine valve opening, the piston dimensions and positions of the piston elements could be validated as the prototype enables an easy inspection of each piston's control edges opening and closing the slots in the relevant servo cylinder. Hence the rapid prototyping confirms the design layout of the control unit and servo valve and allows to proceed with the manufacturing without the need to change any dimensions.

6.2 Material choice

As indicated in Subsection 5.2.1 containing the layout of one of the compression springs, this section introduces the two materials that predominantly came into use for manufacturing. The materials and the properties they feature will be presented. Finally, it will be explained which material has been used for each component of the FVVT system.

6.2.1 Properties of the material AlZnMgCu

This material is a 7000 series aluminium (Al) alloy containing zinc (Zn), magnesium (Mg) and copper (Cu). The utilized alloy corresponds to AISI 7075 (AISI for American

Iron and Steel Institute). The very comprehensive American engineering material data base MatWeb (LLC) has been utilized for research on and the comparison of materials used within this project.

Al 7075 features a modulus of elasticity[17] of $71.7\,GPa$ which is slightly increased compared to pure aluminium ($68\,GPa$) due to its alloying components. The ultimate tensile strength[18] (UTS) of Al 7075 is $524\,MPa$, making it one of the strongest aluminium alloys in the range of all 1000 to 7000 series aluminium alloys. In contrast, 1000 series aluminium alloys feature a UTS value of maximal $186\,MPa$, around 65 % reduced compared to Al 7075.

The chosen material is not only very strong compared to other aluminium alloys, but also features a comparatively low density of only $2.8\,{}^{kg}/_{dm^3}$, giving it a remarkable advantage compared to many other materials. This allows for a significantly reduced overall weight of the redesigned FVVT system. Appendix 9.6 contains a datasheet from MatWeb showing all properties of Al 7075. A table listing the components built from this material will be shown in the next but one subsection [26].

6.2.2 Properties of the material 42CrMo4

This material is a 4000 series low alloy steel that amongst others contains the alloying components chromium (Cr), manganese (Mn) and molybdenum (Mo). This steel alloy accords to AISI 4137. Again the mentioned material characteristic values largely originate from the MatWeb database.

The modulus of elasticity of 4137 steel is $205\,GPa$, more than 2.8 times higher

[17] region within the stress-elongation diagram which shows curve linearity and hence reversible/elastic deformation; resistance of a material against plastic deformation

[18] material specific maximum tensile strain before material failure occurs (beginning of necking); the value in general indicates how much load a material can withstand

than the correspondent value of Al 7075 that was introduced beforehand [27]. The UTS value of 4137 steel is in the range of $1100 - 1300\,MPa$, giving it up to 148 % higher tensile strength compared to Al 7075 [28].

The density on the other hand is $7.72\,{}^{kg}/_{dm^3}$ and hence around 176 % higher than the density of the chosen aluminium alloy [28]. This increases the overall weight of the FVVT system, but it is necessary to use a material with properties in this range to ensure fatigue resistance especially within the components that are subject to increased dynamic stress. Appendix 9.7 summarizes all properties of 4137 steel in a datasheet from MatWeb.

6.2.3 Material attribution

Table 6.1 (next page) contains all the components of the redesigned FVVT system that need to be manufactured and lists the materials chosen for the manufacturing process. The table is separated in the components used for the control unit, abbreviated with CU and the required parts for the servo valve, SV.

The manufacturing process was carried out by the Ostfalia University at two of their workshops in Wolfenbüttel and Wolfsburg, Germany. The parts that are subject to vibration at a highly dynamic rate, like the control- and servo piston, or have to be resistant against deformation, like the mechanical stops of the pistons, have been made of 42CrMo4. Parts that will not undergo a high load, for instance some of the covers or adapters, externally mounted to the housings, have been manufactured of AlZnMgCu.

Table 6.1: Material attribution

Part	Material	
	AlZnMgCu	42CrMo4
CU Housing		x
CU Stopper	x	
CU Servo cylinder		x
CU Control piston		x
CU Translation piston	x	
CU Cover top		x
CU Cover low		x
CU Cover	x	
CU Seal lock	x	
CU Adapter press. sens.	x	
CU Adapter solenoid	x	
SV Cover front		x
SV Top cover front		x
SV Top cover mid		x
SV Top cover rear		x
SV Cover rear		x
SV Stopper		x
SV Spring disc		x
SV Servo piston		x

There are two exceptions to the former. While the mechanical stops within the servo valve will be hit under full hydraulic pressure, in the case of the stop in the control unit (CU stopper) it is not necessary to use the stronger material as this stop will experience the force of the compression spring moving the control piston only while the piezo actuator is inactive. As the translation piston of the control unit features a maximum travel range of only $120\,\mu m$ due to the piezo extension and cannot be hit by another component, AlZnMgCu has been used for the manufacturing of this part.

All components of the servo valve have been made of 4137 steel as all of the covers include ducts pressurized with the full hydraulic system pressure. Thus the assembled components will feature the same coefficient of expansion and resistance against the system pressure.

6.3 Peripheral electric and electronic devices

This section introduces all required parts to set up the redesigned FVVT system from the electrical/electronic point of view. This includes the displacement and pressure sensors that are needed to conduct research on the fully variable valve train while in operation and the electronic auxiliaries such as the amplifier for the piezo actuator, the dSPACE control system and the used function generator.

6.3.1 Block diagram of the redesigned FVVT sytem

A block diagram of all required FVVT system components is illustrated in Figure 6.3 (next page).

The abbreviations can be understood as follows:

- AMP = piezo amplifier
- FG = function generator
- LT = lever transmission
- CU = control unit
- SV = servo valve
- EV = engine valve body.

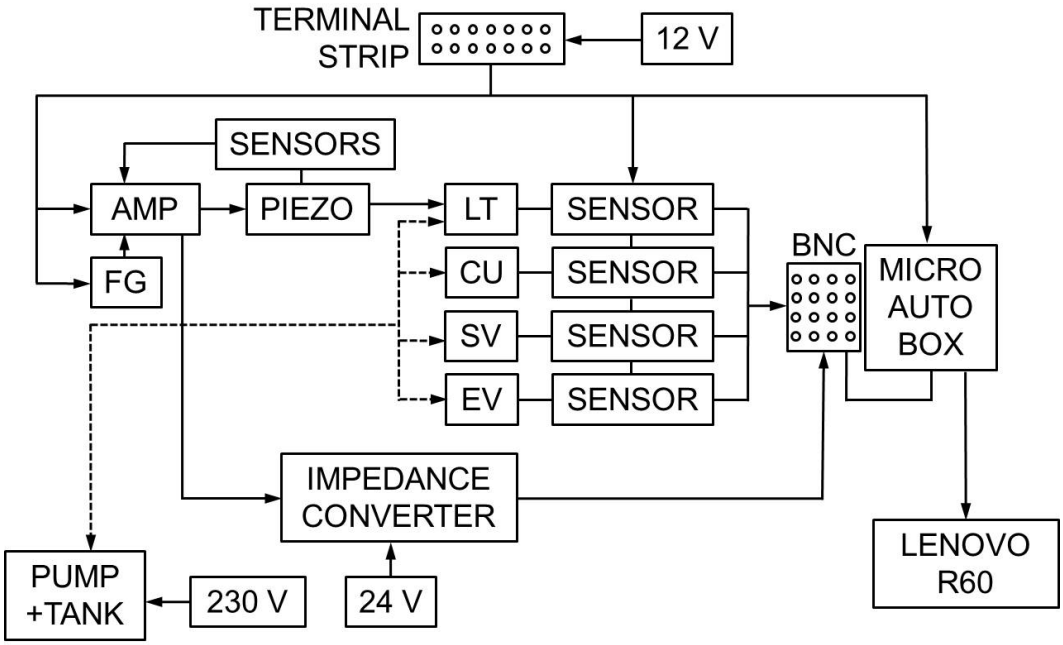

Figure 6.3: Block diagram of the indirectly controlled FVVT system

A terminal strip is powered by a $12\,V$ power supply and supplies voltage to the piezo amplifier, function generator, all external sensors and the MicroAutoBox, which is the control unit used within this project. The function generator connects to the "Control In" of the piezo ampflifier, providing the signal sent to the actuator. The piezo is powered directly by the amplifier and uses a displacement and temperature monitoring sensor that also connect to the amplifier. From here, the position signal output connects to the input of an impedance converter using a modified BNC[19] cable. The converter is used to adjust the voltage range of this signal so it can be read by the MicroAutoBox and is powered by a Siemens PLC $24\,V$ power supply. The output of the impedance converter is designed as a BNC connection. A BNC cable connects from the output "SGPIEZO" of the converter board directly to the BNC input box that is connected to the MicroAutoBox.

Three displacement sensors and one pressure sensor are implemented into the mechanical core of the system (consisting of LT, CU, SV and EV), which is driven by

[19]BNC = Bayonet Neill-Concelman Connector

the piezo actuator and supplied with hydraulic pressure by a pump (compare broken line in Figure 6.3), that requires a $230\,V$ power supply and a tank, which the hydraulic fluid can return to. While the pressure sensor monitors the hydraulic pressure within the lever transmission, displacement sensors need to be chosen to monitor the motion of the

1. control piston in the control unit
2. servo piston within the servo valve
3. engine valves.

The cables of the three displacement sensors and the pressure transducer have been built in such a way as to enable a connection to the terminal strip for the power supply while the sensor signal wires connect to the input box of the MicroAutoBox using a BNC connector. An Ethernet cable is used to connect the MicroAutoBox to the Lenovo R60 research laptop. The actual sensors chosen for this project and the main characteristics of the electronic core components of the redesigned FVVT system will be explained in the following subsections.

6.3.2 Displacement sensors

The use of displacement transducers for all relevant pistons and stems is crucial for the FVVT system control. As only the piezo actuator is equipped with a displacement sensor, the remaining sensors still need to be chosen. Within the previous FVVT system two different displacement sensors have been used on the engine valve stem. Subsequently, these will be introduced and one of them will be chosen for this project.

Sensitec GLM7xxASB-Ax

The functional principle of the GLM700 family sensors from the German sensor manufacturer Sensitec is based on a magneto-resistive measurement. This includes a

ferromagnetic rack featuring teeth with a fixed distance to one another and a sensor element with a magnet being mounted perpendicularly to the rack, as seen in Figure 6.4.

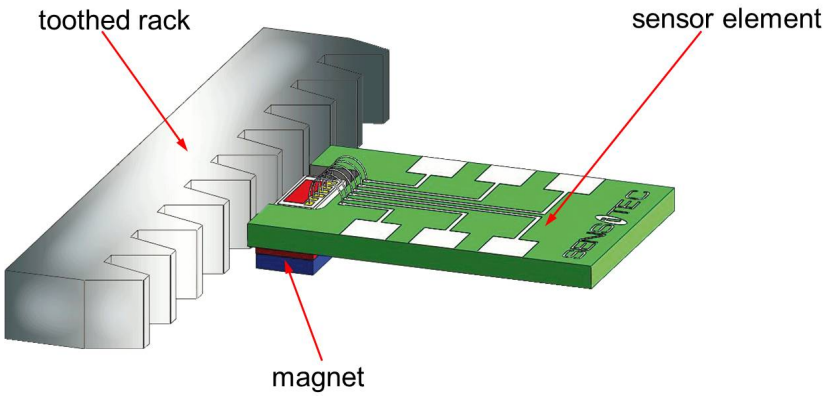

Figure 6.4: Sensitec GLM7xxASB-Ax sensor composition [29]

The magneto-resistive effect was discovered around 150 years ago and has been used in sensors for more than 30 years already. The physical principle of the sensor is based on a change in electrical sensor resistance caused by a magnetic field. The GLM700 uses a "Giant MagnetoResistive" (GMR) tooth sensor with an integrated bias magnet.

This effect was discovered by Fert and Grünberg in 1988, who received the Nobel Prize for Physics in the year 2007. This effect can be seen in systems consisting of layers of at least two ferromagnetic materials with a single non-magnetic metallic layer in between. The direction of magnetization is the determining factor regarding the sensor resistance. If the layers are magnetized non-parallel, the resistance is up to 50 % higher compared to parallel magnetization, which is why this effect is called "giant" [30].

The research of Fert and Grünberg proves that the reason for the increased change in resistance can be explained by one of the ferromagnetic layers influencing the dispersion of electron orientation in the other ferromagnetic layer when those two layers are magnetized antiparallel. This makes it harder for the electrons to pass through the influenced ferromagnetic layer and hence results in higher electrical resistance [31].

The direction of current is not decisive for the change in resistance. The properties of a GMR sensor can be changed depending on the number of layers and their direction of magnetization. By this the sensor can be made suitable for specific applications and measurement requirements [30].

As the toothed rack is moved along the sensor element a change of the magnetic field occurs, depending if a tooth or a gap of the rack is next to the sensor element. This influences the magnetic field and results in a changed voltage signal of the sensor that can be processed and used for a displacement measurement. Figure 6.5 shows the GLM700 sensor application used for the measurement of the engine valve travel within the previous FVVT system.

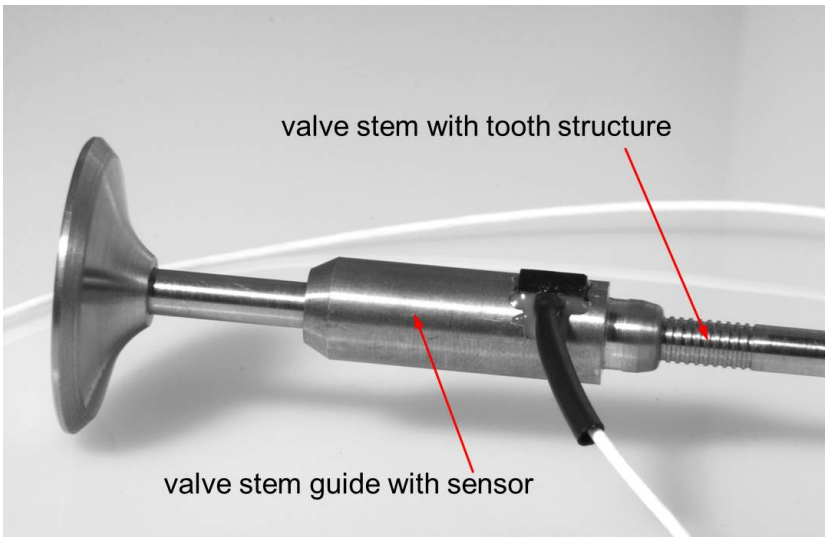

Figure 6.5: Sensitec GLM700 FVVT valve travel sensor application

The sensor element and magnet are integrated into the valve stem guide in this application. The corresponding tooth structure is included directly into the valve stem, replacing the toothed rack shown in the schematic Figure 6.4. The GLM700 sensor works non-contacting and thus is wearless in operation which is a big advantage. Dust and oil on tooth structure and/or sensor have no influence on the measurement. High repeatability makes the sensor suitable for precise measurements. The high

dynamic performance and ability to measure under the conditions of extreme speeds and accelerations make the sensor very eligible for the FVVT system [29]. As it is very small it features very good packaging properties.

On the other hand it is extremly expensive compared to other sensor applications and it is very complex to install the sensor element into the valve stem guide. Appendix 9.8 contains a datasheet listing further technical properties of the sensor.

Gefran PY2C25

The PY2 series sensors are rectilinear displacement transducers that are based on a magnetostrictive principle. According to Deng et al. (2013) magnetostriction in general is a "coupling process between magnetic energy and elastic energy in ferromagnetic materials with high magnetostrictive coefficient" [32]. The way in which this effect can be used in a sensor will be explained subsequently. For better understanding Figure 6.6 shows the setup of a magnetostrictive displacement sensor.

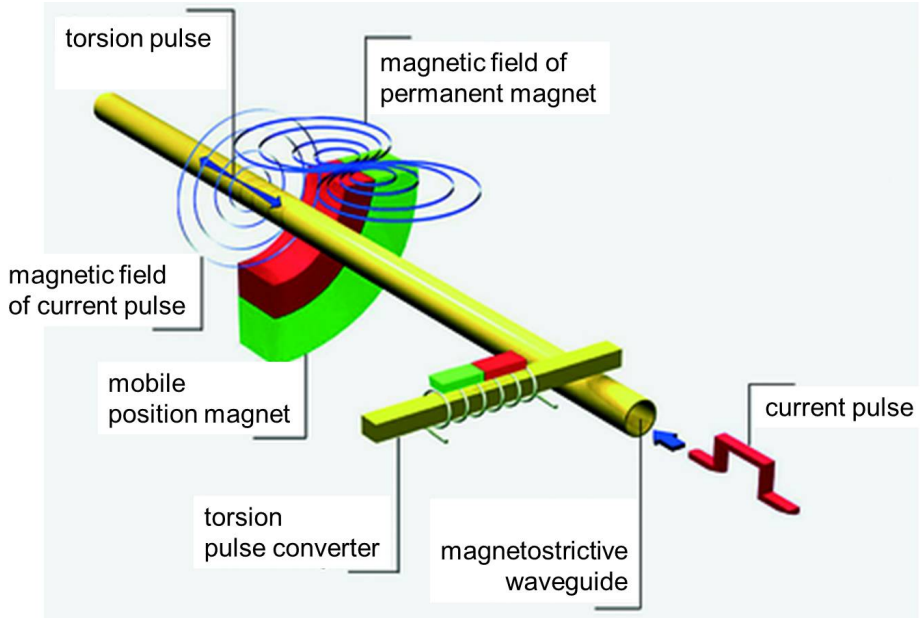

Figure 6.6: Principle of magnetostrictive displacement measurement [33]

The first time magnetostriction was used for displacement measurement applications was in 1970 [33]. The ferromagnetic waveguide as measuring element is the core component of the transducer. A mobile position magnet, mounted to the moving part whose position is meant to be measured, induces a longitudinal magnetic field within the waveguide. While a current pulse is sent through the sensor, a second magnetic field is being induced, this time radially around the waveguide. As soon as both magnetic fields meet and interact at the point of measurement, a torsion pulse is produced which travels as structure-borne sound wave through the waveguide at ultrasonic speed. When this pulse reaches the signal processing (torsion pulse converter) that is integrated in the sensor head, the position of the moving part is being precisely determined by measuring the time elapsed between the dispatch of the current pulse and the arrival of the torsion pulse. Hence the sensor principle is based on a time-of-flight measurement [34]. The actual Gefran PY2 series sensor as used within the previous FVVT system is shown in Figure 6.7.

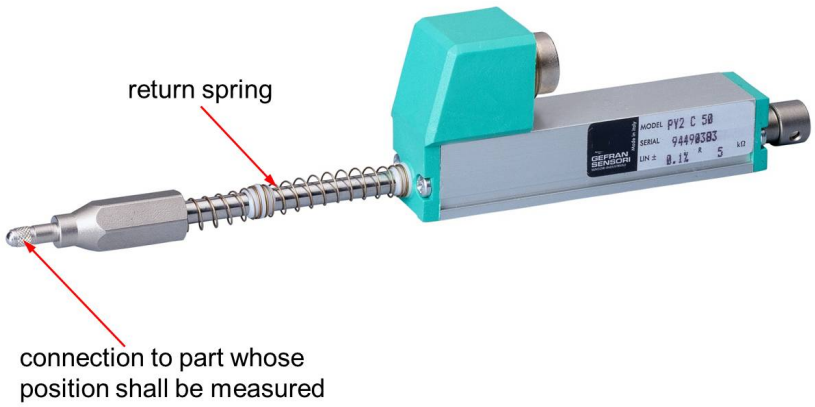

Figure 6.7: Gefran PY2C25 displacement transducer [35]

The sensor end can easily be connected to any rod or stem whose position needs to be measured within this project. The return spring acts as an aid to return the control piston in the control unit when the FVVT system is brought back into its initial position. A further advantage is that this sensor also works on a frictionless, magneto-mechanical basis making it wearless with no need to recalibrate the sensor. The sensor features infinite resolution [34].

With a total length of 138 mm the sensor is far more disadvantageous in terms of packaging, compared with the Sensitec GLM700 sensor. However, this sensor is offered at significantly reduced cost compared to the Sensitec sensor.

The sensor is suitable for measurements of velocities up to 10 $^m/_s$ (compare datasheet of the Gefran PY2 series sensors in Appendix 9.9). With the values shown within the calculations of this research project in Section 5.3, 3.92 ms are available to fulfil the maximum servo piston translation of 10 mm at maximum engine speed. This results in a maximum servo piston velocity of 2.55 $^m/_s$, which is around 25 % of the maximal value, making the sensor suitable for this measurement application.

Cost-benefit analysis

As shown in Table 6.2 a cost-benefit analysis will be conducted to choose the type of displacement transducer that will be used within this project.

Table 6.2: Displacement transducer selection

		Sensitec GLM700		Gefran PY2C25	
Criterion	Weighting	Fulfilment	FxW	Fulfilment	FxW
Cost	4	1	4	8	32
Dynamic performance	3	10	30	8	24
Precision	3	10	30	10	30
Sensor wear	2	10	20	10	20
Package	2	10	20	5	10
Installation	4	1	4	8	32
Total			108		148
Ranking			**2**		**1**

For the analysis, all criteria relevant for the sensor selection are compared, whilst a weighting indicates the relevance of each criterion. In columns “FxW” the fulfilment

of these criteria (1 lowest to 10 highest) is evaluated by multiplying it with a specific weighting.

The Sensitec transducer does not feature limitations regarding the velocity and acceleration conditions within which it can measure the displacement, resulting in excellent dynamic performance. However, as calculated above, the FVVT system will not reach velocities that exceed the Gefran transducer's range. Even though the Sensitec transducer offers the advantage regarding dimensions and packaging, the complicated installation of the sensor element and the high cost result in a total fulfilment reduced by 27 % compared to the Gefran sensor.

Thus, the Gefran PY2C25 displacement transducer will be used for measuring the positions of the control piston in the control unit, the servo piston within the servo valve and at least one of the two engine valves that move simultaneously, solving another of the sub-objectives of this research, as mentioned in Section 1.2.

6.3.3 Pressure transducer

The transducer type PTDVB1001B1C1 by the manufacturer Parker Hannifin has been used for monitoring the pressure in the lever transmission within the previous FVVT system. This sensor will also be used for the indirectly controlled FVVT system as it proved to be suitable for this application. The pressure needs to be monitored to ensure that it neither exceeds its designated maximum value nor drops too low due to a leak or void formation, affecting the FVVT system control.

The sensor thread fits into an adapter that will be fitted to the control unit housing, as shown in the exploded view of the control unit (see Figure 4.4). A drill $1\,mm$ in diameter leads from the adapter into the lever transmission, enabling the measurement of the hydraulic pressure.

The filtration transducer uses a stainless steel element, coated with alloy and insulation materials, that is in contact with the hydraulic transmitting medium. The transducer can determine pressures up to 100 *bar* and uses ASIC (Application Specific Integrated Circuit) programmable software. The maximum overload pressure is 250 *bar* [36]. The full system pressure of 150 *bar* will not in any case be applied to the lever transmission. A datasheet of the Parker PTD ASIC transducer can be found in Appendix 9.10.

6.3.4 Piezo amplifier

An energy recovery power amplifier type HVPZT E-482 will be used to supply the required voltage to the piezo actuator. It is from the manufacturer PI, the same company that delivered the piezo actuator for this project. This amplifier has been designed especially for the dynamic analogue operation of piezo actuators with high electrical capacitance and features an output voltage range of 0 to 1050 V. The input voltage is 0 to 10 V which means the use of an external high voltage power supply is not necessary. The DC (direct current) offset can be configured with the aid of a 10-turn potentiometer, adding 0 to $\pm 10\,V$ to the input voltage.

According to PI the energy recovery system allows the amplifier to save up to 80 % energy using switched control. Pulse width modulation (PWM) of the piezo output voltage is being used and during discharge of the actuator, the energy partly is being returned into a capacitor storage. This energy can be utilized for the next charging process of the piezo. Thus the amplifier features lower temperatures and provides improved stability.

For this project the optional E-509 PZT-Servo Controller has been added. This enables closed-loop control, including a position feedback sensor. According to the manufacturer, this allows for positioning accuracy and repeatability in the nanometre range and even below. This is very important for this project as the control of

the FVVT system has to rely on the effectively used travel range of the piezo of $\Delta l_{eff} = 120\,\mu m$, as explained in Section 3.2.

Moreover, the amplifier has an included temperature sensor. Piezo and this sensor are connected to the amplifier by LEMO sockets[20]. The temperature sensor deactivates the piezo output voltage when the actuator reaches a temperature of $120\,°C$. As the operating temperature range is 5 to $40\,°C$ with a loss effect of around $10\,\%$ at over $40\,°C$ this measure is helpful to protect the actuator [37]. To ensure that the piezo reaches its full displacement under any circumstances and never overheats, its housing will be connected to compressed air in order to enable a convective cooling of the stack. A summary of the technical specifications of the E-482 amplifier can be found in Appendix 9.11.

6.3.5 Development control system

The MicroAutoBox type 1401/1501 from dSPACE that already has been part of the previous FVVT setup, will be used as control system. It is needed for communication purposes between the displacement and pressure transducers and the corresponding ControlDesk software, also provided by dSPACE. The MicroAutoBox works like an engine control unit (ECU) with no user intervention necessary. The box is suitable for many different applications like x-by-wire or powertrain control. An external power supply is necessary to run the MicroAutoBox. It will be introduced in Subsection 6.3.7.

Alongside the standard automotive I/O (Input/Output), an FPGA[21] (Field Programmable Gate Array) is integrated into the MicroAutoBox. The FPGA can be configured in a Simulink environment. A laptop can easily be connected to the MicroAutoBox enabling application download, parameterization of models and the analysis of data using Ethernet. A flight recorder is integrated into the box

[20] push-pull connectors by the Swiss company LEMO S.A.

[21] integrated circuit that can be configured by the user

for long-term data logging [38] [39]. More technical specifications can be found in Appendix 9.12.

6.3.6 Function generator

A function generator type FG200 from the company Digimess Instruments Ltd will be used to generate a voltage signal that will be sent to the piezo actuator. The FG200 is a sweep function generator that is being controlled by a $2\,MHz$ microprocessor. The frequency range is $0.2\,Hz$ to $2\,MHz$ in seven decade ranges, with a frequency accuracy of $\pm 0.5\,\%$. Various output waveforms as sine, square or triangle are available. Besides the frequency and output function signal the amplitude can be adjusted up to $20\,V$ peak-to-peak. Also the amplitude attenuation can be chosen in $20\,dB$ steps from 0 to $60\,dB$ [40]. All further technical specifications can be found in the datasheet in Appendix 9.13.

6.3.7 Power supply

A profitec switchable power supply type SPS 12103 serves two purposes. Firstly, as mentioned before, it delivers the required direct voltage (adjustable from 12 to $14\,V$) for the MicroAutoBox. Secondly, it will supply the displacement and pressure transducers with operating voltage as it is suitable for the operation of any device with $12\,V$ direct current input voltage. The maximum output current in this version is $10\,A$. The residual ripple of $\leq\ 2\,\%$ means that only a very small alternating current voltage component is left in the smoothed direct current output voltage and guarantees a stable power supply of MicroAutoBox and all sensors. The utilized switched-mode technology gives the SPS 12103 advantages relating to weight and size compared to conventional power supplies. Futhermore it features a short-circuit protection and overtemperature shutdown function [42]. The technical specifications are listed in Appendix 9.14.

6.4 Peripheral mechanical devices

This section introduces all required parts to set up the redesigned FVVT system from the mechanical side. This includes the special seals and gaskets that due to the high system pressure are essential for preventing oil leaks, and the calculated compression springs.

6.4.1 Rod seals for moved pistons

As mentioned in Subsections 4.3.1 and 4.3.2, five rod seals in total have to be used in order to seal the moved pistons and the lever transmission against the atmosphere. These are custom-built rod seals from Guilliard & Dörr GmbH, a plastic and seal manufacturer from Germany.

The largest of the three rod seals used within the control unit has been designed specifically for this project. The dimensions of this seal are 20.00x28.00x33.00x5.00x1.30. How these measurements are meant to be understood can be seen in a technical drawing in Appendix 9.15. The remaining two small rod seals used for the control unit and both seals used for the servo valve are identical and consistent with the rod seals used within the previous FVVT system. The dimensions of the small rod seal are 4.00x12.00x17.00x5.00x1.30. The measurements again correlate to the technical drawing mentioned above.

The rod seals are suitable for maximum piston speeds up to $10\,{}^{m}/_{s}$ and can withstand the system pressure of $15\,MPa$. Grooves have been embedded within the relevant components of the redesigned system to carry the rod seals that will be press-fitted to remain in their designated position.

6.4.2 Properties of the chosen o-rings

O-rings will be used for the housings of both the control unit and the servo valve on the contact surfaces with the covers that contain the hydraulic ducts. This way leakages in these ducts can be avoided. As mentioned before, at the same time eight o-rings for the servo cylinder of the control unit will be installed in the positions indicated in black in Figure 5.1. The quantity and dimensions of o-rings used can be found in the correspondent list in Appendix 9.16.

All o-rings are made by the German industrial technology company HUG GmbH and are manufactured in FPM75 quality which is a synthetic rubber comparable to Viton, Fluorel or Technoflon. The FPM75 o-rings are fully adequate for this project as they can be used within a temperature range between -20 to $+200\,°C$ and are resistant to mineral oils and hydraulic pressure.

6.4.3 Compression springs

After sending a technical enquiry to the German spring company Gutekunst + Co.KG in Germany listing all calculated properties of the compression springs that will be used within the control unit and the servo valve, the company returned a revaluation of the properties that can be met within their production. Datasheets with technical drawings and all dimensions and spring properties can be found in Appendix 9.17 for the single spring of the control unit and in Appendix 9.18 regarding the two identical springs of the servo valve.

Quality class 1 (highest) has been chosen for the manufacturing process of the springs as the calculated properties have to be adhered to as precisely as possible so as to realize an accurate prediction of the actual FVVT system behaviour. The spring used for the control unit features a deviation of only $-2.2\,\%$ with regard to the calculated stiffness; the springs that will be used for the servo valve correspond to the

calculated stiffness with 0 % deviation. Also all other properties comply excellently with the values demanded in the calculations. As all compression springs have to withstand a high dynamic stress they have been shot-peened which is a measure to increase the dynamic lifespan of a spring.

6.5 Conclusion

In order to execute the production of the actual FVVT system components according to the prototype, the manufacturing materials have been chosen. To get a step closer to the test assembly of the redesigned FVVT system, the mechanical and electronic components that will be required for this research project have been determined. In the following chapter, the manufactured FVVT components will be assembled and all sensors and electronic connections will be implemented to prepare a first test of the system on the BMW K71 cylinder head.

7 Experimental setup and test results

In this chapter the laboratory test setup of the redesigned FVVT system will be introduced as an integrated system. A look at the physical composition of the engine valve actuator test bench will be followed by a presentation of of the Matlab Simulink model that is being implemented into the dSPACE engine control system. Necessary modifications to the system hardware will be discussed, that were required to enable testing with the system. Finally, the test results will be analysed, showing the possibilities of the system at its early development stage and emphasizing the limits of the system, that still need to be overcome to enable a flawless system operation in future.

7.1 System setup on mobile test bench

This section illustrates the test bench setup referring to the components that have been introduced in the previous Sections 6.3 and 6.4. The section takes a look at the fixture of the assembled cylinder head and piezo actuator, explains why it was required to change the compression springs and highlights the implementation of sensors, electronics and the hydraulic components.

7.1.1 System component composition

Figure 7.1 (next page) shows the assembled test bench, carrying all components required for testing the redesigned FVVT system.

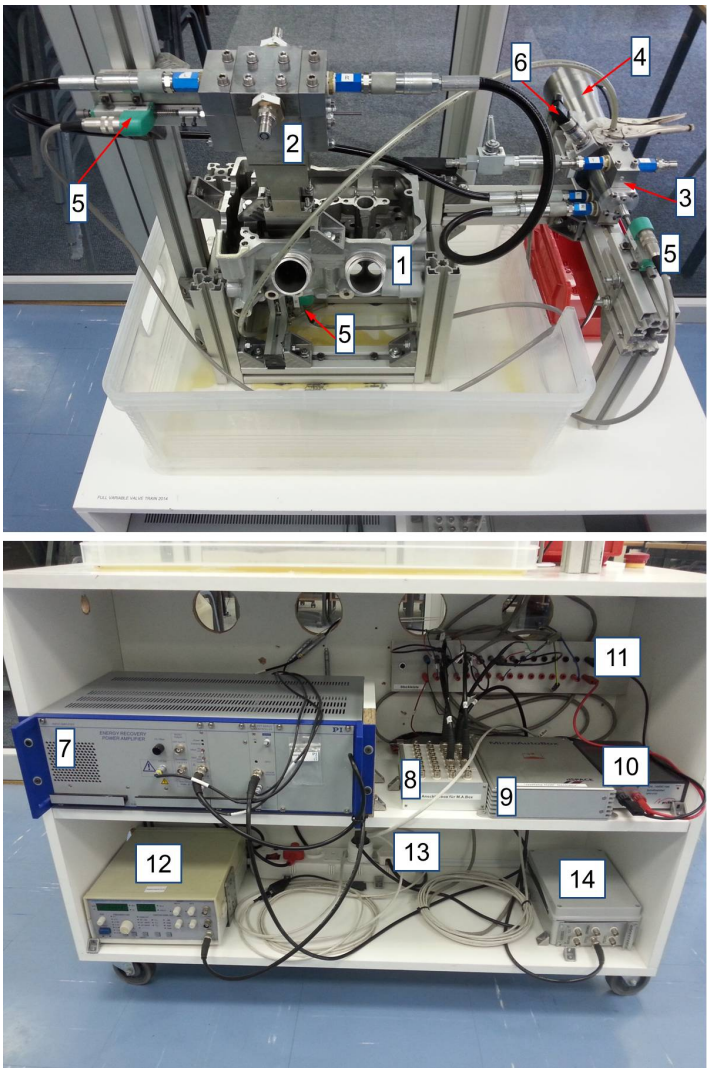

1: K71 cylinder head
2: Servo valve and valve body
3: Control unit
4: Piezo actuator
5: Displacement transducers
6: Pressure transducer
7: Piezo amplifier
8: BNC input box for sensors
9: MicroAutoBox
10: $12\,V$ power supply
11: Terminal strip
12: Function generator
13: $24\,V$ power supply
14: Impedance converter

Figure 7.1: Test setup of the indirectly controlled FVVT system

The test bench is designed to be mobile in order to run experiments with the FESTO hydraulic training facilities of the "Nelson Mandela Metropolitan University". For this purpose all components are mounted on a movable table.

The core of the test setup is the BMW K71 cylinder head (1) with the engine valve body and servo valve (2) mounted on top. Since the cylinder head was not designed to carry the components of the FVVT system, it needed to be modified. The bearing bridges that normally the intake and exhaust camshaft rest on have been removed to produce the space required in vertical direction. Hydraulic lines are used to connect the servo valve with the control unit (3). The piezo actuator (4) is directly connected to the control unit. The displacement transducers (5) are mounted to the servo piston of the servo valve, to the control piston of the control unit and to one of the two intake valves of the engine, that open and close simultaneously. As mentioned before, the test bench at this stage of development is simplified to operate one pair of intake valves and does not operate all eight engine valves at the same time. The pressure transducer (6) connects to the lever transmission. A plastic collection pan has been added to keep any spilling hydraulic oil from entering the inside of the table, where the electronic components of the test bench are accommodated.

The ampflifier for the piezo actuator (7), the MicroAutoBox (9) with the connected BNC input box for the sensors (8), the $12\,V$ power supply (10) for the sensors and the MicroAutoBox, and a terminal strip (11) are placed on the center level of the table. The function generator (12) that generates the signal sent to the piezo actuator and a $24\,V$ power supply (13), connected to an impedance converter (14), are stored in the bottom level of the table. The connection between the components correlates to the block diagram that was shown in the previous chapter (compare Figure 6.3).

7.1.2 Cylinder head and piezo actuator fixture

Extrusions have been used to form solid mounts for the test bench hardware and sensors. The cylinder head is carried by four upright profiles that are supported by six cross-member profiles that are tightly connected using $90\,^\circ$ angles. The piezo actuator and connected control unit are mounted onto an independent profile that is supported by a cross-member to the cylinder head fixture. The fixture is bolted onto the table at eight symmetrically chosen locations.

7.1.3 Substituted compression springs

Due to the fact that the parcel containing the custom made compression springs by the Gutekunst spring factory never reached South Africa, a prompt solution needed to be found to guarantee that the test of the redesigned FVVT system was not being delayed. Fortunately the manufacturer Springwell (Pty) Ltd, located in Port Elizabeth, was able to produce two identical compression springs for the servo valve and the single spring for the control unit. The springs fulfil the dimensional requirements and feature the demanded stiffness, but due to slightly larger tolerances in the manufacturing process the spring ends needed a little subsequent machining. The tolerances mentioned in Subsection 6.4.3 might not fully apply to these springs. However, they fit perfectly and no difference in properties could be found for the two identical springs of the servo valve. For that reason the springs are considered suitable for the initial system test.

7.1.4 Sensor mounts

All three Gefran displacement transducers are mounted onto extrusions, that have been chosen to be as short as possible and are supported by several mounting points. By this in combination with the rigid setup of the basic fixtures an influence on the acquired data due to vibration or motion of mounted parts during experimental tests will be avoided or reduced to a minimum. Figure 7.2 explicitly shows the mounting mechanism of the sensors.

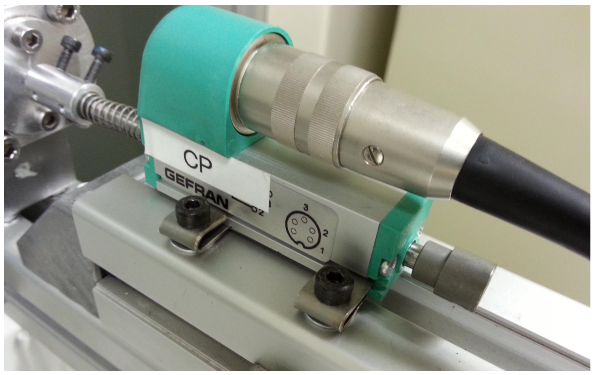

Figure 7.2: Adjustable sensor mount

Special brackets have been built for the sensors that allow for an adjustment of the sensor position in the direction of the magnetostrictive waveguide (compare Figure 6.6) in order to calibrate the sensors' zero-offset. For this the four mounting bolts need to be loosened. After position adjustment and tightening of the bolts the sensors are being secured firmly in the designated position by two u-shaped profiles that grasp into a groove on either side of the sensor body and mount it down onto the extrusion.

Aluminium couplings made out of round stock are used to connect the sensor waveguides to the moving pistons and the engine valve respectively. Four bolts, of which each two have an angular separation of 60 °, can be used to guarantee a tight connection, clamping the movable part within the coupling.

7.1.5 Hydraulic equipment

The hydraulic fittings on the control unit and servo valve have been replaced by suitable FESTO quick connectors, so the system can easily be connected to the supply and return lines of the hydraulic pump that is part of the FESTO training equipment. Pressure control valves allow to adjust the system pressure to the desired value.

Since the FESTO training facilities can be utilized, the implementation of an external oil pump with an included oil tank, hydraulic lines and pressure regulators becomes no longer necessary. As the used H-HA40G-1X2P/230 V50 Hz pump accommodates four high pressure connections and four return line connections and can adjust the applied pressure in the range 0 to 18 MPa, it is suitable for the operation of the FVVT test bench. The "HLP 22" oil used by this pump is in accordance with DIN 51524. As this oil also is a HLP specification oil as the oil that some of the calculations of this research are based on, it shows similar properties as the originally intended "HLP 46" oil and is also very suitable for internal use in hydraulic systems to pressures above 10 MPa. A negative effect by the around 50 % reduced kinematic viscosity compared to "HLP 46" is not expected.

7.1.6 Sensor connection to MicroAutoBox

The correct connection of the sensor cables to the BNC input box of the MicroAutoBox is crucial as otherwise no sensor signals can be read by the box. Figure 7.3 shows the correct input allocation that correlates to the Simulink model.

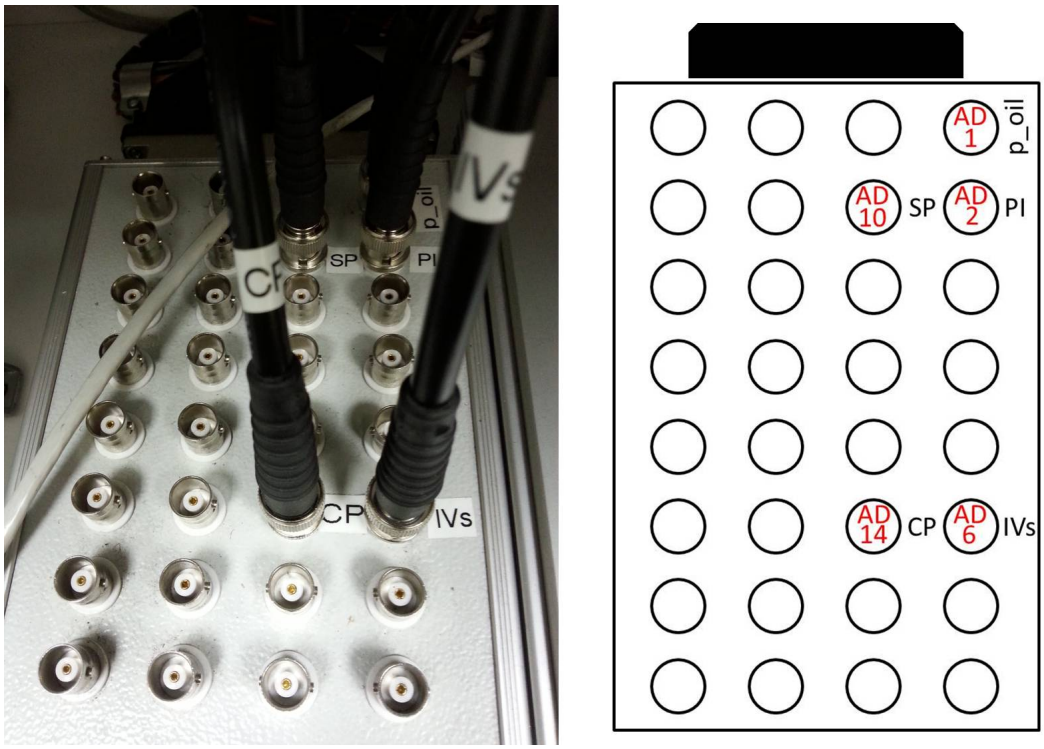

Figure 7.3: Sensor signal input of the MicroAutoBox

The abbreviations can be understood as follows:

- p_{oil} = pressure transducer
- SP = servo piston displacement
- PI = piezo actuator displacement
- CP = control piston displacement
- IVs = engine valve displacement.

The shown ADx (analogue/digital) numbering is important for the allocation of the used BNC ports of the MicroAutoBox to the Simulink model environment, that will be introduced in the next section. The numbering on the BNC input box starts top to bottom on the utmost right column and from there continues top to bottom column by column.

7.2 Model of the electrohydraulic actuator

The FVVT system operation is based on a Simulink model and the correspondent Matlab m-file. The modified model and m-file that guarantee a reliable operation of the redesigned FVVT system will be introduced in this section. A new layout in the dSPACE ControlDesk software was provided to be able to monitor and analyse the system's behaviour.

7.2.1 Simulink model of the redesigned FVVT system

The Simulink model used for the redesigned FVVT system is based on the model that has been used for the directly controlled, previous system. As many different Simulink files with different experimental stages exist for this project it is important to mention that the model used as a basis for this research is the file "Kaskade01072013.mdl". In order to utilize this model a number of modifications and alterations were necessary before a reliably working connection between the dSPACE system and the model could be achieved.

As the previous system had been used in conjunction with one of the engine test benches at the Ostfalia University, the model included blocks that referred to the optional "RapidPro" system that has been connected to the MicroAutoBox but will not be part of the test setup at the NMMU as it is still being used at the Ostfalia University and the use of this system is not indispensable. All "RapidPro" related blocks have been removed from the model.

The sampling time of the model had to be changed from $50\,\mu s$ to $90\,\mu s$ as after the implementation of the additional measurement equipment for this system a timeout failure would occur directly after the start of the data acquisition. This has been caused by the hardware limitations of the Lenovo R60 laptop used and the increased amount of acquired data. By using $90\,\mu s$ timeout overruns can be avoided. The number of recorded values is more than sufficient for any simulated engine speed. As the redesigned FVVT system features one more moving piston compared to the previous system, another displacement transducer was added to the Simulink model. The modified model is shown in Figure 7.4 (next page).

The illustration shows the top layer of the Simulink model that helps understanding the basic layout of the sensor input into the MicroAutoBox. The model, however, contains far more model subsystems underneath the top layer, that have been built at the Ostfalia University. The broken red lines highlight the model components of each of the four sensors that have been implemented for use within the previous FVVT system. These are the pressure transducer monitoring the hydraulic pressure within the lever transmission and displacement transducers for the piezo, engine valves and servo piston. The broken green line at the bottom emphasizes all blocks required for the signal input of the control piston displacement. As this sensor needed to be added to the model the block structure was largely built according to the existing blocks of the servo piston.

The basic structure of all sensors contains an ADC (analogue-to-digital converter) block, a multiplier of the value using a constant of 100 in case of the pressure transducer and a constant of five in case of the displacement sensors, and finally an AD/"Goto" block. For the displacement transducers additional blocks are interconnected, for instance, "Lookup" blocks that are required to calibrate the actual sensor displacement to the occurring voltage and gain blocks that reduce the displacement from metres into millimetres.

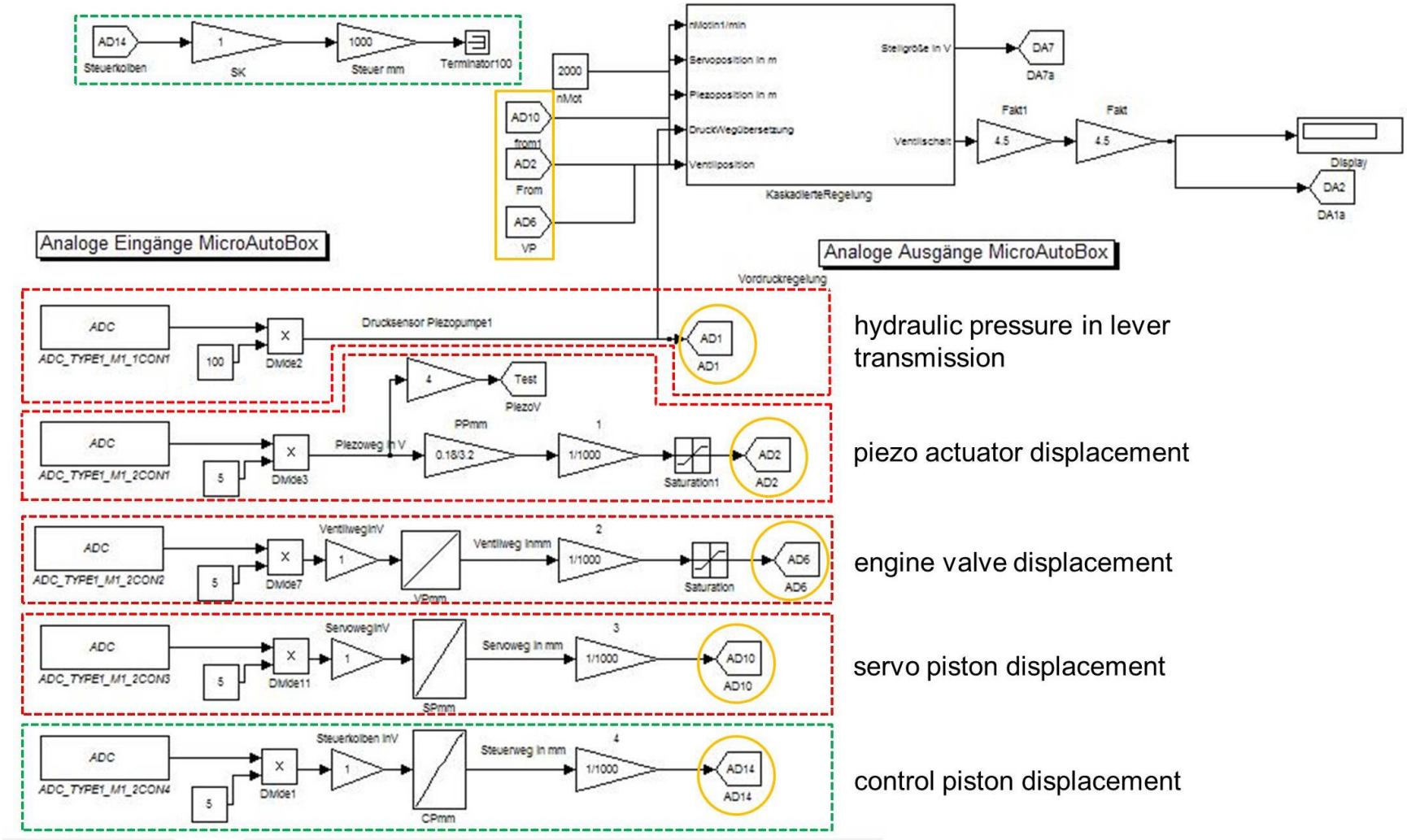

hydraulic pressure in lever transmission

piezo actuator displacement

engine valve displacement

servo piston displacement

control piston displacement

Figure 7.4: Modified Simulink model

The AD/"Goto" block numbering, highlighted by yellow circles, correlates to the BNC inputs of the MicroAutoBox, as mentioned in Subsection 7.1.6 (compare Figure 7.3). For further processing purposes the sensor signals AD1, AD2, AD6 and AD10 that were already used in the previous FVVT setup, enter a sublayer of the model (see yellow box and AD1 path in Figure 7.4). The sublayers can be seen by entering the black box that is named "Kaskadierte Regelung", which is German for cascaded control.

The broken green line at the top of the illustration shows the block assembly that is required to see an actual displacement of the added control piston sensor in the dSPACE ControlDesk software. These blocks have been created according to the blocks used for the other sensors within the model sublayers. The terminator block is used to cap blocks with unconnected outputs and hence allows for the sensor displacement to be read in ControlDesk.

7.2.2 Matlab m-File of the redesigned FVVT system

The m-File that is being used within this research project is called "Piezo26042013.m" and has been designed with Matlab version 7.6.0 (R2008a). The m-File is almost identical to the one used for the previous FVVT system. The modified model sampling time that has been mentioned before also involves changes within the m-File, of which an extraction is shown in Figure 7.5 (next page).

The red boxes show the two lines of the m-File where the values needed to be altered according to the model's sampling time. This m-File "Piezo26042013.m" can only be used in combination with the modified Simulink model "Kaskade01072013.mdl" and will not work with any older or altered FVVT system files.

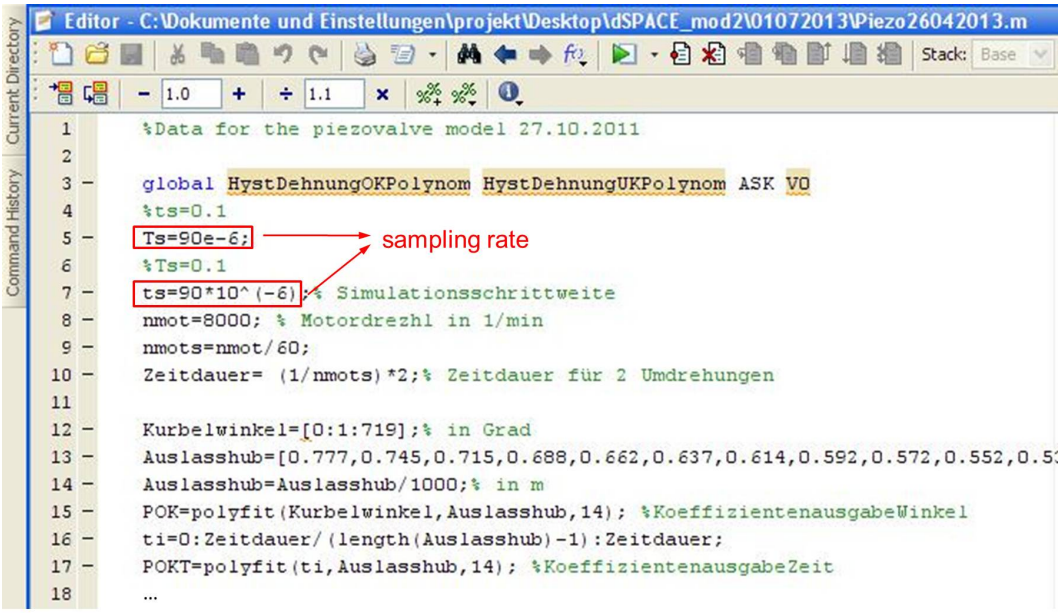

Figure 7.5: Modified Matlab m-File

7.2.3 Modified dSPACE ControlDesk layout

The ControlDesk software by dSPACE allows one to visualize model variables from the Simuliunk model that is directly linked to the MicroAutoBox, in an instrument-based interface on screen. The exact software used is "ControlDesk Developer Version 3.2.2 P2 - Standard" using a "DS815 Transmitter Card Vs 2.0" that is connected to the MicroAutoBox via Ethernet.

The ControlDesk experiment that has been designed to work exclusively with the above mentioned Simulink model and m-File is called "Exp_Herr_Behre.cdx" and involves the project file "kaskade01072013.sdf" and the layout "06032013.lay". The layout is illustrated in Figure 7.6 (next page).

ControlDesk is linked to the model root in Simulink. By linking a signal from the model to a ControlDesk instrument the signal can be visualized in real-time. The layout shown in Figure 7.6 has been designed especially for use with the redesigned, indirectly controlled FVVT system.

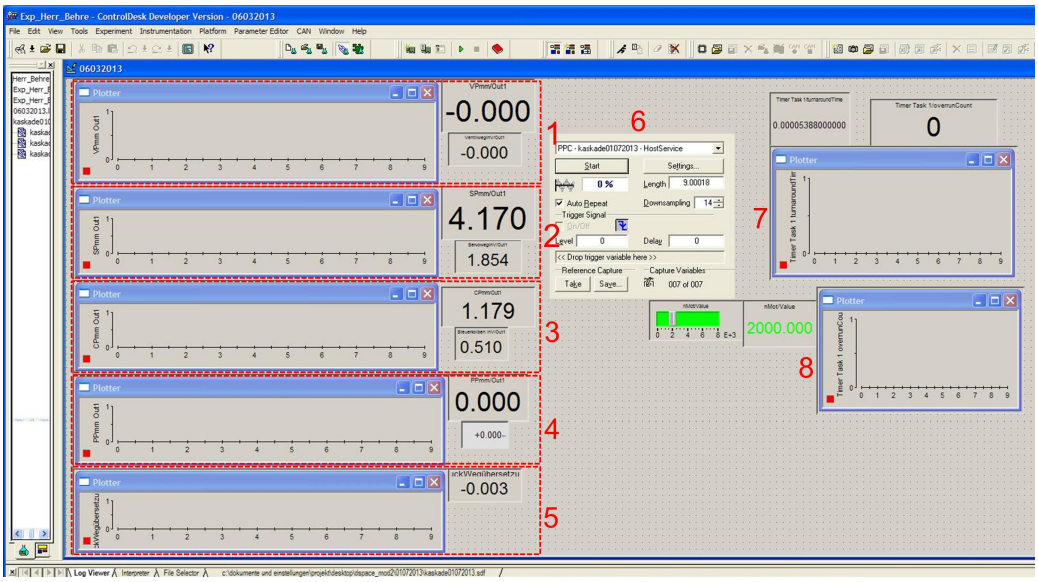

1: Engine valve position 2: Servo piston position 3: Control piston position

4: Piezo position 5: Hydraulic pressure 6: Capture settings

7: Turnaround time 8: Overrun counter

Figure 7.6: ControlDesk layout

Boxes labelled (1) to (4) contain instruments that visualize the signals obtained from the displacement sensors, while box (5) includes the signal from the pressure transducer. These five boxes each feature plotter arrays that show the actual displacement/pressure over sampling time and display blocks for displacement in millimetres, the according voltage and relative pressure in the case of box (5). Summarized the boxes show:

1. VPmm Out1 = (engine) valve position
2. SPmm Out1 = servo piston position
3. CPmm Out1 = control piston position
4. PPmm Out1 = piezo position
5. DruckWegübersetzung = pressure within lever transmission.

A capture settings control block (6) is used to determine the basic prerequisites of experimental runs like recording length or auto repeat and is used to set the starting

and end time of the data capture. The capture then amongst others can be saved as .csv (comma-separated values) file and processed in Microsoft Excel.

The green slider control block below the capture settings block is a residual of the previous FVVT system control and, in combination with the display block next to it can be used to change the simulated engine speed during experiments. Timer Task instruments measuring turnaround time (7) and counting overrun situations (8) have been added to the experiment. Above these two plotter arrays two displays can be seen that illustrate the actual turnaround time and number of overruns. Thus, the stability of the model can be monitored during experiments. This became necessary due to the fact that the model could not be executed in real-time after it had been modified, unless overruns would be ignored in the settings. This is undesirable and a timeout overrun would occur directly after the start of the capture. This happens when the turnaround time exceeds the sampling time of the model. While data is still being processed, the next model step begins too early and a crash of the capture occurs.

In the according block an average turnaround time of approximately $54\,\mu s$ can be read. This allows the assumption that the decision to change the sampling time to $90\,\mu s$ still leaves potential for reduction. However, when a capture is started, initially the turnaround time increases to just over $80\,\mu s$. Hence, the model sampling time of $90\,\mu s$ leaves a small safety buffer concerning eventual overruns and still allows a very narrow sampling time as in the previous FVVT system's control.

7.3 Modifications and optimizations

The initial test of the redesigned FVVT system showed that a number of modifications were required to allow an uncomplicated and reliable use of the system. After implementing measures to seal the system against hydraulic leaks and adding components to control the hydraulic flow, the redesigned FVVT system could be operated.

7.3.1 Improvements of the servo valve

Initially the servo valve and control unit have been tested independently from each other to simplify troubleshooting. The valve body underneath the servo valve carrying the intake valves as one component from the previous FVVT system produces a leak through the engine valve stems. As soon as pressure is applied to the bottom of the valve stem pistons, the hydraulic fluid can escape through the valve stem guides that are not designed for pressures exceeding around $0.4\,MPa$, which is a typical oil pressure of an internal combustion engine's oil circuit. The tested pressure was $3\,MPa$. As the valve stem piston seals are custom made, a provisional solution of the leak was provided by installing an oil catch reservoir that connects to a low pressure fuel pump by the manufacturer "Facet" and feeds the oil back into the tank of the FESTO pump. The "Facet" pump has been equipped with plugs that directly connect to the terminal strip of the test bench allowing the engagement of the pump whenever required. The oil reservoir with attached pump can be seen in Figure 7.7.

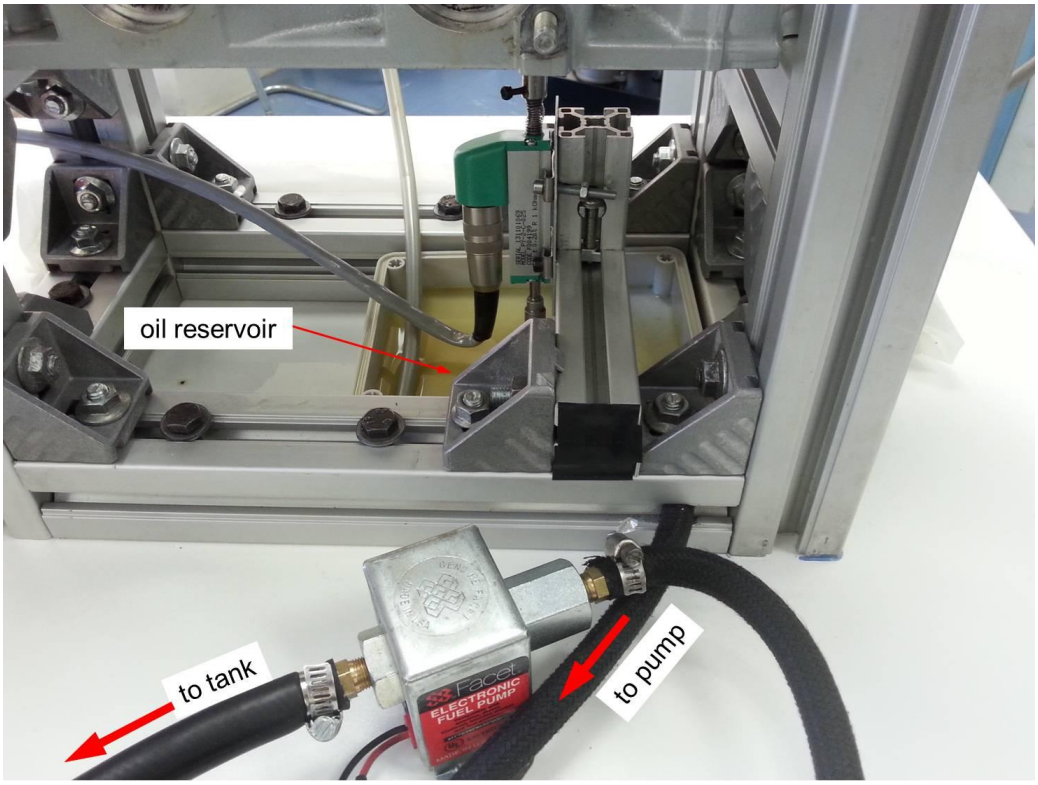

Figure 7.7: Oil catch reservoir with pump

To prevent the servo valve components from leaking under high pressure, a gasket maker has been used to support the o-rings that are used between mating components. A test proved this measure successful.

7.3.2 Improvements of the control unit

The control unit showed similar minor leakages that could be solved by using a gasket maker. The more problematic issue was that the lever transmission did not work in a way so as to move the control piston in a reciprocating manner. This problem occurred due to a constant pressure supply being connected to the lever transmission.

On examining the control piston movement, it became obvious that the piston would gradually be pushed out of the control unit housing in small increments while the piezo actuator was operated with a low frequency of $10\,Hz$. The translation piston that is connected to the piezo would transmit force through the oil in the lever transmission onto the smaller surface area of the control piston. However, when the piezo contracts, the volume within the lever transmission will increase as the translation piston is being returned. The control piston at the same time cannot be returned as full hydraulic pressure is still being supplied into the lever transmission and completely fills it with oil. Within the next extension of the piezo actuator the larger oil volume would result in a movement of the control piston further out of the control unit. The lever transmission acts like a pump in this case pushing more and more oil into the lever transmission as the piezo reciprocates. This problem could be solved by implementing a cut-off cock into the pressure supply of the lever transmission. The assembly can be seen in Figure 7.8 (next page).

By this the lever transmission can be filled and bled initially and the piezo actuator is turned on only once the cock is closed. Now the translation piston pushes the control piston out of the control unit and when the piezo contracts the control piston is returned by the spring in the control unit while the oil volume in the lever transmission remains constant. This way the control piston fulfils a reciprocating movement as desired.

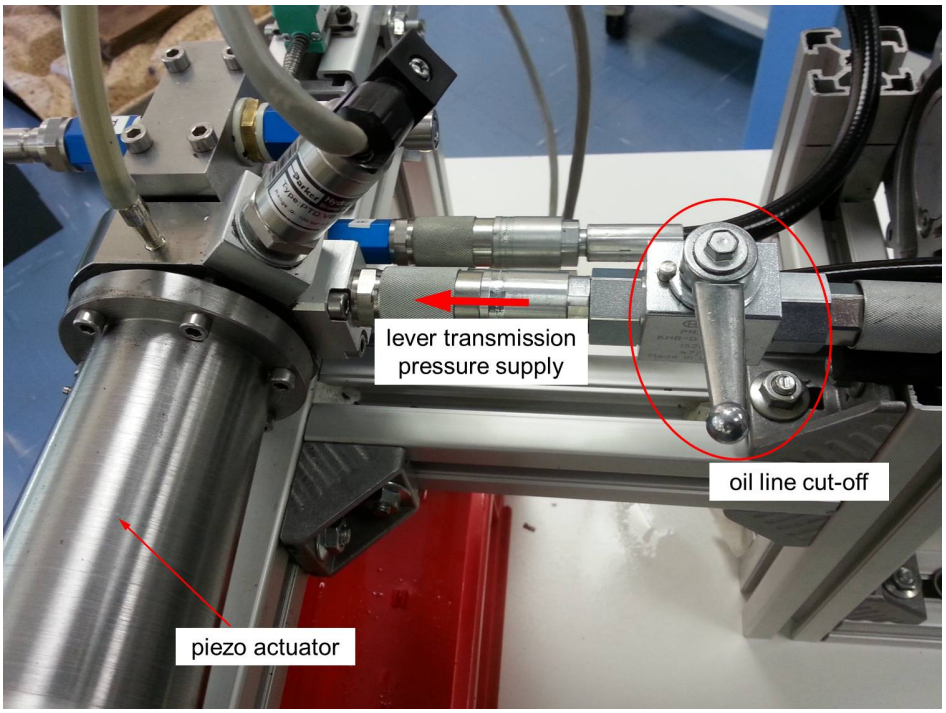

Figure 7.8: Oil cut-off cock for lever transmission

Another disadvantage arose because of the reduction of the translation piston's surface area. With a diameter of henceforth 20 mm the piston mounts directly onto the piezo adapter of the same diameter. This results in a two-piece piston that needs to be sealed by the rod seal in the lever transmission. While the piezo was operated, a significant amount of oil would be transported out of the lever transmission through the groove the two-piece piston forms. The oil pressure within the lever transmission would then drop quickly while the oil is moved into the piezo actuator housing. As a solution an adapter ring with a thickness of 4 mm has been manufactured that fits between the piezo actuator and lever transmission, as shown in Figure 7.9 (next page).

This results in a slightly increased oil volume within the lever transmission and hence slightly increased inertia for high frequency system operation, but at the same time ensures that only the front part of the translation piston in front of the groove reaches into the rod seal. This way the pressure within the lever transmission remains high and a system operation is possible.

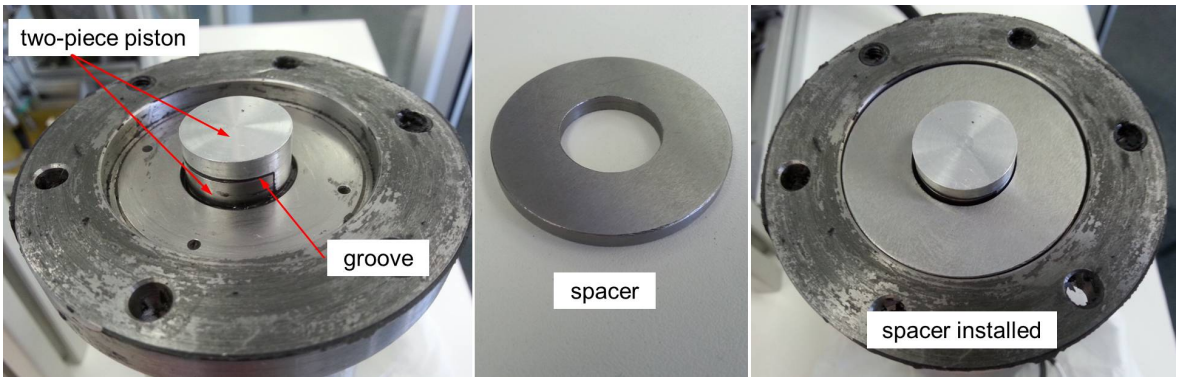

Figure 7.9: Installed spacer for lever transmission

7.4 Test results

The first test results proved that the return spring within the control unit was not yet sufficient to reach all required switching positions. Elimination measures will be introduced in this section. In the following step gradually all system components are added to the setup for consecutive experiments, that will be analysed. Then, recorded valve lift curves, subject to different boundary conditions, will be discussed. Finally, an approach for an engine valve brake implementation, one of the introduced research problems to be solved (compare Section 4.2), will be presented.

7.4.1 Control piston movement

In a subsequent experiment with the lever transmission, after implementation of the afore-mentioned measures, it became apparent that even though the control piston reciprocates, without an increased preload it does not reach its initial position, which the return spring should return it to. The results of an experimental approach with different return spring preloads can be seen in Figure 7.10. (next page)

The pressure in the lever transmission was set to $4\,MPa$ for this experiment, the piezo actuator operated with a sine wave showing a frequency of $7\,Hz$.

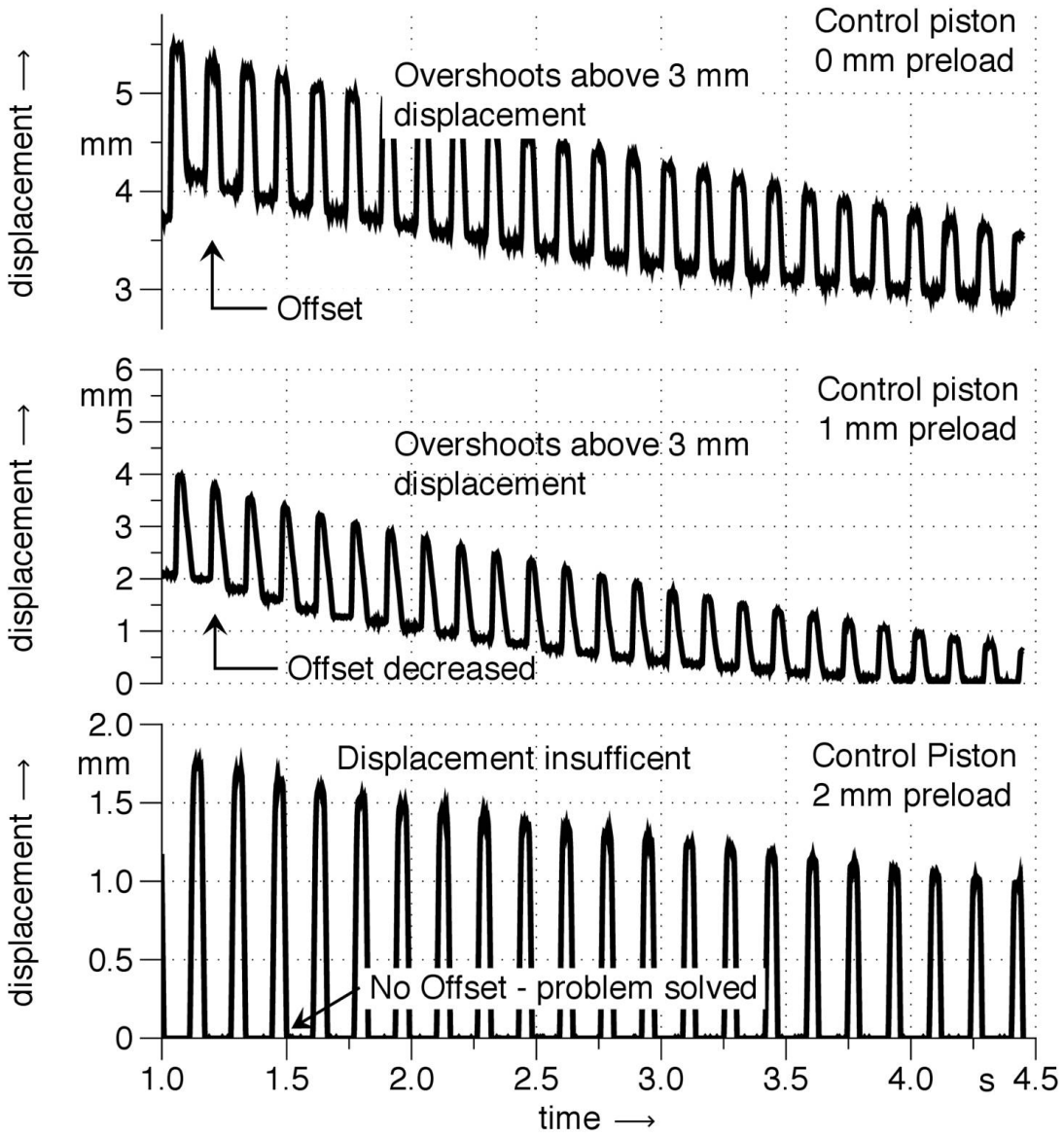

Figure 7.10: Control piston displacement in dependency of chosen return spring preload

Additional return spring preload: 0 mm

While the piezo actuator displacement would be absolutely symmetrical and alternate between 0 and 120 μm, the reciprocating control piston displacement takes place with a permanent offset far from zero on the ordinate. This is due to the tight tolerances of the control piston guides within the control unit. As the piston is guided in the servo cylinder and in the back of the control unit, after the assembly initially a minimal

misalignment of the components was found, that could not completely be eliminated by a reaming of these guides.

Hence, the control piston movement could only be enabled by increasing the pressure within the lever transmission to the stated $4\,MPa$. This leads to a higher force acting on the surface area of the piston, pushing it around $3.8\,mm$ out of the control unit housing initially. For this case the used return spring is not strong enough, meaning that the following reciprocating movement would take place with a displacement that would not be of use for the system operation. Also the amplitude of maximal $1.6\,mm$ peak-to-peak was insufficient yet.

What can also be seen is that the amplitude decreases within the recorded time of around 3.5 seconds. As the piezo showed a constant amplitude over the complete time of testing, this means that the pressure within the lever transmission still slightly reduces over time, even after modifying the lever transmission with a spacer. The problem can be found with the translation piston. The surface finish is not accurate enough to perfectly seal against the high pressure within the lever transmission. An additional complication is that the piston permanently moves within the rod seal that should maintain the pressure. Even though the manufacturer claims the seal is suitable for the piston velocity and applied pressure, it still shows difficulties when used with the translation piston.

Additional return spring preload: 1 mm

As both the maximum and minimum of the control piston displacement were of too high a value on the ordinate, a first attempt to move the displacement into the required operating range of the control piston between 0 and $3\,mm$ was to increase the preload on the return spring in the control unit by supporting it with a $1\,mm$ washer. It was expected that this would keep the piston from exceeding the $3\,mm$ range too far and would allow a higher return force to act on the piston and against the pressure in the lever transmission.

The boundary conditions piezo frequency and hydraulic pressure were maintained as in the previous test without spacers. According to the assumption the curve is located in a lower range on the ordinate, initially reaching $4\,mm$ as maximum displacement. The control piston, however, only reaches its zero position after a recording time of three seconds, while the amplitude is still steadily decreasing into an insufficient range.

With the higher preload on the return spring the amplitude is found to decrease quicker over the recording time. When the lever transmission is filled with oil and bled, the control piston acts with a higher return force against being pushed out of the control unit housing by the hydraulic pressure. Compared to the previous experiment with standard spring preload this results in a smaller oil volume within the lever transmission. As the reduction in amplitude is related to the translation piston seal leakage, a smaller overall oil volume leads to a quicker loss in control piston motion as the transmitting medium within the lever transmission fades. This implies that in general a higher preload moves the reciprocating curve lower towards the usable range, but sacrifizes recordable time within which an experiment can be run in a controlled manner.

Additional return spring preload: 2 mm

The use of two spacers for the return spring proved to solve one problem as the control piston always comes back to the zero position after a forward displacement. The maximum displacement further decreases compared to the two afore-mentioned cases, being now circa $1.2\,mm$ away from the desired $3\,mm$ position. Since the zero position could be reached throughout with this setup, it was decided not to add any more washers. In general a sensitive dependency between spring preload and lever transmission pressure could be observed in all previous experiments.

Increased piezo amplitude

All tests have been undertaken with a piezo actuator displacement of $120\,\mu m$. To ensure that the control piston both reaches the zero position and reaches at least $3\,mm$ displacement at the same time, the piezo displacement was increased by 50 % to the maximum value of $180\,\mu m$. All other boundary conditions remain unchanged. Figure 7.11 shows the result.

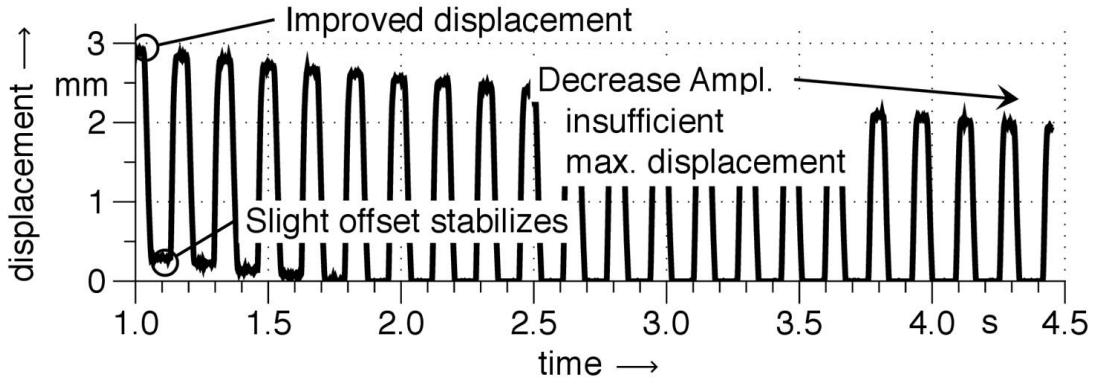

Figure 7.11: Control piston displacement: increased piezo amplitude

Even though the control piston movement shows a fundamental improvement compared to that of the previous cases, a slight zero-offset of the piston return position can be seen due to the enhanced piezo displacement. Also the desired maximum displacement of $3\,mm$ cannot be fully reached and is not being maintained. The value quickly drops to $2\,mm$.

Frequency of the generated function

Continuous testing showed that there is a strong dependency between actuator frequency, piezo amplitude and control piston position. Figure 7.12 (next page) shows the result of an experiment that is identical to the previous one except for that the piezo actuator frequency was changed from $7\,Hz$ to $14\,Hz$, which equals a simulated engine speed of $1680\,{}^{1}/_{min}$.

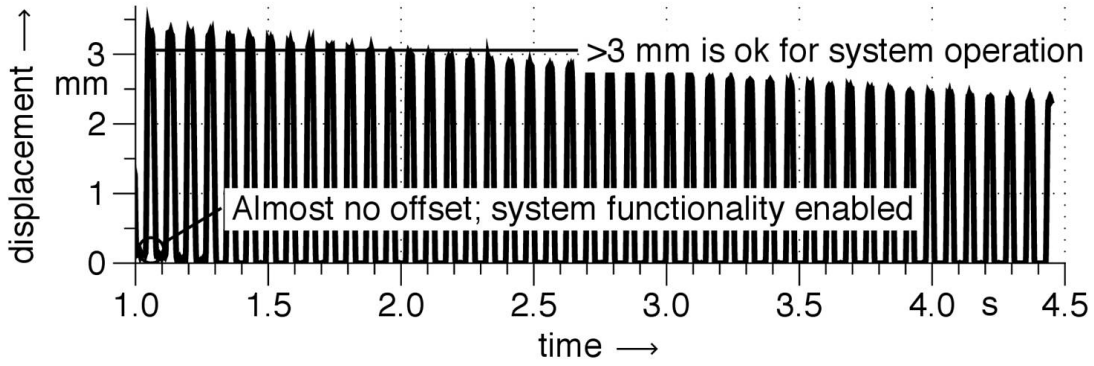

Figure 7.12: Control piston displacement: increased frequency

The higher frequency results in a minimal residual zero-offset that disappears within the first second of recording. Interestingly, the maximum displacement of the control piston exceeds $3\,mm$, allowing all required switching positions to be reached. Only after the two seconds mark on the abscissa the maximum amplitude starts to drop below $3\,mm$. In the previous case the maximum amplitude dropped much quicker and after two seconds, decreased to around $2.6\,mm$. Thus, a higher actuator frequency increases the maximum displacement of the control piston by about $15\,\%$ at two seconds recording time under otherwise identical conditions.

As the best results were gained with two spring spacers for the control unit return spring, this setup will be maintained throughout all further tests. The remaining problem is the drop in amplitude over recording time. Experiments with the servo valve being connected to the control unit have been executed in the next step to gradually involve the FVVT system components and analyse their reaction on the gained control piston displacement.

7.4.2 Servo piston motion

A subsequent experiment involving the servo valve and an actuator frequency of $14\,Hz$ which proved successful in the afore-mentioned tests, allows analysis of the servo piston's reaction to the control piston displacement.

Servo piston motion: sine function

The first attempt with a sine function sent from the function generator to the piezo actuator can be seen in Figure 7.13.

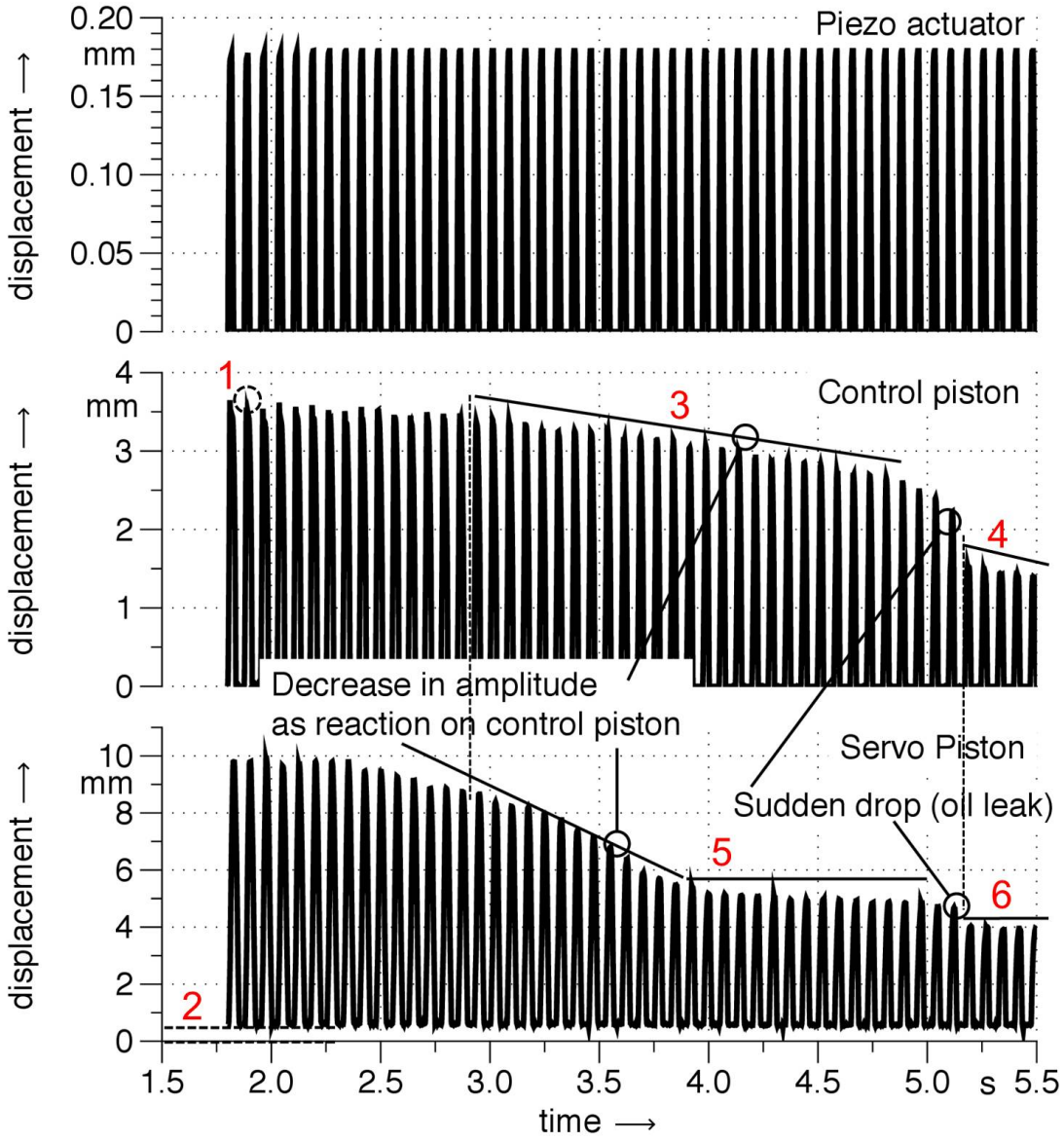

Figure 7.13: Servo piston movement in dependency of control piston position; sine function

The pressure within the lever transmission for this experiment was set to $5.1\,MPa$, while a pressure of $2\,MPa$ was used for the lines connecting the control unit and

the servo valve. The piezo actuator displacement behaves exactly according to the function generator frequency, reciprocating 14 times per second between 0 and the maximum displacement of $180\,\mu m$. Within the first second of recording time the control piston trajectory shows an overshoot in the area of the peaks close to $3.5\,mm$ displacement (1). A close-up analysis of the individual peaks and all correspondent acquisition data showed that the initial pressure within the lever transmission peaks close to $9.5\,MPa$, while the piezo actuator extends. This pressure peak clears during the first second of initial testing and hence the overshoot is not present any more in the further control piston trajectory.

A constant zero-offset of the servo piston motion (2) was found to be caused by an imprecise sensor calibration. As $0.5\,mm$ in the real test setup equals $0\,mm$, the shown maximum displacement also needs to be deducted by $0.5\,mm$ to a maximum value of initially around $9.3\,mm$. As the mechanical stops within the servo valve are $10\,mm$ apart from each other, determining the maximum displacement of the servo piston, the control edges of the servo piston elements open the hydraulic ducts within the servo valve by $4.3\,mm$ of their width of $5\,mm$. Thus, a malfunction of engine valve opening and closing is not expected by the servo piston not fully reaching the mechanical stop. The slightly reduced maximum displacement may be caused by the comparatively low pressure within the hydraulic lines and the piston having too much friction within its guides in the servo valve.

However, while the experiment progresses over recording time, the maximum displacement of the control piston decreases steadily, as discovered in previous experiments (3). At around $5.1\,s$ the displacement drops significantly and abruptly (4). Analysing the pressure transducer's signal shows that the pressure within the lever transmission drops gradually, not abruptly around the viewed time. Still, it does not seem to be sufficient to move the control piston out of the control unit further, due to the lever transmission seal permanently leaking oil in small increments.

The black vertical broken lines in Figure 7.13 indicate that the servo piston displacement is directly influenced by the control piston motion, which proves a very fast reaction time of the system with regard to the tested actuator frequency. The decrease in displacement initially shows a steeper gradient at the beginning, compared to the control piston, and then levels out (5). This means the servo piston reacts sensitively to the control piston motion. In this area already, it can be expected that the servo piston displacement is not sufficient any more to enable engine valve opening and closing. The abrupt drop in maximum displacement to the end of the experiment, can also be found for the servo piston (6).

Servo piston motion: rectangular function

To analyse if a different actuator function has an influence on the results, in the next step the same experiment was run with a rectangular function instead of the sine function. For optimal comparison to the previous case the sampling time on the abscissa and the shown recording duration have been chosen to be identical. Figure 7.14 (next page) shows the results.

The servo controller of the piezo actuator amplifier reacts in a very sensitive way to the amplitude settings of the function generator. Unfortunately, the gained rectangular function within this test shows a two-stage peak for the piezo actuator displacement throughout. However, the function can be used for the further investigations of the redesigned FVVT system.

Compared to the previous set of graphs, the considered characteristics remain very similar. Yet, it becomes obvious that the servo piston displacement reaches its peak more consistently and for a longer time at the beginning of the experiment. The first 12 maxima maintain a very similar value on the ordinate, while each peak is much wider in horizontal direction. This means that the switching positions within the servo valve can be reached better and maintained longer, which may have a positive influence on engine valve opening and closing once the complete system is being operated. This will be further examined in the following step.

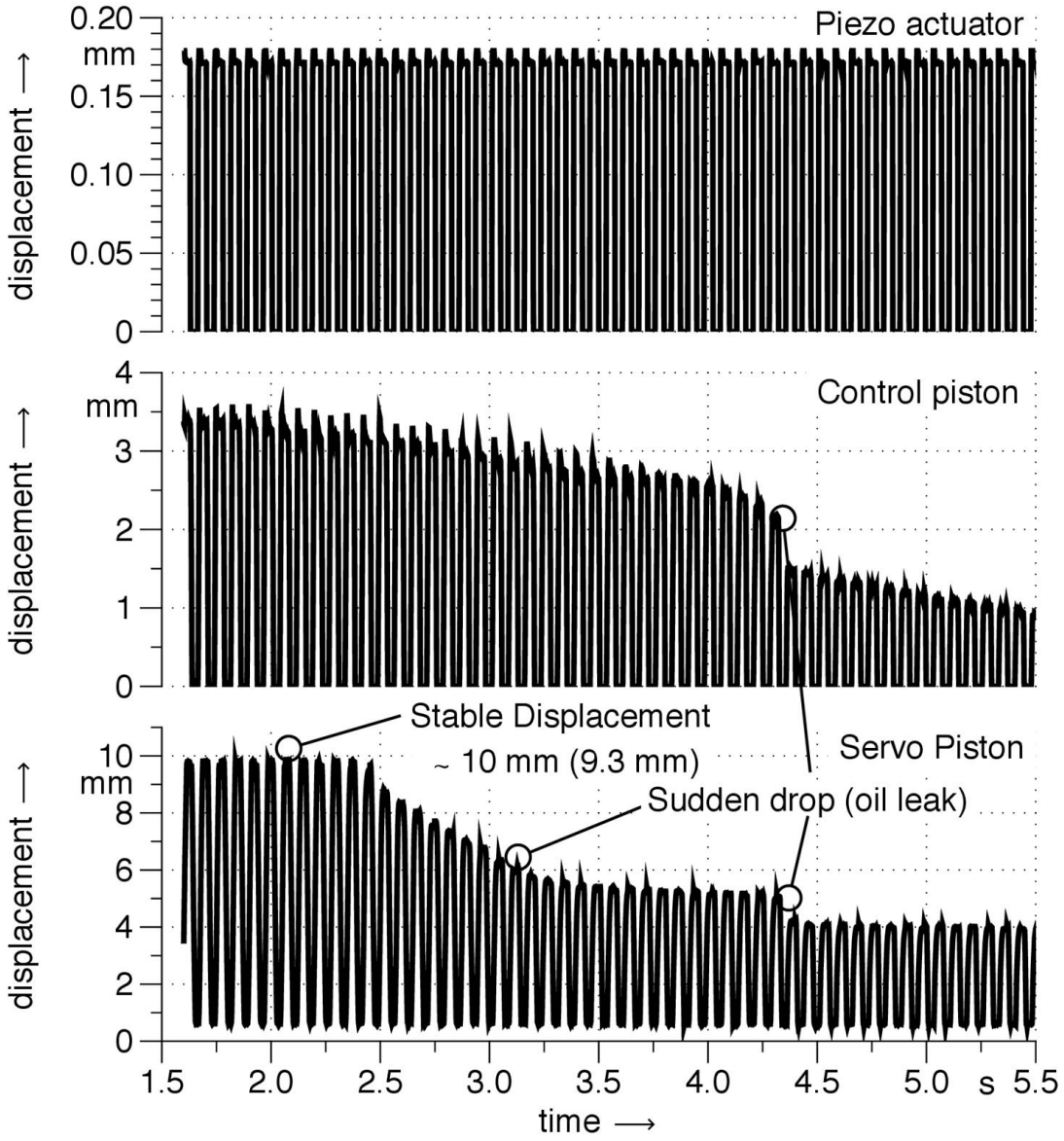

Figure 7.14: Servo piston movement in dependency of control piston position; rectangular function

7.4.3 Engine valve lift curve

To complete the experimental setup, in the next step the servo valve has been connected to all hydraulic lines, so as to add the engine valve motion to the data being acquired.

Engine valve motion: sine function

The results of a test, run with a sine signal at a frequency of circa $12\,Hz$, are shown in Figure 7.15 (next page).

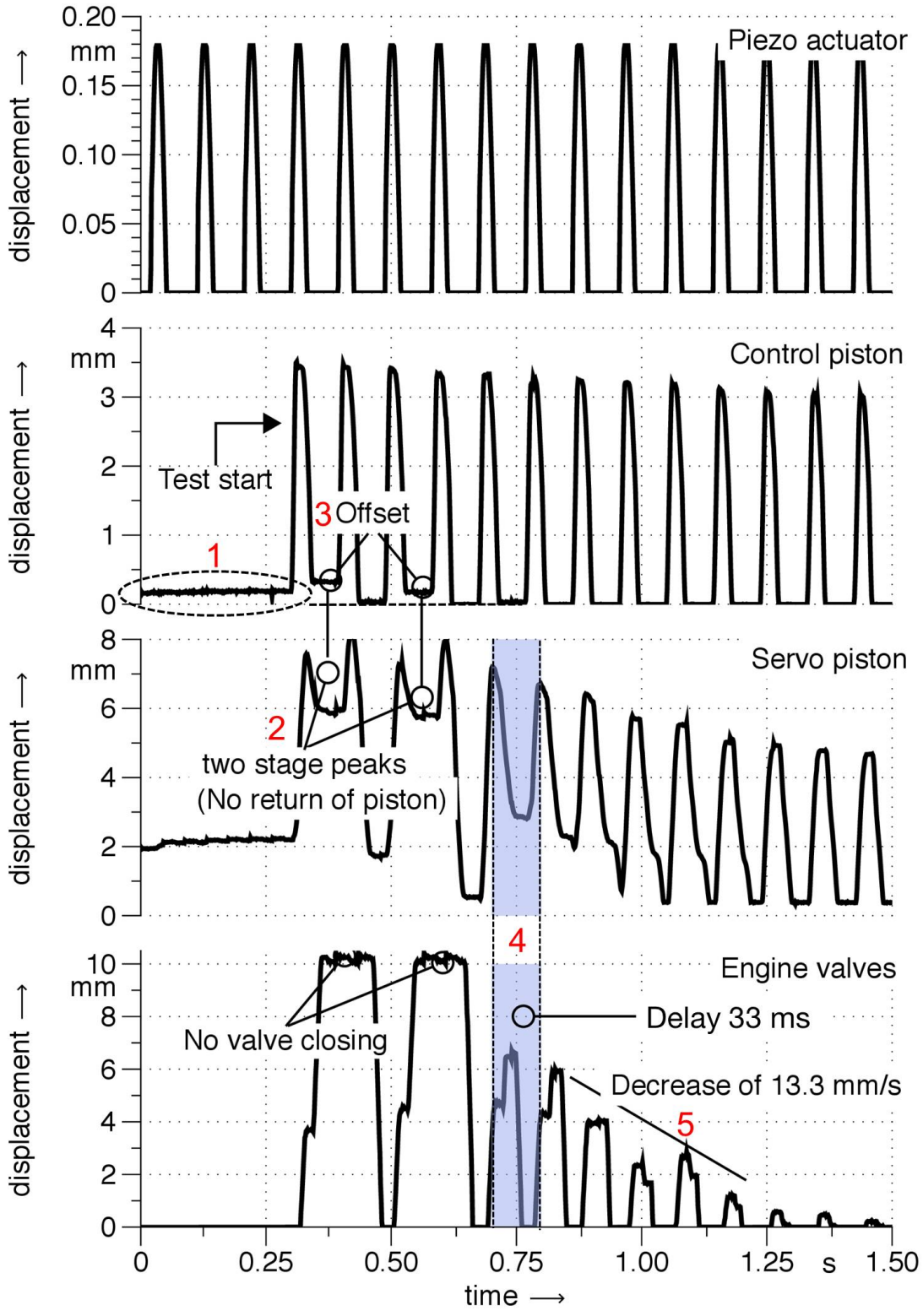

Figure 7.15: Full experimental setup; sine function

The initial time delay of around $0.3\,s$ (1), seen on the control piston, servo piston and engine valve displacement, is caused by the oil cut-off cock in the supply line of the lever transmission. While the piezo is turned on already with the cut-off cock being closed, the reciprocating movement of all piloted movable pistons only starts once the cut-off cock is opened, filling the lever transmission and is closed again quickly afterwards, enabling the control piston to oscillate. Servo piston and engine valve motion graphs are formed in consequence of the latter.

A first experiment with only $7\,Hz$ actuator frequency did not produce any usable acquisition data in case of servo piston and engine valve motion. After increasing the frequency, however, the servo piston displacement initially shows a different behaviour, compared to the experiment, in which the engine valve movement has not yet been recorded, and the servo piston showed a more consistent graph (compare Figure 7.13). Now, the servo piston displacement shows two wide, two-stage maxima (2), directly influencing the maxima of the engine valve displacement. Each two-stage maximum, judged from the actuation frequency, is supposed to consist of two individual reciprocating motions of the servo piston. Within the first two peaks the servo piston only returns to $6\,mm$ and only with increasing recording time reaches low values close to zero, as supposed to. The reduced return position of the servo piston can be explained by the control piston's behaviour within the same time frame. For both discussed wide maxima the control piston does not fully reach its initial position, leaving a gap between 0.2 and $0.4\,mm$ to zero (3). This means, the switching position enabling engine valve closing, could not be fully reached, allowing oil pressure to reach both end faces of the servo piston. Once the control piston reaches the zero position continuously within the remaining recording time, the wide two-stage maxima as seen no longer occur.

The only change undertaken compared to the previous tests is the addition of the engine valve motion to the setup. This shows an influence on the servo piston oscillation, especially in comparison to the servo piston motion without added engine

valve motion (compare Figure 7.13). In the latest experiment it can be seen that the servo piston motion is affected by the additional, vertical oil flow through the servo cylinder, reaching down to the engine valve stem pistons through the additionally connected lines (H), (D) and (F) (compare Figure 4.8). The pressure used in the supply (D) is identical to the maximal hydraulic pressure acting on the servo piston end faces via lines (J) and (L) (compare Figure 4.8). The graph showing the servo piston oscillation is affected almost throughout, stabilizing only from the $1.2\,s$ mark and hence close to the end of the experiment. The peak displacement of the servo piston maximal reaches just over $8\,mm$ and cannot be held constant as is the case when the engine valve motion is not added to the experiment.

Comparing the reciprocating servo piston motion to the correspondent engine valve motion, it can be seen that the engine valves' reaction is slightly delayed to the piston's movement. To show this, one peak-to-peak movement of the servo piston has been compared to the correspondent engine valve motion (4). The actual time delay is around $33\,ms$. A plausible explanation of this delay would be the oil leak of the engine valve body, as the valve stems push a significant amount of oil out of the valve body, not allowing the hydraulic pressure and very fast reaction times to be maintained within this component.

The drop in engine valve displacement is very abrupt with a decrease of around $13.3\,{}^{mm}/_{s}$ (5). This is a reaction to the servo piston motion, with gradually decreasing maxima not being able anymore to overcome the center position within the servo valve, which would be necessary to enable engine valve opening.

Engine valve motion: rectangular function

Next, another test involving all system components was executed, this time using a rectangular instead of a sine function. For improved comparison, the experiment shows the same duration as the previous one. Figure 7.16 (next page) shows the results.

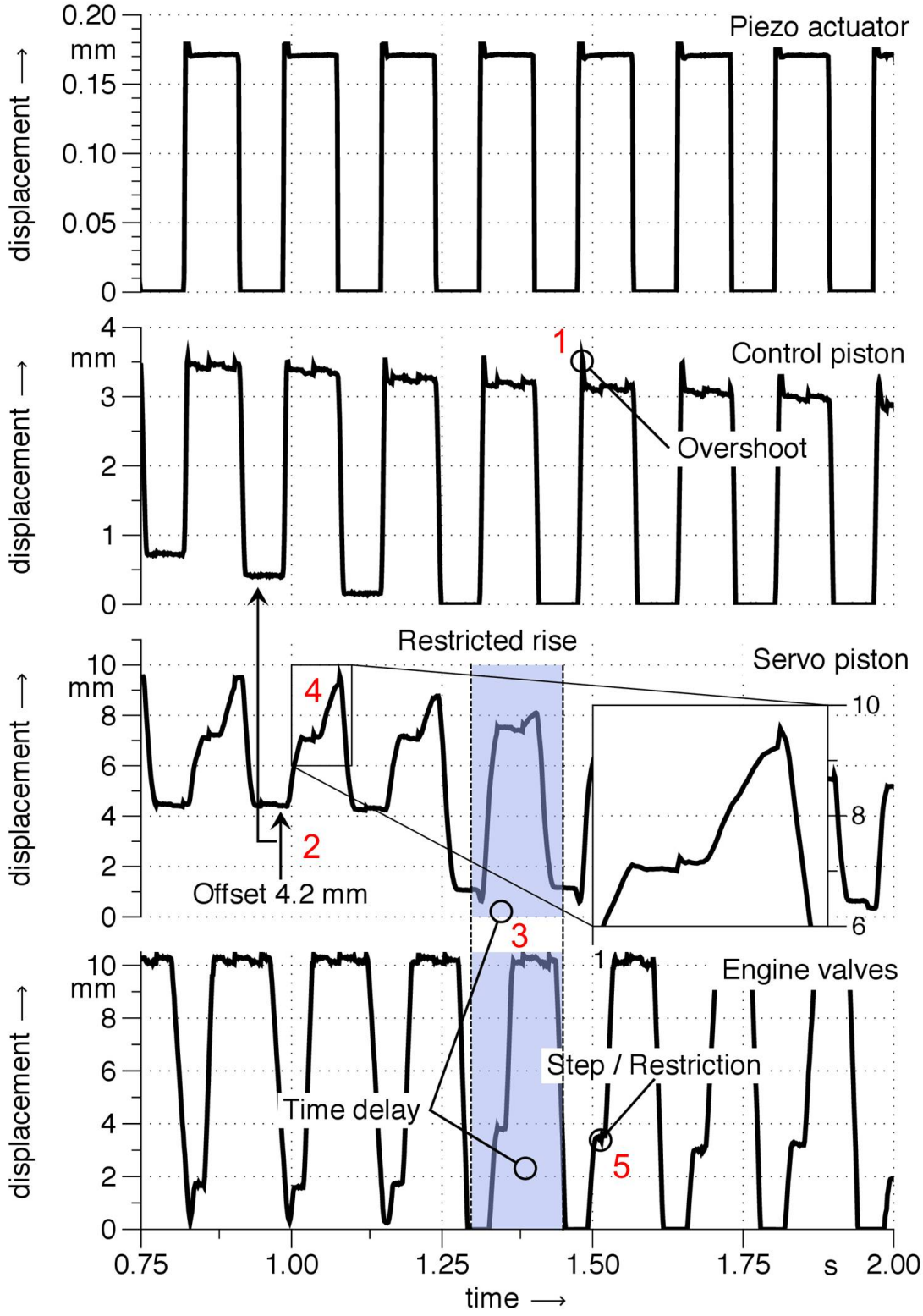

Figure 7.16: Full experimental setup; rectangular function

The rectangular function still shows some imperfections in the area of the maxima of the piezo actuator motion, as found before the engine valve motion was added (compare Figure 7.14). The small peaks at the beginning of the maxima are reflected in the control piston displacement, where they can also clearly be seen (1). Further, the control piston motion is subject to an undesired oscillation in the area of the maxima, where the piezo actuator motion is perfectly level. This deviation is within the range of a tenth of a millimetre and can either be caused by vibration of the test bench or the return spring in the control unit.

Same as in the previous experiment with sine fuction, the servo piston shows a significant zero-offset (2), here around $4.2\,mm$ within its first two minima, while the control piston is not being fully returned to its initial position. This is the case for the first three minima shown in Figure 7.16. Otherwise, the servo piston displacement improved at its peaks to close to $9.5\,mm$, compared to the just over $8\,mm$ from the previous experiment.

The slight delay in reaction time of the engine valve motion following the servo piston displacement, also occurs in this experiment (3). The range of delay is reduced compared to the experiment shown before, with a maximum value of about $16\,ms$.

For the first four reciprocating servo piston motions the graph reaches its maximum slightly delayed. Each maximum rises in two stages (4). This will also be related to the control piston not fully reaching its initial position, as the effect cannot be seen any more after the control piston reaches its zero position again. Once this is the case the servo piston also reaches displacements closer to zero, which enables it to carry more momentum for the following full reciprocating movement, meaning only now can it overcome the counteracting forces and the spring force of the opposing spring in the servo valve.

A characteristic step in all engine valve trajectories can be seen (5). This may occur due to the afore-mentioned oil leak of the engine valve body, hindering engine

valve opening for a very short time. Interestingly, this effect occurs at different engine valve displacements and never on a decrease of the graph. This might point out that the leak originates from the volume on top of the engine valve stem pistons.

Even though the engine valve displacement leaves some room for discussion, as expected from the very first experiment with a rectangular function, compared to the previous engine valve trajectory with sine function (compare Figure 7.15), the engine valve movement is by far the more consistent and reaches the $10\,mm$ valve lift throughout.

Engine valve motion: final result

As the previous results to a certain extent still showed unsatisfactory trajectories for all moving parts, the amplitude and offset settings of the function generator were modified, until a flawless rectangular function for the piezo actuator was achieved. The reactional motions of all moving parts could be significantly improved, as seen in Figure 7.17 (next page).

The experiment has been run with a lever transmission pressure of $4.2\,MPa$. A low frequency of $2.5\,Hz$, equaling a theoretical engine speed of $300\,{}^{1}/_{min}$, has been chosen to allow for a precise analysis of all events occurring during the engine valve actuation process. The engine valve opening time as seen in the graph equals $0.26\,s$ for the viewed case. With the model sampling time of $90\,\mu s$ in combination with the preset downsampling factor of 14 in ControlDesk (compare Figure 7.6), a data point is being recorded every $1.26\,ms$, or reciprocal 793 data points are collected in one second respectively. Multiplying these with the mentioned engine valve opening time, emphasizes that the chosen low experimental frequency displays each valve lift trajectory using 206 data points. In comparison, with the preset downsampling factor, for a simulated engine speed of $2000\,{}^{1}/_{min}$, one valve lift curve would be represented by only circa 30 data points, not allowing the same degree of detail for a precise analysis of the occurring events.

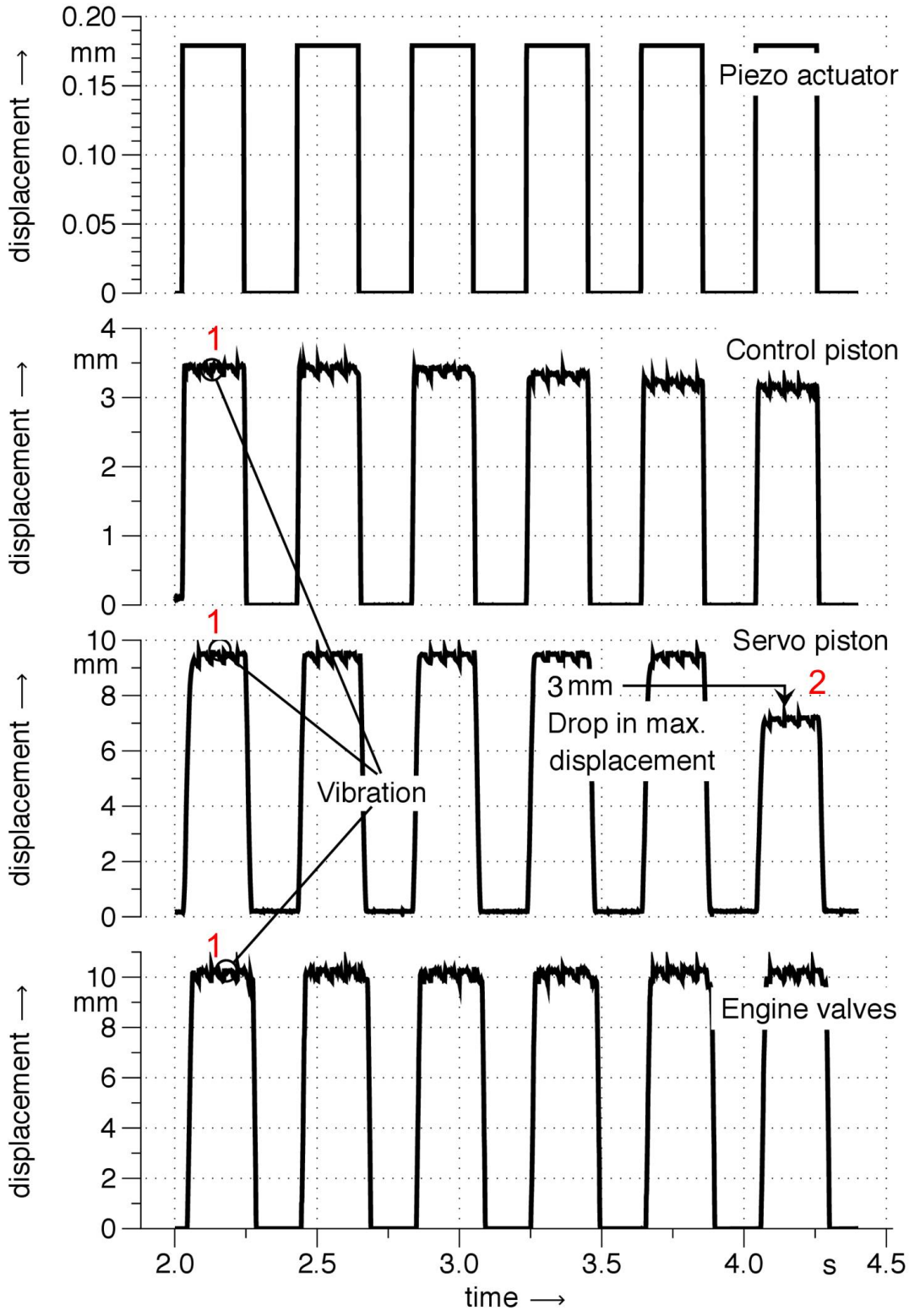

Figure 7.17: Full experimental setup; optimized rectangular function

In Figure 7.17, the piezo actuator graph shows horizontal maxima throughout without any overshoot or inconsistency. As a consequence, the trajectories of control piston, servo piston and engine valves follow this behaviour accurately. In all graphs, except for the piezo actuator, a form of vibration can still be seen (1), that originates from the control piston and is reflected in all subsequent graphs.

However, there is no longer a problem of the servo piston graph showing two-stage peaks and a zero-offset. The servo piston reciprocates between 0 and close to $10\,mm$ as desired, being very uniform until the last maximum (2) that drops to $7\,mm$ due to the decreasing control piston displacement caused by the slight oil leak within the lever transmission, as discussed before.

The final output, the engine valve trajectory, is oscillating between 0 and $10\,mm$ accurately and repetitively. Even the last shown, reduced servo piston maximum, is sufficient to enable full engine valve opening. In Figure 7.18 the graph showing the dynamic lever transmission pressure can be seen.

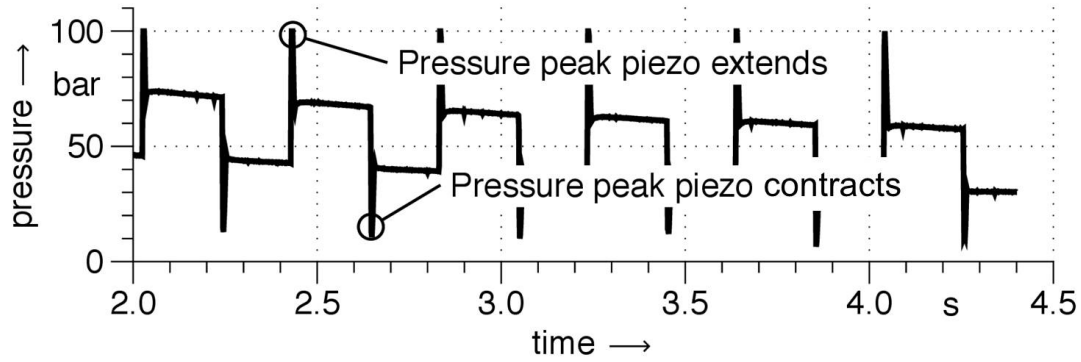

Figure 7.18: Dynamic lever transmission pressure; optimized rectangular function

The graph directly correlates to the piezo actuator motion. For each reciprocating movement two distinctive peaks can be found. The first peak is a narrow maximum reaching $10\,MPa$, that occurs as the piezo actuator pushes the translation piston into the oil volume of the lever transmission. After a fraction of a second the pressure

drops quickly by about $3\,MPa$ and later in the experiment by about $4\,MPa$ and stays relatively level. As soon as the piezo actuator and connected translation piston reach the zero position, the pressure drops down abruptly, forming a peak heading downwards, that looks similar to an inversion of the afore-mentioned $10\,MPa$ peak. During the experiment, the pressure drops to values close to $1\,MPa$ and below. While the piezo actuator remains at zero displacement, the pressure initially levels out at around $4.2\,MPa$, equal to the pressure supplied to the lever transmission, and from there in the subsequent steps drops gradually due to the afore-mentioned oil leak of the rod seal within the lever transmission. The explained event repeats in an identical way for each reciprocating movement of the piezo.

A full adjustability of the engine valve lift curve for any simulated engine speed is not yet fully enabled, but after finishing touches on the mechanical side of the system, it definitely has the potential to be operated in an even far wider range. Concluding the presentation of graphs, the last shown results represent the best optainable data of the system yet at its early stage of development.

Generally speaking for the redesigned FVVT system, during experimentation the center position of the servo piston within the servo valve at no point needed to be fine-adjusted, as this is determined by the two identical compression springs used in the valve, which is an advantage compared to the previous FVVT system, where the center position needed to be approached gradually to reach the initial setpoint to start tests.

Another advantage is that in the case of a power cut, the piezo contracts immediately, and due to the layout of the hydraulic ducts, in this position instantaneously closes the engine valves. This is important with regard to an implementation of the system on a combustion engine, where the piston otherwise may interfere with the engine valves in TDC when an electrical fault occurs, which would lead to deterioration of the engine. This cannot occur with the redesigned FVVT system.

Further, the indirectly controlled system features unrestrained motion of the hydraulic transmitting medium in all hydraulic lines, giving the system an advantage over the design in the presented feasibility study (compare Section 4.1) and solving one of the research requirements (compare Section 4.2) at the same time.

7.4.4 Engine valve brake

An approach for an engine valve brake has been presented within the previous, directly controlled FVVT system. As this system also still is at an experimental stage, the engine valve brake is a concept that has not been implemented into the test setup yet. The concept is illustrated in Figure 7.19 (next page).

In the graph above a standard servo piston trajectory is shown, as used within the directly controlled FVVT system, incorporating no valve brake. In this setup a displacement increasing from the center position within the servo valve ($5\,mm$) means engine valve closing; in the range below $5\,mm$ the engine valves are being opened. In the final setup of the previous FVVT system, and within the redesigned system the servo piston motion has an inverted effect on the engine valve motion. Hence, a rising servo piston trajectory within the redesigned FVVT system is in accordance with engine valve opening while a decreasing trajectory represents engine valve closing. This, however only depends on whether the piezo actuator is mounted to the left or right side of the servo valve as this inverts the function of its inner hydraulic ducts leading to the top or bottom of the valve stem pistons (compare areas 7/8 in Figure 3.4) and has no negative effect on the basic idea of the engine valve brake.

The graph at the bottom of Figure 7.19 shows the same servo piston motion with integrated engine valve brake. The timeframe of one valve actuation cycle is only about $8\,ms$, which according to Figure 4.2 and previous calculations is consistent with the maximum simulated engine speed of $8000\,{}^{1}/_{min}$ or an actuation frequency of $67\,Hz$.

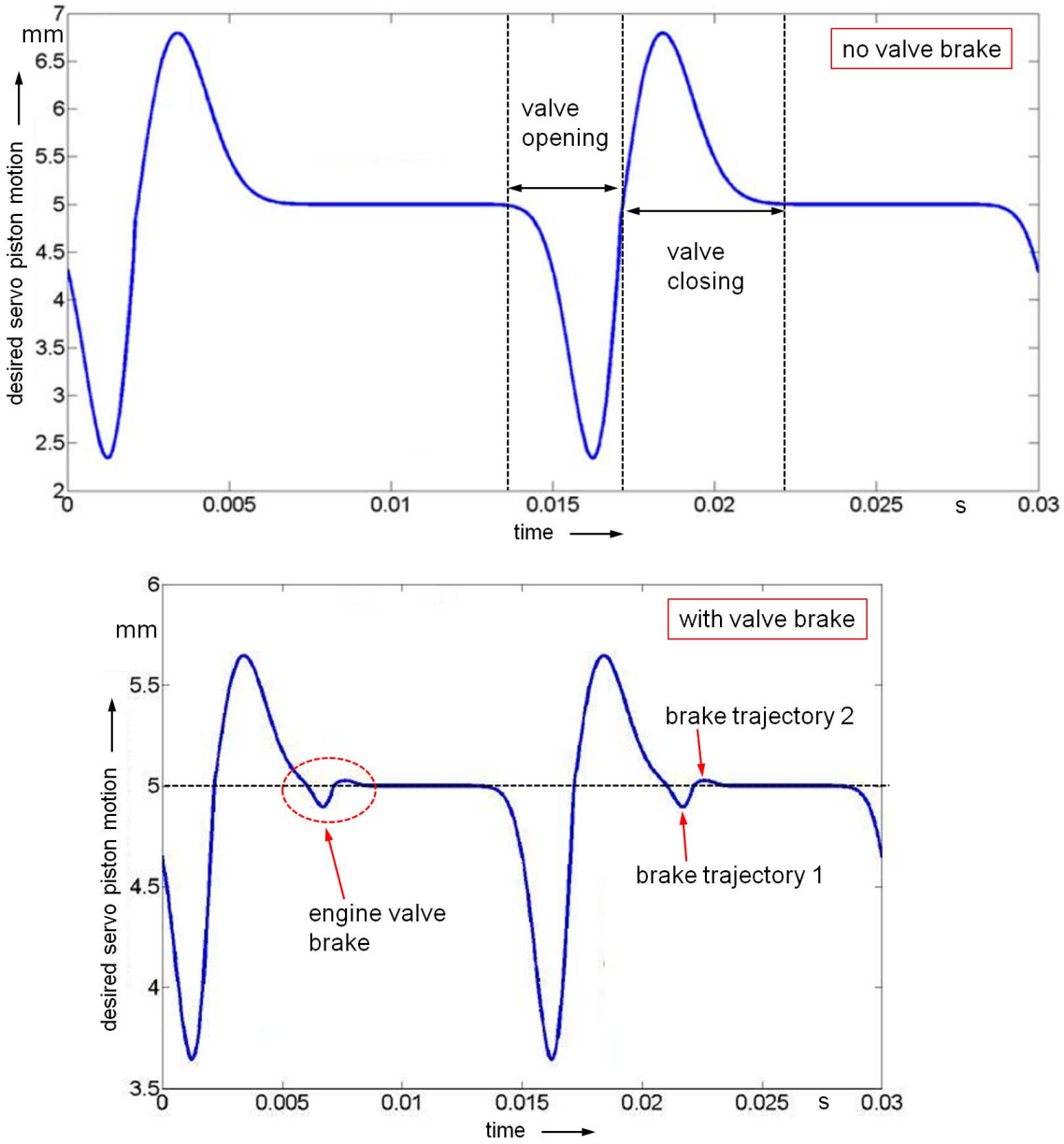

Figure 7.19: FVVT engine valve brake concept

Following one of the two repetitive events shown in the bottom illustration in Figure 7.19, it becomes apparent that the main oscillation of the servo piston in either direction orientates itself around the center position within the servo valve at $5\,mm$ on the ordinate. A horizontal broken line has been added to emphasize this. With the valve brake implemented, the engine valve opening remains unchanged, yet at the end of valve closing, the servo piston motion is dropped below the center position

for a time of not even $2\,ms$ (compare brake trajectory 1). This means the pressure distribution above and underneath the valve stem piston is abruptly being inverted, just before the engine valves, approaching the bottom of the cylinder head at high velocity, would hit the valve seats, causing damage in a long-term application. The pressure building up on top of the valve stem pistons, brakes the engine valve velocity down significantly and might not yet enable fully closed engine valves.

Hence, in the following step another closing trajectory is added, rising just above the center position of $5\,mm$ (compare brake trajectory 2). As this has to compensate only a minimal remaining engine valve lift, the piston oscillation is even smaller than seen at brake trajectory 1. As pressure will build up gradually while the servo piston opens the according control edge within the servo cylinder, the engine valves will not experience a critical acceleration and soft landing is enabled. The brake trajectories can be seen as an additional scaled-down valve opening and closing feature within a minimal displacement range of both servo piston and engine valves.

The functionality of the redesigned FVVT system allows an implementation of the valve brake concept. Even though the control unit is an interconnected component of the setup that has not been part of the previous system, the previous experiment proved that the servo piston motion follows the control piston motion accurately and without noticeable time delay.

Identical to the previous FVVT system it would be necessary to incorporate a changed function that is being sent to the piezo actuator, resulting directly in the modified servo piston movement in the case of the previous system and indirectly in the case of the redesigned FVVT system, where another (control) piston is added to the setup. However, further investigations would be necessary to analyse if the engine valve brake works up to the maximum simulated engine speed. This conclusion is valid for both the directly and indirectly controlled system. That the system within this project allows the implementation of the engine valve brake concept, solves one of the research sub-problems and shows that in this matter no disadvantage compared to the previous system is obtained by the modifications.

7.5 Conclusion

After the completion of the test bench for the redesigned FVVT system and several improvement activities with regard to the physical system and the "MatLab/Simulink" and dSPACE software on the other hand, test results with the indirectly controlled engine valve actuator could be obtained. A continuous variation of actuator signal form, amplitude and frequency settings led to enhanced results, reaching an optimum by using a rectangular actuation function. The implementation of the engine valve brake approach, originally researched for the directly controlled system, can be implemented into the redesigned system throughout. Overall, the stated research requirements could be met to a large extent.

8 Research summary and future development

The core of this project is based on previous research and development results on a fully variable engine valve actuator for combustion engines, carried out at the "Ostfalia University of Applied Sciences" in Wolfsburg, Germany. The innovative electrohydraulic FVVT system makes use of the properties of a piezo-ceramic-based stack actuator, combining the piezo's precision with the force of a hydraulic actuator, operating the engine valve motion.

To further enhance the system, which aims at an improved overall efficiency of the combustion engine, lowering fuel consumption and CO_2 emissions while improving power output by replacing the conventional standard components camshaft, cam followers and valve springs, this research project focuses on the modification of the engine valve actuator to an indirectly controlled system, improving the system control.

Based on a feasibility study from 2010, a largely redesigned engine valve actuator could be manufactured and tested at the "Nelson Mandela Metropolitan University" in Port Elizabeth, South Africa, based on mathematical considerations and computer aided component design.

The redesign offers the advantage of a reduced effective piezo actuator displacement, allowing the implementation of a smaller actuator in future, which leads to

reduced velocities and mass forces of the movable parts the piezo acts upon. After several improvement activities the indirect control of the hybrid electrohydraulic actuator proves to be successful. The existing Simulink model, subject to previous research at the Ostfalia University, has been used as a basis for the system control and could successfully be adapted to the new actuator design. The modification of the Simulink model included the deleting of all signal connections to the "RapidPro" system, a yet unused optional component connecting to the utilized dSPACE "MicroAutoBox", making the overall system more compact and simplified. Through the implementation of lightweight aluminium alloys the overall mass of the system could be reduced significantly.

Since the system still features limitations regarding full adjustability of the valve lift curve and usable signal function forms due to slight oil leaks and its early stage of development, future research should focus on refining the mechanical properties of the system to realize its full potential. The overall dimensions and the weight of the test setup could be significantly improved by using smaller components made out of lightweight material.

An approach using rotary instead of poppet engine valves, while maintaining the benefits of a piezo actuator, is imaginable. Research in this direction is currently being undertaken by Zibani, Chuma, and Marumo (2014), featuring flexible valve event control on a single piston rotary valve engine control unit [43].

This continuous research and its results are a contribution to the development of more efficient, environment friendly engines for motor vehicles, implementing innovative technology into conventional powertrains, that are able to meet the latest emissions legislation and industry demands.

9 Appendices

9.1 Technical specifications BMW K71 engine [44]

Engine	
Type	Water-cooled 4-stroke in-line two-cylinder engine, two overhead camshafts, four valves per cylinder, dry sump lubrication
Bore x stroke	82 mm x 75.6 mm
Capacity	798 cc
Rated output	90 hp (66 kW) at 8,000 rpm
Max. torque	63 lb/ft (86 Nm) at 5,800 rpm
Compression ratio	12.0 : 1
Mixture control / engine management	Electronic intake pipe injection, digital engine management (BMS-K+)
Emission control	Closed-loop 3-way catalytic converter, emission standard EU-3
Performance / fuel consumption	
Maximum speed	Over 125 mph
Fuel consumption per 100 km at constant 90 km/h	69 mpg, at a constant 55 mph
Fuel consumption per 100 km at constant 120 km/h	55 mpg, at a constant 75 mph
Fuel type	Unleaded super
Electrical system	
Alternator	three-phase alternator 400 W
Battery	12 V / 12 Ah, maintenance-free
Power transmission	
Clutch	Multiple-disc clutch in oil bath, mechanically operated
Gearbox	Constant mesh 6-speed gearbox integrated into crankcase
Drive	Belt drive

9.2 Technical drawings: control unit

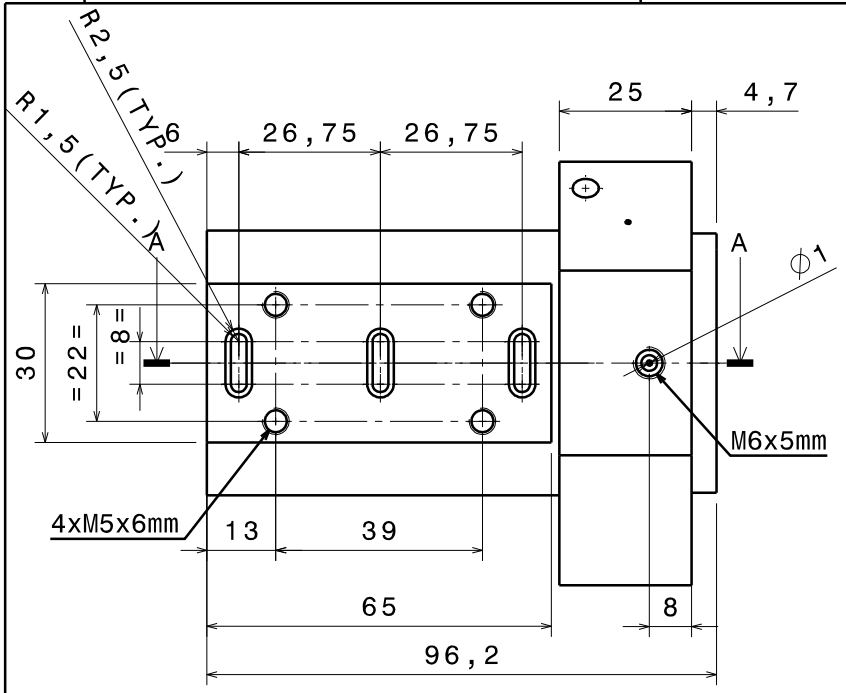

Top View

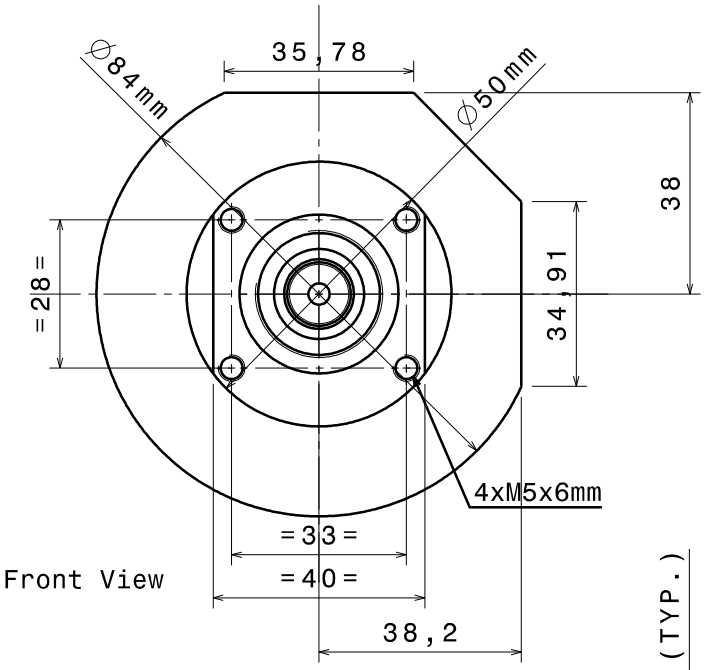

Front View

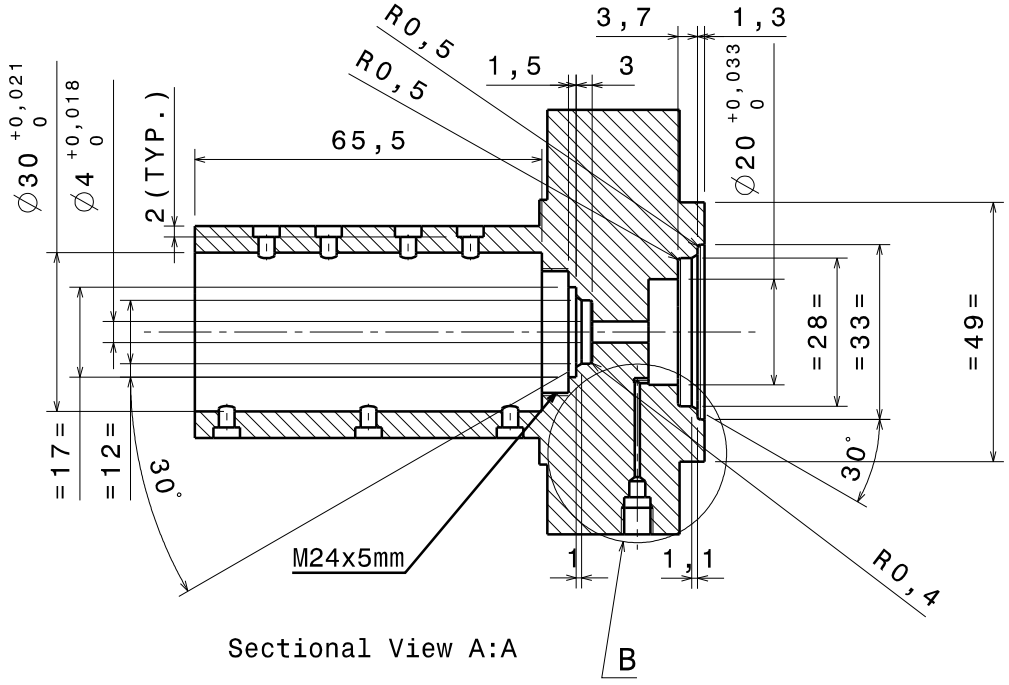

Sectional View A:A

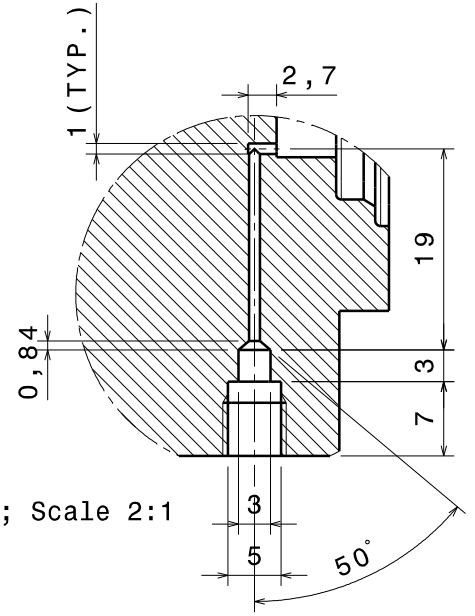

Detail B; Scale 2:1

		Scale: 1:1, 2:1	Quantity: 1
		Name: Behre First Name: Leander	
Date	Name	Component Description	
06/12/13	Behre	CONTROL UNIT HOUSING	
		Material 42CrMo4	
		Drawing No.	Sheet 1/3
Created with CATIA V5			DIN A3

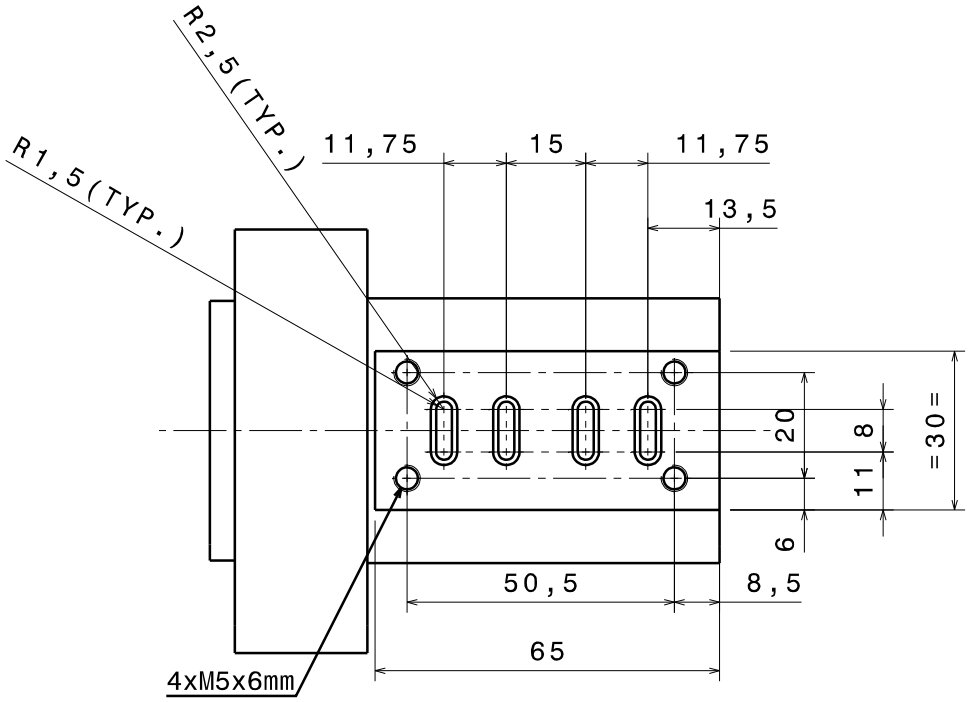

Bottom View

Numbers 1-2 show the surfaces for angular side views

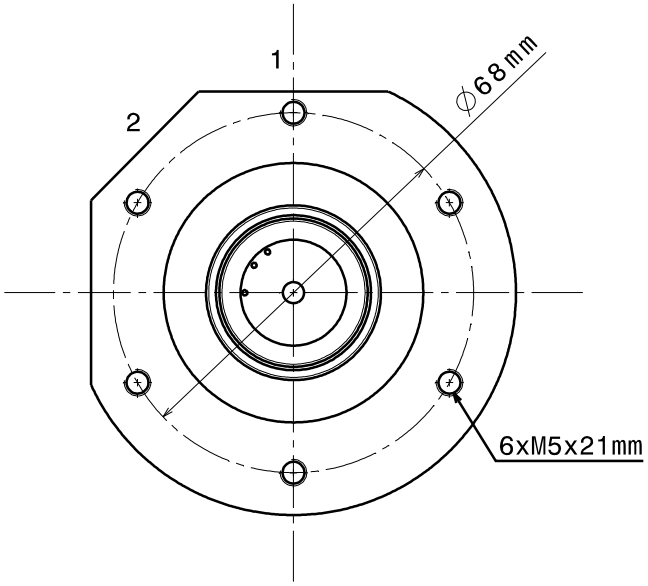

Rear View

						Scale: 1:1	Quantity: 1
						Name: Behre First Name: Leander	
				Date	Name	Component Description CONTROL UNIT HOUSING	
				06/12/13	Behre		
						Material 42CrMo4	
						Drawing No.	Sheet 2/3
							DIN AX
				Created with CATIA V5			

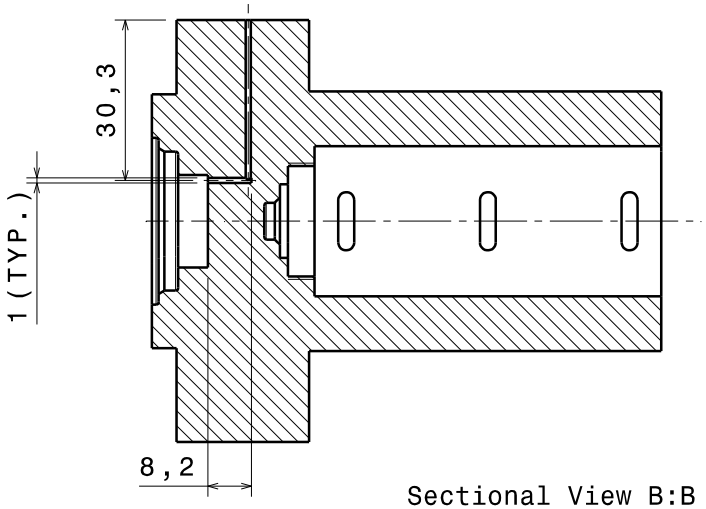

Sectional View B:B

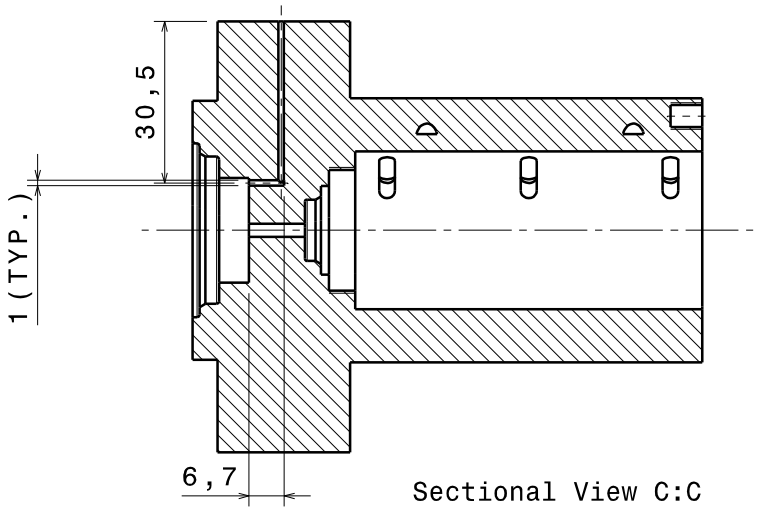

Sectional View C:C

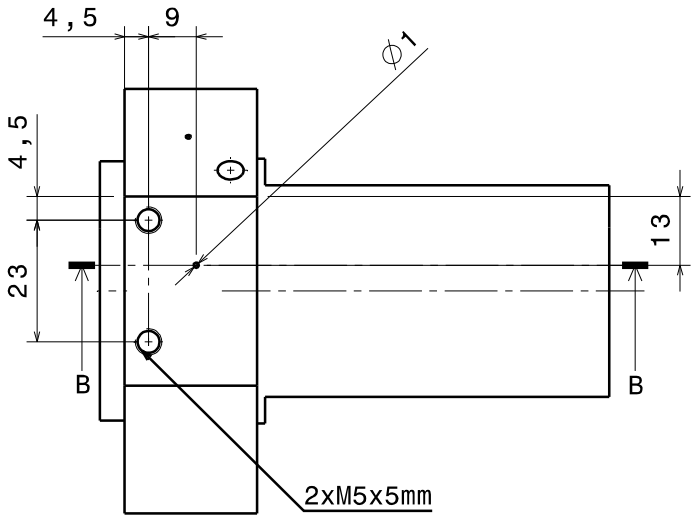

Side View 1

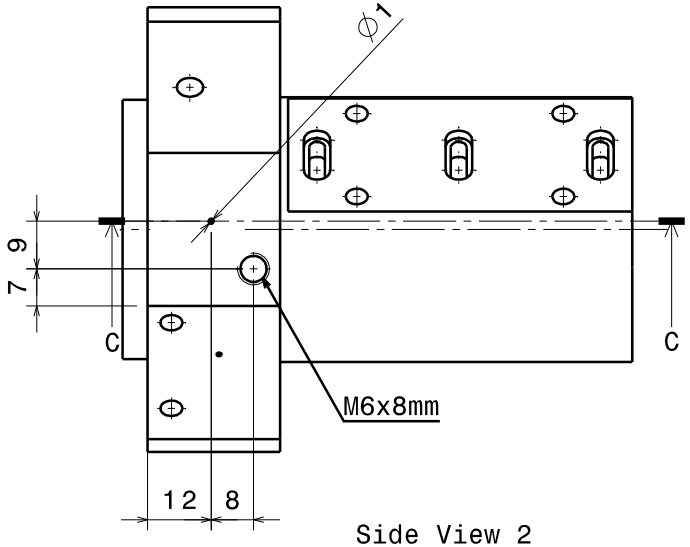

Side View 2

						Scale: 1:1	Quantity: 1
						Name: Behre First Name: Leander	
				Date	Name	Component Description CONTROL UNIT HOUSING	
				06/12/13	Behre		
						Material 42CrMo4	
						Drawing No.	Sheet 3/3
							DIN AX
				Created with CATIA V5			

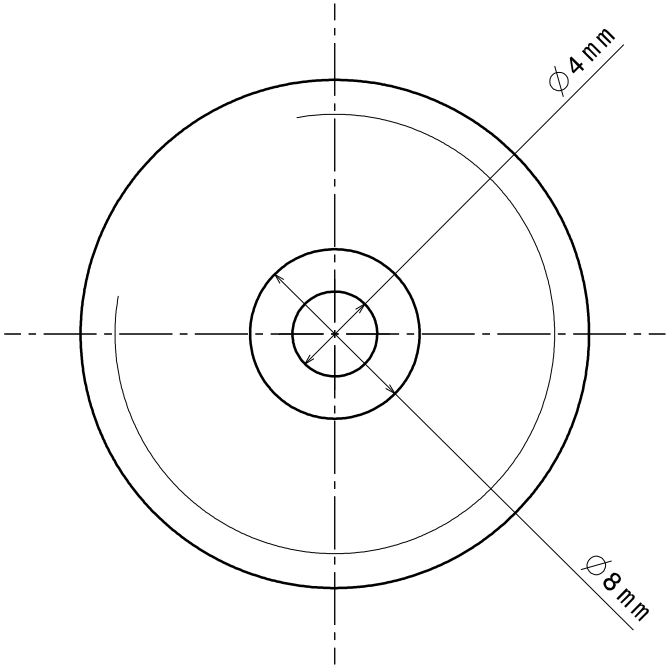

Front View

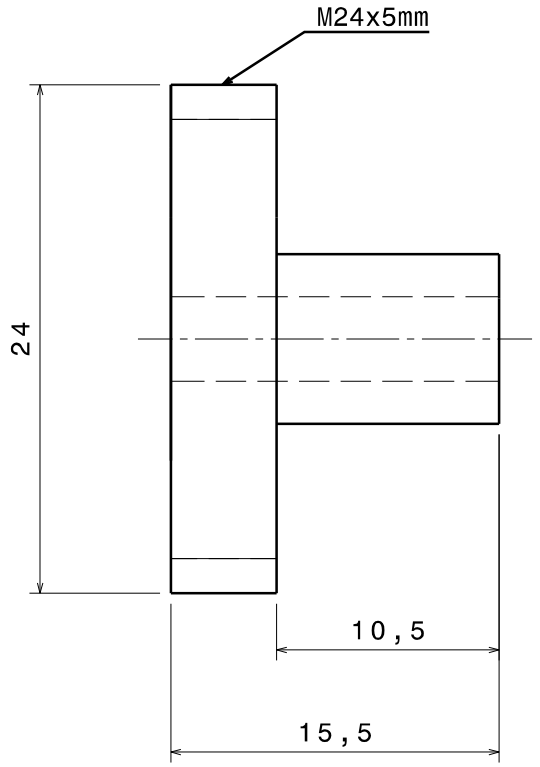

Side View

								Scale: 4:1	Quantity: 1
								Name: Behre First Name: Leander	
						Date	Name	Component Description	
						06/12/13	Behre	CONTROL UNIT STOPPER_CU	
								Material 42CrMo4	
								Drawing No.	Sheet
									DIN AX
					Created with CATIA V5				

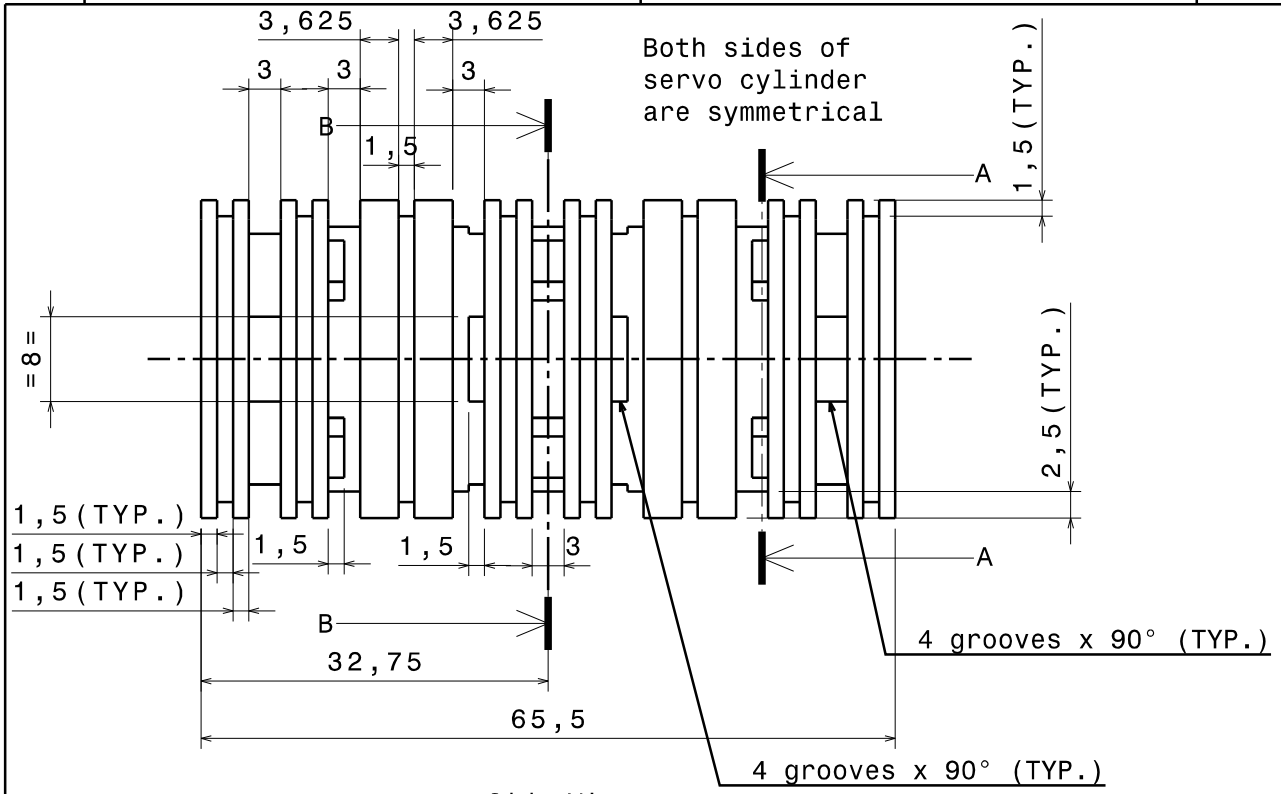

Side View

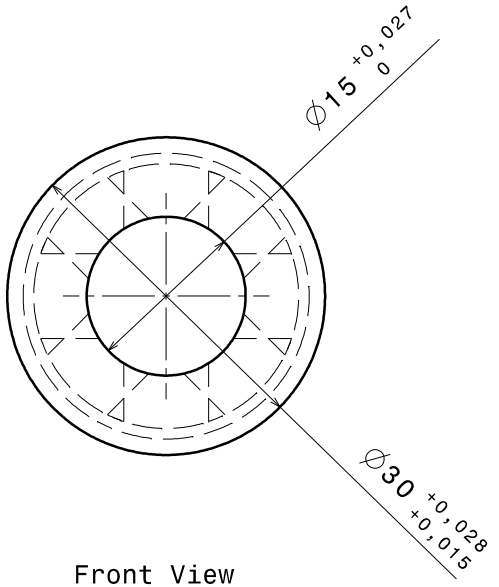

Front View

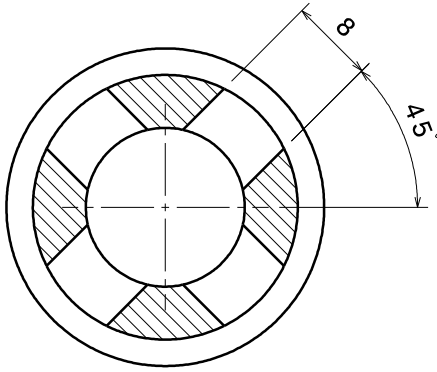

Sectional View A:A

4 grooves x 90°

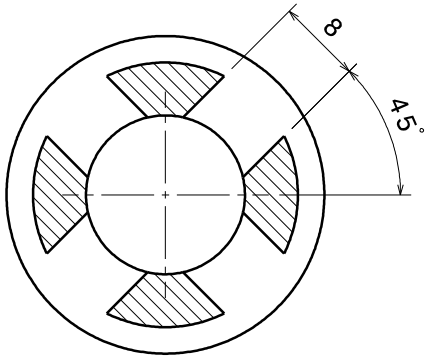

Sectional View B:B

4 grooves x 90°

7 grooves are t=2,5 mm
8 grooves are t=1,5mm

7 x 4 = 28 windows
in servo cylinder
in total

						Scale: 2:1	Quantity: 1
						Name: Behre First Name: Leander	
				Date	Name	Component Description	
				06/12/13	Behre	CONTROL UNIT SERVO_CYLINDER	
						Material 42CrMo4	
						Drawing No.	Sheet
							DIN AX
				Created with CATIA V5			

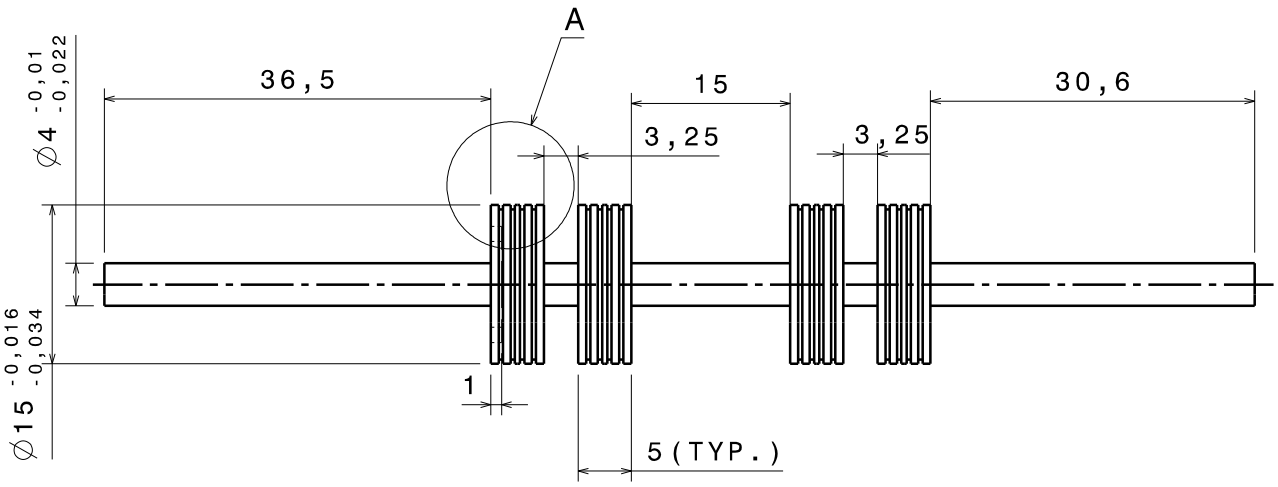

Side View

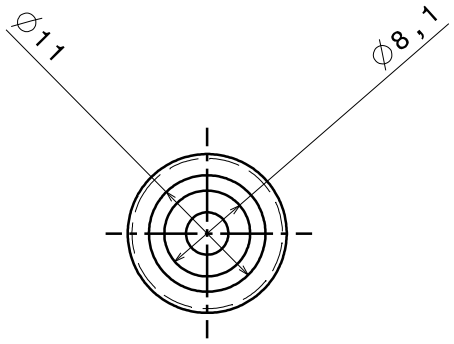

Front View

these measures are for a groove where a spring will fit into

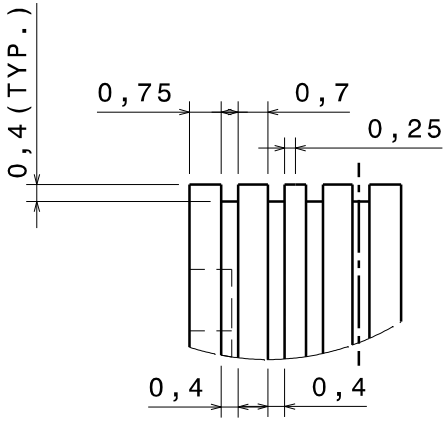

Detail A

grooves on the right of the vertical are symmetrical; identical grooves on all four piston elements

						Scale: 2:1; 8:1	Quantity: 1
						Name: Behre First Name: Leander	
				Date	Name	Component Description	
				06/12/13	Behre	CONTROL UNIT CONTROL_PISTON	
						Material 42CrMo4	
						Drawing No.	Sheet
							DIN AX
				Created with CATIA V5			

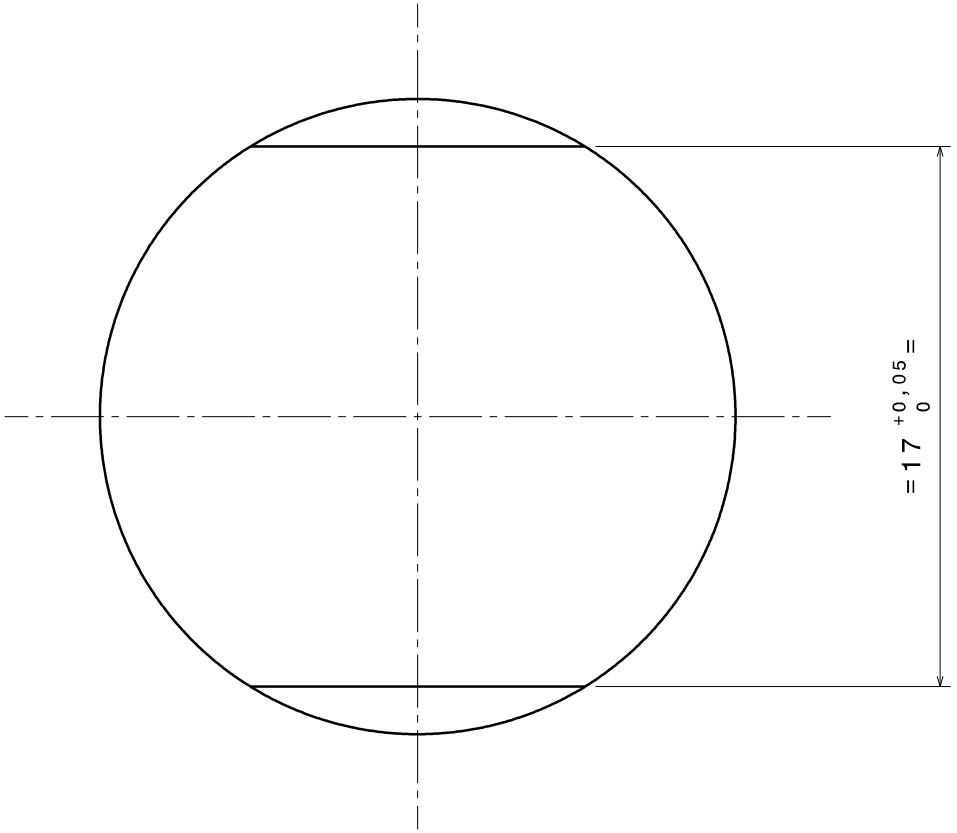

Front View

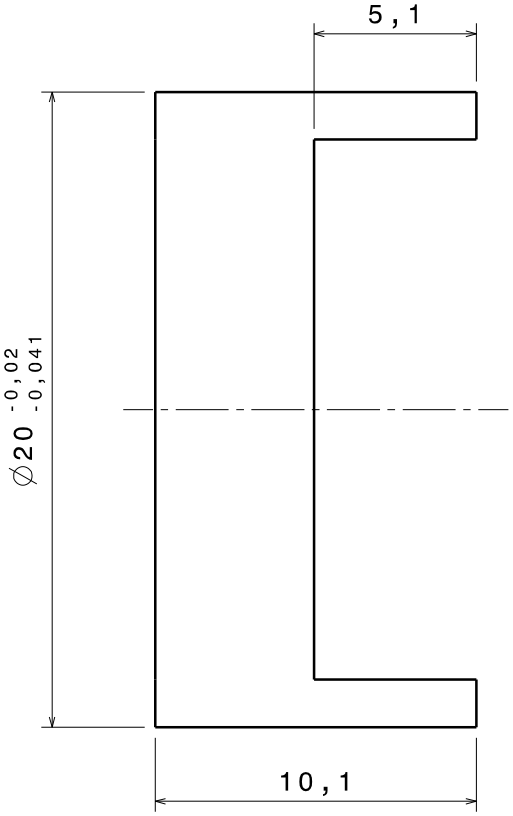

Side View

						Scale: 6:1	Quantity: 1
						Name: Behre First Name: Leander	
				Date	Name	Component Description CONTROL UNIT TRANSL._PISTON	
				06/12/13	Behre		
						Material 42CrMo4	
						Drawing No.	Sheet
							DIN AX
				Created with CATIA V5			

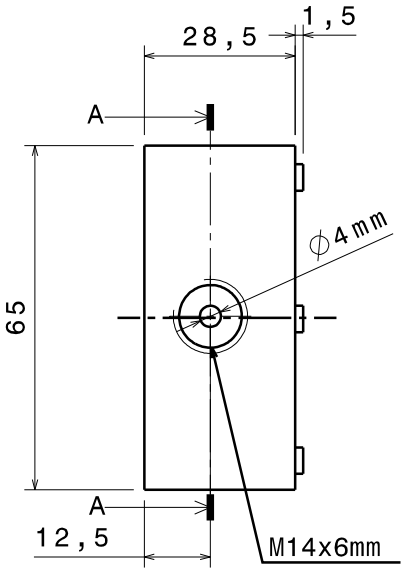

Front View

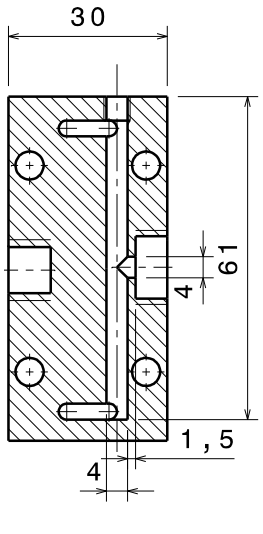

Sectional View A:A

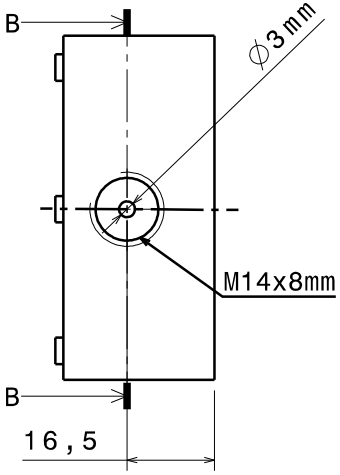

Rear View

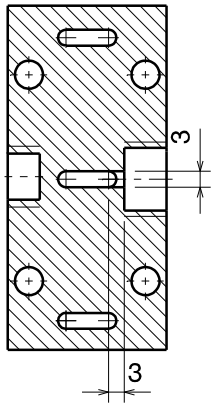

Sectional View B:B

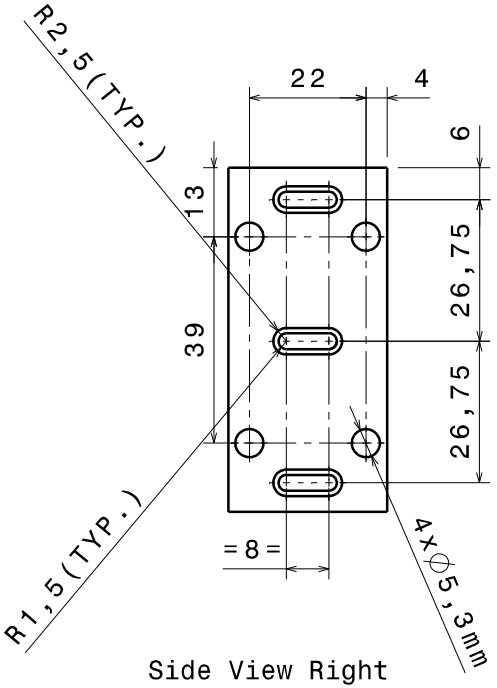

Side View Right

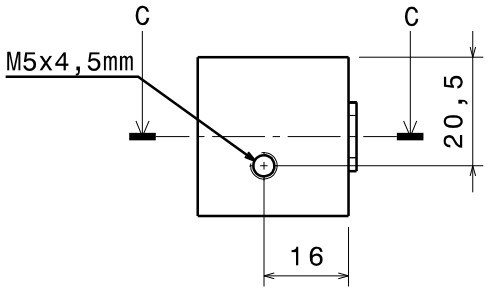

Top View

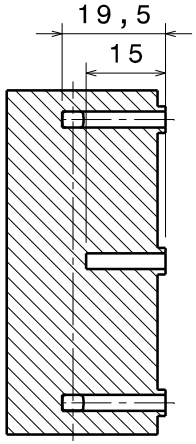

Sectional View C:C

							Scale: 1:1	Quantity: 1
							Name: Behre First Name: Leander	
					Date	Name	Component Description	
					06/12/13	Behre	CONTROL UNIT COVER_TOP	
							Material 42CrMo4	
							Drawing No.	Sheet
								DIN AX
					Created with CATIA V5			

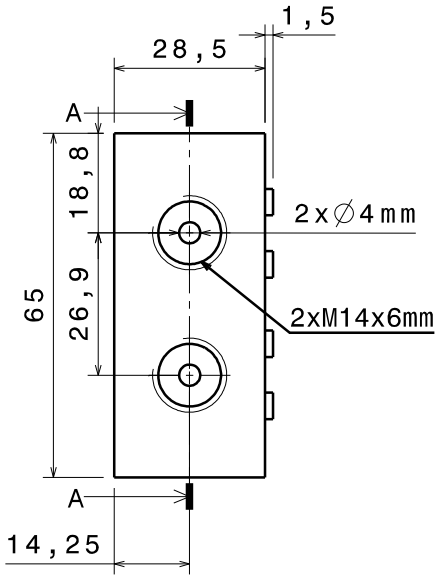

Front View

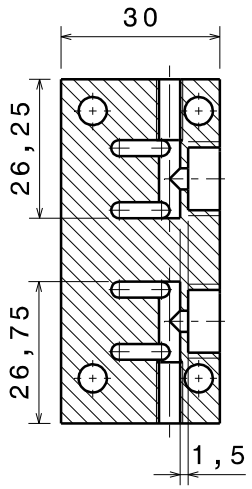

Sectional View A:A

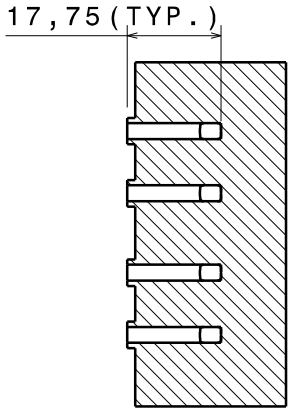

Sectional View B:B

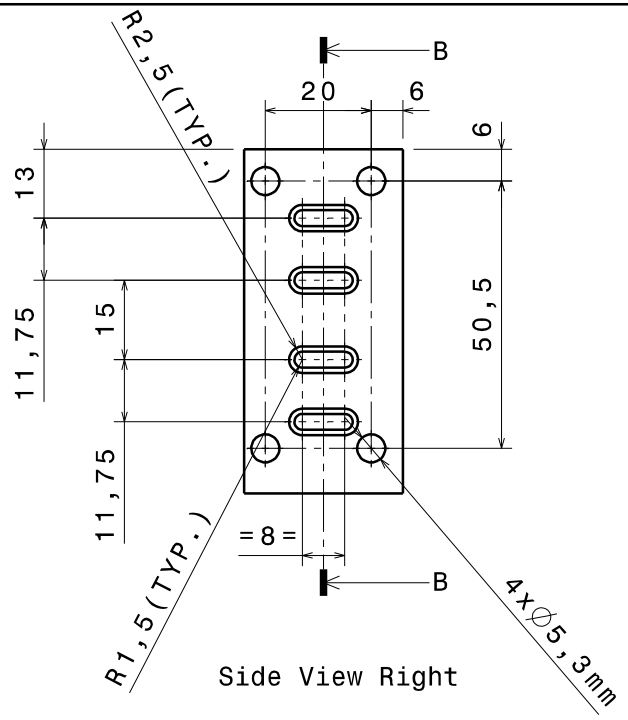

Side View Right

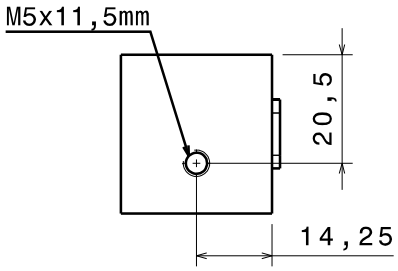

Top View

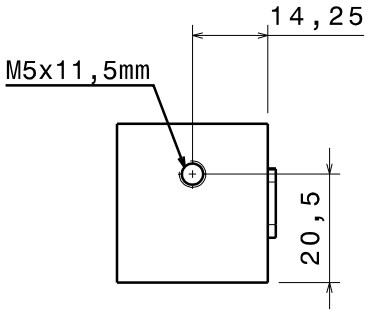

Bottom View

						Scale: 1:1	Quantity: 1
						Name: Behre First Name: Leander	
				Date	Name	Component Description CONTROL UNIT COVER_LOW	
				06/12/13	Behre		
						Material 42CrMo4	
						Drawing No.	Sheet
							DIN AX
				Created with CATIA V5			

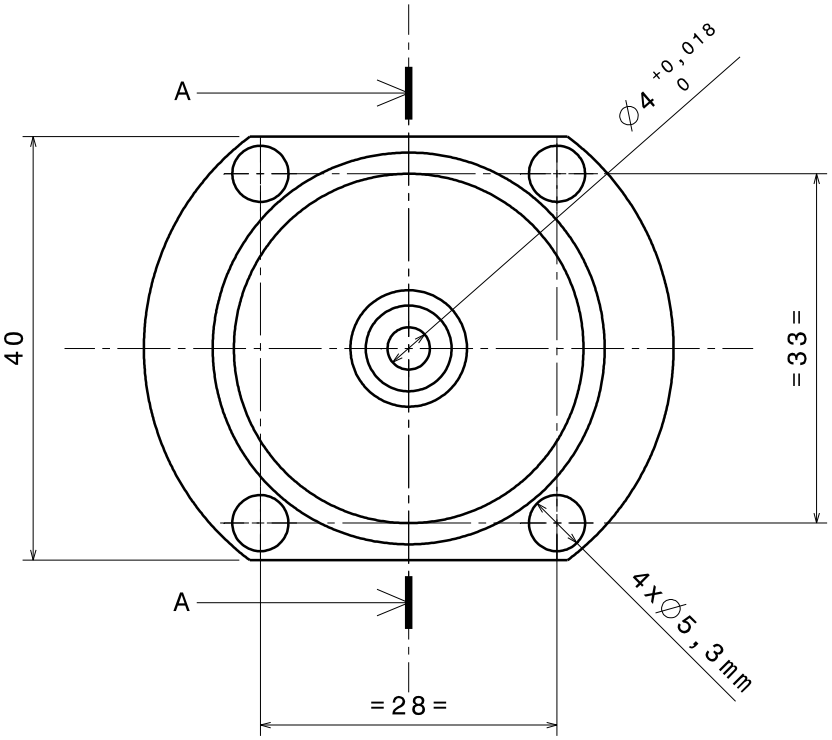

Front View

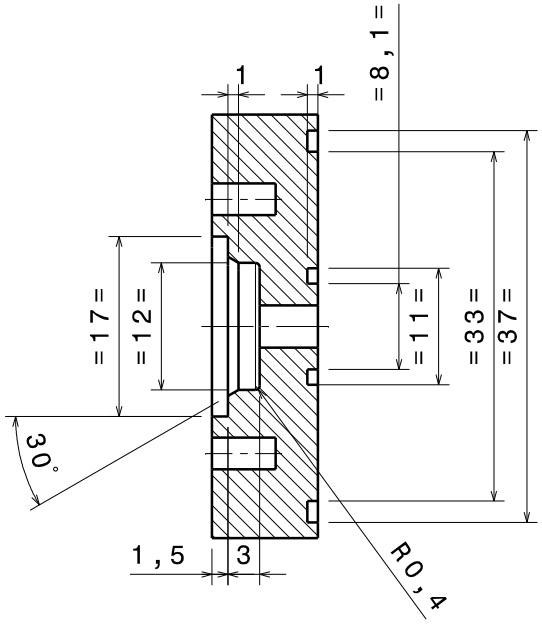

Sectional View A:A

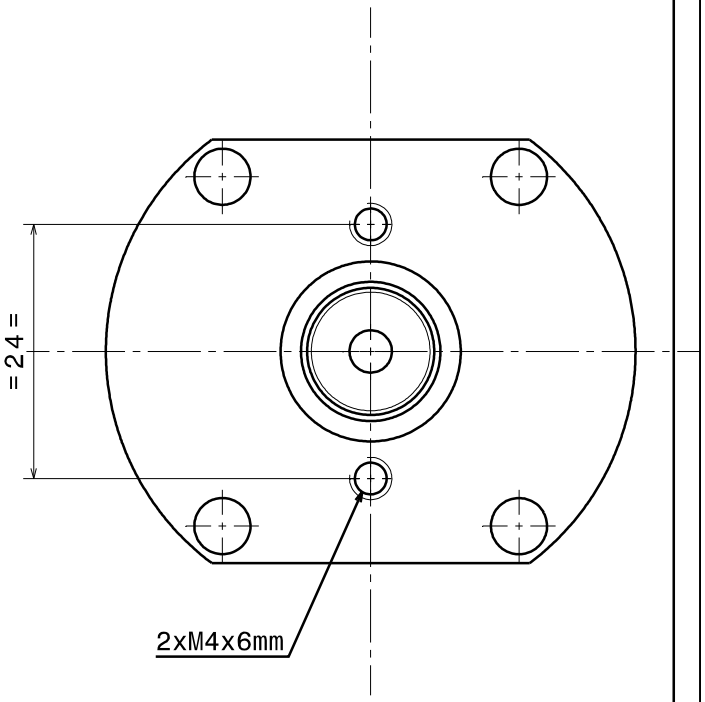

Rear View

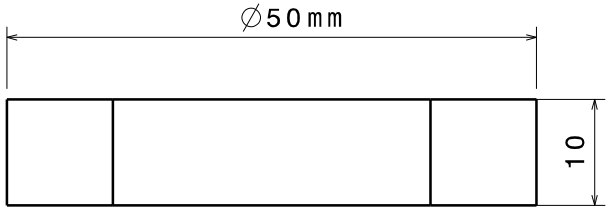

Top View

						Scale: 2:1	Quantity: 1
						Name: Behre First Name: Leander	
				Date	Name	Component Description CONTROL UNIT COVER	
				11/02/14	Behre		
						Material 42CrMo4	
						Drawing No.	Sheet
							DIN AX
				Created with CATIA V5			

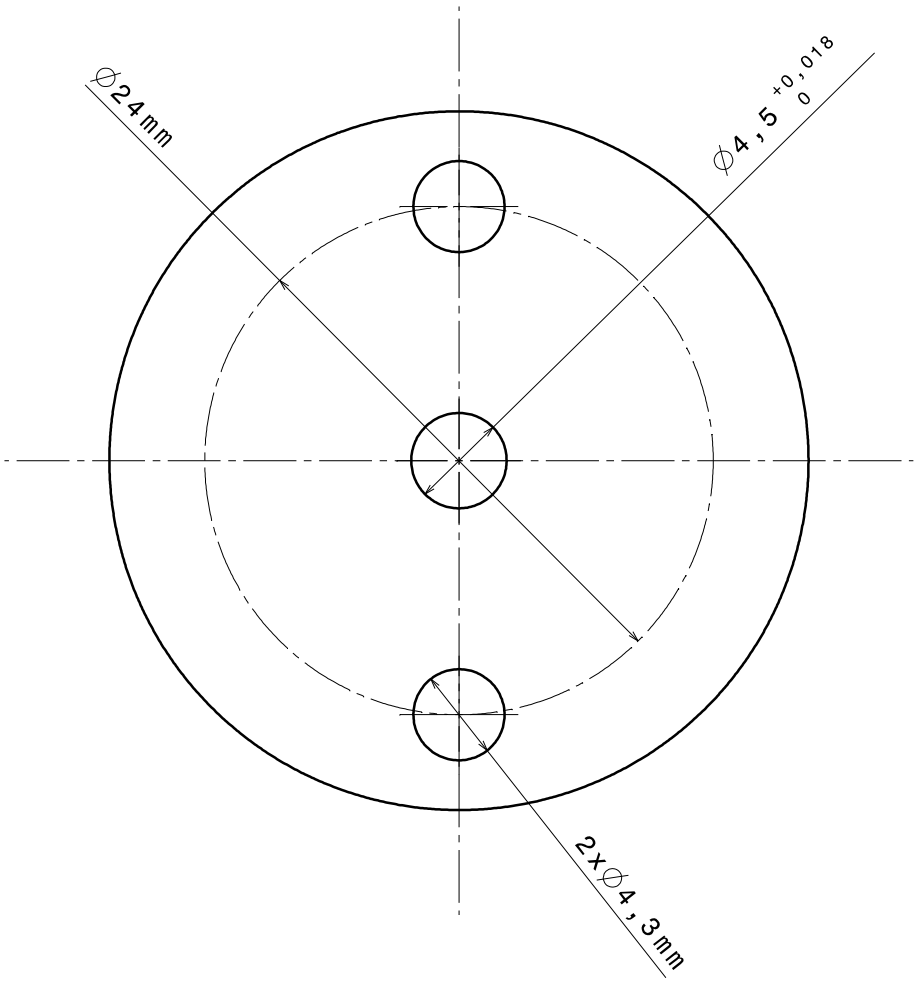

Front View

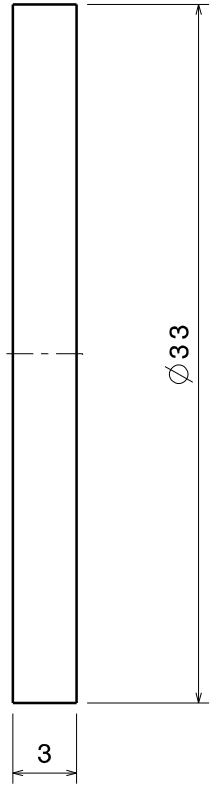

Side View

						Scale: 4:1	Quantity: 3
						Name: Behre First Name: Leander	
				Date	Name	Component Description CONTROL UNIT SEAL_LOCK	
				06/12/13	Behre		
						Material 42CrMo4	
						Drawing No.	Sheet
							DIN AX
				Created with CATIA V5			

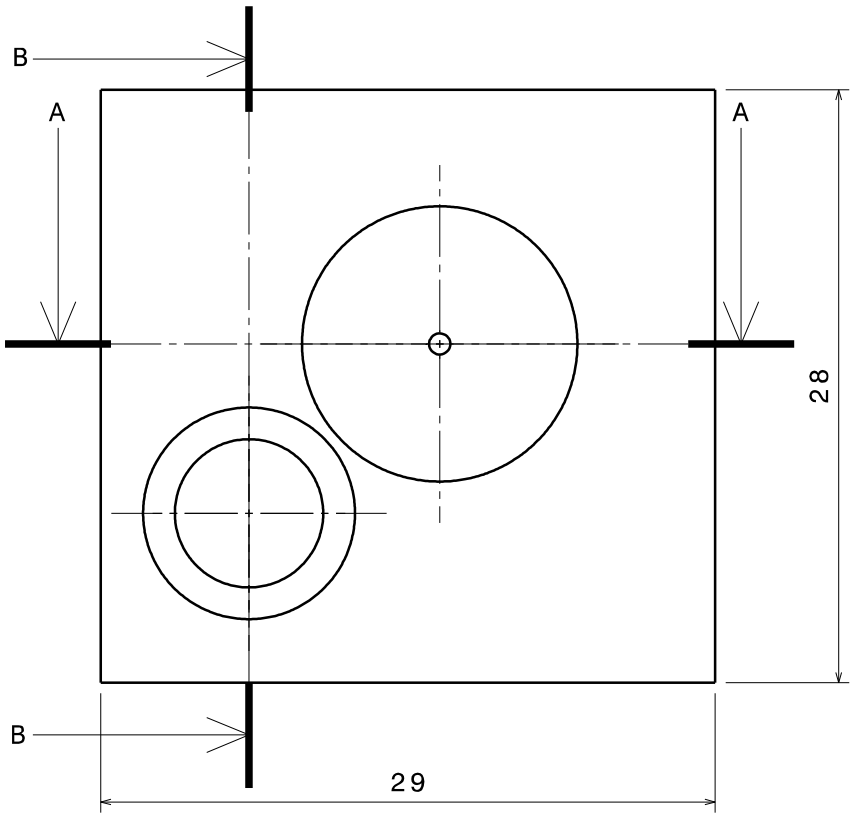

Top View

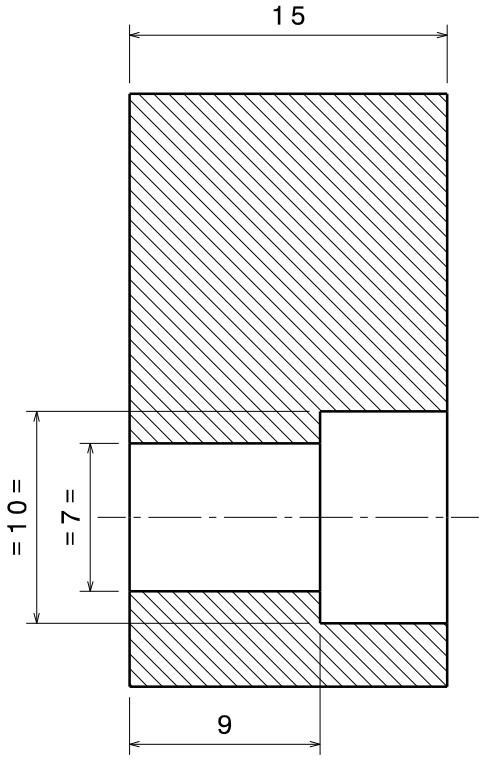

Sectional View B:B

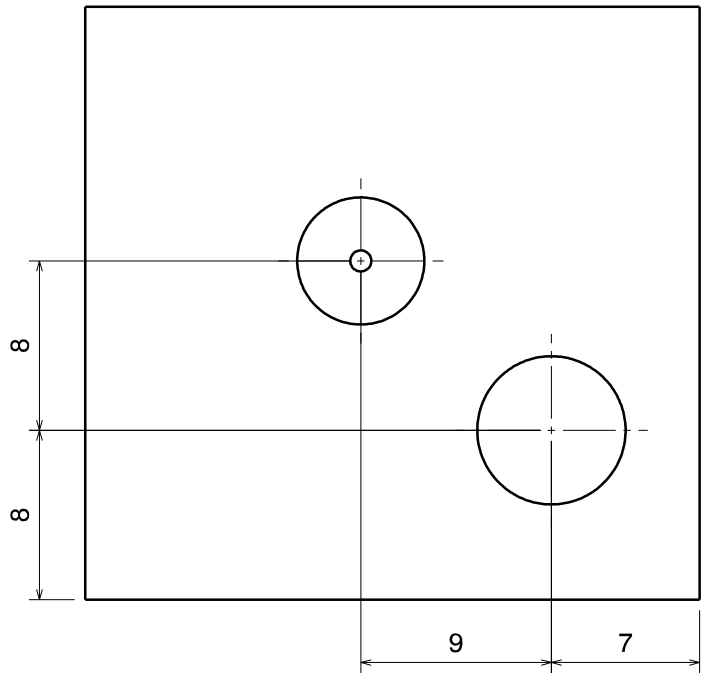

Bottom View

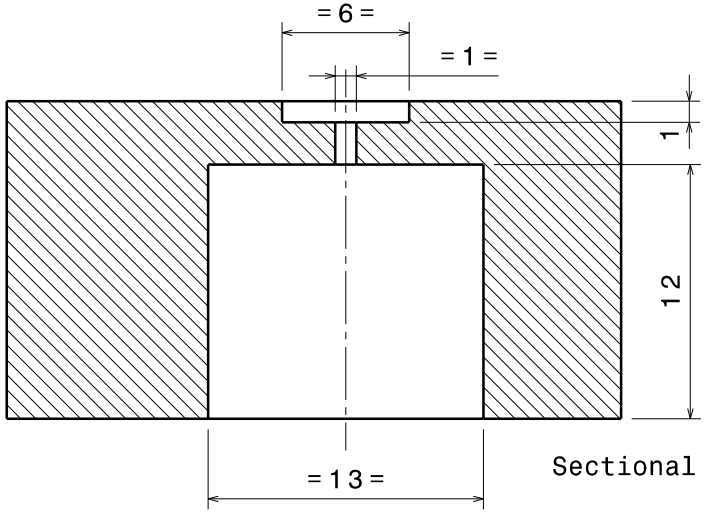

Sectional View A:A

		Scale: 4:1	Quantity: 1
		Name: Behre First Name: Leander	
Date	Name	Component Description CONTROL UNIT ADAPT.PRESS.SENS.	
06/12/13	Behre		
		Material 42CrMo4	
		Drawing No.	Sheet
			DIN AX
Created with CATIA V5			

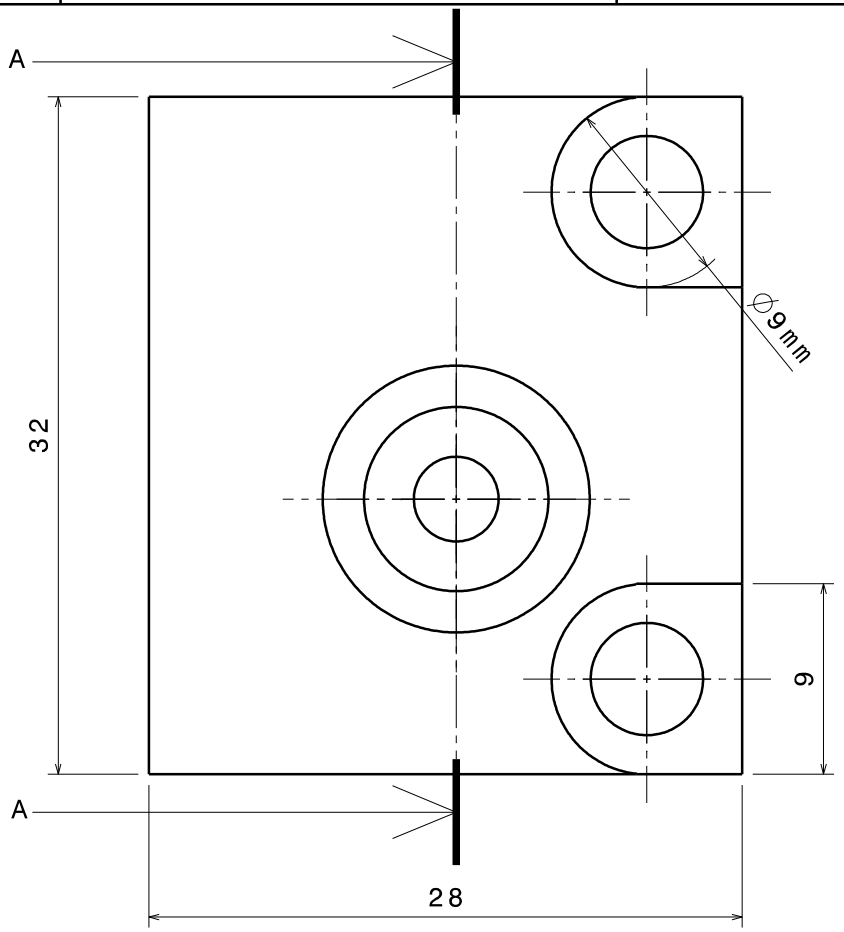

Front View

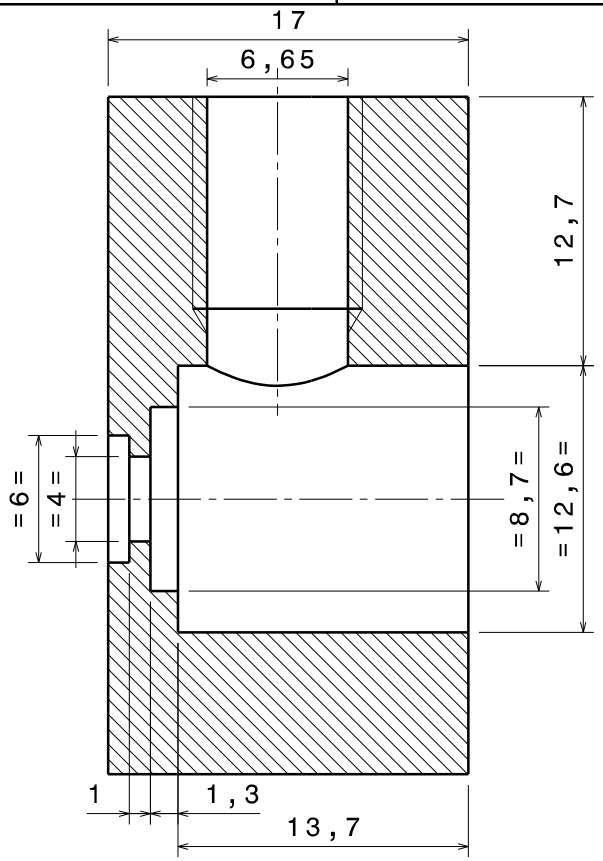

Sectional View A:A

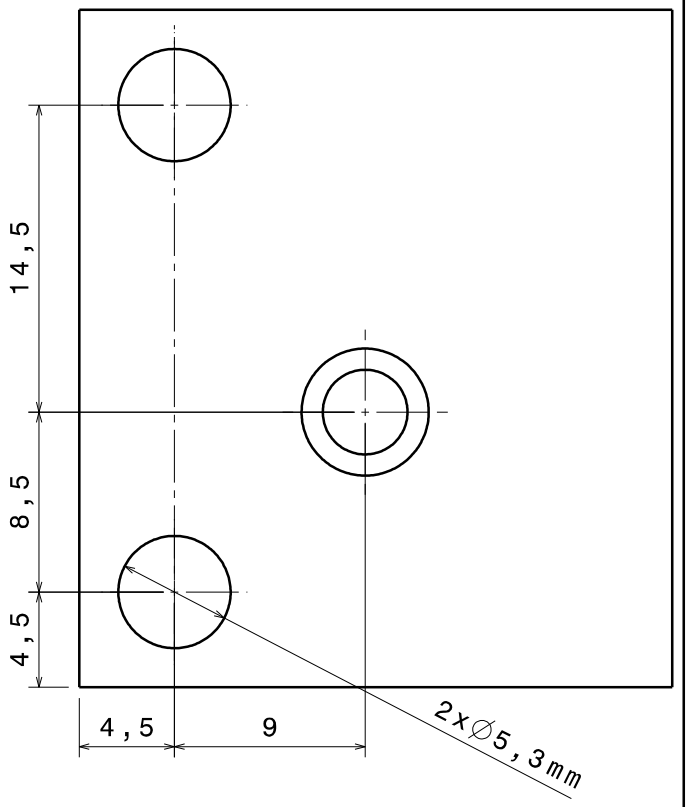

Rear View

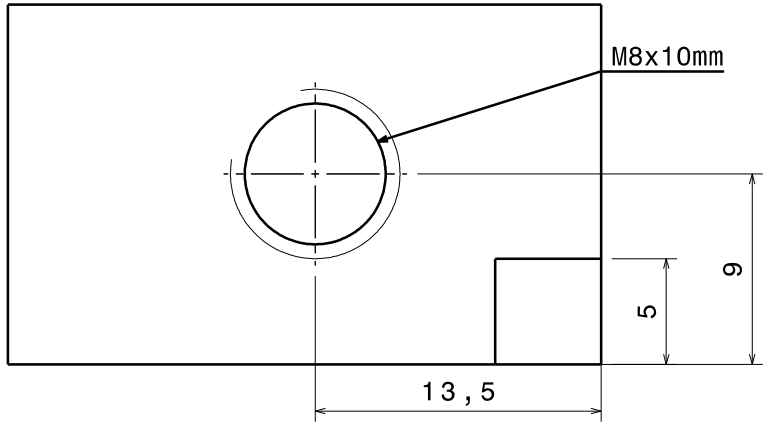

Top View

						Scale: 4:1	Quantity: 1
						Name: Behre First Name: Leander	
				Date	Name	Component Description	
				06/12/13	Behre	CONTROL UNIT ADAPT. SOLENOID	
						Material 42CrMo4	
						Drawing No.	Sheet
							DIN AX
				Created with CATIA V5			

9.3 Technical drawings: redesigned servo valve

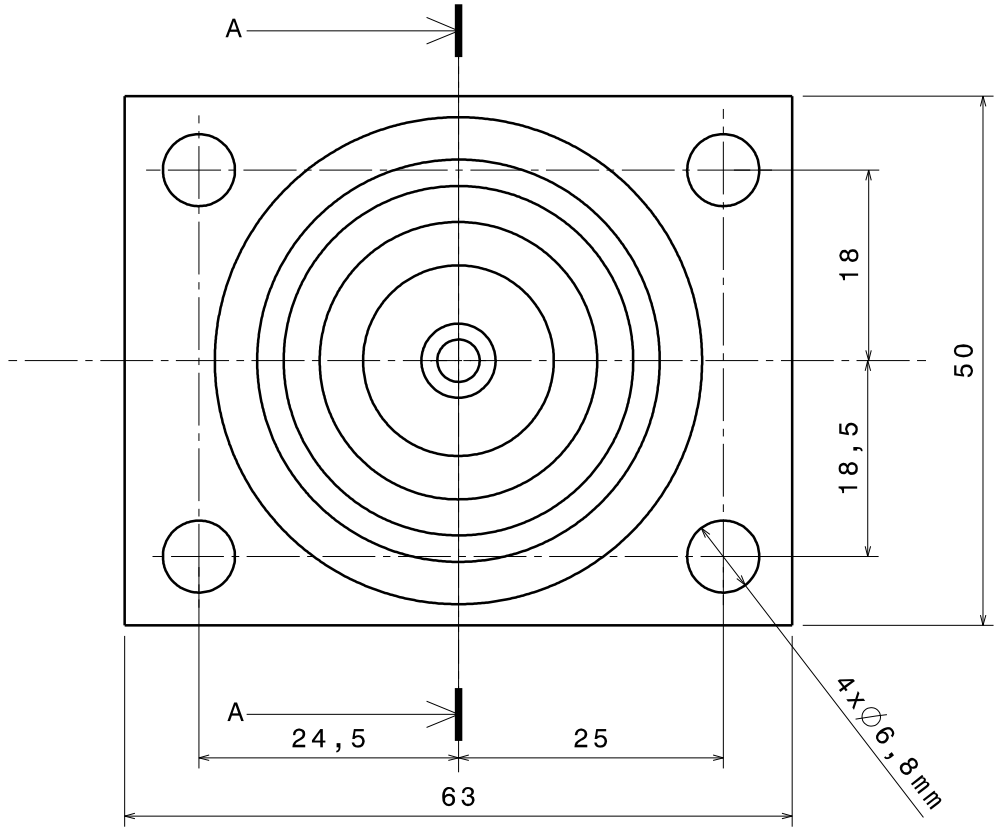

Front View; Scale 2:1

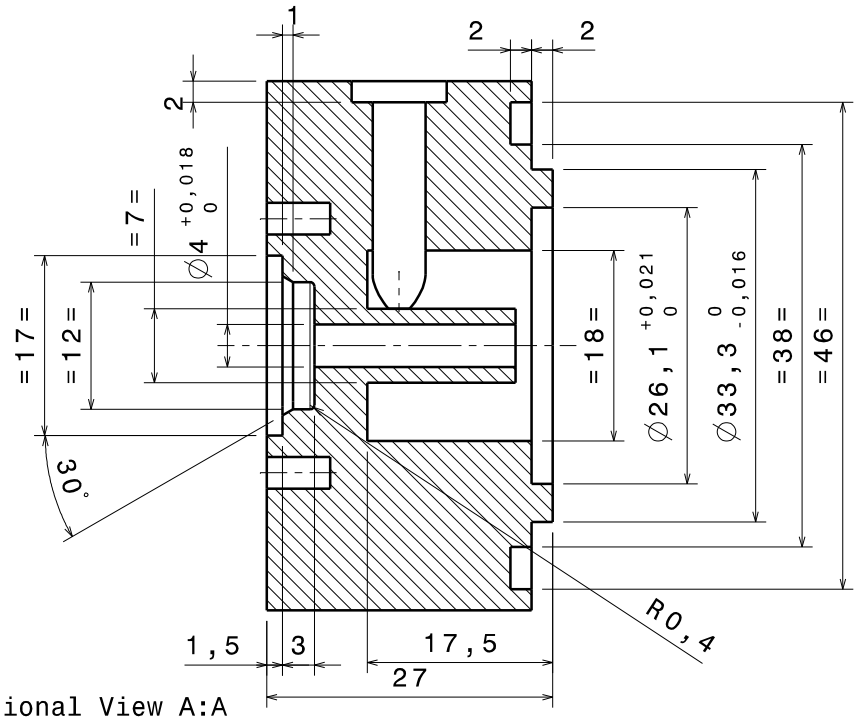

Sectional View A:A

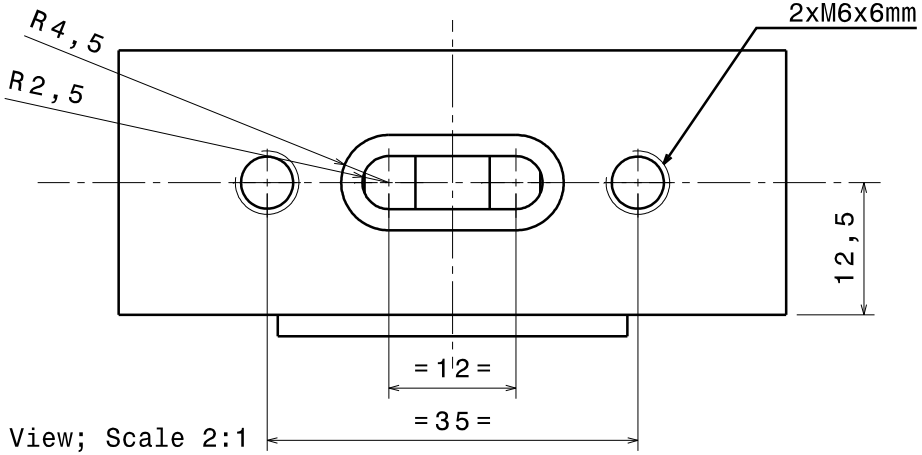

Top View; Scale 2:1

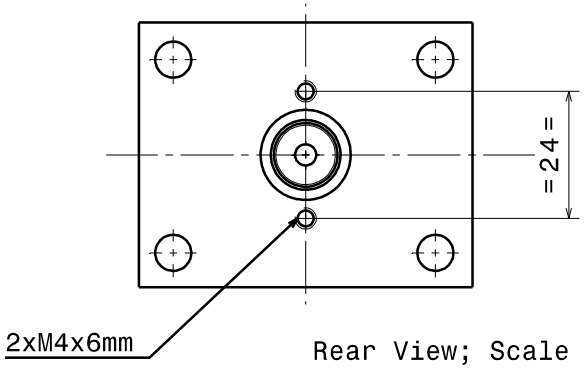

Rear View; Scale 1:1

		Scale: 2:1, 1:1	Quantity: 1
		Name: Behre First Name: Leander	
Date	Name	Component Description	
02/12/13	Behre	SERVO VALVE COVER_FRONT	
		Material 42CrMo4	
		Drawing No.	Sheet
			DIN AX
Created with CATIA V5			

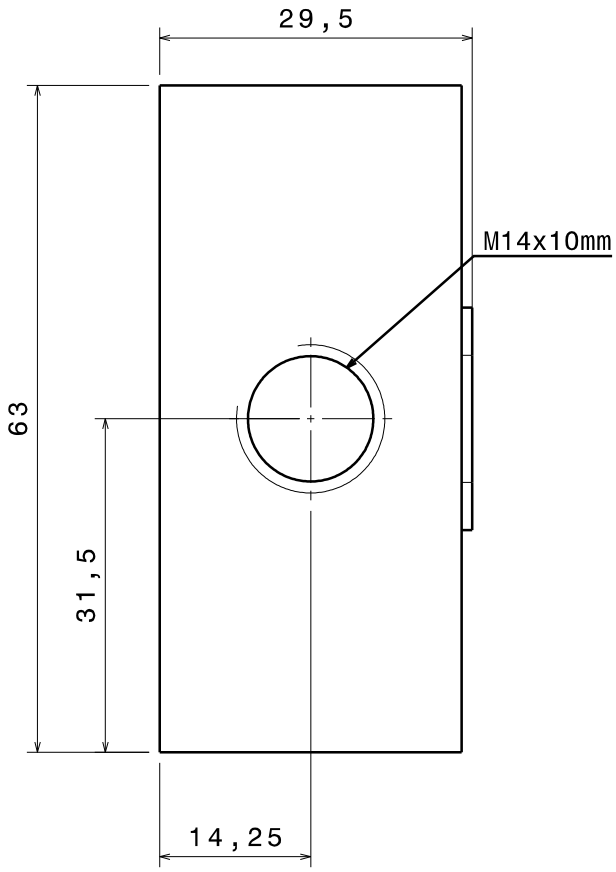

Side View Left

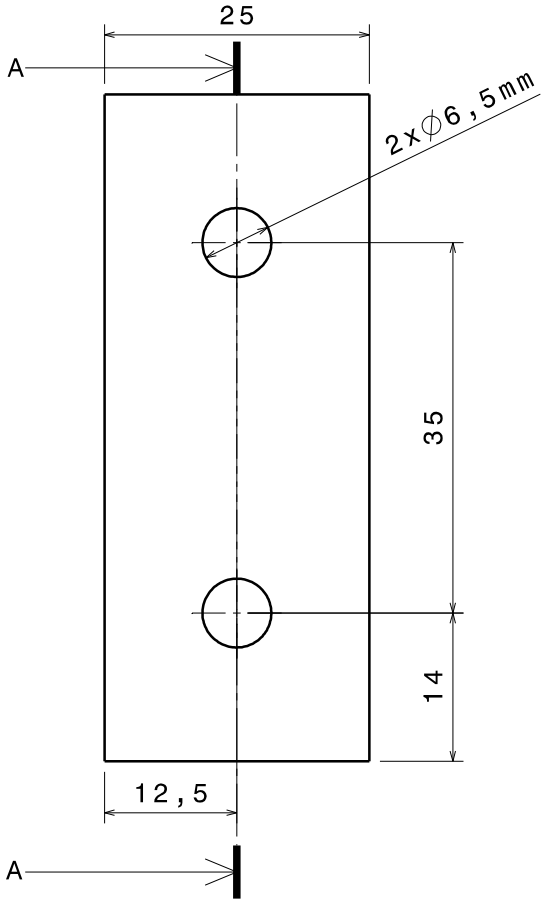

Bottom View

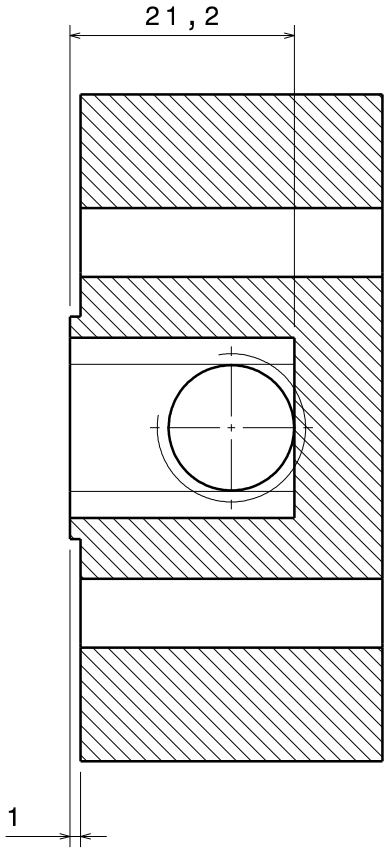

Sectional View A:A

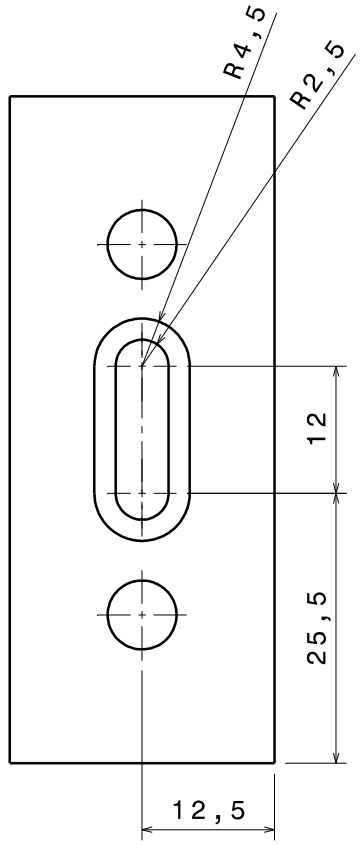

Top View

Drill Hole M14 only
located on left side
of component, not on
the right

						Scale: 2:1	Quantity: 1
						Name: Behre First Name: Leander	
				Date	Name	Component Description	
				03/12/13	Behre	SERVO VALVE TOP_COVER_FRONT	
						Material 42CrMo4	
						Drawing No.	Sheet
							DIN AX
				Created with CATIA V5			

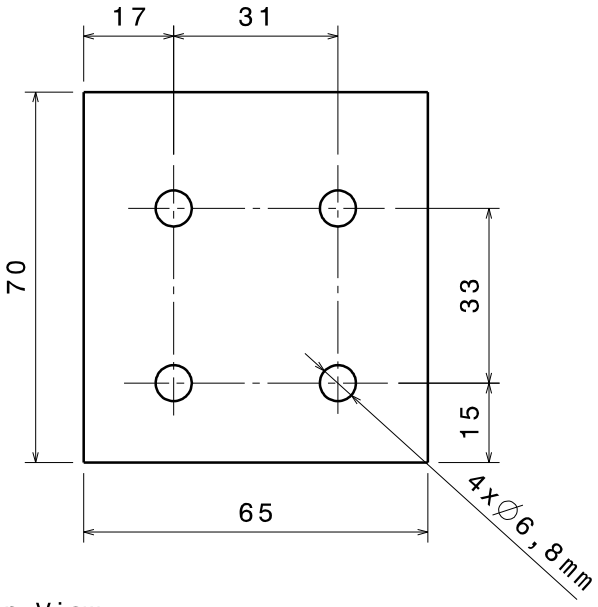

Top View

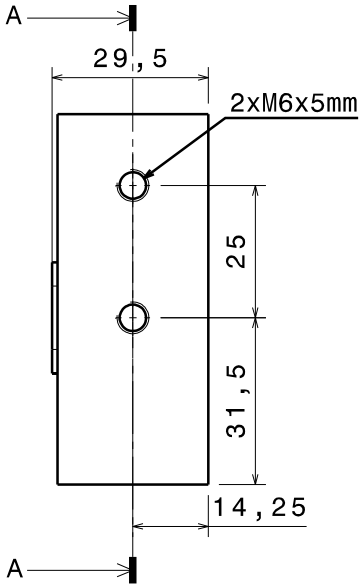

Side View Left

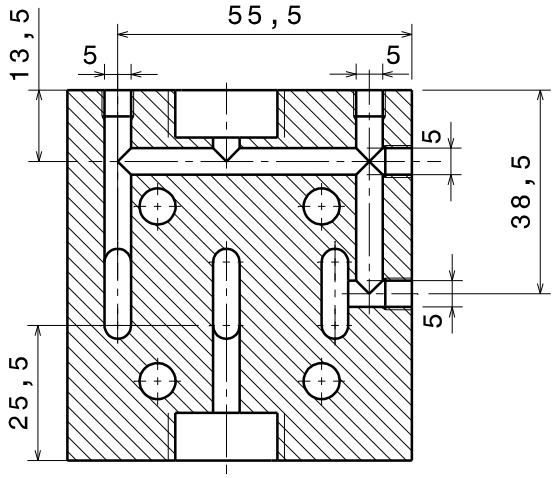

Sectional View A:A

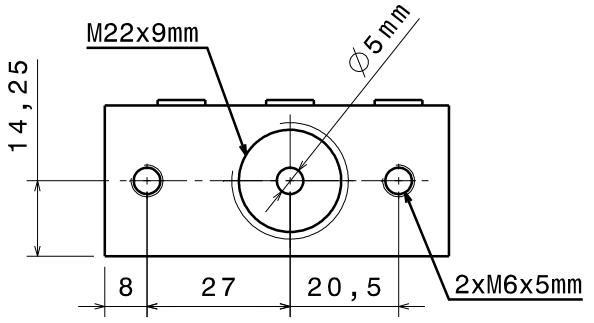

Front View

						Scale: 1:1	Quantity: 1
						Name: Behre First Name: Leander	
				Date	Name	Component Description SERVO VALVE TOP_COVER_MID	
				03/12/13	Behre		
						Material 42CrMo4	
						Drawing No.	Sheet 1/2
							DIN AX
				Created with CATIA V5			

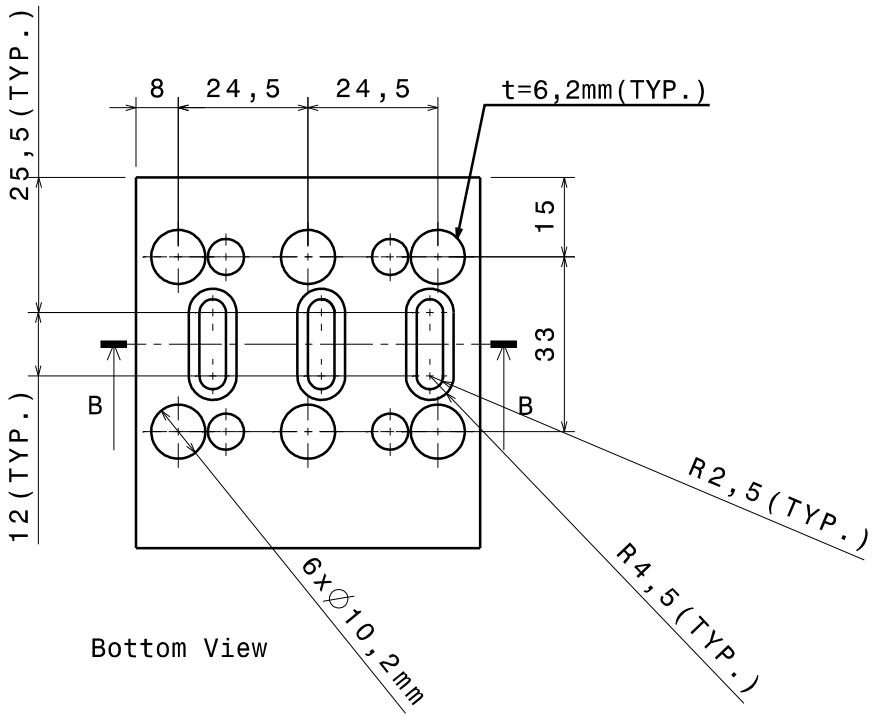

Bottom View

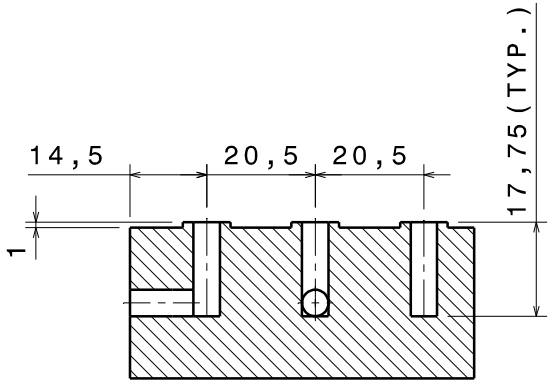

Sectional View B:B

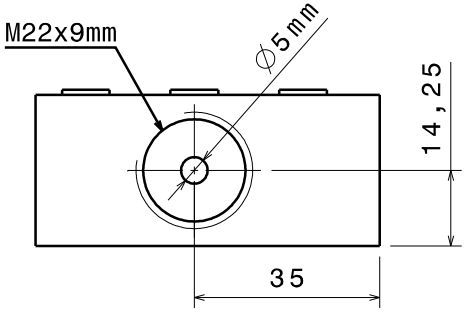

Rear View

						Scale: 1:1	Quantity: 1
						Name: Behre First Name: Leander	
					Date	Name	Component Description
					03/12/13	Behre	SERVO VALVE TOP_COVER_MID
							Material 42CrMo4
							Drawing No.
							Sheet 2/2
							DIN AX
					Created with CATIA V5		

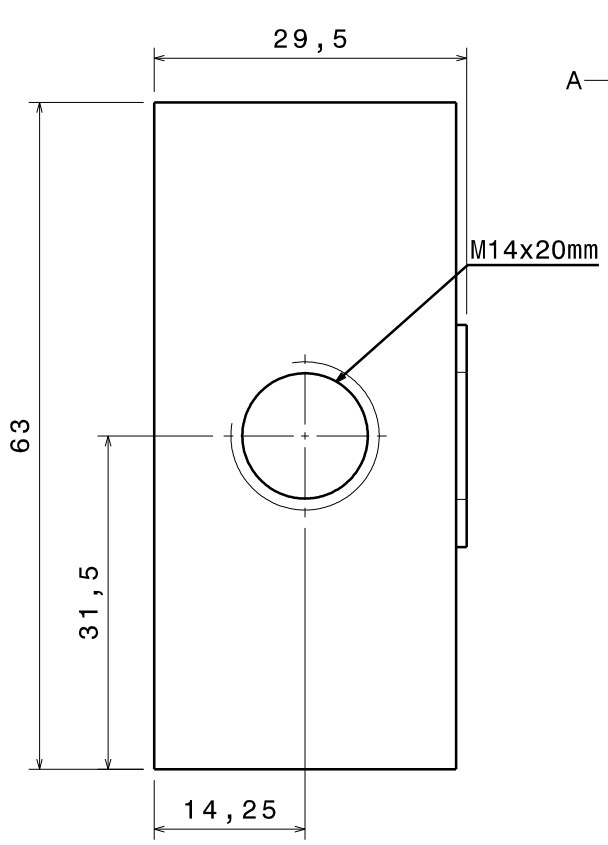

Side View Left

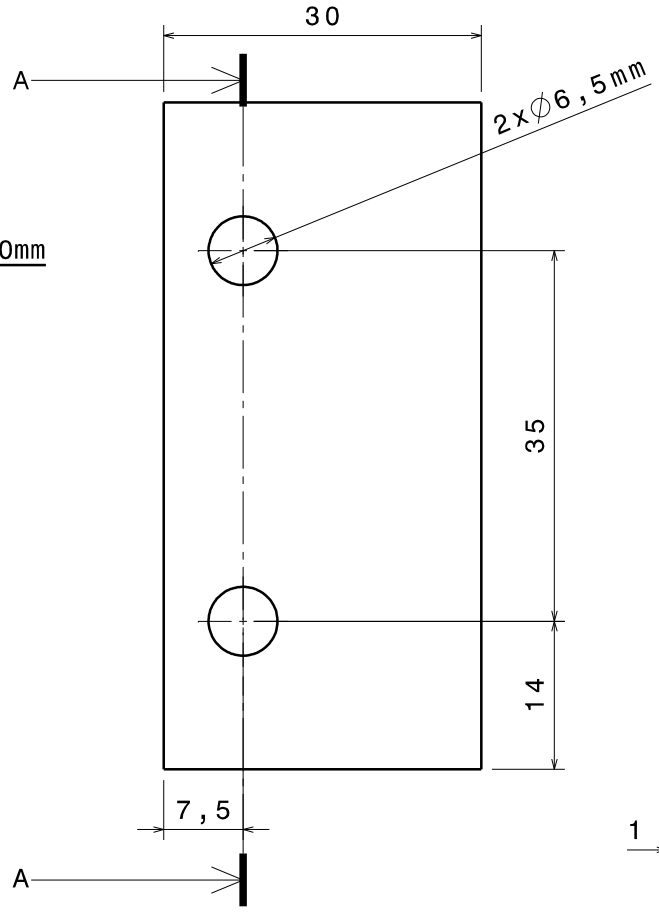

Bottom View

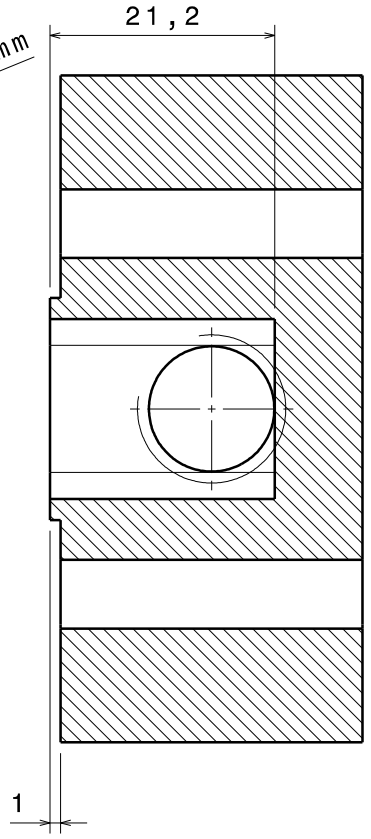

Sectional View A:A

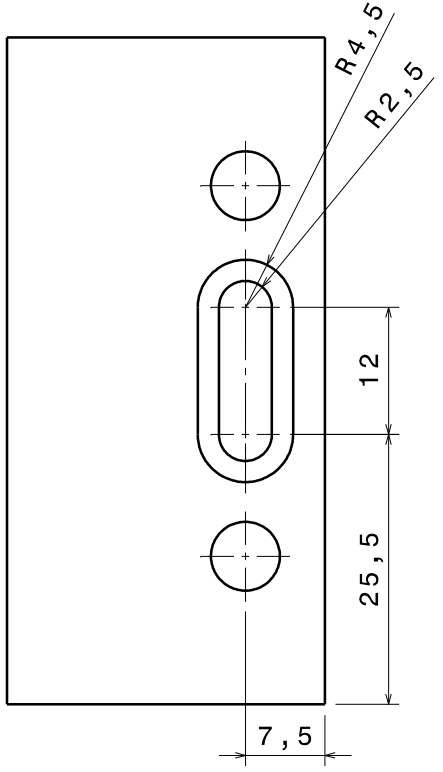

Top View

Drill Hole M14 only
located on left side
of component, not on
the right

						Scale: 2:1	Quantity: 1
						Name: Behre First Name: Leander	
				Date	Name	Component Description	
				03/12/13	Behre	SERVO VALVE TOP_COVER_REAR	
						Material 42CrMo4	
						Drawing No.	Sheet
							DIN AX
				Created with CATIA V5			

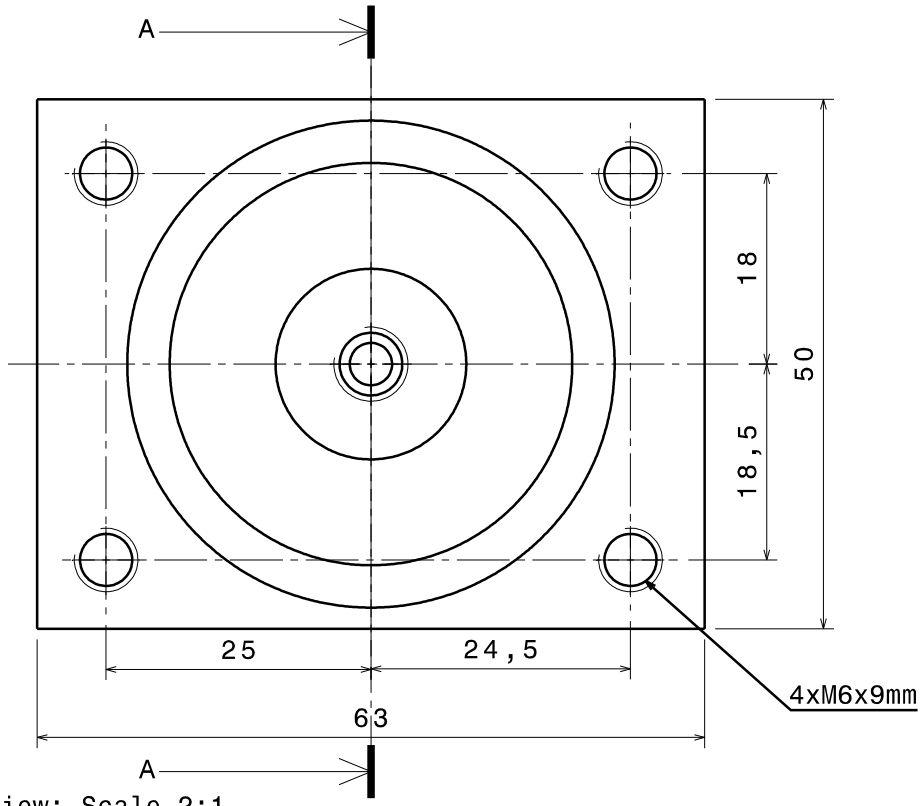

Front View; Scale 2:1

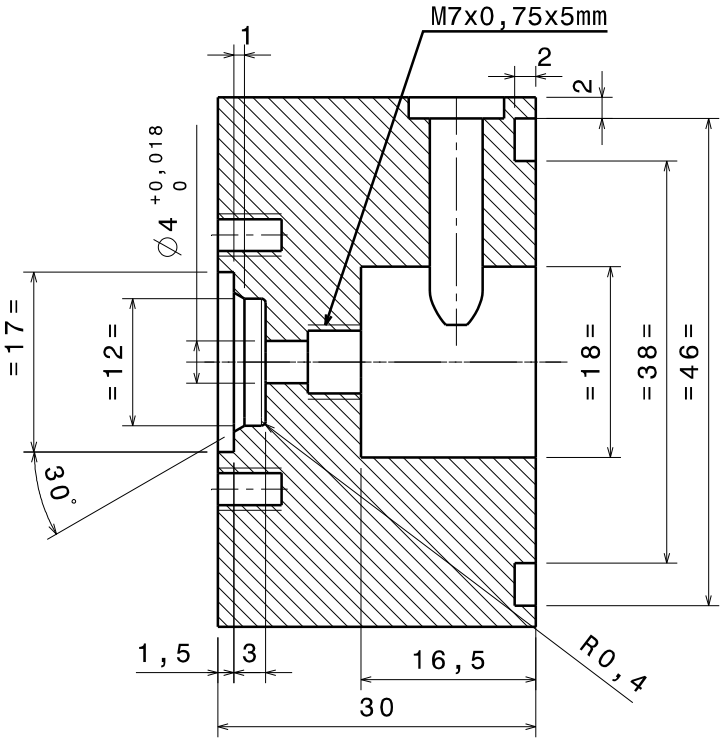

Sectional View A:A

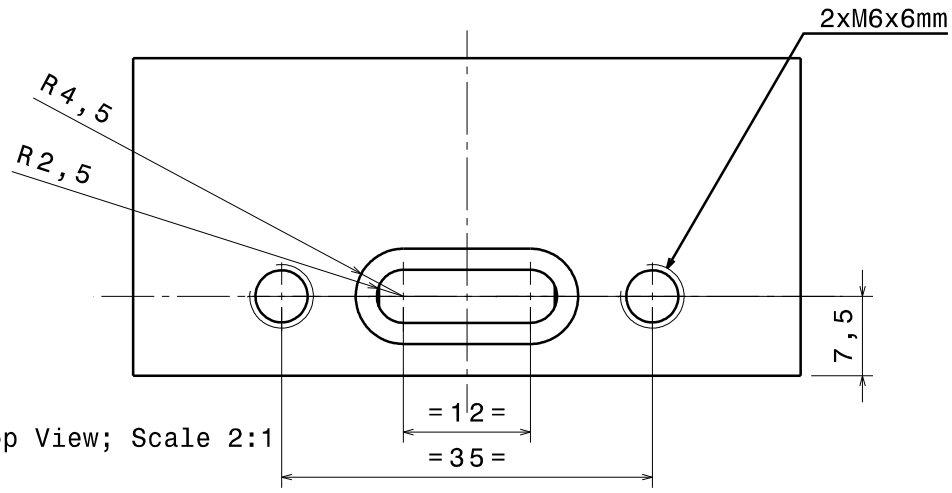

Top View; Scale 2:1

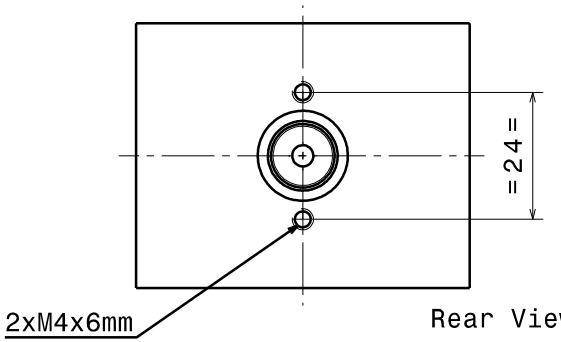

Rear View; Scale 1:1

		Scale: 2:1, 1:1	Quantity: 1
		Name: Behre First Name: Leander	
Date	Name	Component Description	
03/12/13	Behre	SERVO VALVE COVER_REAR	
		Material 42CrMo4	
		Drawing No.	Sheet
			DIN AX
Created with CATIA V5			

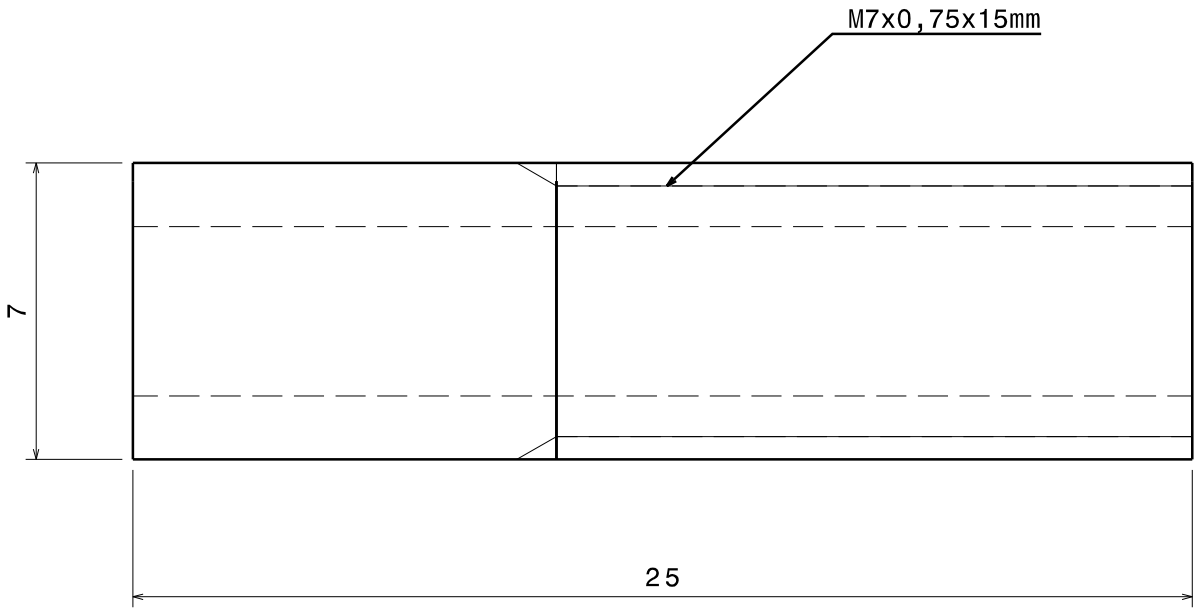

Side View

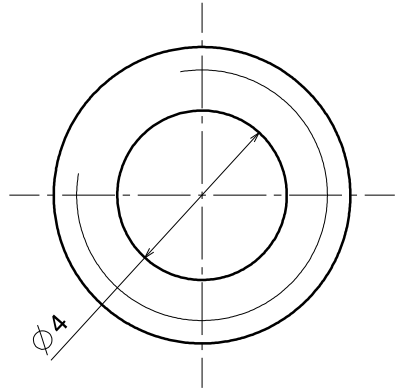

Front View

| | | |

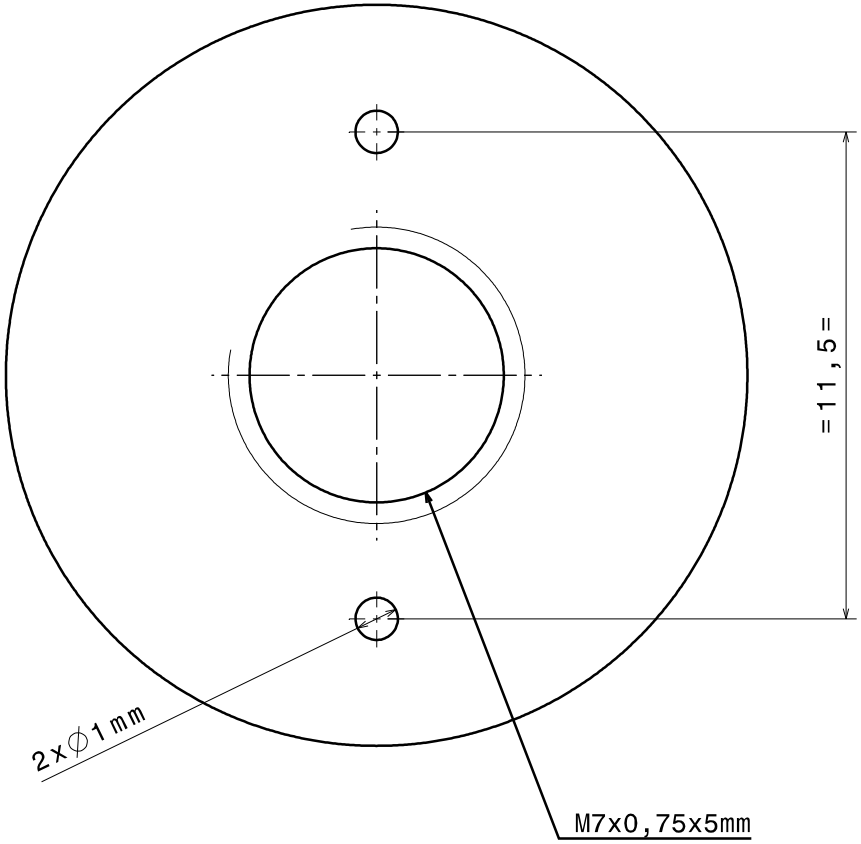

Front View

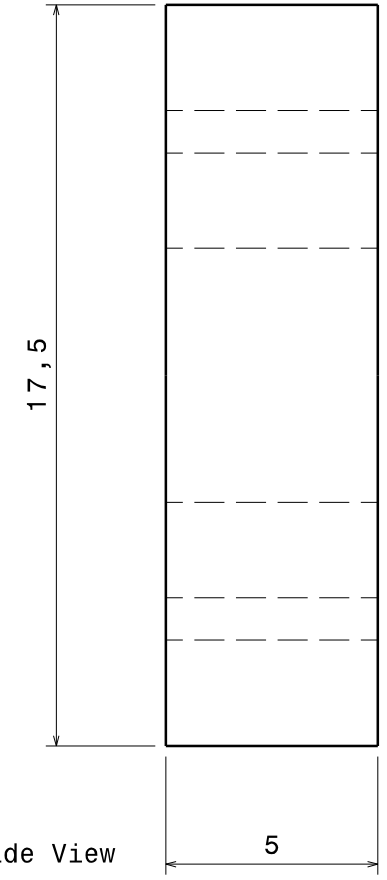

Side View

								Scale: 8:1	Quantity: 1
								Name: Behre First Name: Leander	
					Date	Name		Component Description SERVO VALVE SPRING_DISC	
					03/12/13	Behre			
								Material 42CrMo4	
								Drawing No.	Sheet
									DIN AX
					Created with CATIA V5				

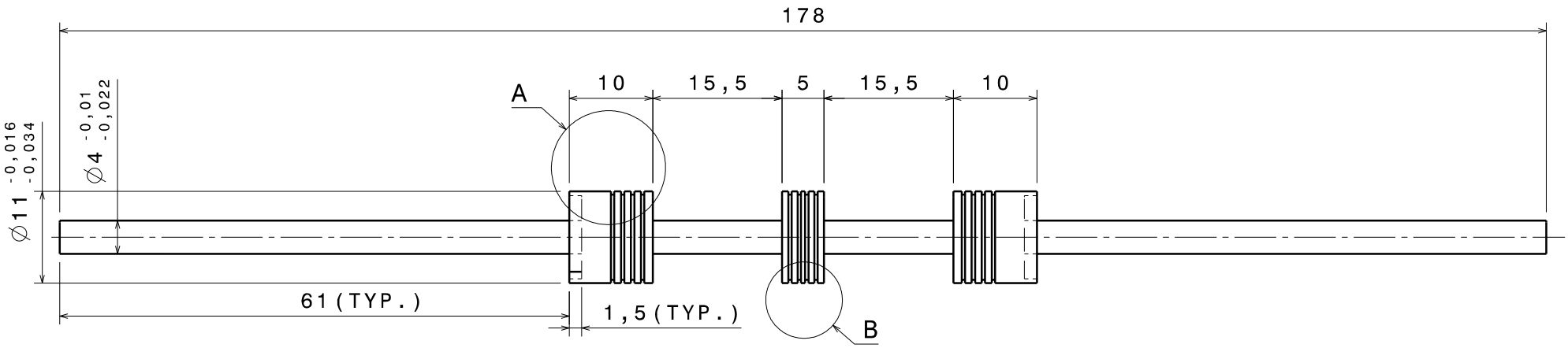

Side View; Scale 2:1

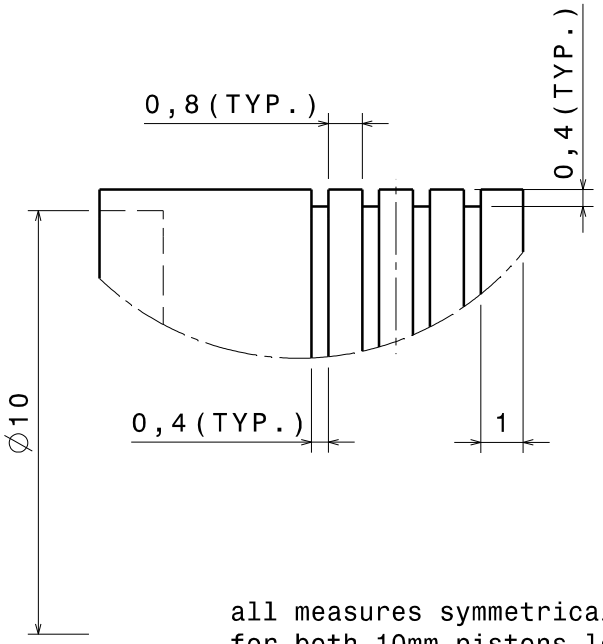

Detail A
Scale 8:1

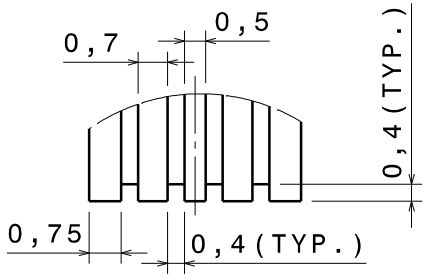

Detail B
Scale 8:1

all measures symmetrical
for both 10mm pistons left
and right

						Scale: 2:1, 8:1	Quantity: 1
						Name: Behre First Name: Leander	
				Date	Name	Component Description SERVO VALVE SERVO_PISTON	
				22/01/14	Behre		
						Material 42CrMo4	
						Drawing No.	Sheet
							DIN AX
				Created with CATIA V5			

9.4 Technical specifications of the "Fortus 250mc" printer [24]

Fortus 250mc Product Specs

Material:
ABS*plus*-P430

Build envelope (XYZ):
254 x 254 x 305 mm (10 x 10 x 12 in.)

Material delivery:
One build material cartridge and one support material cartridge, each 923 cc (56.3 in3)

Layer thicknesses:

0.013 inch (0.330 mm)

0.010 inch (0.254 mm)

0.007 inch (0.178 mm)

Support structure:
Soluble

Available colors:
Ivory, black, blue, dark grey, fluorescent yellow, nectarine, olive green, red, white, and custom colors

System size/weight:
838 x 737 x 1143 mm (33 x 29 x 45 in.)/with crate: 186 kg (409 lbs.), without crate: 148 kg (326 lbs.)

Achievable accuracy:
Parts are produced within an accuracy of ± .241 mm (± .0095 in.). (Accuracy is geometry dependent. Achievable accuracy specification derived from statistical data at 95% dimensional yield.)

Network communication:
10/100 base T connection; Ethernet protocol

9.5 Technical specifications of the "Dimension Elite" printer [25]

Dimension Elite Product Specs

Model material:
ABS*plus* in nine colors

Support material:
Soluble or breakaway

Build size:
203 x 203 x 305 mm (8 x 8 x 12 in.)

Layer thickness:
0.254 mm (0.010 in.) or 0.178 mm (0.007 in.)

Workstation compatibility:
Windows XP/Windows 7

Network connectivity:
Ethernet TCP/IP 10/100 base T

Size and weight:
686 x 914 x 1041 mm (27 x 36 x 41 in.); 136 kg (300 lbs.)

Power Requirements:

Dimension Elite 3D Printer: 100–120 VAC 60 Hz, minimum 15A dedicated circuit or 220–240 VAC 50/60 Hz, minimum 7A dedicated circuit

SCA-1200 support-removal system: 100-120 VAC, 15A, 60 Hz or 220-240 VAC, 10A, 50 Hz

Regulatory Compliance:

Dimension Elite 3D Printer: CE/ETL

SCA-1200 Support Removal System: CE

Special Facility Requirements:
None

9.6 Datasheet Al 7075: material properties [26]

Alclad Aluminum 7075-T6, T651

Categories:	Metal; Nonferrous Metal; Aluminum Alloy; 7000 Series Aluminum Alloy
Material Notes:	Data points with the AA note have been provided by the Aluminum Association, Inc. and are NOT FOR DESIGN. **Composition Notes:** Composition for AA 7075 (not Alclad 7075 specifically). Composition information provided by the Aluminum Association and is not for design.
Key Words:	Alclad 7075-T6, T651; Alclad 7075-T6, T651
Vendors:	**Click here to view all available suppliers for this material.** Please click here if you are a supplier and would like information on how to add your listing to this material.

Physical Properties	Metric	English	Comments
Density	2.81 g/cc	0.102 lb/in³	For AA7075 (Not Alclad)

Mechanical Properties	Metric	English	Comments
Tensile Strength, Ultimate	524 MPa	76000 psi	AA; Typical
	115 MPa @Temperature 181 °C, Time 3.60e+6 sec	16700 psi @Temperature 358 °F, Time 1000 hour	
	220 MPa @Temperature 150 °C, Time 3.60e+6 sec	31900 psi @Temperature 302 °F, Time 1000 hour	
	399 MPa @Temperature 125 °C, Time 3.60e+6 sec	57900 psi @Temperature 257 °F, Time 1000 hour	
	485 MPa @Temperature 100 °C, Time 3.60e+6 sec	70300 psi @Temperature 212 °F, Time 1000 hour	
	525 MPa @Temperature 24.0 °C, Time 3.60e+6 sec	76100 psi @Temperature 75.2 °F, Time 1000 hour	
	>= 462 MPa @Thickness 88.93 - 102 mm	>= 67000 psi @Thickness 3.501 - 4.00 in	Plate; T62, T651
	>= 469 MPa @Thickness 0.203 - 0.279 mm	>= 68000 psi @Thickness 0.00800 - 0.0110 in	Sheet; T6, T62
	>= 483 MPa @Thickness 0.305 - 0.991 mm	>= 70100 psi @Thickness 0.0120 - 0.0390 in	Sheet; T6, T62
	>= 490 MPa @Thickness 76.23 - 88.9 mm	>= 71100 psi @Thickness 3.001 - 3.50 in	Plate; T62, T651
	>= 496 MPa @Thickness 1.02 - 1.57 mm	>= 71900 psi @Thickness 0.0400 - 0.0620 in	Sheet; T6, T62
	>= 496 MPa @Thickness 63.53 - 76.2 mm	>= 71900 psi @Thickness 2.501 - 3.00 in	Plate; T62, T651
	>= 503 MPa @Thickness 1.60 - 4.75 mm	>= 73000 psi @Thickness 0.0630 - 0.187 in	Sheet; T6, T62
	>= 517 MPa @Thickness 4.78 - 6.32 mm	>= 75000 psi @Thickness 0.188 - 0.249 in	Sheet; T6, T62
	>= 517 MPa @Thickness 6.35 - 12.7 mm	>= 75000 psi @Thickness 0.250 - 0.499 in	Plate; T62, T651
	>= 524 MPa @Thickness 50.83 - 63.5 mm	>= 76000 psi @Thickness 2.001 - 2.50 in	Plate; T62, T651
	>= 531 MPa @Thickness 25.43 - 50.8 mm	>= 77000 psi @Thickness 1.001 - 2.00 in	Plate; T62, T651
	>= 538 MPa @Thickness 12.7 - 25.4 mm	>= 78000 psi @Thickness 0.500 - 1.00 in	Plate; T62, T651
Tensile Strength, Yield	462 MPa	67000 psi	AA; Typical
	110 MPa @Temperature 180 °C, Time 3.60e+6 sec	16000 psi @Temperature 356 °F, Time 1000 hour	
	210 MPa @Temperature 150 °C, Time 3.60e+6 sec	30500 psi @Temperature 302 °F, Time 1000 hour	
	375 MPa @Temperature 120 °C, Time 3.60e+6 sec	54400 psi @Temperature 248 °F, Time 1000 hour	
	422 MPa @Temperature 100 °C, Time 3.60e+6 sec	61200 psi @Temperature 212 °F, Time 1000 hour	
	475 MPa @Temperature 24.0 °C,	68900 psi @Temperature 75.2 °F,	

	Time 3.60e+6 sec	Time 1000 hour	
	>= 372 MPa @Thickness 88.93 - 102 mm	>= 54000 psi @Thickness 3.501 - 4.00 in	Plate; T62, T651
	>= 400 MPa @Thickness 0.203 - 0.279 mm	>= 58000 psi @Thickness 0.00800 - 0.0110 in	Sheet; T6, T62
	>= 400 MPa @Thickness 76.23 - 88.9 mm	>= 58000 psi @Thickness 3.001 - 3.50 in	Plate; T62, T651
	>= 414 MPa @Thickness 0.305 - 0.991 mm	>= 60000 psi @Thickness 0.0120 - 0.0390 in	Sheet; T6, T62
	>= 421 MPa @Thickness 63.53 - 76.2 mm	>= 61100 psi @Thickness 2.501 - 3.00 in	Plate; T62, T651
	>= 427 MPa @Thickness 1.02 - 1.57 mm	>= 61900 psi @Thickness 0.0400 - 0.0620 in	Sheet; T6, T62
	>= 434 MPa @Thickness 1.60 - 4.75 mm	>= 62900 psi @Thickness 0.0630 - 0.187 in	Sheet; T6, T62
	>= 441 MPa @Thickness 4.78 - 6.32 mm	>= 64000 psi @Thickness 0.188 - 0.249 in	Sheet; T6, T62
	>= 441 MPa @Thickness 50.83 - 63.5 mm	>= 64000 psi @Thickness 2.001 - 2.50 in	Plate; T62, T651
	>= 448 MPa @Thickness 6.35 - 12.7 mm	>= 65000 psi @Thickness 0.250 - 0.499 in	Plate; T62, T651
	>= 462 MPa @Thickness 25.43 - 50.8 mm	>= 67000 psi @Thickness 1.001 - 2.00 in	Plate; T62, T651
	>= 469 MPa @Thickness 12.7 - 25.4 mm	>= 68000 psi @Thickness 0.500 - 1.00 in	Plate; T62, T651
Elongation at Break	>= 3.0 % @Thickness 88.93 - 102 mm	>= 3.0 % @Thickness 3.501 - 4.00 in	Plate; T62, T651
	>= 5.0 % @Thickness 0.203 - 0.279 mm	>= 5.0 % @Thickness 0.00800 - 0.0110 in	Sheet; T6, T62
	>= 5.0 % @Thickness 50.83 - 63.5 mm	>= 5.0 % @Thickness 2.001 - 2.50 in	Plate; T62, T651
	>= 5.0 % @Thickness 63.53 - 76.2 mm	>= 5.0 % @Thickness 2.501 - 3.00 in	Plate; T62, T651
	>= 5.0 % @Thickness 76.23 - 88.9 mm	>= 5.0 % @Thickness 3.001 - 3.50 in	Plate; T62, T651
	>= 6.0 % @Thickness 25.43 - 50.8 mm	>= 6.0 % @Thickness 1.001 - 2.00 in	Plate; T62, T651
	>= 7.0 % @Thickness 0.305 - 0.991 mm	>= 7.0 % @Thickness 0.0120 - 0.0390 in	Sheet; T6, T62
	>= 7.0 % @Thickness 12.7 - 25.4 mm	>= 7.0 % @Thickness 0.500 - 1.00 in	Plate; T62, T651
	>= 8.0 % @Thickness 1.02 - 1.57 mm	>= 8.0 % @Thickness 0.0400 - 0.0620 in	Sheet; T6, T62
	>= 8.0 % @Thickness 1.60 - 4.75 mm	>= 8.0 % @Thickness 0.0630 - 0.187 in	Sheet; T6, T62
	>= 8.0 % @Thickness 4.78 - 6.32 mm	>= 8.0 % @Thickness 0.188 - 0.249 in	Sheet; T6, T62
	>= 9.0 % @Thickness 6.35 - 12.7 mm	>= 9.0 % @Thickness 0.250 - 0.499 in	Plate; T62, T651
	11 % @Thickness 1.59 mm	11 % @Thickness 0.0625 in	AA; Typical
Creep Strength	85.0 MPa @Temperature 185 °C	12300 psi @Temperature 365 °F	.01mm/m-h
	175 MPa @Temperature 150 °C	25400 psi @Temperature 302 °F	.01mm/m-h
	250 MPa @Temperature 185 °C	36300 psi @Temperature 365 °F	10mm/m-h
	350 MPa @Temperature 150 °C	50800 psi @Temperature 302 °F	10mm/m-h
	350 MPa @Temperature 100 °C	50800 psi @Temperature 212 °F	.01mm/m-h
	425 MPa @Temperature 100 °C	61600 psi @Temperature 212 °F	10mm/m-h
	475 MPa @Temperature 30.0 °C	68900 psi @Temperature 86.0 °F	.01mm/m-h
	515 MPa @Temperature 30.0 °C	74700 psi @Temperature 86.0 °F	10mm/m-h
Rupture Strength	95.0 MPa @Temperature 190 °C, Time 1.44e+6 sec	13800 psi @Temperature 374 °F, Time 400 hour	
	105 MPa @Temperature 190 °C, Time 360000 sec	15200 psi @Temperature 374 °F, Time 100 hour	
	150 MPa	21800 psi	

	@Temperature 150 °C, Time 3.60e+6 sec	@Temperature 302 °F, Time 1000 hour	
	175 MPa @Temperature 190 °C, Time 36000 sec	25400 psi @Temperature 374 °F, Time 10.0 hour	
	240 MPa @Temperature 150 °C, Time 360000 sec	34800 psi @Temperature 302 °F, Time 100 hour	
	280 MPa @Temperature 190 °C, Time 1440 sec	40600 psi @Temperature 374 °F, Time 0.400 hour	
	310 MPa @Temperature 150 °C, Time 36000 sec	45000 psi @Temperature 302 °F, Time 10.0 hour	
	355 MPa @Temperature 99.0 °C, Time 3.60e+6 sec	51500 psi @Temperature 210 °F, Time 1000 hour	
	370 MPa @Temperature 150 °C, Time 1260 sec	53700 psi @Temperature 302 °F, Time 0.350 hour	
	400 MPa @Temperature 99.0 °C, Time 342000 sec	58000 psi @Temperature 210 °F, Time 95.0 hour	
	425 MPa @Temperature 99.0 °C, Time 32400 sec	61600 psi @Temperature 210 °F, Time 9.00 hour	
	470 MPa @Temperature 99.0 °C, Time 900 sec	68200 psi @Temperature 210 °F, Time 0.250 hour	
	495 MPa @Temperature 34.0 °C, Time 2.70e+6 sec	71800 psi @Temperature 93.2 °F, Time 750 hour	
	510 MPa @Temperature 34.0 °C, Time 720000 sec	74000 psi @Temperature 93.2 °F, Time 200 hour	
	525 MPa @Temperature 34.0 °C, Time 360 sec	76100 psi @Temperature 93.2 °F, Time 0.100 hour	
	530 MPa @Temperature 34.0 °C, Time 108000 sec	76900 psi @Temperature 93.2 °F, Time 30.0 hour	
Modulus of Elasticity	71.7 GPa	10400 ksi	AA; Typical; Average of tension and compression. Compression modulus is about 2% greater than tensile modulus.
Shear Strength	317 MPa	46000 psi	AA; Typical

Processing Properties	Metric	English	Comments
Annealing Temperature	413 °C	775 °F	
Solution Temperature	466 - 482 °C	870 - 900 °F	
Aging Temperature	121 °C	250 °F	

Component Elements Properties	Metric	English	Comments
Aluminum, Al	87.1 - 91.4 %	87.1 - 91.4 %	As remainder
Chromium, Cr	0.18 - 0.28 %	0.18 - 0.28 %	
Copper, Cu	1.2 - 2.0 %	1.2 - 2.0 %	
Iron, Fe	<= 0.50 %	<= 0.50 %	
Magnesium, Mg	2.1 - 2.9 %	2.1 - 2.9 %	
Manganese, Mn	<= 0.30 %	<= 0.30 %	
Other, each	<= 0.05 %	<= 0.05 %	
Other, total	<= 0.15 %	<= 0.15 %	
Silicon, Si	<= 0.40 %	<= 0.40 %	
Titanium, Ti	<= 0.20 %	<= 0.20 %	
Zinc, Zn	5.1 - 6.1 %	5.1 - 6.1 %	

References for this datasheet.

Some of the values displayed above may have been converted from their original units and/or rounded in order to display the information in a consistent format. Users requiring more precise data for scientific or engineering calculations can click on the property value to see the original value as well as raw conversions to equivalent units. We advise that you only use the original value or one of its raw conversions in your calculations to minimize rounding error. We also ask that you refer to MatWeb's terms of use regarding this information. Click here to view all the property values for this datasheet as they were originally entered into MatWeb.

9.7 Datasheet 4137 steel: material properties [27]

AISI 4137 Steel

Categories: Metal; Ferrous Metal; Alloy Steel; AISI 4000 Series Steel; Low Alloy Steel; Carbon Steel; Medium Carbon Steel

Material Notes: Available as hot rolled and cold rolled sheet and strip, hot rolled and cold rolled finished bar, and cold heading quality wire. Suitable for heat treatment, machining into components, or, in the as-finished condition, constructional applications and similar uses.

Key Words: UNS G41370, ASTM A322, ASTM A331, ASTM A505, ASTM A519, SAE J404, SAE J412, SAE J770, DIN 1.7225, AFNOR 40 CD 4, AFNOR 42 CD 4 (France), B.S. 708 A 42 (UK), B.S. 708 M 40 (UK), B.S. 709 M 40 (UK)

Vendors: No vendors are listed for this material. Please click here if you are a supplier and would like information on how to add your listing to this material.

Physical Properties	Metric	English	Comments
Density	7.85 g/cc	0.284 lb/in³	

Mechanical Properties	Metric	English	Comments
Hardness, Brinell	187 - 229	187 - 229	annealed and cold drawn
Hardness, Knoop	230	230	Converted from Brinell hardness.
Hardness, Rockwell B	94	94	Converted from Brinell hardness.
Hardness, Rockwell C	15	15	Converted from Brinell hardness. Value below normal HRC range, for comparison purposes only.
Hardness, Vickers	218	218	Converted from Brinell hardness.
Modulus of Elasticity	205 GPa	29700 ksi	Typical for steel
Bulk Modulus	140 GPa	20300 ksi	Typical for steel
Poissons Ratio	0.29	0.29	Calculated
Machinability	70 %	70 %	Based on AISI 1212 steel. as 100% machinability
Shear Modulus	80.0 GPa	11600 ksi	Typical for steel

Electrical Properties	Metric	English	Comments
Electrical Resistivity	0.0000223 ohm-cm	0.0000223 ohm-cm	

Thermal Properties	Metric	English	Comments
CTE, linear	11.2 µm/m-°C @Temperature 0.000 - 100 °C	6.22 µin/in-°F @Temperature 32.0 - 212 °F	
	12.4 µm/m-°C @Temperature 0.000 - 300 °C	6.89 µin/in-°F @Temperature 32.0 - 572 °F	
	13.5 µm/m-°C @Temperature 0.000 - 500 °C	7.50 µin/in-°F @Temperature 32.0 - 932 °F	
Specific Heat Capacity	0.477 J/g-°C	0.114 BTU/lb-°F	
Thermal Conductivity	42.7 W/m-K	296 BTU-in/hr-ft²-°F	

Component Elements Properties	Metric	English	Comments
Carbon, C	0.35 - 0.40 %	0.35 - 0.40 %	
Chromium, Cr	0.80 - 1.1 %	0.80 - 1.1 %	
Iron, Fe	96.93 - 97.85 %	96.93 - 97.85 %	As remainder
Manganese, Mn	0.70 - 0.90 %	0.70 - 0.90 %	
Molybdenum, Mo	0.15 - 0.25 %	0.15 - 0.25 %	
Phosphorous, P	<= 0.035 %	<= 0.035 %	
Silicon, Si	0.15 - 0.35 %	0.15 - 0.35 %	
Sulfur, S	<= 0.040 %	<= 0.040 %	

References for this datasheet.

Some of the values displayed above may have been converted from their original units and/or rounded in order to display the information in a consistent format. Users requiring more precise data for scientific or engineering calculations can click on the property value to see the original value as well as raw conversions to equivalent units. We advise that you only use the original value or one of its raw conversions in your calculations to minimize rounding error. We also ask that you refer to MatWeb's terms of use regarding this information. Click here to view all the property values for this datasheet as they were originally entered into MatWeb.

9.8 Datasheet of the Sensitec GLM7xxASB-Ax family sensors [45]

SENSITEC
MagnetoResistive Sensors

GLM700ASB family

Tooth sensor module with integrated magnet

Data sheet

The sensor modules of the GLM700ASB-Ax family are designed for use with passive measurement scales. The modules combine a GiantMagnetoResistive (GMR) tooth sensor with an integrated bias magnet in a compact SMD housing, so reducing the design and assembly effort for the user. In addition, the integration of sensor and magnet provides a very high quality of the sensor signals.
Adapted to a variety of tooth pitches, the integrated GMR sensors apply the **FIX**PITCH® technology. This means that the sensor chip is matched to a given tooth pitch.
In use with a ferromagnetic scale and a matching pitch, the module delivers two 90 degree phase shifted analogue signals (sine and cosine).
The table “Product overview” on page 7 shows the modules available with the according pitch.

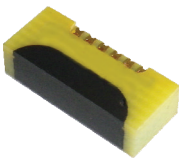

GLM700ASB-Ax

Product overview

Article	Description
GLM7xxASB-Ax	Module, combining a sensor and a magnet for a variety of tooth pitches with sine and cosine output signal.

For order information see page 7.

Quick reference guide

Symbol	Parameter	Min.	Typ.	Max.	Unit
V_{CC}	Supply voltage	-9.0	+5.0	+9.0	V
V_{peak}	Signal amplitude per V_{CC} [1)]	4.0	9.0	20.0	mV/V
T_{amb}	Ambient temperature	-40	-	+125	°C
f	Frequency range	1	-	-	MHz

1) The amplitude depends on the distance between sensor and scale. For further information see Fig. 6 (page 4).

Measurement setup

Depiction	Configuration	Application
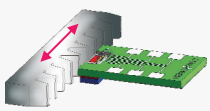	Ferromagnetic toothed rack with fixed pitch; sensor with bias magnet mounted perpendicularly to the rack	Incremental length measurement
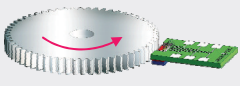	Ferromagnetic toothed wheel with fixed pitch; sensor with bias magnet mounted radially to the toothed wheel	Incremental angle measurement at the shaft circumference

Features

- Gear tooth sensor with integrated magnet
- Differential sine and cosine output signals
- Ambient temperature range from -40 °C to +125 °C
- Designed for vertical or horizontal mounting
- High signal quality due to **FIX**PITCH® technology
- Contactless, wear-free measurement principle

Advantages

- Allows use of simple passive toothed structures as measurement scale; so reducing design, manufacturing and assembly effort
- Flexible design options due to identical pin arrangements
- Reliable operation in difficult environments
- High interpolation possible within tooth pitch for high resolution and high accuracy.
- Low power consumption for battery-driven applications.

Applications

Incremental encoder for linear or rotary motion in various industrial applications, for example:

- Linear position measurement
- Linear direct drive motors
- Linear and rotary bearings

Absolute maximum ratings

In accordance with the absolute maximum rating system (IEC60134).

Symbol	Parameter	Min.	Max.	Unit
V_{CC}	Supply voltage	-9.0	+9.0	V
T_{amb}	Ambient temperature	-40	+125	°C
T_{stg}	Storage temperature	-40	+125	°C
MSL	Moisture sensitivity level	2		

Stresses beyond those listed under “absolute maximum ratings” may cause permanent damage to the device. This is a stress rating only and functional operation of the device at these or any other conditions beyond those indicated in the operational sections of this specification is not implied. Exposure to absolute maximum rating conditions for extended periods may affect device reliability.

Electrical data

T_{amb} = 25 °C; unless otherwise specified.

Symbol	Parameter	Conditions	Min.	Typ.	Max.	Unit
V_{CC}	Supply voltage		-9.0	+5.0	+9.0	V
TC_{RB}	Temperature coefficient of R_B and R_S	T_{amb} = (-40...+125) °C	-	0.12	-	%/K
TC_{Voff}	Temperature coefficient of V_{off}	T_{amb} = (-40...+125) °C	-3	-	+3	µV/V/K
T_{amb}	Ambient temperature		-40	-	+125	°C
V_{peak}	Signal amplitude per V_{CC} [1)]		4.0	9.0	20.0	mV/V
TC_{Vpeak}	Temperature coefficient of V_{peak}	T_{amb} = (-40...+125) °C	-0.08	-0.12	-0.16	%/K
f	Frequency range [2)]		1	-	-	MHz

1) The amplitude depends on the distance between sensor and scale. See Fig. 1 (page 4) for more information.

2) No significant amplitude loss in this frequency range.

Product type specific data

Article description	Pitch	Offset Voltage	Bridge resistance 3)	Sensor resistance 4)	Air gap 5)
GLM711ASB-Ax	1 mm	± 3 mV/V	5.5 kΩ	2.75 kΩ	200 µm
GLM712ASB-Ax	2 mm	± 3.5 mV/V	5.7 kΩ	2.85 kΩ	400 µm
GLM713ASB-Ax	3 mm	± 3.5 mV/V	5.7 kΩ	2.85 kΩ	600 µm
GLM714ASB-Ax	0.94 mm (module 0.3)	± 3 mV/V	5.6 kΩ	2.80 kΩ	190 µm
GLM715ASB-Ax	1.57 mm (module 0.5)	± 3 mV/V	5.8 kΩ	2.90kΩ	310 µm

3) Bridge resistance between pad 1 and 5, 2 and 6. Resistor tolerance ±15 %.

4) Sensor resistance between pad 3 and 4. Resistor tolerance ±15 %.

5) Optimal air gap between sensor and scale - for further information see Fig. 6 (page 4).

9.9 Datasheet of the Gefran PY2 series sensors [35]

GEFRAN

PY2

RECTILINEAR DISPLACEMENT TRANSDUCER WITH BALL TIP

Principal characteristics

- *The side connection creates a through-rod structure with double rod support, guaranteeing greater overall strength of the transducer.*
- *The return spring automatically returns the rod to zero position, making the transducer suitable for comparator applications.*
- *The tip with stainless steel ball is suitable for applications where the object to be measured is not subject to shifts transverse to the transducer axle.*
- *Ideal for checking the flatness or thickness of panels of various materials. Can also be used for valves or mechanical parts when the rod cannot be attached to the moving object.*

TECHNICAL DATA

Useful electrical stroke (C.E.U.)	10/25/50/75/100
Resolution	Infinite
Independent linearity (within C.E.U.)	see table
Displacement speed	≤ 10 m/s
Displacement force	≤ 4 N
Life	>25x10^{6}m strokes,or 100x10^6 operations, whichever is less (within C.E.U.)
Vibrations	5...2000Hz, Amax =0,75 mm amax. = 20 g
Shock	50 g, 11ms.
Tolerance on resistance	± 20%
Recommended cursor current	< 0,1 μA
Maximum cursor current	10mA
Maximum applicable voltage	see table
Electrical isolation	>100MΩ a 500V=, 1bar, 2s
Dielectric strength	< 100 μA a 500V~, 50Hz, 2s, 1bar
Dissipation at 40°C (0W at 120°C)	see table
Actual Temperature Coefficient of the output voltage	< 1,5ppm/°C
Working temperature	-30...+100°C
Storage temperature	-50...+120°C
Case material	Anodised aluminium Nylon 66 G 25
Control rod material	Stainless steel AISI 303
Fixing	Brackets with variable longitudinal axis

MECHANICAL DIMENSIONS

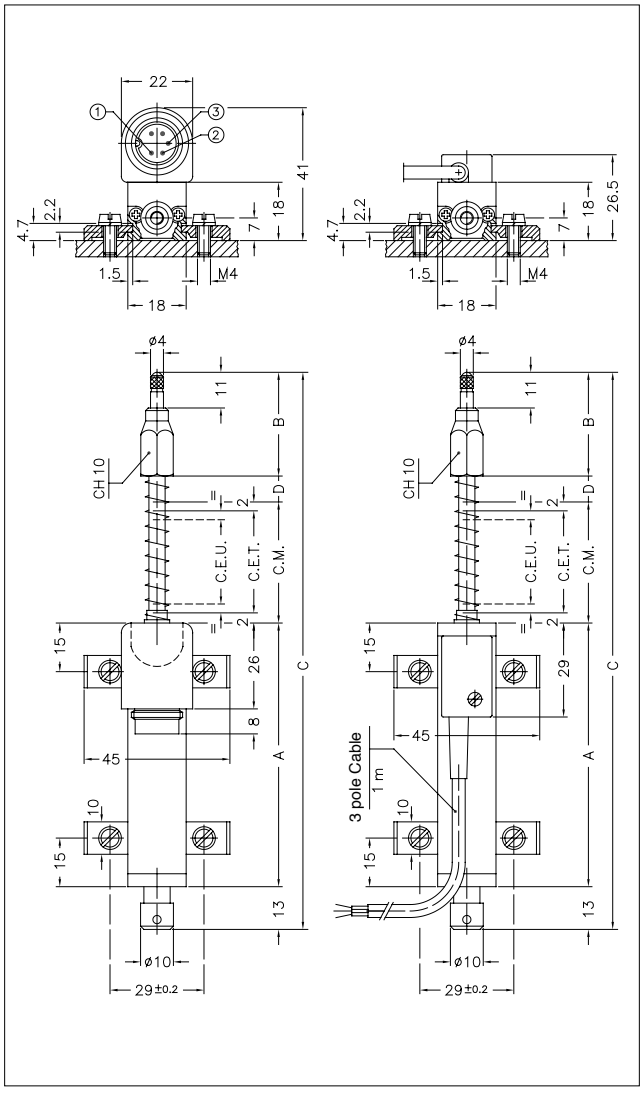

Important: all the data reported in the catalogue linearity, lifetime, temperature coefficient are valid for a sensor utilization as a ratiometric device with a max current across the cursor Ic ≤ 0.1 μA.

MECHANICAL / ELECTRICAL DATA

Model		10	25	50	75	100
Useful electrical stroke (C.E.U.) +1/-0	mm	10	25	50	76	101
Theoretical electrical stroke (C.E.T.) ±1	mm	C.E.U. +1			76	101
Resistance (C.E.T.)	kΩ	1	1	5	5	5
Independent linearity (within C.E.U.)	± %	0.3	0.2	0.1	0.1	0.1
Dissipation at 40° (0W at 120°C)	W	0.2	0.6	1.2	1.8	2.4
Maximum applicable voltage	V	14	25	60	60	60
Mechanical stroke (C.M.)	mm	C.E.U. + 5				
Case length (A)	mm	C.E.U. + 38				
Tip length (B)	mm	32	32	40	40	40
Total length (C)	mm	108	138	196	251	307
Quote (D)	mm	-	-	-	5	11

ELECTRICAL CONNECTIONS

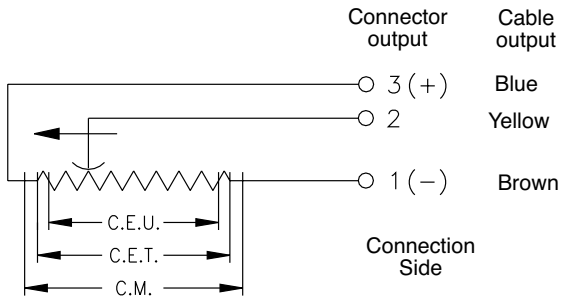

INSTALLATION INSTRUCTIONS

- Respect the indicated electrical connections (DO NOT use the transducer as a variable resistance)
- When calibrating the transducer, be careful to set the stroke so that the output does not drop below 1% or rise beyond 99% of the supply voltage.

OPTIONAL FIXING KIT PKIT006

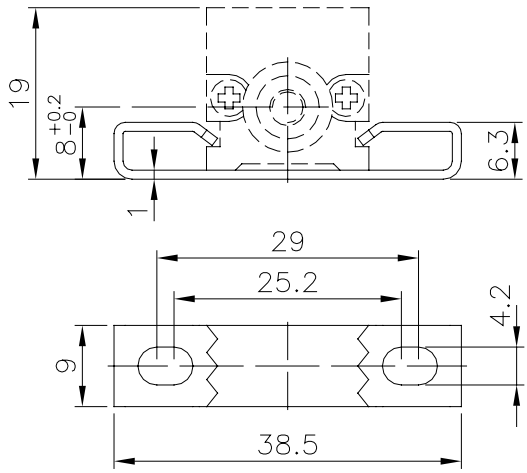

ORDER CODE

Displacement transducer **PY2** □ □ | S □ M | □ □ □ X □ □ □ □ □

3 pole PVC cable output 3x0.25 1m	**F**
5 pole connector output DIN 43322	**C**

Model

Cable length (in metres)

This part of the code only applies to the model with cable output

No certificate attached	**0**
Linearity curve to be attached	**L**

Standard mounting brackets (PKIT005)	**X**
Optional mounting brackets (PKIT006)	**S**

Color of plastic heads (green)	**0**
Color of plastic heads (black)	**N**

Ex.:**PY2 - C - 100**
Displacement transducer model PY2, 5-pole connector output, useful electrical stroke (C.E.U.) 100mm.

ACCESSORIES

STANDARD ACCESSORIES	
Fixing kit: 4 brackets, M4x10 screws, washer	**PKIT005**
Fixing kit: 2 “wraparound” brackets (0000X000S00 configurator option)	**PKIT006**
Tip with bal	**PTAS000**

OPTIONAL ACCESSORIES	
5-pin axial female PCB connector DIN43322 IP40 clamp for wire ø4 - ø6 mm	**CON011**
5-pin axial female PCB connector DIN43322 IP65 clamp PG7 for wire ø4 - ø6 mm	**CON012**
5-pin 90° radial female PCB connector DIN43322 IP40 clamp for wire ø4 - ø6 mm	**CON013**

GEFRAN spa reserves the right to make any kind of design or functional modification at any moment without prior notice

GEFRAN spa
via Sebina, 74
25050 PROVAGLIO D’ISEO (BS) - ITALIA
tel. 0309888.1 - fax. 0309839063
Internet: http://www.gefran.com

9.10 Datasheet of the Parker Hannifin PTD ASIC pressure transducers [36]

Pressure Transducers and Transmitters

ASIC 'Performer'

25, 60, 100, 250, 400 and 600 bar

Brochure: FDHB240UK
March 2007

ASIC 'Performer'

Applications for the ASIC Performer

- Fork lift trucks - braking and load systems.
- Truck mounted cranes - load safety systems.
- Earth moving machinery - hydraulic gearbox control.
- Racing car - gearbox, fuel, cooling and suspension systems.
- Water usage systems - pressurised systems for industrial and hi-rise usage.
- Forest Machinery - felling and logging.
- Paper mills - speed control and weighing systems.

The Parker Filtration ASIC Performer Pressure Transducers and Transmitters.

The ASIC Performer offers a wide range of pressure sensors for mobile or industrial applications.

These sensors have been designed for the requirements of industrial instrumentation systems. Accordingly, the housings and all components in contact with the medium are made of stainless steel. Thus giving compatibility with a wide range of media. There is a choice of two plug connectors of either DIN or M12. There are six measuring ranges available and a choice of outputs in the form of either voltage or current signals. Sensors with output signals from 4...20 mA are available in two wire technology.

The built-in voltage regulator allows the sensors to be operated with a supply voltage of 12-36/9-36 Vdc. All sensors are manufactured in our own production facility, typical of Parker Hannifin's continued commitment to flexibility and quality.

The Complete Performer range utilises ASIC technology (Application Specific Integrated Circuit) programmable software.

A comprehensive range of Pressure Transducers and Transmitters are available from Parker Filtration.

- One-piece body and diaphragm machining ensures long-term product stability.
- All stainless steel construction.
- 6 transducer pressure ratings with 0-5Vdc and 1-6Vdc outputs.
- 6 transmitter pressure ratings with a 2-wire 4-20mA output.
- Microdin din plug and M12 connector options.

AC/DC display unit (DDU1002)

Parker Hannifin
Hydraulic Filter Division Europe
FDHB240UK.

Specification

Pressure ranges:
25, 60, 100, 250, 400, 600 bar.

Pressure Tolerance Specifications:

Rating	Maximum Overload Pressure	Maximum Burst Pressure
25	x 6.0 (150 bar)	x 20.0 (500 Bar)
60	x 2.5 (150 Bar)	x 8.0 (500 Bar)
100	x 2.5 (250 bar)	x 5.0 (500 Bar)
250	x 4.0 (1000 Bar)	x 7.0 (1800 Bar)
400	x 2.5 (1000 Bar)	x 4.5 (1800 Bar)
600	x 1.5 (1000 Bar)	x 3.0 (1800 Bar)

Vibration resistance:
IEC 60068-2-6:
+/- 5mm/10Hz...32Hz
200m/s^2 / 32Hz...2kHz

Installation:
Spanner size 22A/F.
Max. (recommended) tightening torque = 30Nm.

Weight:
200 - 230g

Lifespan:
10 million cycles

Thread Forms

G1/4 (1/4BSP) with ED seal.

All thread forms and sensor interface are made from 1.4301 stainless steel.

Non standard threads - contact Parker CMC

Electrical

Supply voltage	Output
12 - 36Vdc	0 - 5Vdc
12 - 36Vdc	1 - 6Vdc
9 - 36Vdc	4 - 20mA

Transducer current draw = <6mA
Load impedance (ohm) = >10K
Output signal noise = 0.1%FS

Product Performance

Linearity:
Typical: 0.3%FS.
Max: 0.6%FS.

Hysteresis:
Typical: 0.1%FS.
Max: 0.25%FS.

Repeatability:
Typical: 0.2%FS.
Max: 0.4%FS.

Functional temp range:
-40°C to +85°C.

Compensated temperature:
-20°C to +85°C.

Stability:
<0.1%FS/a (typ).

Response time:
= <1mS.

Wiring Information

Connector Industrial Micro Din 9.4mm

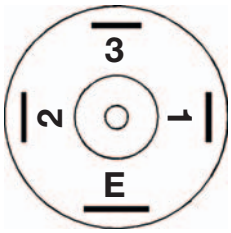

PIN	4 - 20mA	0 - 5Vdc	1 - 6Vdc
1	Do not connect	Signal output	Signal output
2	Supply +ve	Supply +ve	Supply +ve
3	Do not connect	Do not connect	Do not connect
E	Return	Supply ref. (0v)	Supply ref. (0v)

Connector M12

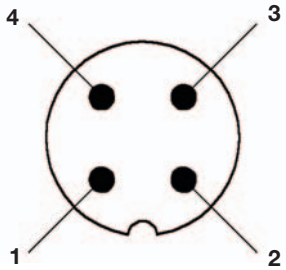

PIN	4 - 20mA	0 - 5Vdc	1 - 6Vdc
1	Supply +ve	Supply +ve	Supply +ve
2	Do not connect	Signal output	Signal output
3	Return	Supply ref. (0v)	Supply ref. (0v)
4	Do not connect	Do not connect	Do not connect

Installation Details

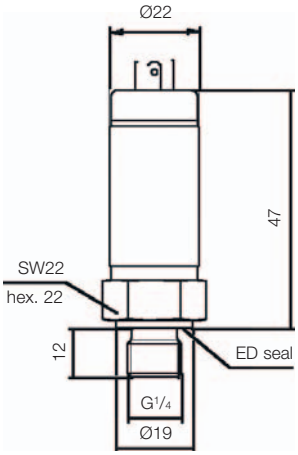

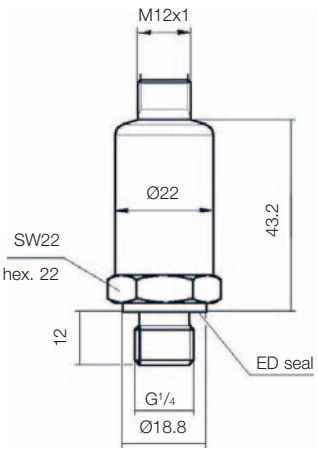

ASIC 'Performer'

Ordering Information

Standard products table

Product number	Description - pressure transducer	Model	Output	Pressure	Thread form	Connector
PTDVB2501B1C1	0 - 5 Vdc 250 bar 1/4 BSP ED seal micro-din	PTD	VB	250	1	B1C1
PTDVB4001B1C1	0 - 5 Vdc 400 bar 1/4 BSP ED seal micro-din	PTD	VB	400	1	B1C1
PTDVB2501B1C2	0 - 5 Vdc 250 bar 1/4 BSP ED seal M12	PTD	VB	250	1	B1C2
PTDVB4001B1C2	0 - 5 Vdc 400 bar 1/4 BSP ED seal M12	PTD	VB	400	1	B1C2
PTDVB0251B1C1	0 - 5 Vdc 25 bar 1/4 BSP ED seal micro-din	PTD	VB	025	1	B1C1
PTDVB0251B1C2	0 - 5 Vdc 25 bar 1/4 BSP ED seal M12	PTD	VB	025	1	B1C2

Product number	Description - pressure transmitter	Model	Output	Pressure	Thread form	Connector
PTXB4001B1C2	4 - 20 mA 400 bar 1/4 BSP ED seal M12	PTX	B	400	1	B1C2
PTXB0251B1C1	4 - 20 mA 25 bar 1/4 BSP ED seal micro-din	PTX	B	025	1	B1C1
PTXB0251B1C2	4 - 20 mA 25 bar 1/4 BSP ED seal M12	PTX	B	025	1	B1C2
PTXB4001B1C1	4 - 20 mA 400 bar 1/4 BSP ED seal micro-din	PTX	B	400	1	B1C1
PTXB2501B1C1	4 - 20 mA 250 bar 1/4 BSP ED seal micro-din	PTX	B	250	1	B1C1
PTXB2501B1C2	4 - 20 mA 250 bar 1/4 BSP ED seal M12	PTX	B	250	1	B1C2

Accessories

Product number	Supercedes	Description
P833PVC2M	P.833PVC-2M	2 meter PVC coated 4 core cable
P833PVC5M	P.833PVC-5M	5 meter PVC coated 4 core cable
P833PVC10M	P.833PVC-10M	10 meter PVC coated 4 core cable

Note 1: Part numbers featured with bold highlighted codes will ensure a 'standard' product selection.
Note 2: Alternate displayed part number selection will require you to contact Parker Filtration for availability.

Product configurator

Product number	Output options		Pressure range (bar)		Thread form		Connector	
PTD	**VB**	0 - 5 Vdc	**025**	0 - 25	**1**	1/4 BSP with ED seal	**B1C1**	Micro-din
PTX	SB	1 - 6 Vdc	060	0 - 60			**B1C2**	M12
	B	4 - 20mA (PTX only)	100	0 - 100				
	RB	0.5 - 4.5 ratiometric	**250**	0 - 250				
	PB	0.1 - 4.9	**400**	0 - 400				
			600	0 - 600				

Note 1: Part numbers featured with bold highlighted codes will ensure a 'standard' product selection.
Note 2: Alternate displayed part number selection will require you to contact Parker Filtration for availability.

Examples of standard part number product ordering

PTDVB2501B1C1
0 – 5 volt output transducer
250 bar maximum pressure
1/4" BSP with ED seal
Industrial micro-din 9.4mm connector

PTDSB4001B1C2
1 – 6 volt output transducer
400 bar maximum pressure
1/4" BSP with ED seal
M12 connector
(See accessories for IP68 protected cable)

PTXB0251B1C2
4 – 20mA output transmitter
25 bar maximum pressure
1/4" BSP with ED seal
M12 connector
(See accessories for IP68 protected cable)

Condition Monitoring website: www.parker.com/cmc
Condition Monitoring email: conmoninfo@parker.com
For further information on other Parker Products,
call EPIC free on 00800 27 27 5374

Brochure Ref: FDHB240UK
Hydraulic Filter Division Europe

© Copyright 2007
Parker Hannifin Corporation
All rights reserved.

9.11 Datasheet of the Physik Instrumente HVPZT E-482 amplifier [37]

PICA High-Power Piezo Driver/ Servo Controller

HIGH ENERGY EFFICIENCY THROUGH ENERGY RECOVERY

E-482

- Peak current 6 A
- Output voltage to 1050 V
- Integrated energy recovery
- Temperature sensor protects piezo actuator from overheating

PICA high power piezo driver
19-inch bench top for dynamic continuous operation of PICA piezo actuators with high electrical capacitance. Analog operation. Output voltage up to 1050 V, bipolar selectable. 6 A peak current, 2 A average current

Energy saving of up to 80% due to switched control principle
Switching amplifier with pulse width modulation (PWM) of the piezo output voltage. When the piezo actuator is discharged, a patented circuitry for energy recovery stores part of the returning energy in a capacitor makes it reusable for the next charging cycle. The amplifier runs cooler and provides better stability.

Upgrading to a Servo Controller
Optional E-509 position servo control module for closed-loop control with a position feedback sensor. Optional E-517 digital module with wave generator, data recorder, display, 24-bit interfaces (USB, etc)

© Physik Instrumente (PI) GmbH & Co. KG 2012. Subject to change without notice. Latest releases available at www.pi.ws. 12/11/22.0

	E-482.00	Unit
Function	Power amplifier with energy recovery for PICA high-voltage piezo actuators	
Amplifier		
Output voltage	Default: 0 to 1050 V Selectable: -260 to +780 V, -525 to +525 V	
Amplifier channels	1	
Average current (idle current)	2	A
Peak current, <5 ms	6	A
Current limitation	Short-circuit-proof	
Voltage gain	100	
Amplifier bandwidth, small signal	2 kHz (1 µF)	
Amplifier bandwidth, large signal	400 Hz (5 µF)	
Ripple, noise, 0 to 10 kHz, 1 µF	300	mV_{rms}
Suggested capacitive load	1 µF (min.), 17 µF (max.)	
Input impedance	100	kΩ
Control input voltage	Servo off: ±1/100 of selected output range; servo on: 0 to 10 V	
Interface and operation		
Piezo connector	LEMO EGG.0B.701.CJL1173	
Analog input	BNC socket	
Temperature sensor (piezo actuator)	LEMO socket; deactivation of the piezo voltage output at 120 °C	
DC offset	10-turn potentiometer, adds 0 to ±10 V to input voltage	
Miscellaneous		
Operating voltage	100 to 120 / 220 to 240 VAC, 50 to 60 Hz (fuse change required)	
Operating temperature range	5 to 40	°C
Mass	10.4	kg
Dimensions	288 mm × 450 mm × 158 mm + handles	

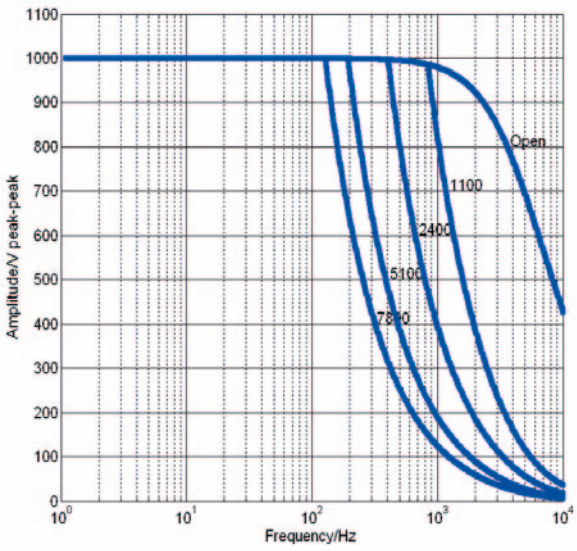

Operating limits with various PZT loads (open-loop), capacitance is measured in nF

9.12 Technical specifications: dSPACE MicroAutoBox type 1401/1501 [46]

Embedded Success dSPACE

Technical Details

Certifications

Compact, stand-alone prototyping unit

Parameter		Specification			
MicroAutoBox		1401/1501	1401/1504	1401/1505/1507	NEW: 1401/1507
Processor		NEW: IBM PPC 750GL, 800 MHz (incl. 1 MB level 2 cache) z			
Memory		NEW: 16 MB main memory 4 MB memory exclusively for communication between MicroAutoBox and PC/notebook 16 MB nonvolatile flash memory containing code section and flight recorder data Clock/calendar function for time-stamping of flight recorder data			
Interfaces	CAN interface	Dual CAN interface; 2 CAN channels in total	Two dual CAN interfaces; 4 CAN channels in total	Two dual CAN interfaces; 4 CAN channels in total	Two dual CAN interfaces; 4 CAN channels in total
	Serial interface (based on CAN processor)	1 x RS232 interface	1 x RS232 interface	2 x RS232 interface	2 x RS232 interface
		1 x serial interface usable as K/L-Line or LIN interface	1 x serial interface usable as K/L-Line or LIN interface	2 x serial interface usable as K/L-Line or LIN interface	2 x serial interface usable as K/L-Line or LIN interface
	ECU interface	Dual-port memory interface, 16 K x 16-bit DPRAM	–	2 x dual-port memory interfaces, 16 K x 16-bit DPRAM	Dual-port memory interface, 16 K x 16-bit DPRAM
	FlexRay interface	–	–	Up to 2 slots[1)] for FlexRay modules	1 slot[1)] for a FlexRay module
Analog input	Resolution	16 12-bit channels	24 12-bit channels	16 12-bit channels	-
	Sampling	4 to 1 multiplexed Simultaneous sample & hold			-
	Input voltage range	0 ... 5 V			-
Analog output	Resolution	8 12-bit channels	–	8 12-bit channels	-
	Output voltage range	0 ... 4.5 V			-
	Output current	5 mA max. sink/source current			-
Digital I/O	General	Digital I/O on 68336 slave processor, 20 MHz, with time processor unit (TPU) I/O software support for different applications			-
	Bit I/O	16 discrete inputs 10 discrete outputs, 5 mA output current 16 shared discrete inputs/outputs, bit-selectable 16 TPU channels Up to 16-bit resolution			-
	PWM generation/measurement	4 shared inputs for frequency or PWM 4 PWM outputs, PWM frequency 2.5 Hz ... 100 kHz, duty cycle 0 ... 100%			-

		Overcurrent and short circuit protection			
Physical connections		ZIF connector for I/O signals and power supply, mechanically secured			Sub-D connectors for bus interfaces and power supply, LEMO connector for ECU interface
		Connection to a notebook/PC for program load, experiment configuration, signal monitoring and flight recorder read-out ZIF connector for I/O signals and power supply, mechanically secured Additional 78-pin Sub-D connector with MicroAutoBox 1401/1505/1507 High-speed host interface (100 megabits/s technology) Support of PCMCIA, PCI, and ISA host connections Cable length of up to 10 meters			
Physical characteristics	Enclosure material	Cast aluminum box			
	Enclosure size	Approx. 200 x 225 x 50 mm (7.9 x 8.9 x 2.0 in)	Approx. 200 x 225 x 50 mm (7.9 x 8.9 x 2.0 in)	Approx. 200 x 225 x 95 mm (7.9 x 8.9 x 3.8 in)	Approx. 200 x 225 x 50 mm (7.9 x 8.9 x 2.0 in)
	Ambient temperature	Operating temperature: -40 ... +85 °C (-40 ... 185 °F) Storage temperature: -55 ... +125 °C (-67 ... +257 °F)			
	Power supply	6 ... 40 V input power supply, protected against overvoltage and reverse polarity			
	Power consumption	Max. 20 W			

[1] IP module slot. Can also be used for an ARINC interface module (via dSPACE Engineering Services).

Certifications

Further Information

MicroAutoBox Variants
Features that depend on the I/O board type and hardware Revisions

Contact Information

Request Information
Order Product Information

Contact
You can find all the information on contacting dSPACE here.

© 2010 dSPACE GmbH

9.13 Digimess FG 200 function generator datasheet [47]

FG200 2MHz Sweep Function Generator

digimess® concept

Order No: HUC 61-00

CE

The ***digimess***® FG200 is a general purpose microprocessor controlled 2MHz sweep function generator. The unit features a power up self-test and is operated by a combination of soft touch buttons and rotary controls, resulting in a modern and easy to use instrument for engineers of all levels. This versatile instrument includes a 5 digit frequency display for internal or external signals and a 3 digit output amplitude display. The frequency, amplitude and attenuation ranges are indicated by leds as well as the selected waveform shape, the unit also includes both internal and external frequency sweep modes. The instrument is supplied with an operating manual, bnc test lead

Specification	
Frequency range	0.2Hz to 2MHz in 7 decade ranges
Frequency accuracy	+/- 0.5%
Output waveforms	Sine, square and triangle
Output impedence	50ohm
Output voltage	1mVpp to 10Vpp (into 50ohm load) 1mVpp to 20Vpp (into 1kohm load)
Attenuation	0dB, -20dB, -40dB, -60dB
TTL output voltage and impedence	< 0.8V and > 3V, 600ohm
Offset	-5V to +5V
Duty cycle	20% to 80%
Sine wave distortion	< 2%
Triangle wave non-linearity	< 1%
Square wave rise time	< 100nS
Sweep modes	Internal linear, Internal log, External sweep
External counter input	0.2Hz to 20MHz
Input voltage	110/220Vac +/- 10% 50Hz max 30W
Dimensions W x L x H and weight	265 x 215 x 90mm, 2kg

9.14 Technical data: profitec switchable power supply type SPS 12103 [42]

Artikelbezeichnung:	Labornetzgerät 10A
Artikelnummer:	SPS 12103
Fabrikat:	Profitec
Abmessungen ca.:	175 x 110 x 45 mm
Ausgangsspannung:	12-14 VDC
Belastbarkeit:	10A
EAN Code:	4016641161822
Eingangsspannung:	230VAC
Gehäuse:	Kunststoff
Gewicht:	846 g
Kurzschluss-Schutz:	Ja (Ein- und Ausgang)
Lüfter:	Ja
Restwelligkeit:	<2% mV
VPE:	1/16

9.15 Technical drawing of the Guilliard & Dörr rod seals

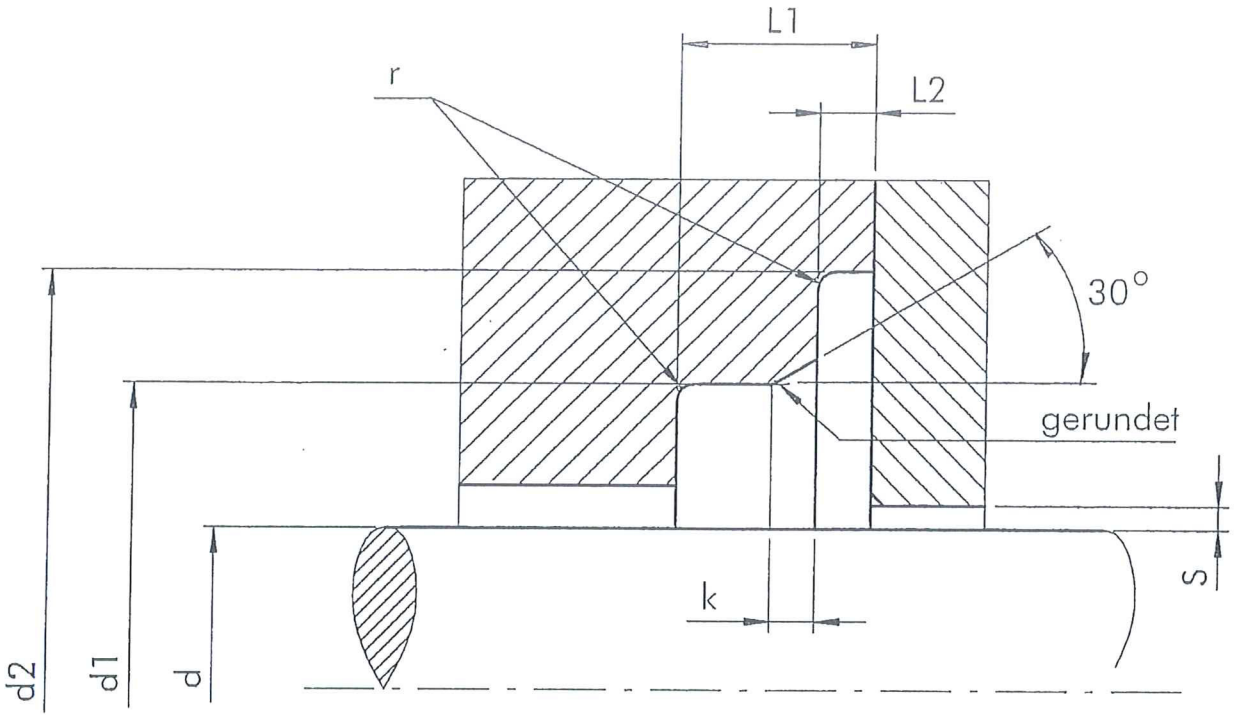

$d = 20,0$

$d_1 = 28,0$

$d_2 = 33,0$

$L_1 = 5,0$

$L_2 = 1,3$

$r = 0,5$

$k = 1,1$

GUILLIARD & DÖRR GmbH
DICHTUNGS- UND KUNSTSTOFFTECHNIK
Neue Heimat 22
74343 Sachsenheim-Ochsenbach
Telefon 0 70 46 / 96 10 - 0
Fax: 0 70 46 / 96 10 - 33

9.16 List of dimensions and quantity of used o-rings

Kasse

	Artikel	Anzahl	Einzelpreis	Summe
	Präzisions O-Ring 38,00 x 3,50 mm FPM75 Lieferzeit: sofort, Zvv.	4	4,43 EUR	17,72 EUR
	Präzisions O-Ring 13,50 x 1,50 mm FPM75 Lieferzeit: sofort, Zvv.	14	1,11 EUR	15,54 EUR
	Präzisions O-Ring 33,00 x 2,00 mm FPM75 Lieferzeit: sofort, Zvv.	3	2,20 EUR	6,60 EUR
	Präzisions O-Ring 8,00 x 1,00 mm FPM75 Lieferzeit: sofort, Zvv.	14	0,77 EUR	10,78 EUR
	Präzisions O-Ring 26,70 x 1,78 mm FPM75 Lieferzeit: sofort, Zvv.	10	1,18 EUR	11,80 EUR
	Präzisions O-Ring 27,00 x 1,50 mm FPM75 Lieferzeit: sofort, Zvv.	10	1,55 EUR	15,50 EUR
	Präzisions O-Ring 27,00 x 2,00 mm FPM75 Lieferzeit: sofort, Zvv.	10	1,90 EUR	19,00 EUR

Versandkostenberechnung:

Lieferland: Germany

Versandgewicht: 1,065 kg

Versandart: Paketdienst DPD - UPS

Zwischensumme:	96,94 EUR
inkl. 19% MwSt.:	15,48 EUR
Summe:	96,94 EUR zzgl. 0,00 EUR Versand

9.17 Properties of the compression spring used in the control unit

Firma/Name	Ostfalia Hochschule Wolfsburg	**Kd.Nr.**	
Ansprechpartner	Leander Behre	**Datum**	09.05.2014 14:10
Straße		☐ **Anfrage**	☐ **Bestellung**
PLZ/Ort		**Ref.Nr.**	G145648
Telefon	**Fax**	**Stück**	
E-mail		**Termin**	

GUTEKUNST FEDERN
Carl-Zeiss-Strasse 15
D-72555 Metzingen
Telefon 0 71 23 / 9 60-0
Telefax 0 71 23 / 9 60-195
technik@gutekunst-co.com
www.gutekunst-federn.de

Druckfedern

d	mm	Drahtdurchmesser
D	mm	Mittlerer Windungsdurchmesser
Dd	mm	Dorndurchmesser
De	mm	Äußerer Windungsdurchmesser
Dh	mm	Hülsendurchmesser
e1	mm	Abweichung von Mantellinie
e2	mm	Abweichung von Parallelität

F1	N	Kraft der Feder vorgespannt
F2	N	Kraft der Feder gespannt
Fn	N	Höchstkraft der Feder
Fc	N	Theo. Federkraft bei Blocklänge
k	-----	Spannungsbeiwert
L0	mm	Ungespannte Länge der Feder
L1	mm	Länge der Feder vorgespannt
L2	mm	Länge der Feder gespannt
Ln	mm	Kleinste Länge der Feder
Lc	mm	Blocklänge
n	St.	Anzahl federnden Windungen
nt	St.	Anzahl der Gesamtwindungen
R	N/mm	Federrate
s	mm	Steigung der Feder

S1	mm	Strecke der Feder vorgespannt
S2	mm	Strecke der Feder gespannt
Sh	mm	Arbeitsweg (Hub)
Sn	mm	Grösste Strecke der Feder
tauzul	N/mm²	Zulässige Schubspannung
tau1	N/mm²	Schubspannung bei F1
tau2	N/mm²	Schubspannung bei F2
taun	N/mm²	Schubspannung bei Fn
tauc	N/mm²	Schubspannung bei Fc
taukozul	N/mm²	Zulässige Oberspannung korrigiert
taukhzul	N/mm²	Zulässige Hubspannung korrigiert
tauk2	N/mm²	Korrigierte Schubspannung bei F2
taukh	N/mm²	Korrigierte Hubspannung

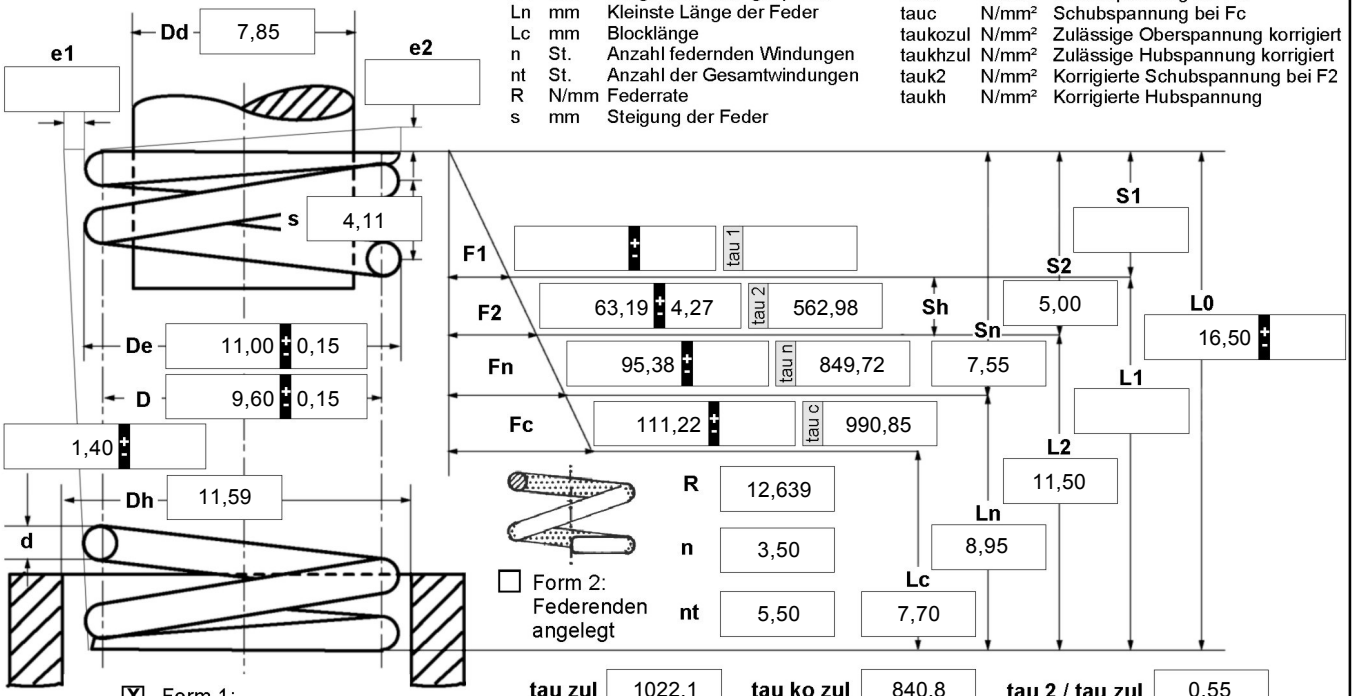

tau zul	1022,1	**tau ko zul**	840,8	**tau 2 / tau zul**	0,55
k	1,205	**tau kh zul**	840,8	**tau n / tau zul**	0,83

1 Windungsrichtung
☐ links ☒ rechts

2 Dynamische Beanspruchung ☒

tau k2	678,21
tau kh	678,21
tau k2 / tau ko zul	0,81
tau kh / tau kh zul	0,81

3 Arbeitsweg Sh 5,00 mm

4 Lastspielzahl N 10000000

5 Lastspielfrequenz n 1574,4 / s

6 Arbeitstemperatur °C

7 Führung und Lagerung DIN EN 13906-1
☐ Dorn ☐ Hülse

Knicklänge bei Lagerungsbeiwert " v " in mm

Fall 1 v=2,0	Fall 2 v=1,0	Fall 3 v=1,0	Fall 4 v=0,7	Fall 5 v=0,5
11,96	0,00	0,00	0,00	0,00

8 Werkstoff
EN 10270-2 VD SiCr (Ventilfederstahldraht)

Schubmodul **G**	81500,0
Elastizitätsmodul **E**	200000,0

9 Draht- oder Staboberfläche
☒ gezogen ☐ gewalzt ☐ spanend bearbeitet

10 Federn entgratet ☐ innen ☐ außen

11 Oberflächenschutz ☒ kugelgestrahlt

12 Toleranzen nach DIN EN 15800

Gütegrad	De,Di,D	L0	F1,F2	e1,e2	Drahtstärke **d** nach DIN 2076
1	☒	☐	☒	☐	
2	☐	☐	☐	☐	
3	☐	☐	☐	☐	☒

13 Fertigungsausgleich durch

Eine Federkraft mit zugehöriger Länge	L0	☐
Eine Federkraft mit zugehöriger Länge und L0	n, d	☐
	n, De, Di	☐
Zwei Federkräfte mit zugehörigen Längen	L0, n, d	☐
	L0,n,De,Di	☐

14 Prüffedern setzen ! LS _____ mm
Übrige Federn ☐ setzen ☐ ungesetzt
Ungesetzte Federn dürfen länger sein als L0 !

Zusätzliche Angaben / Prüf- Werkszeugnis / Zeichnungsnummer …

Zeichnungs-Nr.: G145648
In Werkstoff VDSiCr mit OF und in Gütegrad 01>fein

W.(g)	2,004		1 /	10 /	100 /	1000 /	Lz	

9.18 Properties of the compression springs used in the servo valve

Firma/Name	Ostfalia Hochschule Wolfsburg	**Kd.Nr.**	
Ansprechpartner	Leander Behre	**Datum**	09.05.2014 13:57
Straße		☐ **Anfrage**	☐ **Bestellung**
PLZ/Ort		**Ref.Nr.**	G145647
Telefon	**Fax**	**Stück**	
E-mail		**Termin**	

GUTEKUNST FEDERN
Carl-Zeiss-Strasse 15
D-72555 Metzingen
Telefon 0 71 23 / 9 60-0
Telefax 0 71 23 / 9 60-195
technik@gutekunst-co.com
www.gutekunst-federn.de

Druckfedern

d	mm	Drahtdurchmesser
D	mm	Mittlerer Windungsdurchmesser
Dd	mm	Dorndurchmesser
De	mm	Äußerer Windungsdurchmesser
Dh	mm	Hülsendurchmesser
e1	mm	Abweichung von Mantellinie
e2	mm	Abweichung von Parallelität

F1	N	Kraft der Feder vorgespannt
F2	N	Kraft der Feder gespannt
Fn	N	Höchstkraft der Feder
Fc	N	Theo. Federkraft bei Blocklänge
k	-----	Spannungsbeiwert
L0	mm	Ungespannte Länge der Feder
L1	mm	Länge der Feder vorgespannt
L2	mm	Länge der Feder gespannt
Ln	mm	Kleinste Länge der Feder
Lc	mm	Blocklänge
n	St.	Anzahl federnden Windungen
nt	St.	Anzahl der Gesamtwindungen
R	N/mm	Federrate
s	mm	Steigung der Feder

S1	mm	Strecke der Feder vorgespannt
S2	mm	Strecke der Feder gespannt
Sh	mm	Arbeitsweg (Hub)
Sn	mm	Grösste Strecke der Feder
tauzul	N/mm²	Zulässige Schubspannung
tau1	N/mm²	Schubspannung bei F1
tau2	N/mm²	Schubspannung bei F2
taun	N/mm²	Schubspannung bei Fn
tauc	N/mm²	Schubspannung bei Fc
taukozul	N/mm²	Zulässige Oberspannung korrigiert
taukhzul	N/mm²	Zulässige Hubspannung korrigiert
tauk2	N/mm²	Korrigierte Schubspannung bei F2
taukh	N/mm²	Korrigierte Hubspannung

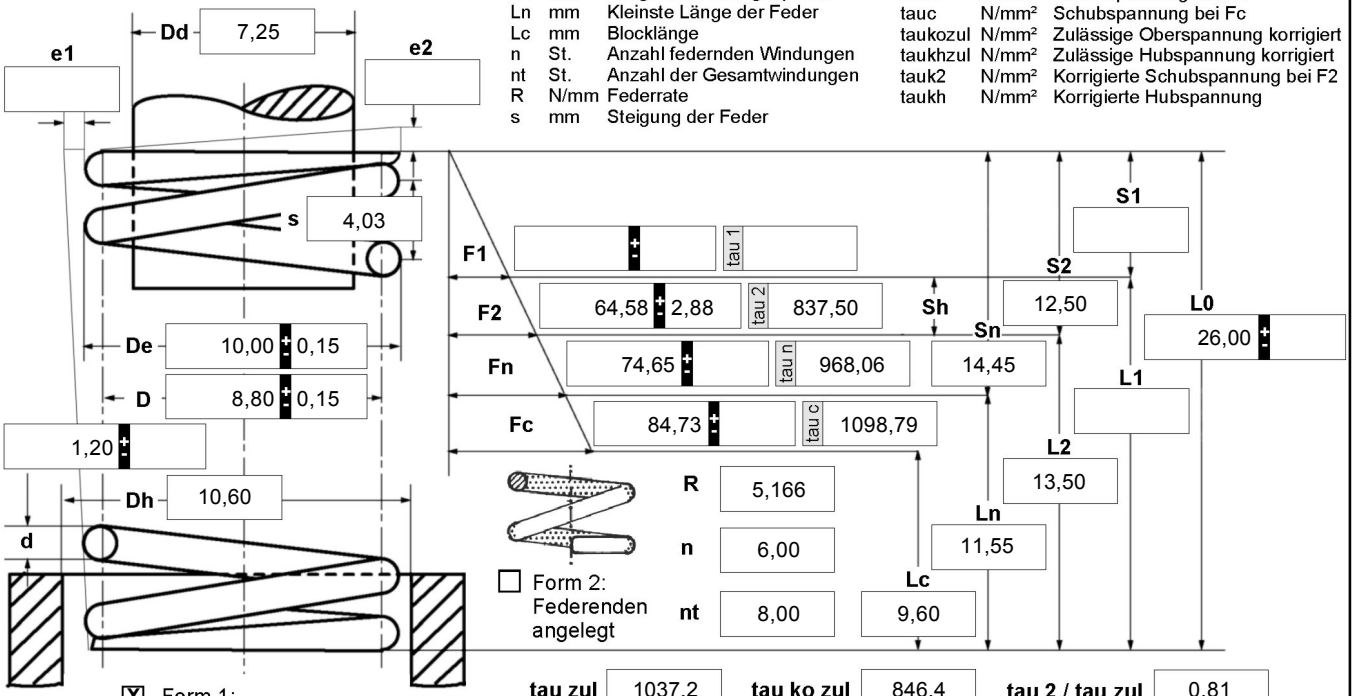

tau zul	1037,2	**tau ko zul**	846,4	**tau 2 / tau zul**	0,81
k	1,190	**tau kh zul**	846,4	**tau n / tau zul**	0,93

1 Windungsrichtung
☐ links ☒ rechts

2 Dynamische Beanspruchung ☒

tau k2	996,51
tau kh	996,51
tau k2 / tau ko zul	1,18
tau kh / tau kh zul	1,18

3 Arbeitsweg Sh 12,50 mm

4 Lastspielzahl N

5 Lastspielfrequenz n 936,8 / s

6 Arbeitstemperatur °C

7 Führung und Lagerung DIN EN 13906-1
☐ Dorn ☐ Hülse

Knicklänge bei Lagerungsbeiwert " v " in mm

Fall 1 v=2,0	Fall 2 v=1,0	Fall 3 v=1,0	Fall 4 v=0,7	Fall 5 v=0,5
23,87	15,29	15,29	0,00	0,00

8 Werkstoff
EN 10270-2 VD SiCr (Ventilfederstahldraht)

Schubmodul **G**	81500,0
Elastizitätsmodul **E**	200000,0

9 Draht- oder Staboberfläche
☒ gezogen ☐ gewalzt ☐ spanend bearbeitet

10 Federn entgratet ☐ innen ☐ außen

11 Oberflächenschutz ☒ kugelgestrahlt

12 Toleranzen nach DIN EN 15800

Gütegrad	De,Di,D	L0	F1,F2	e1,e2	Drahtstärke **d** nach DIN 2076
1	☒	☐	☒	☐	
2	☐	☐	☐	☐	
3	☐	☐	☐	☐	☒

13 Fertigungsausgleich durch

Eine Federkraft mit zugehöriger Länge	L0	☐
Eine Federkraft mit zugehöriger Länge und L0	n, d	☐
	n, De, Di	☐
Zwei Federkräfte mit zugehörigen Längen	L0, n, d	☐
	L0,n,De,Di	☐

14 Prüffedern setzen ! LS _____ mm
Übrige Federn ☐ setzen ☐ ungesetzt
Ungesetzte Federn dürfen länger sein als L0 !

Zusätzliche Angaben / Prüf- Werkszeugnis / Zeichnungsnummer …

Zeichnungs-Nr.: G145647
In Werkstoff VDSiCr mit OF und in Gütegrad 01>fein

! Zul. Oberspannung überschritten (tau k2 > tau ko zul)
Zul. Hubspannung überschritten (tau kh > tau kh zul)

W.(g)	1,964		1 /	10 /	100 /	1000 /	Lz	

Bibliography

[1] European Automobile Manufacturers Association, communications department (2011). The Automobile Industry Pocket Guide. Available from http://www.acea.be/images/uploads/files/20110921_Pocket_Guide_3rd_edition.pdf. (Accessed 08 January 2014).

[2] Jung, A. (2014). Alternativantriebe: Warten auf Grün. Press report by Spiegel Online. Available from http://www.spiegel.de/spiegelwissen/alternativantriebe-wie-umweltfreundlich-elektro-und-hybridmobile-sind-a-1000702.html. (Accessed 24 November 2014).

[3] Kurke, H. (2010). Machbarkeitsstudie einer vollvariablen Ventilsteuerung auf Piezo-Basis an einem BMW K71 Motor. Diploma thesis. Ostfalia University of Applied Sciences: Wolfsburg, Germany.

[4] Behre, B.Eng. L. (2013). Entwicklung und Evaluierung eines vorgesteuerten Hochgeschwindigkeitsservoventils für Piezoaktoren. Bachelor thesis. Ostfalia University of Applied Sciences: Wolfsburg, Germany.

[5] BMW Motorrad Deutschland (2014). Faszination, Technik im Detail, Motor & Antrieb, Zweizylinder Parallel-Twin 800 ccm. Available from http://www.bmw-motorrad.de/de/de/index.html. (Accessed 15 January 2014).

[6] Bozek, J.-W. (1991). Formation and Control of Combustion Pollutants from Gasoline-Fueled Otto Cycle Motor Vehicle Engines. Synopsis of information. United States Environmental Protection Agency (EPA): Washington, D.C., USA.

[7] Jalal, Engr. A. (2006). Pollution by 2-Stroke Engines. Presentation. The Nigerian Conference on Clean Air, Clean Fuels and Vehicles: Abuja, Nigeria.

[8] Becker, Prof. Dr.-Ing. U. (2013). Vorlesung Grundlagen Verbrennungsmotoren und Antriebsstrang, Teil 5: Kraftstoffe und Abgase. Lecture script. Ostfalia University of Applied Sciences: Wolfsburg, Germany.

[9] Van Basshuysen, Dr.-Ing. E.h. R., and Schäfer, Prof. Dr.-Ing. F. (2002) Internal Combustion Engine Handbook: Basics, Components, Systems, and Perspectives. Technical literature. Vieweg-publishing house: Wiesbaden, Germany.

[10] Becker, Prof. Dr.-Ing. U., Werner, M.Sc. N., and Stahlberg, Dipl.-Ing. (FH) M. (2013). Formelsammlung zum Skript Antriebstechnik und Fahrzeugakustik. Formulary. Ostfalia University of Applied Sciences: Wolfsburg, Germany.

[11] He, X., Durrett, R., and Sun, Z. (2008). Late Intake Valve Closing as an Emissions Control Strategy at Tier 2 Bin 5 Engine-Out NOx Level. Paper 2008-01-0637, SAE World Congress & Exhibition. University of Minnesota: Minneapolis, Minnesota, USA.

[12] Eichlseder, Univ.-Prof. Dr. techn. H., Klell, Dr. techn. M., Schutting, Dipl.-Ing. E., Neureiter, Dipl.-Ing. A., Fuchs, Dipl.-Ing. C., Schatzberger, Dipl.-Ing. T., and Kammerdiener, Dipl.-Ing. T (2007). Miller- und Atkinson-Zyklus am aufgeladenen Dieselmotor. Research report. Hamburg University of Applied Sciences: Hamburg, Germany.

[13] Car and Driver (2009). Fiat's Multiair Valve-Lift System Explained. Available from http://www.caranddriver.com/features/fiats-multiair-valve-lift-system-explained. (Accessed 29 January 2014).

[14] United States Environmental Protection Agency (EPA) (2011). Light-Duty Vehicle Technology Cost Analysis, Mild Hybrid and Valvetrain Technology. Technical report. Assessment and Standards Division Office of Transportation and Air Quality: Washington, D.C., USA.

[15] Shekaina, J., and Jayasingh, Dr. T. (2012). Novel Configuration for Air Flow Rationalization and Turbo Lag Reduction in CRDI Engine. Research paper, International Journal of Scientific and Research Publications, Volume 2, Issue 9. Dr. M.G.R Educational and research Institute: Chennai, India.

[16] Ferrari, Dr.-Ing. A. (2009). The Fiat Multiair Technology: A step towards high efficiency SI engines. Technical report. Fiat Powertrain Technologies: Turin, Italy.

[17] Vanhaelst, Prof. Dr.-Ing. R. (2013). Alternative Antriebe: 2. Thermische Antriebe: 2.2 Viertakt-Kolbenmotoren - Potentiale und Trends. Lecture script. Ostfalia University of Applied Sciences: Wolfsburg, Germany.

[18] Schechter, M.-M., and Levin, M.-B. (1996). Electrohydraulic Camless Valvetrain with Rotary Hydraulic Actuator. United States Patent 5,562,070: Dearborn, Michigan, USA.

[19] Sturman Industries (2014). Hydraulic Valve Actuation. Available from http://sturmanindustries.com/Solutions/Products/HVACamless/HydraulicValveActuation/tabid/202/Default.aspx. (Accessed 24 November 2014).

[20] Hochheuser, Dipl.-Ing.(FH) M. (2012). A full variable valve train mechatronic control system. Master thesis. Nelson Mandela Metropolitan University: Port Elizabeth, South Africa.

[21] Stölting, Prof. Dr.-Ing. H.-D., Kallenbach, Prof. Dr.-Ing. habil. Prof. h.c. E., and Amrhein, Prof. Dr. Dipl.-Ing. W. (2011). Handbuch Elektrische Kleinantriebe. Handbook. Hanser-publishing house: Munich, Germany.

[22] Manz, Dipl.-Ing. H. (2001). Aktive Schwingungsreduktion in modal formulierten Strukturen mit Hilfe piezokeramischer Aktorik und Polverschiebung. Progress report VDI No. 475. VDI-publishing house: Düsseldorf, Germany.

[23] Werner, M.Sc. N., Mercorelli, Prof. Dr.-Ing. P., and Becker, Prof. Dr.-Ing. U. (2011). Analyse der Abhängigkeit systemrelevanter Parameter einer vollvariablen piezo-hydraulischen Ventilpositionsregelung auf das Betriebsverhalten eines

Verbrennungsmotors. Presentation. Ostfalia University of Applied Sciences: Wolfsburg, Germany.

[24] Stratasys (2014). 3D Printers, Production Series, Fortus 250mc, Fortus 250mc Spec Sheet. Available from http://www.stratasys.com/3D-Printers/production-series/fortus-250mc. (Accessed 29 April 2014).

[25] Stratasys (2014). 3D Printers, Performance, Dimension Elite, Dimension Elite Brochure. Available from http://www.stratasys.com/3d-printers/design-series/performance/dimension-elite. (Accessed 29 April 2014).

[26] MatWeb (LLC), Material Property Data (2014). Search, Material Property Search, Metal, Nonferrous Metal, Aluminum Alloy, 7000 Series Aluminum Alloy, Alclad Aluminum 7075-T6, T651. Available from http://www.matweb.com/search/DataSheet.aspx?MatGUID=9852e9cdc3d4466ea9f111f3f0025c7d&ckck=1. (Accessed 8 May 2014).

[27] MatWeb (LLC), Material Property Data (2014). Search, Material Property Search, Metal, Ferrous Metal, Alloy Steel, AISI 4000 Series Steel, Low Alloy Steel, Carbon Steel, Medium Carbon Steel. Available from http://www.matweb.com/search/DataSheet.aspx?MatGUID=b9f5c86dc4354e6fa041339280d5e04f. (Accessed 12 May 2014).

[28] Deutsche Edelstahlwerke, Providing special steel solutions (2014). Publikationen, Werkstoffdatenblätter, Baustahl, 1.7225/1.7227. Available from http://www.dew-stahl.com/fileadmin/files/dew-stahl.com/documents/Publikationen/Werkstoffdatenblaetter/Baustahl/1.7225_1.7227_de.pdf. (Accessed 8 May 2014).

[29] Sensitec (2014). Products, Length-And-Path, Details about the technical Principles of the Length and Position Measurement. Available from http://www.sensitec.com/english/products/length-and-path/laengenmessung-erklaerungsseite.html. (Accessed 15 May 2014).

[30] Sensitec (2014). Technology, MR Sensor Technology. Available from

http://www.sensitec.com/english/technology/mr-sensor-technology/mr_sensortechnologie.html. (Accessed 19 May 2014).

[31] Fert, A. L. F., and Grünberg, P. A., compiled by the Class of Physics of the Royal Swedish Academy of Sciences (2007). The Discovery of Giant Magnetoresistance. Scientific Background on the Nobel Prize in Physics 2007. The Royal Swedish Academy of Sciences: Stockholm, Sweden.

[32] Deng, C., Kang, Y., Li, E., Zhang, Y., Cheng, J., and Ge, T. (2013). A new model of the signal generation mechanism on magnetostrictive position sensor. Research journal. State Key Laboratory of Digital Manufacturing Equipment & Technology, and College of Electrical and Electronic Engineering, Huazhong University of Science and Technology: Wuhan, Hubei 430074, China.

[33] SCOPEONLINE (2014). Magnetostriktive Messung: Der Maßstab der Hydraulik. Available from http://www.scope-online.de/th9-Expertenbeitrag_id_10141__dId_22100__app_510-83781_.htm. (Accessed 21 May 2014).

[34] MTS Sensor Technologie GmbH & Co. KG (2014). Die Temposonics® Positionsmessung - magnetostriktiv!. Available from http://www.mtssensor.de/Magnetostriktion.26.0.html. (Accessed 21 May 2014).

[35] Gefran SPA (2014). PY2 Rectilinear displacement transducer. Available from http://www.gefran.com/en/product_categories/38-rectilinear-displacement-transducers%28rc1%29/products/73-py2-rectilinear-displacement-transducer#certifications. (Accessed 21 May 2014).

[36] Parker (2007). Pressure Transducers and Transmitters: ASIC ´Performer´: 25, 60, 100, 250, 400 and 600 bar. Product Brochure FDHB240UK. Parker Hannifin Corporation: Cleveland, Ohio, USA.

[37] Physik Instrumente (PI) (2012). PICA High-Power Piezo Driver/Servo Controller: High Energy Efficiency Through Energy Recovery. PDF Catalogue Datasheet. Physik Instrumente GmbH & Co. KG: Karlsruhe/Palmbach, Germany.

[38] dSPACE (2014). Products, Our Solutions For..., Electric Drive Technology, dSPACE Products, MicroAutoBox. Available from http://www.dspace.co.uk/en/ltd/home/products/our_solutions_for/electricaldrive/dspace_products/microautobox.cfm?nv=n2. (Accessed 05 June 2014).

[39] dSPACE (2013/2014). Exklusive Angebote für Hochschulen: dSPACE ACE Kit. Product Brochure. dSPACE digital signal processing and control engineering GmbH: Paderborn, Germany.

[40] Digimess (2003). FG 200 Function Generator: Operating Instructions. Product Brochure. Digimess Instruments Ltd: Derby, United Kingdom.

[41] Rapid Electronics (2014). Digimess FG200 2 MHz Sweep Function Generator. Available from http://www.rapidonline.com/test-measurement/digimess-fg200-2mhz-sweep-function-generator-68105. (Accessed 06 June 2014).

[42] profitec (2014). Stromversorgung, Labornetzgeräte, Labornetzgerät, Labornetzgerät SPS 12103 / 10A. Available from http://www.profitec.info/stromversorgung/labornetzgeraete/regelbar/3824/labornetzgeraet?c=18236000. (Accessed 07 June 2014).

[43] Zibani, I.B., Chuma, J.M., Marumo, J. (2014). Design, Test and Implementation of a single piston rotary valve Engine Control Unit. Research journal. Department of Electrical Engineering, University of Botswana: Gaborone, Botswana.

[44] BMW Motorrad USA (2014). Motorcycles, Tour, F 800 GT, Technical Data. Available from http://www.bmwmotorcycles.com/us/en/index.html?content=http://www.bmwmotorcycles.com/us/en/bike/enduro/2012/f800gs/f800gs_data.html&prm_action=&notrack=1. (Accessed 17 January 2014).

[45] Sensitec (2014). GLM700ASB family tooth sensor module with integrated magnet: Data sheet. Available from http://www.sensitec.com/upload /SENSITEC/PDF_Downloads/Datenblatt/Sensitec_GLM700ASB_DSE_08.pdf. (Accessed 19 May 2014).

[46] dSPACE (2010). Products, Hardware, MicroAutoBox Hardware, MicroAutoBox - Technical Details. Available from http://www.dspace.co.uk/en/pub/home/products/hw/micautob/technischedaten.cfm.
(Accessed 06 June 2014).

[47] Digimess (2012). FG 200 2 MHz Sweep Function Generator. Datasheet. Digimess Instruments Ltd: Derby, United Kingdom.